

**IDENTIFICATION OF ELASTIC PROPERTIES OF
COMPOSITE PLATES USING NON-DESTRUCTIVE TWO
STAGES DERIVATIVE-BASED METHOD AND META-
HEURISTIC HYBRID OPTIMIZATION METHOD**

TAM JUN HUI

**FACULTY OF ENGINEERING
UNIVERSITY OF MALAYA
KUALA LUMPUR**

2018

**IDENTIFICATION OF ELASTIC PROPERTIES OF
COMPOSITE PLATES USING NON-DESTRUCTIVE
TWO STAGES DERIVATIVE-BASED METHOD AND
META-HEURISTIC HYBRID OPTIMIZATION
METHOD**

TAM JUN HUI

**THESIS SUBMITTED IN FULFILMENT OF THE
REQUIREMENTS FOR THE DEGREE OF DOCTOR OF
PHILOSOPHY**

**FACULTY OF ENGINEERING
UNIVERSITY OF MALAYA
KUALA LUMPUR**

2018

UNIVERSITY OF MALAYA
ORIGINAL LITERARY WORK DECLARATION

Name of Candidate: TAM JUN HUI

Registration/Matric No: KHA140096

Name of Degree: Doctor of Philosophy (Ph.D.)

Title of Project Paper/Research Report/Dissertation/Thesis (“this Work”):

Identification of Elastic Properties of Composite Plates Using Non-Destructive Two Stages Derivative-Based Method and Meta-Heuristic Hybrid Optimization Method

Field of Study: Engineering Design

I do solemnly and sincerely declare that:

- (1) I am the sole author/writer of this Work;
- (2) This Work is original;
- (3) Any use of any work in which copyright exists was done by way of fair dealing and for permitted purposes and any excerpt or extract from, or reference to or reproduction of any copyright work has been disclosed expressly and sufficiently and the title of the Work and its authorship have been acknowledged in this Work;
- (4) I do not have any actual knowledge nor do I ought reasonably to know that the making of this work constitutes an infringement of any copyright work;
- (5) I hereby assign all and every rights in the copyright to this Work to the University of Malaya (“UM”), who henceforth shall be owner of the copyright in this Work and that any reproduction or use in any form or by any means whatsoever is prohibited without the written consent of UM having been first had and obtained;
- (6) I am fully aware that if in the course of making this Work I have infringed any copyright whether intentionally or otherwise, I may be subject to legal action or any other action as may be determined by UM.

Candidate’s Signature

Date:

Subscribed and solemnly declared before,

Witness’s Signature

Date:

Name:

Designation:

**IDENTIFICATION OF ELASTIC PROPERTIES OF COMPOSITE PLATES
USING NON-DESTRUCTIVE TWO STAGES DERIVATIVE-BASED METHOD
AND META-HEURISTIC HYBRID OPTIMIZATION METHOD**

ABSTRACT

Researchers have been investing much time and efforts in investigating non-destructive vibrational methods. Accuracy, repeatability, convergence and robustness are the important aspects determining the reliability of a non-destructive method. Evaluating the reliability of a method on the basis of these aspects is subjective because this depends on the compared methods and the applications. In this research, a derivative-based method is developed to identify the elastic properties of composite plates under various boundary conditions. The novelty consists in its composition, where it is constructed adopting the Fourier method, a weighted least squares method and the mode shape error function. The displacement function of the plate structure is defined in terms of two-dimensional Fourier cosine series which is supplemented with several one-dimensional additional terms to accommodate various boundary conditions. The derivatives of mode shape with respect to stiffness rigidity are derived and computed from the model's displacement function. A two-stage identification approach is proposed, in which stage 1 uses natural frequencies while stage 2 utilises mode shapes. The use of mode shapes in stage 2 is proven vital in improving the identifiability of the in-plane shear modulus and Poisson's ratio. However, the effectiveness of this method is dependent on the initial values. Therefore, a meta-heuristic hybrid optimisation method is proposed to enhance the exploratory and exploitative search processes. In early iterations, the two-point standard mutation is utilised collaboratively with the concept of the ACO unrepeated tour to evade local entrapments, while the one-point refined mutation is used in later iterations to supplement the exploitative search process, which is mainly contributed by the PSO. The proposed method is validated using test

functions and well-known engineering design problems. It exhibits an excellent global search capability in the presence of constraints. Furthermore, the applicability of the proposed method in material identification is investigated and compared with those of the conventional methods, namely, ACO, GA and PSO. It is proven to be relatively better than the conventional methods in various aspects. Instead of adopting the conventional natural frequency error function, the FRF error function is used to improve specifically the identifiability of the in-plane shear modulus and Poisson's ratio. The effectiveness of the FRF error function in material identification consists in the trade-off range between those of the natural frequency error function and mode shape error function. Comparing the two-stage derivative-based method with the meta-heuristic hybrid optimisation method, the latter is better in terms of accuracy and robustness, while the former exhibits superiority in the aspects of repeatability and convergence.

Keywords: composite, derivative-based, frequency response function (FRF), meta-heuristic, non-destructive

**IDENTIFIKASI CIRI-CIRI ELASTIK PLAT KOMPOSIT MENGGUNAKAN
KAEDAH DUA PERINGKAT BERASASKAN DERIVATIF DAN KAEDAH
PENGOPTIMUMAN HIBRID META-HEURISTIK**

ABSTRAK

Para penyelidik telah banyak menghabiskan masa dan usaha dalam mengkaji kaedah tidak musnah secara getaran. Ketepatan, kebolehulangan, kepantasan dan keteguhan merupakan aspek penting yang menentukan kebergantungan pendekatan tidak musnah. Penilaian kebergantungan kaedah berdasarkan aspek-aspek tersebut dikatakan subjektif disebabkan penilaian tersebut bergantung kepada kaedah yang dibandingkan serta jenis aplikasi. Dalam kajian ini, kaedah berasaskan derivatif telah direka untuk mengenalpasti ciri-ciri elastik bahan komposit dalam keadaan sempadan umum. Kebaharuan pendekatan tersebut terdapat dalam pembinaan algoritma yang berlandaskan kaedah Fourier, kaedah “weighted least squares” serta penggunaan fungsi ralat bentuk mod. Fungsi bentuk struktur ditakrifkan sebagai “Fourier cosine series” dua dimensi disertai beberapa istilah tambahan satu dimensi untuk menyesuaikan pelbagai keadaan sempadan umum. Derivatif bentuk mod berlandaskan “stiffness rigidity” dapat diperolehi daripada fungsi bentuk tersebut. Dalam kajian ini, pendekatan pengenalan berasaskan dua peringkat dikemukakan. Frekuensi semula jadi digunakan di peringkat pertama dan bentuk mod digunakan di peringkat kedua. Penggunaan bentuk mod di peringkat kedua dinyatakan penting dalam meningkatkan ketepatan modulus ricih dalam-satah dan nisbah Poisson. Namun, keberkesanan kaedah tersebut dikatakan bergantung kepada nilai permulaan. Oleh itu, kaedah pengoptimuman hibrid meta-heuristik turut direka untuk meningkatkan proses penerokaan dan eksploitasi. Dalam lelaran awal, mutasi standard dua mata digunakan secara kolaboratif dengan konsep penerokaan tidak berulang yang terdapat dalam ACO untuk mengelakkan perangkap tempatan, manakala mutasi halus satu mata digunakan dalam lelaran kemudian untuk

menambahbaikan proses eksploitasi yang disumbangkan oleh PSO. Kaedah yang dicadangkan telah disahkan melalui penggunaan fungsi ujian dan pelbagai masalah reka bentuk kejuruteraan. Pendenkatan yang dicadangkan tersebut mempamerkan keupayaan pencarian global yang tinggi dalam keadaan yang didapati kekangan. Selain itu, penggunaan kaedah yang dicadangkan dalam pengenalan ciri-ciri elastik bahan komposit telah disiasat dan keberkesanan kaedah tersebut dibandingkan dengan kaedah konvensional, seperti ACO, GA dan PSO. Kaedah hibrid tersebut didapati cemerlang dalam pelbagai aspek. Selain menggunakan fungsi ralat frekuensi semula jadi konvensional dalam pengenalan ciri-ciri bahan, fungsi ralat FRF dicadangkan untuk memperbaiki pengenalpastian modulus ricih dalam-satah dan nisbah Poisson. Keberkesanan fungsi ralat “FRF” dalam mengenal pasti ciri-ciri elastik bahan komposit didapati terletak di antara keberkesanan fungsi ralat frekuensi semula jadi dan fungsi ralat bentuk mod. Antara kaedah berasaskan dua-peringkat derivatif dan kaedah pengoptimuman hibrid meta-heuristik, kaedah pengoptimuman hibrid meta-heuristik terbukti lebih baik dari segi ketepatan dan keteguhan, manakala, kaedah kaedah berasaskan dua-peringkat derivatif terbukti lebih unggul dalam aspek kebolehulangan dan kepantasan.

Kata kunci: komposit, derivatif, “frequency response function (FRF)”, meta-heuristik, tidak musnah

ACKNOWLEDGEMENTS

First and foremost, the author would like to address his utmost gratitude to his supervisors, Ir. Dr Ong Zhi Chao, Prof. Dr Zubaidah Ismail and Assoc. Prof. Ir. Dr Ang Bee Chin for giving him an opportunity to conduct and handle this research project. Without their unconditional help and guidance, the author would not have made it this far.

Apart from that, the author would like to express his appreciation to his fellow lab mates of vibration laboratory, Mr Chin Wei Ken, Mr Lim Hong Cheet, Mr Mahmudur Rahman, Mr Md. Sazzad Hossain, Mr Mohd Bakar Mohd Mishani, and Mr Rasel Sarkar for their constructive opinions and encouragement when facing difficulties and complications.

Furthermore, the author wishes to thank the Postgraduate Research Grant (PG009-2015A) of University of Malaya for providing financial assistance. Moreover, the author wishes to deliver his gratitude to his beloved family members, especially, his father, Mr Tam Chong Chien and mother, Mrs Liew Yeok Kheng, for their never-ending support and motivation. Lastly, the author would like to utter a word of appreciation to every party who had, directly and indirectly, involved in the journey of his research project.

TABLE OF CONTENTS

Abstract	iii
Abstrak	v
Acknowledgements	vii
Table of Contents	viii
List of Figures	xiii
List of Tables.....	xviii
List of Symbols and Abbreviations.....	xxiii
CHAPTER 1: INTRODUCTION.....	1
1.1 Problem statement and motivation	1
1.2 Objectives	5
1.3 Contributions	6
1.4 Research flow and scope	8
1.5 Outline of the report.....	9
CHAPTER 2: LITERATURE REVIEW.....	11
2.1 Introduction.....	11
2.2 Overview.....	11
2.3 Experimental measurements (Vibrational methods)	17
2.4 Numerical evaluation.....	22
2.4.1 Forward method	22
2.4.1.1 Rayleigh's method.....	22
2.4.1.2 Rayleigh-Ritz method	25
2.4.1.3 Finite Element Method (FEM).....	28
2.4.1.4 Fourier method	32

2.4.2	Inverse method	33
2.4.2.1	Derivative-based method.....	34
2.4.2.2	Meta-heuristic optimisation method.....	39
2.4.3	Uncertainty	48
2.4.4	Summary	50
2.5	Mathematical theory	51
2.5.1	Forward method (Fourier method).....	51
2.5.2	Inverse method	53
2.5.2.1	Derivative-based method.....	54
2.5.2.2	Meta-heuristic optimisation method.....	60
CHAPTER 3: RESEARCH METHODOLOGY		75
3.1	Introduction.....	75
3.2	Method 1: Two-stage derivative-based method	75
3.2.1	Stage 1: Natural frequencies.....	76
3.2.2	Stage 2: Mode shapes	77
3.3	Method 2: Meta-heuristic hybrid optimisation method (Hybrid GA-ACO-PSO).....	79
3.3.1	General flow of algorithm	80
3.3.2	Verification of the proposed method using test functions and engineering design problems.....	81
3.3.2.1	Test functions	82
3.3.2.2	Engineering design problems	87
3.3.3	Application in vibrational material identification	95
3.3.4	Comparative study of different error functions.....	97
3.4	Experimental validation.....	98
3.4.1	Destructive test	99
3.4.2	Theoretical calculation	100

3.4.3	Non-destructive test.....	102
3.4.3.1	Experimental measurement.....	102
3.4.3.2	Numerical evaluation.....	106
CHAPTER 4: RESULTS AND DISCUSSIONS		109
4.1	Introduction.....	109
4.2	Method 1: Two-stage derivative-based method	109
4.2.1	Accuracy of two-stage derivative-based method in reference plates	109
4.2.2	Repeatability of two-stage derivative-based method in reference plates.....	112
4.2.3	Convergence of two-stage derivative-based method in reference plates.....	112
4.2.4	Analysis of the proposed two-stages derivative-based method in reference plates.....	113
4.3	Method 2: Meta-heuristic hybrid optimisation method (Hybrid GA-ACO-PSO)	116
4.3.1	Verification using test functions and engineering design problems.....	117
4.3.1.1	Test functions	117
4.3.1.2	Engineering design problems	122
4.3.2	Application in vibrational material identification	141
4.3.2.1	Accuracy of meta-heuristic hybrid optimisation method in reference plates.....	141
4.3.2.2	Repeatability of meta-heuristic hybrid optimisation method in reference plates.....	145
4.3.2.3	Convergence of meta-heuristic hybrid optimisation method in reference plates.....	148
4.3.2.4	Robustness of meta-heuristic hybrid optimisation method in reference plates.....	154
4.3.3	Comparative study of different error functions.....	157

4.3.3.1	Accuracy of meta-heuristic hybrid optimisation method with different error functions in reference plates	158
4.3.3.2	Repeatability of meta-heuristic hybrid optimisation method with different error functions in reference plates	161
4.3.3.3	Convergence of meta-heuristic hybrid optimisation method with different error functions in reference plates	163
4.3.3.4	Analysis of meta-heuristic hybrid optimisation method with different error functions in reference plates	165
4.4	Experimental validation.....	166
4.4.1	Destructive test.....	166
4.4.2	Theoretical calculation	167
4.4.3	Non-destructive test.....	167
4.4.3.1	Method 1: Two-stage derivative-based method.....	167
4.4.3.2	Method 2: Meta-heuristic hybrid optimisation method (Hybrid GA-ACO-PSO)	175
4.5	Comparison between two-stage derivative-based method and meta-heuristic hybrid optimisation method.....	195
CHAPTER 5: CONCLUSIONS AND RECOMMENDATIONS.....		200
5.1	Conclusions	200
5.2	Recommendations.....	203
References.....		204
List of Publications and Papers Presented		221
Appendix A.....		222
Appendix B.....		223
Appendix C.....		227
Appendix D.....		228

Appendix E.....	230
Appendix F.....	231

University of Malaya

LIST OF FIGURES

Figure 1.1: Research flow chart	10
Figure 2.1: Overview of composite material properties identification methodologies...	12
Figure 2.2: Distributed loading and point loading static test (Wang & Kam, 2000)	13
Figure 2.3: Flow chart of non-direct evaluation of elastic properties	15
Figure 2.4: Schematic of the impulse technique experimental set-up (Hwang et al., 2009)	19
Figure 2.5: Schematic of the shaker-based experimental set-up (Matter et al., 2011)....	20
Figure 2.6: Schematic of the acoustic-based experimental set-up (Matter et al., 2007) .	21
Figure 2.7: Concept of refined mutation	67
Figure 2.8: Concept of combined discrete and continuous probability distribution scheme.....	68
Figure 2.9: The proposed hybrid GA-ACO-PSO algorithm	70
Figure 3.1: Pseudo code of the proposed hybrid algorithm	81
Figure 3.2: Schematic diagram of a pressure vessel	89
Figure 3.3: Welded beam schematic diagram	90
Figure 3.4: INSTRON universal testing instrument	100
Figure 3.5: Schematic diagram of specimen for thickness of 3mm.....	100
Figure 3.6: Schematic diagram of plate	103
Figure 3.7: Experimental set-up for ABS plate.....	103
Figure 3.8: Experimental set-up for ACP	104
Figure 4.1: Convergence rate achieved by GA, ACO, PSO and the proposed hybrid algorithm for Himmelblau's non-linear optimisation problem case 1	128
Figure 4.2: Convergence rate achieved by GA, ACO, PSO and the proposed hybrid algorithm for Himmelblau's non-linear optimisation problem case 1	128

Figure 4.3: Convergence rate achieved by GA, ACO, PSO and the proposed hybrid algorithm for pressure vessel design optimisation problem.....	128
Figure 4.4: Convergence rate achieved by GA, ACO, PSO and the proposed hybrid algorithm for welded beam design optimisation problem.....	129
Figure 4.5: Convergence rate achieved by GA, ACO, PSO and the proposed hybrid algorithm for gear train design optimisation problem	129
Figure 4.6: Computational time consumed by GA, ACO, PSO and the proposed hybrid algorithm for Himmelblau's non-linear optimisation problem case 1	130
Figure 4.7: Computational time consumed by GA, ACO, PSO and the proposed hybrid algorithm for Himmelblau's non-linear optimisation problem case 2	131
Figure 4.8: Computational time consumed by GA, ACO, PSO and the proposed hybrid algorithm for pressure vessel design optimisation problem.....	131
Figure 4.9: Computational time consumed by GA, ACO, PSO and the proposed hybrid algorithm for welded beam design optimisation problem.....	131
Figure 4.10: Computational time consumed by GA, ACO, PSO and the proposed hybrid algorithm for gear train design optimisation problem	132
Figure 4.11: Comparison of minimised value for aluminium plate using different algorithms.....	142
Figure 4.12: Comparison of minimised value for graphite epoxy plate using different algorithms.....	143
Figure 4.13: Comparison of repeatability for aluminium plate using different algorithms	145
Figure 4.14: Comparison of repeatability for graphite epoxy plate using different algorithms.....	147
Figure 4.15: Convergence rate of different types of algorithms for aluminium plate under F-F-F-F boundary condition	149
Figure 4.16: Convergence rate of different types of algorithms for aluminium plate under C-F-F-F boundary condition	149
Figure 4.17: Convergence rate of different types of algorithms for aluminium plate under C-C-F-C boundary condition	150
Figure 4.18: Convergence rate of different types of algorithms for graphite epoxy plate under F-F-F-F boundary condition	151

Figure 4.19: Convergence rate of different types of algorithms for graphite epoxy plate under C-F-F-F boundary condition	151
Figure 4.20: Convergence rate of different types of algorithms for graphite epoxy plate under C-C-F-C boundary condition	151
Figure 4.21: Computational time of different types of algorithms for aluminium plate under F-F-F-F boundary condition	154
Figure 4.22: Computational time of different types of algorithms for graphite epoxy plate under F-F-F-F boundary condition.....	154
Figure 4.23: Absolute percentage error of evaluated E_x	159
Figure 4.24: Absolute percentage error of evaluated E_y	160
Figure 4.25: Absolute percentage error of evaluated G_{xy}	160
Figure 4.26: Absolute percentage error of evaluated v_{xy}	160
Figure 4.27: Standard deviation of the evaluated E_x	162
Figure 4.28: Standard deviation of the evaluated E_y	162
Figure 4.29: Standard deviation of the evaluated G_{xy}	162
Figure 4.30: Standard deviation of the evaluated v_{xy}	163
Figure 4.31: Computational time of using different types of error functions	164
Figure 4.32: Sensitivity graph of ABS plate	177
Figure 4.33: Sensitivity graph of ACP	177
Figure 4.34: Corresponding mode shapes of ABS plate after stage 1	178
Figure 4.35: Corresponding mode shapes of ACP after stage 1	178
Figure 4.36: 25 measurement DOFs of corresponding modes of the ABS plate determined from the first level FRF selection scheme.....	179
Figure 4.37: 25 measurement DOFs of corresponding modes of ACP determined from the first level FRF selection scheme	179
Figure 4.38: Evaluated and experimental FRFs of ABS plate before (top) and after (bottom) the second stage with input DOF at point 5 and output DOF at point 1. Note: Arrow in black indicates a reduction in magnitude difference before and after the second stage.	181

Figure 4.39: Evaluated and experimental FRFs of ABS plate before (top) and after (bottom) the second stage with input DOF at point 9 and output DOF at point 1. Note: Arrow in black indicates a reduction in magnitude difference before and after the second stage, while arrow in green denotes an increment in magnitude difference before and after the second stage.	182
Figure 4.40: Evaluated and experimental FRFs of ABS plate before (top) and after (bottom) the second stage with input DOF at point 21 and output DOF at point 1. Note: Arrow in black indicates a reduction in magnitude difference before and after the second stage, while arrow in green denotes an increment in magnitude difference before and after the second stage.	183
Figure 4.41: Evaluated and experimental FRFs of ABS plate before (top) and after (bottom) the second stage with input DOF at point 25 and output DOF at point 1.	184
Figure 4.42: Evaluated and experimental FRFs of ACP before (top) and after (bottom) the second stage with input DOF at point 5 and output DOF at point 1. Note: Arrow in black indicates a reduction in magnitude difference before and after the second stage, while arrow in green denotes an increment in magnitude difference before and after the second stage.	188
Figure 4.43: Evaluated and experimental FRFs of ACP before (top) and after (bottom) the second stage with input DOF at point 9 and output DOF at point 1. Note: Arrow in black indicates a reduction in magnitude difference before and after the second stage.	189
Figure 4.44: Evaluated and experimental FRFs of ACP before (top) and after (bottom) the second stage with input DOF at point 21 and output DOF at point 1. Note: Arrow in black indicates a reduction in magnitude difference before and after the second stage, while arrow in green denotes an increment in magnitude difference before and after the second stage.	190
Figure 4.45: Evaluated and experimental FRFs of ACP before (top) and after (bottom) the second stage with input DOF at point 25 and output DOF at point 1. Note: Arrow in black indicates a reduction in magnitude difference before and after the second stage, while arrow in green denotes an increment in magnitude difference before and after the second stage.	191
Figure B.1: Sensitivity graph of aluminium plate under F-F-F-F boundary condition.	224
Figure B.2: Sensitivity graph of aluminium plate under C-F-F-F boundary condition	224
Figure B.3: Sensitivity graph of aluminium plate under C-C-F-C boundary condition	225
Figure B.4: Sensitivity graph of graphite epoxy plate under F-F-F-F boundary condition	226

Figure B.5: Sensitivity graph of graphite epoxy plate under C-F-F-F boundary condition226

Figure B.6: Sensitivity graph of graphite epoxy plate under C-C-F-C boundary condition.....226

University of Malaya

LIST OF TABLES

Table 1.1: Research gap	5
Table 2.1: Final estimates and number of iterations performed for cross-ply laminate (Daghia et al., 2007).....	36
Table 2.2: System identification of orthotropic plate using hybrid RSM–PSO method in time domain with 5% noise (Sankar et al., 2014)	46
Table 3.1: Dimensions and elastic properties of reference plates.....	76
Table 3.2: Number of dimensions used and the optimum solutions for test functions...	83
Table 3.3: Input settings for GA, ACO, PSO and the proposed hybrid algorithm	86
Table 3.4: Notations for welded beam design problem	91
Table 3.5: Input settings for the proposed algorithm	94
Table 3.6: Input settings for GA, ACO, PSO and the proposed hybrid algorithm in material identification	96
Table 3.7: Input settings for hybrid algorithm in FRF-based material identification	98
Table 3.8: Dimension of specimen	100
Table 3.9: Apparatus and equipment specifications	104
Table 4.1: Identification results of aluminium plate under three different boundary conditions.....	110
Table 4.2: Identification results of graphite epoxy plate under three different boundary conditions.....	111
Table 4.3: Average computational time of the proposed two-stage derivative-based method.....	112
Table 4.4: Average minimised function value error and standard deviation achieved by the proposed hybrid algorithm with different features.....	118
Table 4.5: Friedman test on <i>aa</i> variations	119
Table 4.6: Friedman test on <i>D</i> variations	119
Table 4.7: Average minimised function value error <i>fi – Fi</i> achieved by GA, ACO, PSO and the proposed hybrid algorithm	120

Table 4.8: Standard deviation achieved by GA, ACO, PSO and the proposed hybrid algorithm	120
Table 4.9: Average computational time (s) consumed by GA, ACO, PSO and the proposed hybrid algorithm	121
Table 4.10: Average minimised function value error $f_i - F_i$ achieved by established algorithms and the proposed hybrid algorithm	122
Table 4.11: Standard deviation achieved by established algorithms and the proposed hybrid algorithm.....	122
Table 4.12: Friedman test on accuracy and repeatability.....	122
Table 4.13: Best, average and worst minimised objective function values as well as standard deviation achieved by the proposed hybrid algorithm with different features	123
Table 4.14: Friedman test on parameter variations.....	124
Table 4.15: Best, average and worst minimised objective function values as well as standard deviation achieved by GA, ACO, PSO and the proposed hybrid algorithm ..	126
Table 4.16: Comparison of the best solutions for Himmelblau's problem applying different algorithms.....	134
Table 4.17: Repeatability study for Himmelblau's problem.....	135
Table 4.18: Comparison of best solutions for pressure vessel design problem applying different algorithms.....	137
Table 4.19: Repeatability study for pressure vessel design problem.....	137
Table 4.20: Comparison of the best solutions for welded beam design problem applying different algorithms.....	139
Table 4.21: Repeatability study for welded beam design problem.....	139
Table 4.22: Comparison of the best solutions for gear train design problem applying different algorithms.....	140
Table 4.23: Repeatability study for gear train design problem.....	140
Table 4.24: Elastic constants obtained for aluminium plate under F-F-F-F boundary condition.....	142
Table 4.25: Elastic constants obtained for aluminium plate under C-F-F-F boundary condition.....	142

Table 4.26: Elastic constants obtained for aluminium plate under C-C-F-C boundary condition.....	142
Table 4.27: Elastic constants obtained for graphite epoxy plate under F-F-F-F boundary condition.....	144
Table 4.28: Elastic constants obtained for graphite epoxy plate under C-F-F-F boundary condition.....	144
Table 4.29: Elastic constants obtained for graphite epoxy plate under C-C-F-C boundary condition.....	144
Table 4.30: Improvement percentage of identified elastic properties using the proposed algorithm with respect to those of using other algorithms.....	145
Table 4.31: Repeatability study using different type of algorithms for aluminium plate under F-F-F-F boundary condition	146
Table 4.32: Repeatability study using different type of algorithms for aluminium plate under C-F-F-F boundary condition	146
Table 4.33: Repeatability study using different type of algorithms for aluminium plate under C-C-F-C boundary condition	146
Table 4.34: Repeatability study using different type of algorithms for graphite epoxy plate under F-F-F-F boundary condition.....	147
Table 4.35: Repeatability study using different type of algorithms for graphite epoxy plate under C-F-F-F boundary condition	147
Table 4.36: Repeatability study using different type of algorithms for graphite epoxy plate under C-C-F-C boundary condition	147
Table 4.37: Difference of standard deviation of the proposed hybrid algorithm with respect to those of other algorithms	148
Table 4.38: Identified elastic properties of aluminium plate in the presence of increasing errors	157
Table 4.39: Identified elastic properties of graphite epoxy plate in the presence of increasing errors.....	157
Table 4.40: Benchmark elastic properties of ABS plate obtained from tensile test	167
Table 4.41: Benchmark elastic properties of ACP obtained from theoretical calculation	167

Table 4.42: Identification results of ABS plate under F-F-F-F boundary condition	168
Table 4.43: Comparison of experimental and evaluated natural frequencies and mode shapes for ABS plate.....	169
Table 4.44: Average node displacement difference between experimental and evaluated mode shapes for ABS plate.....	170
Table 4.45: Identification results of ACP under F-F-F-F boundary condition	170
Table 4.46: Comparison of experimental and evaluated natural frequencies and mode shapes for ACP.....	172
Table 4.47: Average nodal displacement difference between experimental and evaluated mode shapes for ACP.....	172
Table 4.48: Computational time of ABS plate.....	174
Table 4.49: Identification stopping criteria of ABS plate.....	174
Table 4.50: Convergence results of ABS plate.....	174
Table 4.51: Computational time of ACP.....	175
Table 4.52: Identification stopping criteria of ACP.....	175
Table 4.53: Convergence results of ACP.....	175
Table 4.54: Experimental and evaluated natural frequencies of ABS plate in the first stage.....	180
Table 4.55: Evaluated elastic properties of ABS plate using natural frequency error function in stage 1	185
Table 4.56: Evaluated elastic properties of ABS plate using FRF error function in stage 2.....	186
Table 4.57: Experimental and evaluated natural frequencies of ACP after the first stage.....	186
Table 4.58: Evaluated elastic properties of ACP using natural frequency error function in stage 1	192
Table 4.59: Evaluated elastic properties of ACP using FRF error function in stage 2 .	193
Table 4.60: Standard deviations of evaluated elastic properties of ABS plate	194
Table 4.61: Standard deviations of evaluated elastic properties of ACP.....	194

Table 4.62: Computational time of the proposed meta-heuristic hybrid algorithm in determining the elastic properties of ABS plate	195
Table 4.63: Computational time of the proposed meta-heuristic hybrid algorithm in determining the elastic properties of ACP	195
Table 4.64: Comparison of evaluated elastic properties using two-stage derivative-based method and meta-heuristic hybrid optimisation method.....	196
Table 4.65: Comparison of standard deviations of evaluated elastic properties using two-stage derivative-based method and meta-heuristic hybrid optimisation method...	197
Table 4.66: Comparison of average computational time of evaluated elastic properties using two-stage derivative-based method and meta-heuristic hybrid optimisation method.....	197
Table 4.67: Robustness of the proposed two-stage derivative-based method and meta-heuristic hybrid optimisation method	199
Table A.1: Test functions used for validation purposes.....	222
Table B.1: Benchmark natural frequencies and mode shapes of aluminium plate	223
Table B.2: Benchmark natural frequencies and mode shapes of graphite epoxy plate.....	225
Table C.1: The computational time of using two-stage derivative-based method in reference study	227
Table D.1: Average minimised function value error $f_i - F_i$ achieved by the proposed hybrid algorithm of feature 2 with different parameter aa and D	228
Table E.1: Best, average and worst minimised objective function values as well as standard deviation achieved by the proposed hybrid algorithm of feature 1 with different parameter aa	230
Table F.1: The minimised values and evaluated elastic properties using hybrid GA-ACO-PSO incorporated with three different types of error functions	231
Table F.2: The computational time of using hybrid GA-ACO-PSO incorporated with three different types of error functions.....	231

LIST OF SYMBOLS AND ABBREVIATIONS

Symbols

α_{ij}	:	Frequency response function (FRF) at position i and output at position j
$\alpha_{X_i}, \alpha_{A_i}$:	Experimental and analytical frequency response function (FRF), respectively
λ_{am}	:	$m\pi/a$
λ_{bn}	:	$n\pi/b$
τ_{ij}	:	Pheromones
φ_i	:	Scaled mode shapes
θ, ϕ	:	Characteristic beam functions satisfying boundary conditions
ϕ_m, ψ_n	:	Admissible assumed functions used in Rayleigh's quotient
ϕ_{X_i}, ϕ_{A_i}	:	The i^{th} complex experimental and analytical mode shapes, respectively
ϵ	:	Error function
\otimes	:	Element-by-element vector multiplication
ρ	:	Mass density
ϑ	:	Regularization parameter used in stage 1
μ	:	Regularization parameter used in stage 2
ω	:	Angular frequency
\mathbf{A}	:	Double Fourier series coefficients matrix
$\vec{\mathbf{a}}$:	The momentum factor vector
$\vec{\mathbf{b}}_1, \vec{\mathbf{b}}_2$:	The strength of attraction vector
$\vec{\mathbf{c}}, \vec{\mathbf{d}}$:	The coefficients vector
J	:	Objective function
\mathbf{K}	:	Stiffness matrix
\mathbf{M}	:	Mass matrix

\vec{p}_1	:	The previous best position vector
\vec{p}_2	:	The globally best position vector in the whole neighbourhood
ΔPr	:	Solution obtained after minimisation of J
\vec{r}_1, \vec{r}_2	:	Random number vectors within the range from 0 to 1
S	:	Sensitivity matrix
\vec{v}_k	:	The previous velocity vector
\vec{v}_{k+1}	:	The updated velocity vector
W_ϵ	:	Weighting matrices that define the importance of ϵ
W_x	:	Weighting matrices that define the importance of ΔPr
\vec{x}_{cross}	:	The solution vectors after undergoing crossover process
\vec{x}_k	:	The previous position vector
\vec{x}_{k+1}	:	The updated position vector
a	:	Plate dimension in x direction
aa, bb	:	The percentage range of design variables in refined mutation
b	:	Plate dimension in y direction
c_m^l, d_n^l	:	Single Fourier series coefficients
co	:	Crossover point
d_{ij}	:	Distance between cities i and j
ev	:	Evaporation rate
f_i	:	Minimised value of cost function i
fr_i, \overline{fr}_i	:	Evaluated and experimental natural frequencies, respectively of mode i
h	:	Plate thickness
g_i	:	Constraint i
k_{x0}, k_{xa}	:	Translational stiffness at $x = 0$ and $x = a$, respectively
k_{y0}, k_{yb}	:	Translational stiffness at $y = 0$ and $y = b$, respectively

l	:	1, 2, 3, 4 index in the special functions and single Fourier series
l_{ant}	:	An unvisited city by k^{th} ant
m	:	0,1... $M-1$ Fourier series indices in x -direction
n	:	0,1... $N-1$ Fourier series indices in y -direction
p_{ij}^k	:	Probability function of the amount of pheromone
$rand1,$:	Random numbers ranging from 0 to 1
$rand2$:	
u_i	:	Weighting factor
ν_{xy}	:	Major Poisson's ratio associated with x - y plane of the plate
ν_{yx}	:	Minor Poisson's ratio associated with x - y plane of the plate
ν_{12}	:	Major Poisson's ratio associated with 1 - 2 plane of the fibre
ν_{21}	:	Minor Poisson's ratio associated with 1 - 2 plane of the fibre
x_{new}	:	The mutated variable
A_{mn}	:	Double Fourier series coefficients
$CCABS$:	Weighted absolute relative difference between natural frequencies
$CCMDISP$:	Weighted absolute relative difference between modal displacements
D	:	Number of mutation points
D_{ij}	:	Standard bending stiffness
E_x, E_y	:	Elastic modulus in x - and y -direction of the plate
E_1, E_2	:	Elastic modulus in 1 - and 2 -direction of the fibre
F_i	:	Global optimum of test function i^{th}
G_{xy}	:	Shear modulus associated with x - y plane of the plate
G_{12}	:	Shear modulus associated with 1 - 2 plane of the fibre
H	:	Thickness of plate
HT	:	Hermitian transpose

K_{x0}, K_{xa}	:	Rotational stiffness at $x = 0$ and $x = a$, respectively
K_{y0}, K_{ya}	:	Rotational stiffness at $y = 0$ and $y = b$, respectively
L_k	:	Length of tour built by k^{th} ant
M_x, M_y	:	Bending moments
M_{xy}	:	Twisting moment
N	:	Number of dimensions
$N(s^p)$:	Set of cities available for k^{th} ant
N_x, N_y	:	Constant in-plane forces per unit width
P	:	Single Fourier series coefficients matrix
Q_x, Q_y	:	Shear forces
$R(\omega)$:	Rayleigh's quotient
T_{max}	:	Kinetic energy
UB_i, LB_i	:	The upper and lower boundaries of i^{th} design variable
V_{max}	:	Potential energy
$W(x, y)$:	Flexural displacement

Abbreviations

2D	:	Two-Dimensional
3D	:	Three-Dimensional
ABS	:	Acrylonitrile-Butadine-Styrene
ACO	:	Ant Colony Optimisation
ACP	:	Aluminium Composite Panel
APSO	:	Adaptive Particle Swarm Optimisation
B	:	Bayesian estimator
BC	:	Boundary Condition
C	:	Clamped
CLPSO	:	Comprehensive Learning Particle Swarm Optimisation
CPSO-H	:	Cooperative Particle Swarm Optimisation with Hybrid Swarm
CSF	:	Cross Signature Scale Factor
DAQ	:	Data Acquisition
DASYLab	:	Data Acquisition System Laboratory
DNSCLPSO	:	Diversity Enhanced Comprehensive Learning Particle Swarm Optimisation with Neighbourhood Search
DNSPSO	:	Diversity Enhanced Particle Swarm Optimisation with Neighbourhood Search
DOF	:	Degree Of Freedom
EMA	:	Experimental Modal Analysis
F	:	Free
FEM	:	Finite Element Method
FFT	:	Fast Fourier Transform
FRAC	:	Frequency Response Assurance Criterion

FRF	:	Frequency Response Function
GA	:	Genetic Algorithm
GOPSO	:	Modified PSO which employs Generalised Opposition-Based Learning (GOBL) and Cauchy mutation
LVD	:	Laser Doppler Vibrometer
MAC	:	Modal Assurance Criterion
MATLAB	:	Matrix Laboratory
MVE	:	Minimum Variance Estimator
PSO	:	Particle Swarm Optimisation
RSM	:	Response Surface Methodology
SAC	:	Signature Assurance Criterion

University of Malaya

CHAPTER 1: INTRODUCTION

1.1 Problem statement and motivation

From the viewpoint of practical application, the knowledge of material properties is essential. Material properties must be known in advance before the material is adopted for particular purposes to ensure its application suitability. As time elapses, constructed structures, such as buildings, bridges, infrastructures, etc. may have experienced changes in material properties on account of ageing implications, climatic effects, inexorable fatigue and cyclic load accumulation, etc., and thereby, incurring a great possibility in the occurrence of catastrophic accidents. These undesirable implications can, in fact, be anticipated and avoided via the study of material identification. Therefore, understanding the fundamentals of material identification is imperative.

Since the past decades, material evolution has been occurring incessantly from previous simple isotropic components to present heterogeneous composite structures. Composites are hybrid materials that are composed of at least two constituents at a macroscopic scale. They are manufactured in layers of laminates, and each layer is arranged in a specific orientation. Superiority in material properties has been the contributing factor leading to the widespread usage of composite materials in multiple industries. Corresponding to the advancement of emerging materials, material identification methods have as well been experiencing a breakthrough from traditional destructive identification approaches to current non-destructive evaluation techniques. Classical identification methods, such as tensile tests, compressive tests, etc., tend to be destructive, time-consuming and expensive. Therefore, a number of identification approaches have been developed to circumvent these drawbacks.

A combined experimental and numerical technique has often been the primary choice in material identification owing to its non-destructive nature, promising accuracy as

well as cost- and time-saving advantages. This technique involves experimental measurement and numerical evaluation. It requires only a single experimental test to evaluate the elastic properties of a composite material, unlike conventional destructive tests. Experimental modal analysis (EMA) is conducted to acquire the modal parameters of a structure that define its dynamic behaviours. Subsequently, the modal parameters, namely, natural frequencies, mode shapes and damping properties are utilised as the reference parameters in numerical evaluation to identify the elastic properties of the target structure. Numerical evaluation involves the use of a forward method and an inverse method as well as the definition of an objective function. A forward method is used to construct a virtual plate model, in which, the input and output parameters of the model are the elastic properties and the modal parameters of a structure, respectively. Conversely, an inverse method is used to derive an inverse form of the plate model to evaluate the elastic properties by minimising the error difference between evaluated and reference modal parameters.

Accuracy, repeatability, convergence and robustness are the important aspects determining the reliability of a non-destructive method. Evaluating the reliability of a method on the basis of these aspects is subjective because this depends on the compared methods and the applications. In material identification, the accuracy of a non-destructive method can be evaluated based on the absolute percentage error between the identified and reference elastic properties, as well as the minimised value of the cost function. Furthermore, the repeatability of a non-destructive method can be studied by computing the standard deviations of several sets of the identified elastic properties, as well as those of the minimised value of the cost function. In the study of convergence, the computational time and the convergence rate in terms of iterations can be the relevant indicators. Apart, the robustness of a non-destructive approach can be defined by its range of applicability in the variation of boundary conditions, objective functions

and dimension number, as well as its degree of adaptation to problems that are prone to uncertainties. In brief, the reliability of a non-destructive method depends substantially on the accuracy, repeatability, convergence and robustness of the forward methods and the inverse or optimisation methods. Definition of an objective function is also one of the important factors affecting the effectiveness of an identification method. In non-destructive vibrational material identification, the discrepancy between the reference and evaluated natural frequencies is commonly used to define the objective function (Hwang et al., 2010; Lin & Chang, 2010; Pagnotta & Stigliano, 2009). The main reason leading to its prevalent usage is due to the uniqueness and simple acquisition of natural frequencies. A natural frequency is unique such that it is expressed as a global value that defines a particular mode of a structure. Due to its uniqueness, natural frequencies can be computed by solving an Eigen problem, in which, the eigenvalues represent the natural frequencies. However, the drawback of using natural frequencies in material identification consists in its low sensitivity with respect to the Poisson's ratio. Alternatively, this issue can be solved by adjusting the parameters pertaining to the plate geometry, for examples, aspect ratio, angle of orthotropy and thickness to improve the sensitivity of resonant frequencies with respect to the Poisson's ratio, as proven in (Ragauskas & Belevičius, 2009; Silva et al., 2004). Furthermore, the drawback can be circumvented by including a higher quantity of resonant frequencies during computation, as discussed by Hwang et al. (2009). Instead of using only natural frequencies, Cugnoni et al. (2007) proposed the integrated use of the natural frequency error norm, diagonal modal assurance criteria (MAC) error norm, off-diagonal MAC error norm, mode shape error norm, and nodal line error norm to improve the accuracy of the in-plane Poisson's ratio and the out-of-plane shear moduli of thick composite plates.

The finite element method (FEM) has been widely used in material identification in conjunction with various derivative-based methods, mainly, due to its excellent flexibility and robustness. Nevertheless, in the aspect of accuracy, the Fourier method is proven better than the FEM due to its analytical quality. Developing a derivative-based method based on the Fourier method is challenging because of their infinite and complex natures. Despite, Ismail et al. (2013) successfully developed an inverse method to identify the elastic properties of orthotropic plates under general boundary conditions adopting the integrated use of the Fourier method and Newton-Raphson method. In the study, the discrepancy between the reference and evaluated natural frequencies is used to define the objective function in constructing the inverse algorithm. The approach is proven robust to general boundary conditions. However, the accuracy of this approach in identifying the in-plane shear modulus and the Poisson's ratio can be further improved due to the relatively low sensitivity of natural frequency with respect to both the properties. On the contrary, mode shapes are relatively more local than natural frequencies and hence, relatively more sensitive to the in-plane shear modulus. In addition, knowing that mode shapes and the Poisson's ratio are much related, the influence of mode shapes on the Poisson's ratio is relatively higher than that of natural frequencies. Therefore, to resolve this complication, a derivative-based method incorporated with the Fourier method and the mode shape error function can be the relevant solution.

The proposed method can be an effective solution to a relevant problem. However, it incurs some drawbacks. Derivative-based methods are known to be problem dependent and less robust to the variation of initial values, number of parameters, etc. Furthermore, the coupled-implementation of natural frequencies and mode shapes error functions may complicate the identification procedures. The need of performing modal parameter extraction from the experimental frequency response function (FRF) may

consume relatively more processing time and affect the credibility of the results. Therefore, a more robust meta-heuristic optimisation method, integrated with the FRF error function can be the potential alternative to circumvent those drawbacks. Generally, the reliability of an identification method depends substantially on the effectiveness of the forward method, inverse method and error function. Based on the review of previous study, the research gaps are briefed in Table 1.1.

Table 1.1: Research gap

No.	Aspects	Previous Study	Research Gap	Current Study
1	Forward method	The use of Rayleigh's method, Rayleigh-Ritz method and finite element method (FEM) in material identification is common and abundant.	Numerous analytical forward methods have been developed; however, the application of these methods in material identification is limited.	The use of an analytical forward method, namely, Fourier method in material identification is proposed and studied.
2	Inverse method	Various derivative-based inverse methods and meta-heuristic optimisation methods have been widely studied and developed.	The application of a derivative-based method incorporated with an analytical forward method is uncommon. The use of a meta-heuristic hybrid algorithm that is composed of three conventional methods is limited.	The use of a derivative-based method incorporated with an analytical method used for material identification is studied. A new hybrid meta-heuristic algorithm, integrating three conventional methods is proposed and investigated.
3	Error function	Natural frequency error function has been widely used in material identification.	The separate use of natural frequency and mode shape error functions is limited. The use of frequency response functions (FRFs) in material identification is rare.	The separate use of natural frequency and mode shape error functions is investigated. The use of the Fourier-generated FRFs is proposed and studied.

1.2 Objectives

The aim of this research is to develop non-destructive identification methods for composite materials. In this regards, two methods, namely, derivative-based and meta-heuristic methods, of different applicability are explored. Notably, the reliability of an identification method is dependent on the type of the forward method, inverse method

and objective function used. On the basis of these factors, the objectives of the current research are presented as follows:

- i. To design a two-stage derivative-based method in determining the elastic properties of composite plates, in which, stage 1 involves the use natural frequencies and stage 2 involves the use of mode shapes
- ii. To design a meta-heuristic hybrid optimisation method in solving engineering design problems and in material identification as compared to three conventional algorithms, namely, genetic algorithm (GA), ant colony optimisation (ACO) and particle swarm optimisation (PSO)
- iii. To investigate the effectiveness of the proposed meta-heuristic optimisation method incorporated with three different objective functions, namely, natural frequency, mode shape and frequency response function (FRF) error functions
- iv. To validate the proposed two-stage derivative-based method and meta-heuristic hybrid optimisation method in material identification with the benchmark

1.3 Contributions

Due to their non-destructive nature and time- and cost-saving advantages, the proposed methods can be more useful than the conventional destructive methods in manufacturing and construction industries, where operational cost and time are the main concerns. In the aspects of accuracy, repeatability, convergence and robustness, the specific contributions of the research corresponding to the objectives are elaborated as follows:

- i. The proposed two-stage derivative-based method is different from the existing methods, in which, the Fourier method is employed as the forward

method, while, a weighted least squares method is utilised as the inverse method. The natural frequency error function is used in stage 1, while, the mode shape error function is used in stage 2 to improve specifically the identifiability of the in-plane shear modulus and the Poisson's ratio. The proposed method is useful for the identification of elastic properties of simple structures, such as plates under general boundary conditions, due to its excellent repeatability and convergence, as well as its satisfactory accuracy and robustness.

- ii. The proposed meta-heuristic hybrid optimisation method is composed of three different conventional algorithms, namely, genetic algorithm (GA), ant colony optimisation (ACO) and particle swarm optimisation (PSO). Hence, it is known as meta-heuristic hybrid GA-ACO-PSO optimisation method. New features are introduced to improve the overall performance. The proposed method is effective in solving wide-ranging problems, including problems with multimodality, constraints and a large number of dimensions. It exhibits excellent accuracy and robustness, as well as considerably good repeatability and convergence.
- iii. The integrated use of the Fourier method, the proposed hybrid method and the FRF error function is inferred to be more effective in improving the identifiability of the in-plane shear modulus and the Poisson's ratio if compared to those of using the natural frequency error function, as well as the mode shape error function due to the direct exploitation of the experimental FRF data, which are not subjected to processing procedures. Selection of suitable FRFs can be made based on the sensitivity of natural modes with respect to elastic properties, as well as based on the location of impact that lies in the high response region of the corresponding modes to

improve the identifiability of the in-plane shear modulus and Poisson's ratio.

- iv. The experimental validation of the two-stage derivative-based method, as well as the meta-heuristic hybrid optimisation method confirms the feasibility and applicability of both the methods on real structures and thus, might be useful for on-site practical applications.

1.4 Research flow and scope

The research flow chart is constructed as shown in Figure 1.1. The current non-destructive vibrational evaluation approaches are reviewed and surveyed critically. As mentioned, a non-destructive vibrational evaluation approach comprises a forward method and an inverse method. The present research proposes two identification methods, namely, two-stage derivative-based method and meta-heuristic hybrid GA-ACO-PSO optimisation method. The research begins with the modelling of method 1. A two-stage procedure is involved in the first method, in which, stage 1 uses the natural frequency error function, whereas, stage 2 utilises the mode shape error function. The effects of using the proposed method on two different reference plates, namely, aluminium plate and graphite epoxy plate, as well as, under several sets of boundary conditions, namely, F-F-F-F, C-F-F-F and C-C-F-C (C: Clamped, F: Free) are studied. After the completion of method 1, the research continues with the modelling of method 2. The feasibility of method 2 in solving 10 sets of test functions and four sets of engineering design problems, which are taken from the past literature, is first verified. The applicability of method 2 in material identification is then investigated. In this regards, the effectiveness of the proposed algorithm in identifying the elastic properties of two reference plates under several sets of boundary conditions, namely, F-F-F-F, C-F-F-F and C-C-F-C, are studied and compared with those of the conventional algorithms, including, genetic algorithm (GA), ant colony optimisation (ACO) and

particle swarm optimisation (PSO). Furthermore, the effectiveness of the proposed meta-heuristic hybrid optimisation method, incorporated with different types of error functions (natural frequency, mode shape and frequency response function (FRF) error functions), is examined and the best error function is determined. Eventually, both of the proposed two-stage derivative-based method and meta-heuristic hybrid optimisation method are validated using real specimens. The elastic properties obtained from the conventional destructive test and the theoretical calculation are used as the benchmark parameters and compared with the results evaluated from the non-destructive evaluation approaches. In addition, the overall performances of the proposed two-stage derivative-based method and the proposed meta-heuristic hybrid optimisation method are compared and summarized.

1.5 Outline of the report

The report consists of five major chapters, namely, introduction, literature review, research methodology, results and discussions, as well as conclusions and recommendations. The first chapter explains the problem statement and motivation of the research, as well as introduces the main idea of the research. Chapter two reviews the works done by previous researchers and presents the mathematical theories used in this research. Chapter three elaborates the procedures of performing the proposed two-stage derivative-based method and the proposed meta-heuristic hybrid optimisation method during numerical verification stage, as well as the procedures of conducting the destructive test, theoretical calculation, and the proposed non-destructive tests during experimental validation stage. Chapter four presents and discusses the outcomes of the research. The last chapter concludes the research and provides some recommendations for future development.

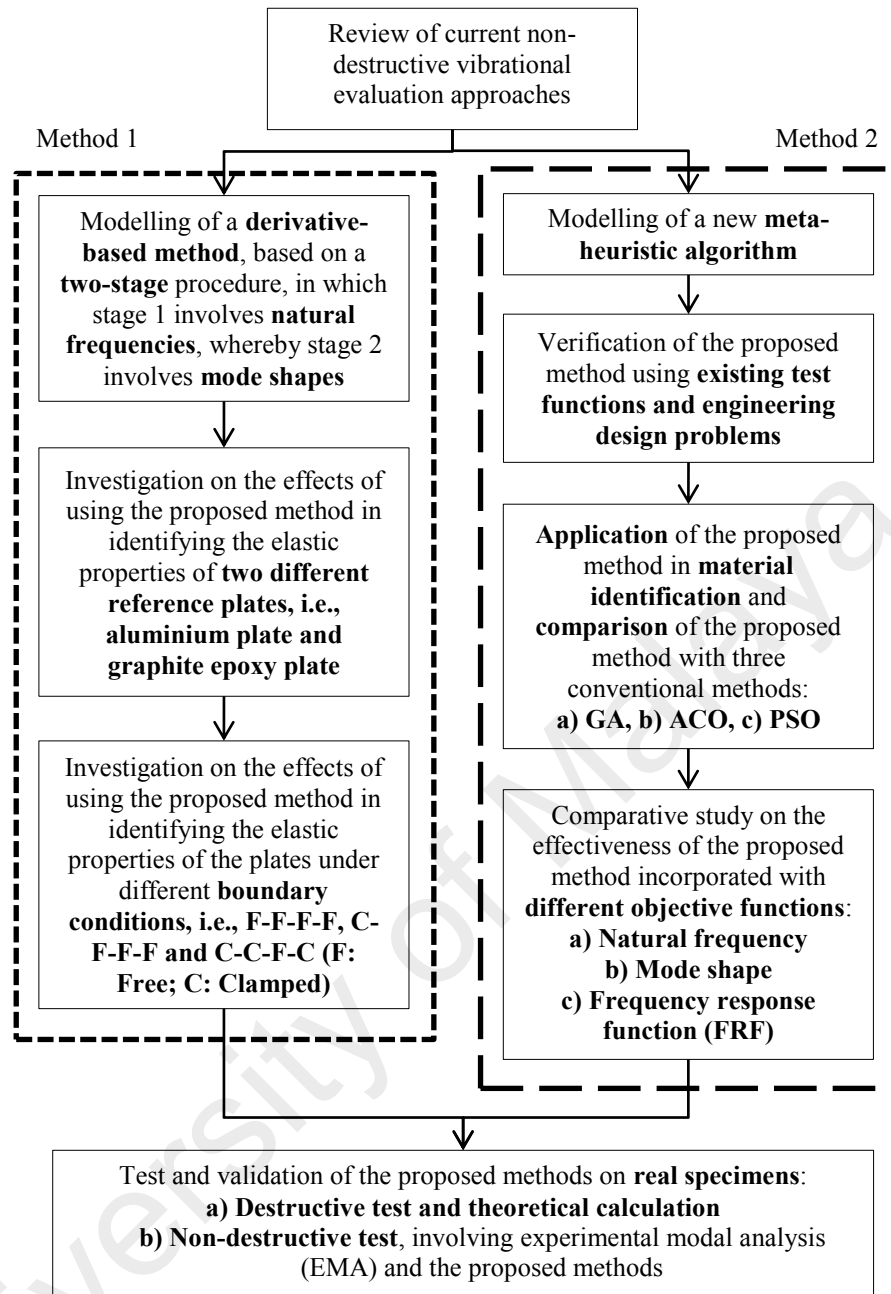


Figure 1.1: Research flow chart

CHAPTER 2: LITERATURE REVIEW

2.1 Introduction

This chapter presents a review of the development of non-destructive vibrational evaluation approaches in determining the elastic properties of composite plates. Numerous experimental techniques, as well as numerical forward and inverse approaches are critically reviewed. Besides, this chapter also includes the mathematical theories of derivative-based methods and meta-heuristic optimisation methods.

2.2 Overview

Composite materials can be referred to as hybrid materials, which are made of two or more materials at a macroscopic scale. Nowadays, composite materials are drawing global interest and attention due to their prominent physical and chemical properties, such as lightweight, high strength and high corrosion resistance. Consequently, the production of a great assortment of composite materials is getting prevalent, and hence, inciting the development of identification methods for composite materials. Due to the substantial impact of composite materials to various industries, researchers have thus been devoting much effort to studying and developing material identification methods for composites since the past decades.

Generally, the identification of elastic constants or elastic properties can be categorised into two main techniques, namely, destructive technique and non-destructive technique, as shown in Figure 2.1. A destructive technique can be referred to as a classical static approach involving static mechanical tests, such as, tensile test, compressive test, bending test, torsional test, etc. to acquire the stresses and strains of a specimen. Direct identification of elastic constants can be performed based on the fundamental stress-strain theory. Due to the anisotropic characteristics of composites,

several tests need to be performed to identify the properties of different directions, hence, complicating the overall procedures.

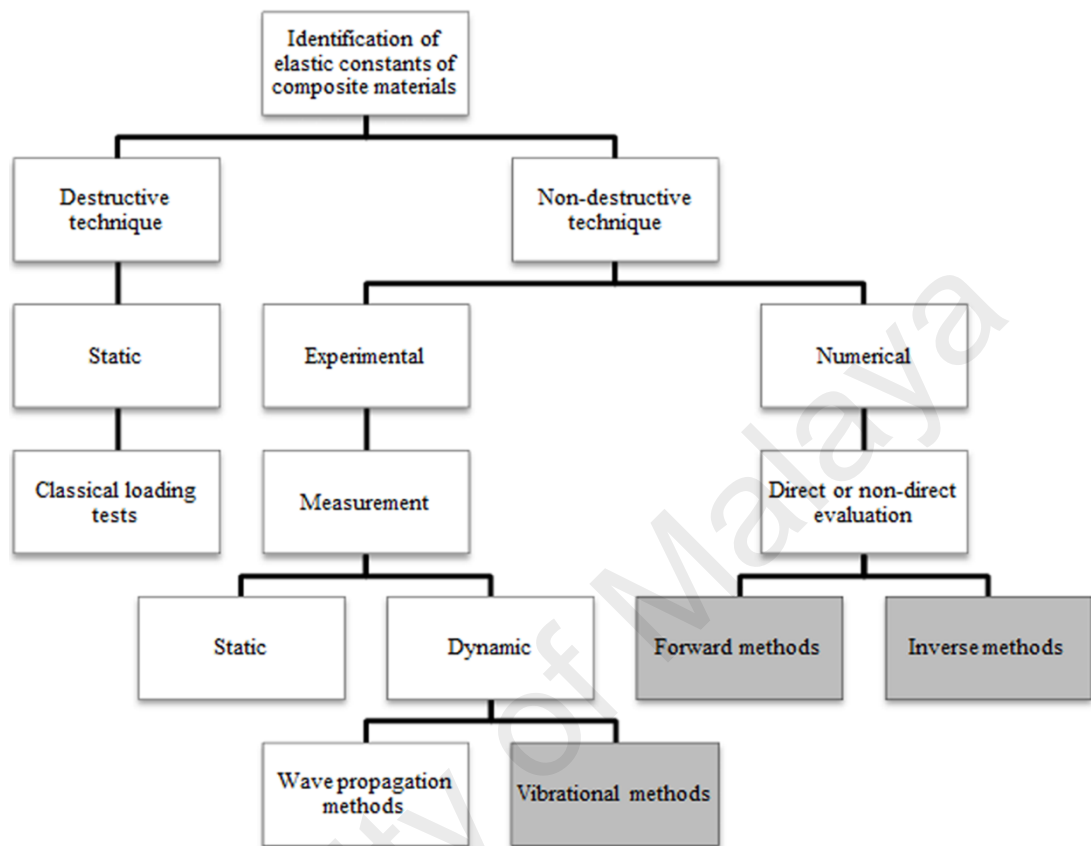


Figure 2.1: Overview of composite material properties identification methodologies

A non-destructive technique involves two primary procedures, namely, experimental measurement and numerical evaluation. Experimental measurement involves the measurement and extraction of significant parameters employing a non-destructive experimental technique, while, numerical evaluation involves the evaluation of elastic properties of a composite material adopting a forward method and an inverse method.

Experimental measurement can be categorised into two main approaches, namely, static approach and dynamic approach. In some cases, static tests are carried out in non-destructive manners. These tests involve transverse quasi-static loadings on a specimen, in which the induced strains must not exceed 0.5% so that the elasticity of the specimen can be maintained and thus, the deflection could fully recover at the end of the test

(Wesolowski et al., 2009). The boundary conditions of the plate specimen are either simply-supported or clamped and the deformational parameters, namely, displacements and strains are acquired without damaging the specimen (Bruno et al., 2008; Kam et al., 2009; Wesolowski et al., 2009). Unlike the destructive static approach, this approach requires the involvement of numerical evaluation to determine the elastic properties. Figure 2.2 presents the experimental set-up of the non-destructive static approach and the detailed procedures can be retrieved from (Wang & Kam, 2000).

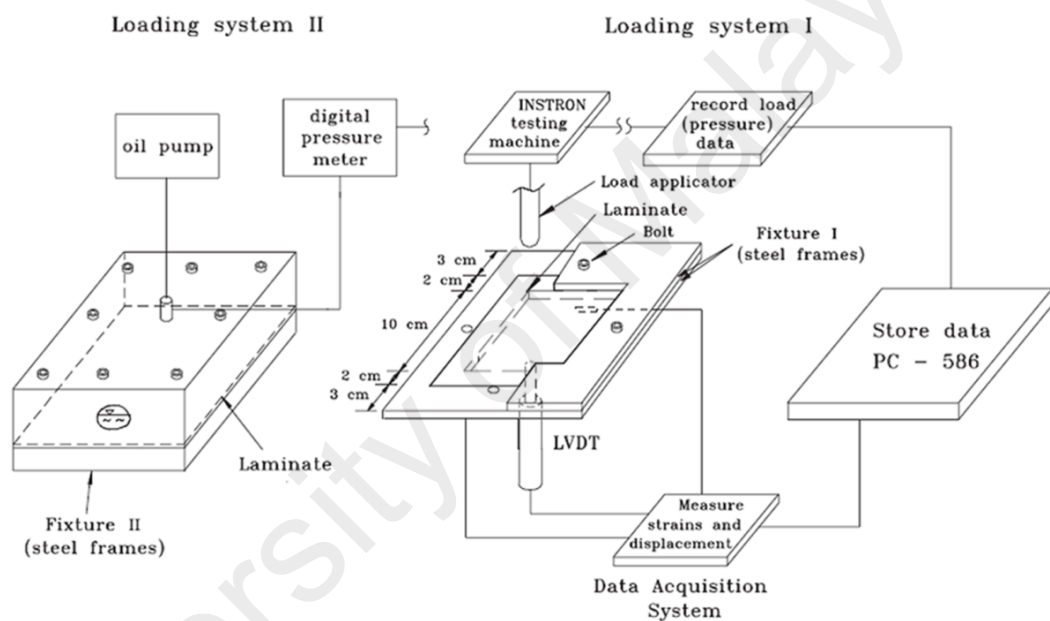


Figure 2.2: Distributed loading and point loading static test (Wang & Kam, 2000)

A dynamic approach is one of the commonly-used non-destructive approaches. Basically, dynamic approach comprises two methods, namely, wave propagative methods and vibrational methods. Wave propagative methods usually adopt the application of ultrasonic wave passing through a specimen, where, the wave signal velocity and transit time of flight (TOF) of the wave from the emitting transducer to the receiving transducer, are recorded. The commonly-used emitting and receiving transducers are piezoelectric transducers due to the factors of low price and lightweight. Wave propagative methods can be further classified into bulk-wave-based methods (Castellano et al., 2014; Dahmen et al., 2010; Vishnuvardhan et al., 2007) and guided-

wave-based methods (Glushkov et al., 2014; Marzani & De Marchi, 2013; Sale et al., 2011). Bulk-wave-based methods are usually used in the identification of thick composite materials via through-transmission or back-reflection techniques. On the contrary, in guided-wave-based methods, Lamb waves or guided waves are usually generated and remained guided between two parallel free surfaces of a plate or shell. Lamb-wave-based methods are normally adopted for the investigation of thin plates. Nevertheless, due to several drawbacks of wave propagation methods, such as complex dispersive characteristics of waves, the formation of several waveforms in single frequency waves, complex procedures, and the need of active power, vibrational methods emerge as the best alternatives in material identification to circumvent those drawbacks. In vibrational methods, an external impact is placed on the specimen and the response of the vibrating specimen is measured and recorded in terms of frequency response functions (FRFs). Modal parameters, namely, natural frequencies, modal damping and mode shapes, which define the dynamic behaviours of the specimen, are then extracted from the acquired FRFs. Commonly, the obtained experimental natural frequencies are utilised in the subsequent numerical stage as the reference parameters.

In numerical stage, direct evaluation refers to the direct identification of elastic properties of a material from a derived inverse equation with the experimental resonant frequencies served as the inputs. On the contrary, non-direct evaluation involves iterations and the minimisation or maximisation of an objective function. As shown in Figure 2.3, the non-direct evaluation of elastic properties of composite materials involves a forward method and an inverse method. In the forward method, parameters, such as natural frequencies, mode shapes, etc. of a specimen are evaluated using the inputs of elastic properties of the material, depending on respective identification approaches. In the inverse method, an error function, which is defined by the difference between the experimental and evaluated parameters, is minimised and an optimisation

algorithm is used to perform the solution search process. Generally, two types of non-direct evaluation methods are reviewed in the present research, namely, derivative-based methods (bayesian estimation method, feasible directions method, Newton's method, and nonlinear least squares method) and meta-heuristic optimisation methods (ant colony optimisation (ACO), genetic algorithm (GA), particle swarm optimisation (PSO) and response surface methodology (RSM)).

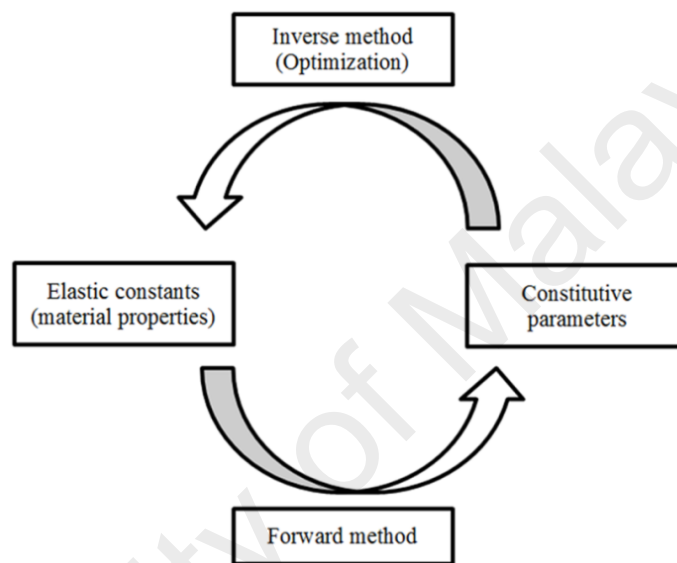


Figure 2.3: Flow chart of non-direct evaluation of elastic properties

The general procedures of a derivative-based method begin with the specification of the input parameters. Initially, the maximum number of iterations, the minimum improvement percentage, and the minimum value of convergence are specified. The benchmark or experimental modal parameters (natural frequencies, mode shapes or/and damping properties) are also specified in the error function. Most importantly, an initial set of elastic parameters are needed to initialise the algorithm. Given an initial set of elastic properties, the algorithm begins with the forward evaluation of the modal parameters. Based on the error function, the error between the benchmark and evaluated modal parameters is then evaluated. Subsequently, the derivative of the evaluated modal parameter with respect to the elastic property is computed. Afterthat, the step vector is evaluated from the derived inverse algorithm, involving the use of the evaluated

derivative matrix and error function values. The computed step vector signifies the distance between the assigned and actual elastic properties that will reduce the error between the benchmark and evaluated modal parameters. The next iteration begins with the addition of the step vector to the previous assigned elastic parameters. The iterations are carried on until either of the termination criteria is satisfied. The termination criteria include the maximum number of iterations, the minimum improvement percentage, and the minimum value of convergence. The elastic properties are eventually identified once the running algorithm is terminated.

With regard to a meta-heuristic optimisation method, it does not involve the evaluation of derivatives. A slight difference exists in the procedures between the present and the former methods. Instead of assigning only an initial set of elastic parameters at once, a specific number of populations and boundaries of search region need to be defined initially. For the first iteration, several sets of elastic properties are randomly picked within the specified search region according to the predefined number of populations. In this approach, minimisation or maximisation of the error function is involved. An individual set of elastic parameters with a relatively better function value will be prioritised and the search will emphasize more on its surrounding area in the next iteration. The iterations persist until either of the stopping criteria is achieved. In the end, the elastic properties are evaluated once the running algorithm is stopped.

A number of review articles pertaining to elastic parameter identification methods have been published, for instances, a review of elastic properties identification methods based on full-field measurements presented by Avril et al. (2008) and a review of recent progress of elastic characterization methods developed at the University of Calabria by Pagnotta (2008). In this chapter, the focus will be placed on reviewing the development of non-destructive vibrational experimental and numerical methods, as highlighted in

Figure 2.1. The type of the vibrational experimental method, as well as the type of the forward method, inverse method and objective function, incur significant influences on the accuracy, repeatability, convergence and robustness of an identification approach.

2.3 Experimental measurements (Vibrational methods)

Much research has been attempted employing vibrational methods in evaluating the elastic properties of composite materials. A vibrational method is often associated with experimental modal analysis (EMA), as studied by Schwarz and Richardson (1999). It is an experimental technique used to study the dynamic behaviours of elastic structures. The dynamic behaviours of a structure are normally expressed in terms of modal parameters, namely, natural frequencies, mode shapes and damping properties. Generally, there are two common types of excitations, namely, impulse excitation (Huang & Luo, 2013; Hwang et al., 2010; Hwang et al., 2009) and continuous variable excitation (Barkanov et al., 2015; Matter et al., 2011; Schwaar et al., 2012; Xu & Zhu, 2013). Referring to impulse excitation, an impulser, such as an impact hammer is usually used to strike the specimen mechanically and elastically, as described in the ASTM standard (E1876-09, 2009). On the other hand, continuous variable excitation commonly involves the use of loud-speakers or shakers fed by a variable frequency oscillator.

In accordance with the development of Fast Fourier Transform (FFT) analysers and virtual instruments, the impulse excitation technique has been widely used since the late 1970s. The impulse technique is often the primary choice in the study of material identification due to its simple and inexpensive procedures, as shown in past literature (Hwang et al., 2010; Hwang et al., 2009; Lee & Kam, 2006a; Lee et al., 2007). At present, there is only an ASTM standard procedure specifically meant for isotropic materials but none for anisotropic materials. Despite, multiples studies have been

adopting such a procedure on orthotropic and anisotropic laminated materials, as shown in most of the mentioned publications. With regard to layer-wise identification of a multi-layered laminated plate, instead of conducting only a single experimental test, a number of tests are needed depending on the number of materials embedded in the multi-layered laminated plate (Lauwagie et al., 2004; Lauwagie et al., 2003). A large number of vibration tests are required when a large number of materials used in a multi-layered plate. The vibrational experiment adopting impulse technique is commonly known as impact testing, as demonstrated in Figure 2.4 (Hwang et al., 2009). An impact hammer is usually used as the exciter and contactless eddy current proximity transducers (displacement) (Deobald & Gibson, 1988), accelerometers (De Wilde & Sol, 1986; Hwang et al., 2010; Hwang et al., 2009; Lee et al., 2007), microphones (Araujo et al., 2000; Araujo et al., 1996), or laser Doppler vibrometer (LDV) (Alfano & Pagnotta, 2005; Berthelot & Angoulvant, 2002; Lauwagie et al., 2003) are used as the response detectors. However, the shortcomings of this technique consist in its low reproducibility of input characteristics (manual excitation) and non-applicability to light and brittle objects.

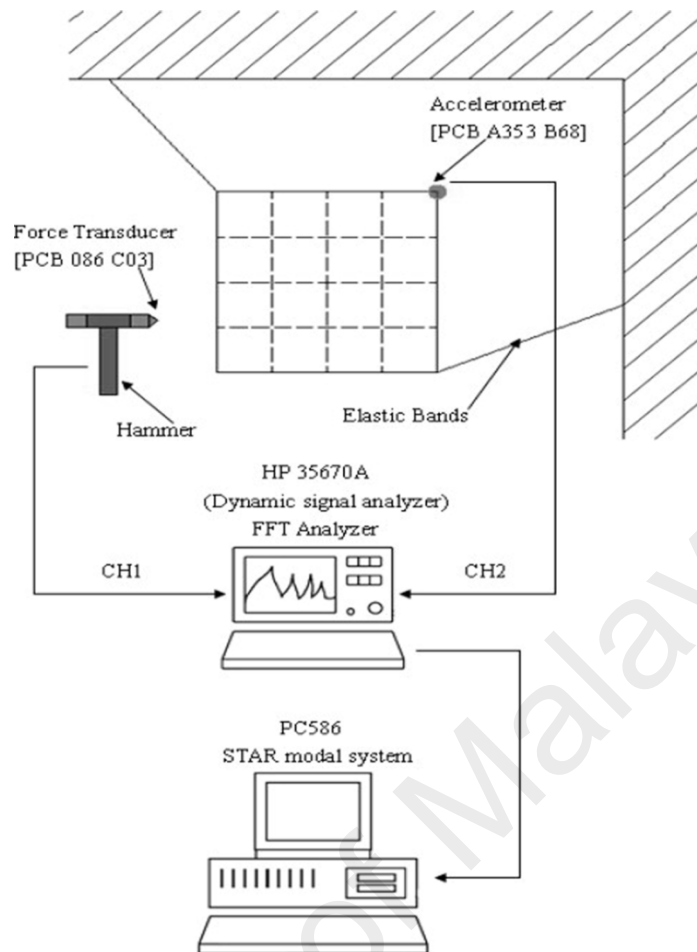


Figure 2.4: Schematic of the impulse technique experimental set-up (Hwang et al., 2009)

Referring to a continuous variable excitation technique, the shaker excitation is commonly used and often compared with the impact excitation. Both of these excitations are developed since the creation of FFT analysers. As shown in Figure 2.5 (Matter et al., 2011), the shaker testing is utilised to eliminate the drawbacks of the impact testing, such as the use of impact hammer might damage delicate surfaces and its limited frequency range of excitation, etc. Common types of shakers, namely, electrodynamic shakers and hydraulic shakers are used along with a stinger, which is a long slender rod, in order to specify the direction of the excitation force applied. There are several types of broadband signals for shaker measurements with FFT analysers, including transient signal, true random signal, pseudo-random signal, burst random signal, fast sine sweep (chirp) signal and burst chirp signal. This shaker excitation technique is widely used in various applications, including in the study of material

identification (Batista et al., 2009; Catania & Sorrentino, 2009; Giraudeau et al., 2010; Matter et al., 2011). Accelerometers (Catania & Sorrentino, 2009), LDV (Batista et al., 2009; Matter et al., 2011) and non-interferometric (Giraudeau et al., 2010) transducers are the common response-measuring transducers used in shaker-based experiment. Although shakers exhibit better applicability in broadband frequency-wise, complications in setting up the experiment, as well as the mass loading effects due to the attached accelerometers on the specimen seem to impede the widespread usage.

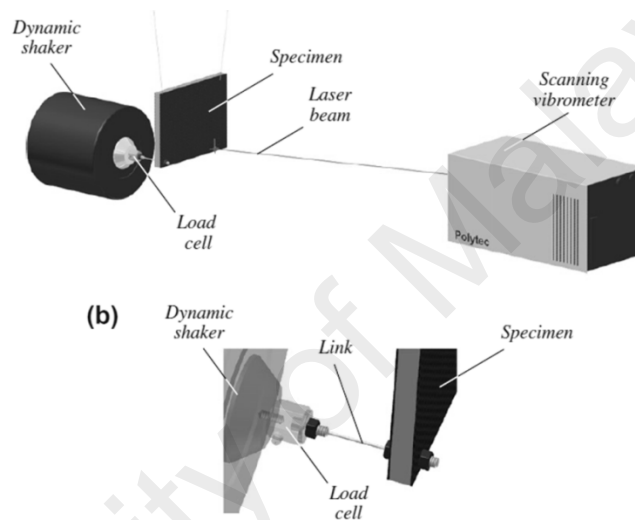


Figure 2.5: Schematic of the shaker-based experimental set-up (Matter et al., 2011)

Apart from the shaker excitation, an alternative technique, which is known as the acoustic excitation has been developed as well, as shown in Figure 2.6 (Matter et al., 2007). In the acoustic-based experiment, a loudspeaker fed by a signal generator with a power amplifier is used as the source of excitation. This excitation is more advantageous over the shaker excitation in the sense that the source of excitation and the specimen are contactless, thereby, avoiding mass loading implication. Besides, it is useful when dealing with structures having relatively low internal damping properties. Similar to the shaker excitation, several types of broadband signals can be configured. The application of this technique is considerably popular in identifying the elastic properties of materials (Barkanov et al., 2015; Schwaar et al., 2012; Xu & Zhu, 2013).

Normally, acoustic loudspeakers are used as the exciter and LDV (Schwaar et al., 2012; Xu & Zhu, 2013) is used as the response detector. Furthermore, interferometric transducers are also used to measure the dynamic response (Borza, 2004; Sato et al., 2008). In terms of signal to noise ratio, the value is found to be comparatively low at low amplitudes, indicating that the noise level is relatively high. Despite, the accuracy of the natural frequencies educed from a narrow frequency band is barely affected.

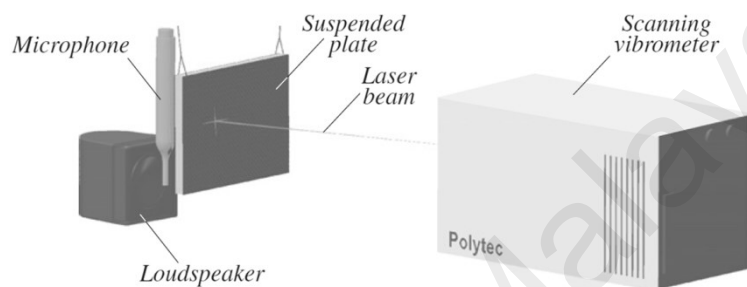


Figure 2.6: Schematic of the acoustic-based experimental set-up (Matter et al., 2007)

The impulse technique, shaker excitation technique and acoustic excitation technique incorporated with a variety of measuring techniques, such as the conventional contact accelerometers, contactless non-interferometric transducers, laser Doppler vibrometers and microphones can be seen to be equally high in demand and widely used due to their respective advantages and disadvantages that complement each other. The selection of either technique depends on the objectives and requirements of a research. In fact, there is no discernible difference in the procedures for each technique when handling a particular type of plate, such as isotropic, orthotropic, anisotropic and laminated plates. Certainly, when dealing with anisotropic and laminated plates, a number of experimental tests are required. Among those aforementioned techniques, the impulse technique appears to be the most popular approach at present in the research of material identification because of the ease of implementation, inexpensive procedures and wide-ranging applicability. In terms of accuracy, those mentioned techniques provide reliable results only if proper and correct procedures are followed.

2.4 Numerical evaluation

2.4.1 Forward method

In a vibrational approach, forward methods are needed to determine the modal parameters, namely, natural frequencies, mode shapes or/and damping properties of a structure for subsequent use in the identification process. The details of the Rayleigh's method, Rayleigh-Ritz method, finite element method (FEM), and Fourier method, including the correlation parameters, type of plates used with respective geometrical shapes, boundary conditions, as well as principle of methods used are presented.

2.4.1.1 Rayleigh's method

In the Rayleigh's method, the maximum kinetic and potential energies of a plate are needed to compose the Rayleigh's quotient. Referring to the study done by Dickinson (1978), for an orthotropic plate, the potential energy, V_{max} and kinetic energy, T_{max} can be expressed as follows:

$$V_{max} = \frac{1}{2} \int_0^a \int_0^b \left[D_x \left(\frac{\partial^2 W}{\partial x^2} \right)^2 + 2v_{xy} D_y \frac{\partial^2 W}{\partial x^2} \frac{\partial^2 W}{\partial y^2} + D_y \left(\frac{\partial^2 W}{\partial y^2} \right)^2 + 4D_{xy} \left(\frac{\partial^2 W}{\partial x \partial y} \right)^2 + N_x \left(\frac{\partial W}{\partial x} \right)^2 + N_y \left(\frac{\partial W}{\partial y} \right)^2 \right] dy dx \quad (2.1)$$

$$T_{max} = \frac{1}{2} \rho h \omega^2 \int_0^a \int_0^b W^2 dy dx \quad (2.2)$$

where, $D_x = E_x h^3 / 12(1 - v_{xy}v_{yx})$, $D_y = D_x E_y / E_x$, and $D_{xy} = G_{xy} h^3 / 12$, E_x and E_y are the elastic moduli, G_{xy} is the in-plane shear modulus, v_{xy} and v_{yx} are the Poisson's ratios, $W(x, y)$ is the transverse displacement of the plate, h denotes the thickness of the plate, ρ is the density of plate material, N_x and N_y are the constant in-plane forces per unit width and the double integral is taken over the area of the plate. The Rayleigh's

quotient is defined by the ratio of total potential to kinetic energy for a mode of vibration, which can be expressed as follows:

$$R(\omega) = \omega^2 = \frac{V_{max}}{T_{max}}$$

$$= \frac{\int_0^a \int_0^b \left[D_x \left(\frac{\partial^2 W}{\partial x^2} \right)^2 + 2v_{xy} D_y \frac{\partial^2 W}{\partial x^2} \frac{\partial^2 W}{\partial y^2} + D_y \left(\frac{\partial^2 W}{\partial y^2} \right)^2 + 4D_{xy} \left(\frac{\partial^2 W}{\partial x \partial y} \right)^2 + N_x \left(\frac{\partial W}{\partial x} \right)^2 + N_y \left(\frac{\partial W}{\partial y} \right)^2 \right] dy dx}{\rho h \int_0^a \int_0^b W^2 dy dx} \quad (2.3)$$

Let $H = v_{xy} D_y + 2D_{xy}$ and the assumed shape function $W(x, y) = \theta(x)\phi(y) \times constant$, where $\theta(x)$ and $\phi(y)$ are the characteristic beam functions which satisfy the boundary conditions on $x = 0, a$ and $y = 0, b$ respectively, and can be rearranged and expressed as follows:

$$\frac{\rho h \omega^2}{H}$$

$$= \frac{\int_0^a \int_0^b \left[\frac{D_x}{H} (\theta'' \phi)^2 + 2\theta \theta'' \phi \phi'' + \frac{D_y}{H} (\theta \phi'')^2 + 4 \frac{D_{xy}}{H} \{(\theta' \phi')^2 - \theta \theta'' \phi \phi''\} + \frac{N_x}{H} (\theta' \phi)^2 + \frac{N_y}{H} (\theta \phi')^2 \right] dy dx}{\int_0^a \int_0^b (\theta \phi)^2 dy dx} \quad (2.4)$$

Given the tables of beam characteristic functions by Felgar (1950), the frequently-used orthotropic plate frequency parameter can be presented as follows:

$$\lambda_{ortho}^2 = \frac{\rho h \omega^2 a^2 b^2}{\pi^4 H} = \frac{D_x}{H} G_x^4 \frac{b^2}{a^2} + \frac{D_y}{H} G_y^4 \frac{a^2}{b^2} + 2 \left[H_x H_y + 2 \frac{D_{xy}}{H} (J_x J_y - H_x H_y) \right] + \frac{N_x b^2}{\pi^2 H} J_x + \frac{N_y a^2}{\pi^2 H} J_y \quad (2.5)$$

where, the coefficients G_x, G_y, H_x, H_y, J_x and J_y can be found in the article written by Warburton (1954).

Several studies have been performed utilising the Rayleigh's method for forward evaluation of natural frequencies of isotropic (Alfano & Pagnotta, 2007; Dickinson &

Diblasio, 1986) and orthotropic composite plates (Ayorinde, 1995; Kim & Dickinson, 1985) in material identification, in which, both thin plates (Ayorinde & Gibson, 1993; Fallstrom, 1991), as well as thick plates (Ayorinde, 1995) are investigated. Most of the studies are carried out involving rectangular plates under free-free boundary conditions. Warburton (1954) was the first who proposed the use of characteristic beam vibration functions in the Rayleigh's method to study the vibration of thin, isotropic plates. His work was further investigated by Hearmon (1959), who applied such method to specially orthotropic composite plates, in which, the load was exerted either in parallel or perpendicular to the plates' fibres. Even though Warburton's expression allows straightforward calculation of plates' natural frequencies, the accuracy might be adversely affected if one or more free edges are involved in the study. Since the presence of free edge(s) affects the reliability of Warburton's equation, Alfano and Pagnotta (2006) proposed the use of Warburton's equation, which is supplemented with appropriate correction factors to identify the elastic properties of thin isotropic rectangular plates with free edges. The two elastic properties, namely, the elastic modulus and Poisson's ratio of the isotropic plate were finally identified using the equation derived from Warburton's equation involving at least two of the first four experimental natural frequencies. Later, Alfano and Pagnotta (2007) adopted the polynomial interpolating functions and more accurate correction factors, which were accounted for the variation of Poisson's ratio, to identify the Poisson's ratio and elastic modulus of the similar plate. In the research done by Ayorinde and Gibson (1993), the Rayleigh's method was employed based on the classical lamination theory to evaluate the natural frequencies of a thin rectangular orthotropic plate with free edges. The proposed method was validated using thin isotropic, orthotropic and laminated plates. McIntyre and Woodhouse (1988) used the similar method to identify the elastic and damping constants of thin, orthotropic composite plates. In fact, this approach was

conducted on the basis of frequencies analysis and damping factors of low vibration modes, which enabling its applicability on various materials. Meanwhile, in the research done by Ayorinde (1995), the applicability of similar method on thick orthotropic plates with free edges was as well investigated. Instead of solely utilising the previous classical lamination theory, through-thickness shear and rotatory inertia were taken into account in the Rayleigh's method to evaluate the plate's resonant frequencies. In summary, the Rayleigh's method can be used to study the vibration of isotropic and orthotropic composite plates. When dealing with isotropic problems, only two elastic properties were involved, while, minimum of four elastic properties were needed when involving orthotropic structures. The Rayleigh's method is adopted in the modelling of the dynamic behaviour of rectangular plates, mainly because of its ease of implementation. However, its restriction in providing only information about the lowest or the first resonant frequency as well as its mediocre accuracy are the main reasons that lead to the development of the Rayleigh-Ritz method.

2.4.1.2 Rayleigh-Ritz method

The Rayleigh-Ritz method is an extension of the Rayleigh's method. Instead of using a single assumed function (static deflection shape), several assumed functions are superimposed to obtain a better approximation. This method allows the evaluation of natural frequencies of higher modes depending on the arbitrary number of assumed functions used. Referring to the article published by Deobald and Gibson (1988), the similar Rayleigh's quotient is expressed as follows:

$$R(\omega) = \omega^2 = \frac{V_{max}}{\rho h \int_0^a \int_0^b W^2 dy dx} \quad (2.6)$$

$$W(x, y) = \sum_{m=1}^p \sum_{n=1}^q A_{mn} \phi_m(x) \psi_n(y) \quad (2.7)$$

In Equations (2.6) and (2.7), A_{mn} denotes the coefficients and $W(x, y)$ represents the transverse displacement or the mode shape of the plate, which is composed of several admissible assumed functions ϕ_m and ψ_n as well as ω indicates the natural frequency, which can eventually be obtained by solving the corresponding eigenvalue problem. In practice, the Rayleigh-Ritz method is said to be applicable to all plate problems (linear or nonlinear), since the principle of virtual displacements applies to all plate problems (Reddy, 2006). The applicability of the Rayleigh-Ritz method in material identification has received considerable recognition among researchers (Berthelot & Angoulvant, 2002; Lee et al., 2007; Rebillat & Boutillon, 2011). Most of the investigations are conducted on thin rectangular orthotropic plates (Berthelot & Angoulvant, 2002; Muthurajan et al., 2004), followed by thin rectangular laminated plates (Lee & Kam, 2006a, 2006b) and thick rectangular Sandwich plates (Lee et al., 2007; Rebillat & Boutillon, 2011) with combinations of free-clamped edges (Berthelot & Angoulvant, 2002; Deobald & Gibson, 1988), free edges (Muthurajan et al., 2004; Rebillat & Boutillon, 2011), and elastically-restrained edges (Lee & Kam, 2006b; Lee et al., 2007). To solve problems involving isotropic or specially orthotropic plates, the use of trigonometric series can be the simplest solution due to the presence of diagonal stiffness and mass matrices. However, when dealing with problems involving plates under arbitrary boundary conditions (excepts simply-supported) or problems involving generally orthotropic laminates, the use of trigonometric series is not recommended because of its complicated procedures. Therefore, polynomial series has come into existence and has been extensively used in computing the natural frequencies of plates owing to its straightforward algebraic manipulation. The use of this series is limited in the mid-1980s due to the difficulty in setting up the series to accommodate a variety of geometric boundary conditions. This issue can be solved by generating higher terms of the series on the basis of the starting polynomials specific to the boundary conditions, as

proposed by Bhat (1985). The Gram-Schmit process was used to produce orthogonal sets of polynomials. The outcomes revealed that the use of orthogonal polynomials led to better convergence. Lee and Kam adopted a set of Legendre's orthogonal polynomials to predict the natural frequencies of partially restrained thin laminated plates (Lee & Kam, 2006b), elastically restrained thin laminated plates (Lee & Kam, 2006a), and free-edged thick laminated Sandwich plates (Lee et al., 2007). The difference between the partially and elastically restrained boundary conditions was the inclusion of additional strain energy stored in the centre spring in the elastically restrained boundary condition. Compared to the partially restrained boundary condition, the laminated plate under elastically restrained boundary condition performed better in the aspect of accuracy. In the absence of centre support, only five measured natural frequencies were needed in the identification process for better accuracy. However, for elastically restrained laminated plates with the number of the unknown spring constants and elastic constants of the elastic supports larger than two, more than seven measured natural frequencies were required to determine the elastic properties. Furthermore, Rebillat and Boutillon (2011) adopted the use of basic orthogonal polynomials with reference to the article published by Bhat (1985) to estimate the resonant frequencies of a thick sandwich plate under free-free boundary condition. In the reference article (Bhat, 1985), the characteristic orthogonal polynomials were proven to be exceptionally useful for the study of lower modes of free-edged plates. As stated by Alobeid and Cooper (1995), the Rayleigh-Ritz approaches were in fact designated for the investigation of symmetric balanced and unbalanced cases. A more general shape function was introduced to curb some previously unsolved orthotropic composite plate boundary conditions, such as C-S-C-F, C-C-C-F, and C-F-C-F (C: Clamped, F: Free, S: Simply-supported). Instead of using the Ashton approach (Chow et al., 1992), a summation of polynomial products was adopted as it was comparatively simpler. When compared

with previous Rayleigh-Ritz approaches, improved convergence properties were obtained. Apart from using polynomial series, the use of the vibrating beam characteristic functions has also been widely utilised to obtain the natural frequencies of plate structures in the study of elastic properties identification (Lai & Ip, 1996; Lai & Lau, 1993; Muthurajan et al., 2004). The selection of the characteristic equations of a vibrating beam is normally made based on the boundary conditions of the plate to represent its assumed mode shapes. In the article written by Deobald and Gibson (1988), a complication was found, in which the computed natural frequencies using such method was not closely matched with the reference experimental natural frequencies when involving orthotropic rectangular plates under free-clamped boundary conditions. However, the percentage of discrepancy between the experimental and predicted resonant frequencies was found to be much smaller (at most around 5%) for lower modes when applying the aforementioned method on free-edged orthotropic rectangular plates (Lai & Lau, 1993). The similar method was then utilised to obtain the natural frequencies of thin specially orthotropic plates with free edges and the introduction of influence coefficients in the frequency expression was found to be effective in reducing the errors (Muthurajan et al., 2004). A major challenge of the Rayleigh-Ritz method consists in the selection of appropriate shape functions for specific problems. The use of appropriate shape functions is of great importance as the quality of the outcomes is substantially relying on it. Apart, due to the limited flexibility of the Rayleigh-Ritz method, which is subjected to boundary constraints, the finite element method has thus come into existence to circumvent the shortcomings.

2.4.1.3 Finite Element Method (FEM)

The FEM has gained its usage prevalence in the study of material identification in recent years on account of its great flexibility and robustness to various boundary conditions and geometrical shapes. Basically, finite element models are created in order

to obtain the numerical modal parameters using given elastic properties as inputs. Natural frequencies or/and mode shapes are computed from the model for subsequent application in the identification process, as it can be observed in several published articles (Auzins et al., 2015; Li et al., 2016; Petrone & Meruane, 2017; Saito et al., 2016). Plates of rectangular (Li et al., 2016; Petrone & Meruane, 2017; Saito et al., 2016) and square (Kong et al., 2014; Ručevskis, 2014) geometrical shapes have often been investigated. Besides, few studies have been conducted on plates of various geometrical shapes, as shown in (Pagnotta & Stigliano, 2008, 2009). In the aspect of boundary condition, plates with free-free edges (Hwang et al., 2010; Petrone & Meruane, 2017), simply-supported edges (Garshasbinia & Jam, 2005) and clamped edges (Borza, 2004; Kong et al., 2014) have prevalently been the topics of interest. Mostly, laminated plates are utilised in previous studies (Kovalovs & Rucevskis, 2011; Petrone & Meruane, 2017). The thickness of plate plays a cardinal role as well in deciding the use of appropriate plate theory in finite element modelling. Hence, the collection of previous studies can be classified into thin isotropic (Pagnotta & Stigliano, 2008, 2009), thin anisotropic (Fallstrom & Jonsson, 1991; Larsson, 1997), thin orthotropic (Fallstrom & Molin, 1987; Lauwagie et al., 2003), thin laminated plates (Kovalovs & Rucevskis, 2011; Petrone & Meruane, 2017) as well as thick anisotropic (Sol et al., 1997) and thick laminated plates (Cugnoni et al., 2007; Matter et al., 2009). Referring to thin laminated plates, the finite element model is usually constructed, based on the Love-Kirchhoff theory or Classical Lamination Plate (CLP) theory, while, for thick laminated plates, the Mindlin theory, First-order Shear deformation theory or higher-order theory are the commonly-used theories, where, the effects due to through-thickness shear deformation or/and rotary inertia are taken into account. Pagnotta and colleagues (Pagnotta & Stigliano, 2008, 2009) developed several two-dimensional and three-dimensional models of isotropic plates of various shapes, based on a theory

considering small deformations and linear elastic characteristic of the material. The plate model was assumed to be subjected to vibration in the absence of damping as well as made of homogeneous and isotropic material. Theoretically, its geometry and nominal size were supposed to be closely identical to the actual plate with a low degree of discrepancy and the difference between the evaluated and actual natural frequencies can be the relevant indicator. A discrepancy was discovered probably due to the inhomogeneity of the material as well as the low degree of resemblance between the dimensions of the model and those of the actual plate. In the research done by Garshasbinia and Jam (2005), the FEM was used to determine the natural frequencies of isotropic, orthotropic and anti-symmetric angle ply plates. Since only two elastic properties were needed in an isotropic problem, the equation of fundamental frequency was much simpler compared to orthotropic and anti-symmetric angle ply plates. Pertaining to the study of anti-symmetric angle ply plate, the properties of each layer were included in the governing equation. At least four resonant frequencies were required to accurately determine the two unknown elastic properties of isotropic plates, as stated by Pagnotta and Stigliano (2008). Sol (1986) constructed a finite element model of a medium thick anisotropic plate on the basis of Reissner-Mindlin theory for the identification of anisotropic plate rigidities. The presence of local material anisotropy was found to have influences on the numerical natural frequencies; hence, a single test was not advisable when dealing with inhomogeneous materials. Besides, in the study done by Lauwagie et al. (2003), Love-Kirchhoff theory was adopted in developing the finite element model of orthotropic plates, whereby, eight order polynomial Lagrange functions were used as the shape functions. The main drawback of this theory consists in the limitation in the thickness of a plate. Thus, an adapted Resonalyser procedure was used based on a more complex 3D finite element model in identifying the elastic properties of moderately-thick isotropic and orthotropic materials.

However, this procedure was not recommended when the homogeneity of the material was the subject of investigation. Later, they developed a novel method, based on an extension of the 'Resonalyser' procedure to identify the elastic properties of a plate with an arbitrary number of layers, each with respective elastic properties (Lauwagie et al., 2004). The classical lamination theory was used to surmount the problem of non-uniqueness. Single test vibration data was not sufficient for subsequent use in the identification process. Instead, several test plates vibration data were needed, depending on the number of layered materials to be identified. The more the layered materials were used, the more the plate configurations were required, and thus, the more the plate vibration data were needed. Maletta and Pagnotta (2004) proposed the use of an over-determined number of natural frequencies of an anisotropic plate to identify its elastic properties. Neither mode shapes, nor modal indices of particular modes were needed since frequencies were correlated simply by their number in a sequential order of magnitude. This method was said to be applicable to orthotropic and laminated plates. Later, Matter et al. (2007), Cugnoni et al. (2007), as well as Matter et al. (2009) developed finite element models, resembling multi-layered composite plates, based on a variable p -order shear deformation theory (PSDT). This generalised higher-order theory was adopted specifically for the study of inherent structure as well as thick or moderately thick multi-layered plates. The shape functions representing the through-thickness displacement were said to be flexible and thus, adaptable to accuracy and computation time requirements. As proven in the article written by Cugnoni et al. (2004), the simulations of thick multi-layered composite plate model with the order of three and above utilising PSDT were well-correlated with those of using third-order layer-wised plate theory, as well as the computational effort was much reduced. Araujo and co-workers (Araujo et al., 2006a; Araujo et al., 2006b) adopted the FEM to construct an active plate model with surface-bonded piezoelectric patches, based on a

displacement field using third order expansions in the thickness coordinate the in-plane displacements and a constant transverse displacement. This model allowed the analysis of arbitrary thin and thick plate and shell structures with more accurate results. Hwang and teammates (Hwang et al., 2010; Hwang et al., 2009) adopted the FEM to model laminated composite plates. The use of more resonant frequencies was recommended to improve accuracy. As of today, the use of the FEM is of great interest due to its prominent flexibility and robustness; however, from the viewpoint of accuracy as compared to an analytical method, such as the Fourier method, the FEM certainly comes second.

2.4.1.4 Fourier method

Referring to the study performed by Ismail and co-authors (Ismail et al., 2011, 2013), an accurate analytical forward method, which was constructed based on the Fourier series, was utilised to generate the natural frequencies of orthotropic plates under general elastic boundary conditions. Equation (2.8) describes the motion of an orthotropic plate, assuming that a harmonic excitation is given.

$$D_{11} \frac{\partial^4 W}{\partial x^4} + 4D_{16} \frac{\partial^4 W}{\partial x^3 \partial y} + 2(D_{12} + 2D_{66}) \frac{\partial^4 W}{\partial x^2 \partial y^2} + 4D_{26} \frac{\partial^4 W}{\partial x \partial y^2} + D_{22} \frac{\partial^4 W}{\partial y^4} - \rho h \omega^2 W(x, y) = q(\omega, x, y) \quad (2.8)$$

$$W(x, y) = \sum_{m=0}^{\infty} \sum_{n=0}^{\infty} A_{mn} \cos(\lambda_{am}x) \cos(\lambda_{bn}y) + \sum_{l=1}^4 \left(\xi_b^l(y) \sum_{m=0}^{\infty} c_m^l \cos(\lambda_{am}x) + \xi_a^l(x) \sum_{m=0}^{\infty} d_m^l \times \cos(\lambda_{bn}y) \right) \quad (2.9)$$

A relationship between the elastic constants, D_{ij} and the plate deflection displacement, $W(x, y)$ is established, in which the displacement deflection function is expressed in a more robust form of Fourier series expansion, as shown in equation (2.9). It is noted that for a thin orthotropic plate, $D_{11} = E_1 h^3 / 12 (1 - \nu_{12} \nu_{21})$, $D_{22} = E_2 h^3 / 12 (1 - \nu_{12} \nu_{21})$, $D_{12} = \nu_{12} D_{22}$, $D_{66} = G_{12} h^3 / 12$, $D_{16} = 0$, $D_{26} = 0$, in which, E_1 and E_2 are the elastic moduli, h is the plate thickness, ν_{12} and ν_{21} are the Poisson's ratios and G_{12} is the shear modulus. Basically, the displacement function was composed of a two-dimensional Fourier cosine series supplemented with a number of terms in the form of one-dimensional series. Direct evaluation of the series expansions for all the related derivatives was done via term-by-term differentiation of the displacement series and a classical solution was derived by allowing the series to exactly fulfil the governing differential equation and all the boundary conditions at every field and boundary point. Eventually, the modal parameters, including the natural frequencies were computed by resolving a standard matrix eigenvalue problem. The salient advantage of this approach consists in its solution exactness and accuracy, in which, the governing differential equation and the boundary conditions are satisfied entirely and exactly on a point-wise basis. This method is also applicable to plates under arbitrary boundary conditions, loading features, and/or load conditions. Extensive studies have been done applying the Fourier method on plate vibration analysis; however, as of today, the use of this method in material characterization is not common. Though, with its outstanding accuracy and versatility, the application of this Fourier method in the field of material identification can be promising.

2.4.2 Inverse method

An inverse method plays an important role in determining elastic properties of a material as the accuracy, repeatability, convergence and robustness of the identification method reflect its reliability. Inverse methods can be classified into two main categories,

namely, derivative-based methods and meta-heuristic optimisation methods. Bayesian estimation method, feasible directions method, Newton's method, and nonlinear least squares method (Levenberg- Marquardt method) are the examples of derivative-based methods, while, ant colony optimisation (ACO), genetic algorithm (GA), particle swarm optimisation (PSO) and response surface methodology (RSM) are the examples of meta-heuristic optimisation methods. In the current section, the aforementioned methods, which are commonly used in material identification or other related fields, are reviewed.

2.4.2.1 Derivative-based method

(a) Bayesian estimation method

In the Bayesian parameter estimation expression, weighting coefficients on the parameters and the responses are taken into consideration. The deviation between the initial model estimates and the experimental data is reduced by minimising a weighted error function. From the previous studies, the Bayesian estimation method was adopted by Lai and Ip (1996) to determine the material properties of unidirectional laminated composite plates under free-free boundary condition. An error function was defined by the discrepancy between the theoretical and experimental responses (natural frequencies) as well as the difference between the initial and updated parameters (estimated elastic constants), along with the presence of two weighting matrices. Sensitivity matrix, denoting the derivatives of the natural frequencies with respect to the four stiffnesses was evaluated as well for subsequent use in the identification process. Iteration process was initialised by assigning an initial guess of elastic constants and the process persisted until the updated elastic constants fell within 0.1% of the previous values. The complete procedures can be found in the aforementioned article. Generally, the number of iteration in Bayesian estimation would not exceed 10 and it is notable that the use of confidence on the initial estimates would, in fact, improve the

convergence. The comparison between the confidence matrices for the initial estimates and the updated parameters signifies the accuracy of the identified elastic properties. The results obtained using the Bayesian estimation method were found to be in good agreement with the results obtained from static testing. Hence, the use of the Bayesian estimation method involving modal data can be said to be one of the best alternatives of replacing static tests in material identification. Furthermore, Daghia et al. (2007) proposed a very different approach in determining the elastic constants of free-edged thick laminated plates within a Bayesian framework, applying two estimators, which were the Bayesian estimator (B) and the minimum variance estimator (MVE). Although the B estimator showed better performances in terms of efficiency and robustness, it was biased by the a priori information. As the deviation was reducing, the parameters were biased to remain close to the initial guesses. In contrast, the MVE estimator exhibited higher accuracy without any bias, but it was only sensitive to local minima and lower in convergence rate. The MVE estimator was then modified to improve its convergence rate by introducing a two-step procedure. From Table 2.1 (Daghia et al., 2007), the modified MVE estimator can be seen improving in convergence rate with outstanding accuracy. The Bayesian estimation method in parameter identification is quite common; however, the amount of research conducted using this method in material identification is quite limited, mainly due to its mediocre accuracy and rate of convergence. The accuracy of this method is often questionable as the selection of an a priori parameter is very subjective and the way of defining and selecting an a priori parameter requires skills and experiences.

Table 2.1: Final estimates and number of iterations performed for cross-ply laminate (Daghia et al., 2007)

	E_1 (GPa)	E_2 (GPa)	ν_{12}	G_{12} (GPa)	G_{13} (GPa)	G_{23} (GPa)	No. iter.
Initial	150	17	0.25	8	8	5	
Deviation	17.5	4	0.05	1.5	1.5	1.5	
B	120.1	13.69	0.2812	5.989	6.206	3.206	3
MVE	125	9.458	0.3058	6	5.996	3	39
MVE-modified							
Stage 1	124.9	9.449	0.3306	5.999	5.983	2.985	10
Stage 2	125	9.491	0.3013	6	5.999	3	13
Target	125	9.5	0.3	6	6	3	

(b) Feasible direction interior-point method

Feasible direction method has once been utilised in material identification since 1990's due to its simplicity in coding and efficiency, in which, penalty functions, active set strategies or quadratic programming sub-problems are not involved in the solutions (Araujo et al., 2006a; Araújo et al., 2002; Araujo et al., 2000; Araujo et al., 1996; Araujo et al., 2006b; Herskovits, 1998). It is very useful for problems with objective function or constraint functions that are not defined at infeasible points, for example, the identification of material properties of laminated composite plates with surface-bonded piezoelectric patches proposed by Araujo and collaborators (Araujo et al., 2006a; Araújo et al., 2002; Araujo et al., 2006b). As stated in the article by Araújo et al. (2002), simultaneous identification of elastic constants, piezoelectric and dielectric coefficients was impractical, thus, a separate evaluation of each category was required using the proposed method. This study also investigated the feasibility of the proposed method in determining elastic properties of multi-material laminated composite plates. In other studies (Araujo et al., 2006a; Araujo et al., 2006b), two different approaches were adopted and compared. The first method was the gradient-based technique, specifically, the use of Gauss-Newton algorithm (gradient-based) integrated with the feasible arc interior point algorithm (FAIPA) for unconstrained and constrained optimisations, respectively. The second method was the use of the meta-modeling method based on

artificial neural network (ANN) technique. Both approaches produced convincing results as the evaluated elastic properties were found to be reasonably accurate. However, in a close comparison, the error residuals of using FAIPA technique were found to be slightly lower as compared to those of using ANN technique. In the meantime, the convergence rate of FAIPA was discovered to be 1.2 to 2.4 times higher than that of ANN. Overall, FAIPA technique can be claimed to be the better technique.

(c) Newton method

Ismail et al. (2013) proposed the integrated use of the Newton-Raphson multivariate iterative method and the Fourier method to identify the elastic properties of orthotropic plates under general boundary conditions. Validations were done on plates under three different sets of boundary conditions, comprising combinations of free and clamped edges. The formulation of Newton-Raphson multivariate method started with the definition of a weighted error function, describing the square difference between experimental and predicted natural frequencies. The derivative of the error function with respect to the derivative of each parameter to be identified was expected to be zero. In the formulation, the sensitivity matrix denoting the derivative of the eigenvalues with respect to the derivative of the parameters to be identified was utilised as well. The effects of using four, five, six and seven natural frequencies with the definition of three different sets of weighting conditions were investigated. The weighting conditions were expressed in terms of error formulation, in which, absolute error ($w = 1$), absolute percentage error ($w = \frac{1}{\omega^2}$) and the error in between the formers ($w = \frac{1}{\omega}$) were defined. The results revealed that the root means squared (RSM) error of the identified elastic properties was found to be decreasing with respect to increasing number of natural frequencies. Besides, the use of the absolute error and the absolute percentage error in the formulation was found to have improved the identification results as well. As of today, the integrated use of the Newton method with the Fourier method to determine

elastic properties is considerably new and not popular since Newton method is a root-finding method, which is only useful for simple identification problems, but not very practical for complex material identification problems.

(d) Nonlinear least squares method (Levenberg-Marquardt method)

Cugnoni et al. (2007) utilised nonlinear least squares algorithm (Levenberg-Marquardt algorithm) to identify the elastic properties of multilayered laminated composite plates, based on a global error function, which was composed of the natural frequency error function, mode shape-related error functions as well as the nodal line error function. The error functions pertaining to mode shape can be expressed in terms of Modal Assurance Criteria (MAC) error function and in terms of mode shape error function. In fact, MAC error function can be further decomposed into two classical error norms, which are the diagonal and off-diagonal MAC error norms. Meanwhile, mode shape error function was defined by the sum difference between the numerical and experimental of mode shapes in absolute values. Considering the difficulty in obtaining accurate Poisson's ratio using conventional error function (natural frequencies only), information on the nodal lines of the mode shapes, which were sensitive to the Poisson's ratio, should be taken into account in the determination process. Hence, nodal line error function was developed via interpolation of the mode shapes into grey-shaded 2D images. Eventually, these five error functions were combined and weighted to form a general error function that would be minimised using Levenberg-Marquardt algorithm. The advantages of the proposed method were found in its prominent convergence rate as well as its great robustness. Only few iterations were needed in the determination of in-plane Young's and shear moduli with an uncertainty of 2 to 5%. Meanwhile, the transverse moduli of thin plates showed an uncertainty of about 10% and the deviation diminished as the thickness-to-span ratio of the plate increased. Later, Matter and teammates (Matter et al., 2007, 2009) further improved the method

developed by Cugnoni et al. (2007) to come out with a two-stage identification method. There were two ways of conducting the two-stage identification method, including the identification by parameter subset and the identification by progressive refinement. The identification by parameter subset was conducted by separating the evaluation of Poisson's ratio from the identification of the Young's and shear moduli, whereas, identification by progressive refinement was meant by determining the entire set of elastic properties via two consecutive steps from rough prediction to refined estimation. From the findings, this two-stage identification method showed positive identification results especially the Poisson's ratio and demonstrated excellent convergence rate as compared to the conventional one-step optimisation method.

2.4.2.2 Meta-heuristic optimisation method

(a) Ant Colony Optimisation (ACO)

Since decades ago, ACO has been actively used in dynamic applications, comprising scheduling problems, vehicle routing problems, assignment problems, and set problems on account of its directive search strategy and its ability to adapt to changes in real time. Yu and Xu (2010) proposed the use of continuous ACO (CnACO) to locate the structural damages as well as quantify the severity of damages of a frame. The objective function was defined by the discrepancy between the experimental and analytical natural frequencies and mode shapes. The proposed method was found to be effective and robust to various types of damages even in the presence of noise. Besides, Majumdar et al. (2012) utilised ACO to specifically locate and quantify structural damages on truss structures. It was proven that the use of first three natural frequencies was sufficient enough to locate the damage and the method was evident to be capable of handling noisy data. Daei and Mirmohammadi (2015) employed a modified continuous ACO to determine the location of structural damages and its severity, involving the use of flexibility matrix error function. In the study, the objective function was defined by

the discrepancy between the flexibility matrix of the reference and damaged structures, in which, the flexibility matrix of the damaged structure was actually composed of the natural frequencies and mode shapes of the damaged structure. The use of flexibility matrix in defining the objective function was said to be advantageous as only a few of the lower frequencies were needed in obtaining the flexibility matrix. Jalil et al. (2015) developed a modified version of ACO to construct a model representing a flexible plate structure. ACO with roulette wheel selection was proposed and the results revealed that the proposed ACO performed better, in terms of accuracy and convergence rate compared to the previous version of ACO. Koide et al. (2013) utilised ACO in identifying the optimal stacking sequence of laminated composite rectangular plates. There were four cases, in which, the optimal orientations of the piles were determined by (i) minimising the material cost, (ii) maximising the critical load factor, (iii) maximising the fundamental frequency of rectangular composite plates, and (iv) maximising the fundamental frequency of square composite plates with central hole. From the aforementioned articles, it is evident that the application of ACO in structural health monitoring is prevalent, probably, due to its excellent global search capability. Nevertheless, in the study of material identification, the use of ACO is not as overwhelming as that of in structural health monitoring, perhaps, due to its inferiority in convergence rate as compared to other meta-heuristic algorithms.

(b) Genetic Algorithm (GA)

Generally, GA is a useful tool for the evaluation of optimal solutions in scientific, technical and productions problems. It is a class of stochastic search algorithm owning the global search capability as well as requiring no initial estimation to initialise the optimisation process. Owing to its global search capability, GA has been widely employed in material identification. Similar to other meta-heuristic algorithms, the definition of an optimisation cost function is needed in GA. In the study of vibrational

method, the objective function is usually defined by the relative difference between the experimental and predicted natural frequencies as it can be found in several publications (Hwang et al., 2010; Lin & Chang, 2010; Pagnotta & Stigliano, 2009). Elastic properties of various types of plates have been studied using GA, including orthotropic plates (Maletta & Pagnotta, 2004; Silva et al., 2004) and laminated composite plates (Hwang et al., 2010; Lin & Chang, 2009, 2010). Rectangular plates under free (Hwang et al., 2010; Hwang et al., 2009; Lin & Chang, 2009) and simply-supported (Garshasbinia & Jam, 2005) boundary conditions are often the subjects of investigation. Referring to several relevant articles (Pagnotta & Stigliano, 2008, 2009; Silva et al., 2004), the use of basic GA is found prevalent among researchers on account of its simplicity. As stated in the research done by Maletta and Pagnotta (2004), the involvement of the mode shape and the modal indices in the objective function was not necessary as the simple correlation of frequencies by their number in a sequential order of magnitude was said to be sufficient. The apparent advantage of such function can be observed in reducing the effect due to large experimental errors that may be incurred at higher frequencies. The identification of four and five elastic constants was claimed to be adequate for the study of thin laminated plates and thick laminated plates, respectively. Instead of using a minimisation objective, a maximisation objective function was utilised in GA (Garshasbinia & Jam, 2005). The cost function was defined by the difference between unity and the absolute percentage error between the experimental and numerical natural frequencies. The elastic properties of the orthotropic and laminated plates were then evaluated via the use of GA. Furthermore, an inverse method involving simple GA was proven to be viable for the study of orthotropic and laminated rectangular plates with arbitrary thickness as well as free edges. In the investigation of laminated plates (Ragauskas & Belevičius, 2009; Silva et al., 2004), the deviation between the identified and reference Poisson's ratio was found to be relatively

large as compared to the other properties, due to the low sensitivity of natural frequencies with respect to the Poisson's ratio. In addition, the change in the through-thickness shear moduli was also discovered to be relatively low in variations of natural frequencies. Solutions to these issues can be undertaken by tailoring and determining the optimum plate geometric parameters, including, the plate side aspect ratio, orthotropy angles, and thickness so that the sensitivity of natural frequencies with respect to the through-thickness shear modulus as well as the Poisson's ratio can be enhanced. In this study, a two-step identification was performed. The first step was the identification of the plate geometric parameters as mentioned above, while the second step involved the ordinary material identification procedures adopting the optimised geometric parameters determined in the first step. GA was utilised in both of the steps. From the investigation, the use of plate geometric parameter optimisation procedure engaging genetic algorithm was proven to be necessary for achieving better identification results. On the other hand, four types of objective functions, as well as optimisation methods were investigated in elastic properties determination (Pagnotta & Stigliano, 2008, 2009). The efficiency of each objective function coupled with each type of optimisation method was investigated and compared in terms of the number of the FEM code runs. All the objective functions were applicable to GA and the results revealed that GA performed the best in terms of accuracy due to its global search ability; however, its convergence speed was the least convincing among them.

Furthermore, the use of hybrid GA with improved efficiency in material identification can be found in the previous publications (Hwang et al., 2010; Hwang et al., 2009; Lin & Chang, 2009, 2010). Referring to the work done by Hwang et al. (2010), a hybrid algorithm, known as, real-parameter GA(RGA) (Hwang & He, 2006) was adopted to determine the elastic properties of rectangular laminated composite plates under free-free boundary conditions. RGA was employed in the crossover and

mutation processes, as well as, simulated annealing was utilised in another mutation process. Adaptive mechanisms were introduced to tailor the probabilities of the crossover and mutation operators to enhance the hill-climbing ability in the search of the optimum solution. Only the first six measured natural frequencies were considered in the identification of the four elastic constants of a thin laminated plate due to the difficulty in acquiring a large number of experimental natural frequencies. In addition, natural frequencies of higher modes were negligible since only four elastic properties were the parameters of interest. Similarly, the estimation of the Poisson's ratio was found to be inconsistent, unlike the other elastic properties, which showed high repeatability. Despite, the deviation in the Poisson's ratio could be reduced if more resonant frequencies were taken into account in the computation. In the article presented by Hwang et al. (2009), the similar hybrid GA was utilised to evaluate the effective elastic properties of a rectangular woven composite plate and two rectangular printed circuit boards (PCBs) under free-free boundary condition. Distinctively, a two-step procedure was used in the determination process. The first step was performed by taking into account the first four measured frequencies, in which the first three were fixed and the fourth was free to match to identify the missing frequencies. After the identification of missing frequencies was done in the first step, the identification of the effective elastic properties of the plates was continued using more measured frequencies according to the mode sequence. Comparisons of the effective elastic properties obtained in the first step and second step were done. The second step yielded better results, showing improved objective function values, as well as improved repeatability in the Poisson's ratio. This can be explained by the inclusion of more frequencies in the objective function. At present, it can be seen that the use of GA in material identification is getting prevalent, primarily, because of its excellent global search ability and its great accuracy.

(c) Particle Swarm Optimisation (PSO)

PSO is one of the most prevalently-used meta-heuristic algorithms in wide-ranging applications due to its promising search quality and excellent rate of convergence. Leiderman and Castello (2016) proposed the integrated use of Quasi-Static-Approximation with PSO to solve a time-harmonic inverse scattering problem in quantifying the interfacial defects incurred at an interface between two elastic solid half-spaces. The proposed method was proven to be feasible in interfacial defect quantification as well as robust to noisy data. Liu et al. (2016) suggested the collaborative use of modified fuzzy C-Means (FCM) clustering algorithm with chaotic quantum particle swarm optimisation (CQPSO) for carbonate fluid identification. CQPSO algorithm was assigned to perform initialization and to produce globally optimum cluster centre with intention of evading premature convergence as well as local entrapment. The proposed approach was proven to be effective in determining fluid properties with total coincidence rate of fluid prediction approaching 97.10%. Xu and Gao (2016) introduced a hybrid approach integrating micromechanical modelling and backpropagation (BP) neural network to determine the thermal-elastic properties of composite materials. PSO was introduced into the proposed hybrid approach to evaluate the optimal multi-layered matrix thicknesses by minimising the coefficient of thermal expansion (CTE) of composites with the constraint of elastic modulus. Kutanaei and Choobbasti (2015) utilised PSO to study the combined effects of fibre and cement contents on the unconfined compression strength, modulus of elasticity, and axial strain at the peak strength of sand. The role of PSO was to approximate and build a polynomial model on the basis of experimental data and the constructed model was used to study the relationship between the cement content and the mechanical properties of sand as well as the relationship between the fibre content and the mechanical properties of sand. Similarly, Sun et al. (2015) adopted the use of PSO to determine the

temperature-dependent properties of a thermo-elastic structure, in which, PSO algorithm was designated to minimise a global objective function, which was defined by the errors of instantaneous frequencies and the sum of the highest order of the polynomials that were composed of the temperature-dependent properties. Referring to the reviews above, it can be observed that PSO is preferably adopted for collaborative application primarily because of its ease of implementation and high convergence rate.

(d) Response Surface Methodology (RSM)

Response surface methodology (RSM) is a collection of statistical and mathematical techniques beneficial for developing and optimising processes. Extensive studies have been done in identifying the elastic properties of laminated composite plates utilising the integration of the design of experiments and RSM (Bledzki et al., 1999; Hwang & Chang, 2000; Rikards et al., 2003; Rikards et al., 2001; Rikards et al., 1999). The use of RSM substantially improves the rate of convergence (approximately 50-100 times), thus, inciting the widespread usage of such method. In the study done by Bledzki et al. (1999), the elastic properties of laminated composite plates with two different fibre-surface treatments were studied, namely, the use of epoxy dispersion with aminosilane to enhance fibre/matrix adhesion (EP) and the use of polyethylene to eliminate fibre/matrix adhesion (PE). Apart from the drastic decrease in computational time, only one plate sample was needed to sufficiently determine the entire elastic constants by utilising the proposed RSM. The results revealed that EP composite possessed higher transverse stiffness owing to the excellent fibre/matrix adhesion. Moreover, as discussed by Rikards and teammates (Rikards et al., 2001; Rikards et al., 1999), the transverse shear modulus was discovered to be experiencing relatively large deviation in the study of thin plates due to insignificant transverse deformation. On the other hand, the transverse shear modulus of moderately thick plates was also found to be erroneous probably due to the use of RESINT program, which only considered the main terms of

the regression equation during approximation process. In comparison to the terms defining the in-plane elastic constants, the terms defining the transverse shear modulus were of the second order, thus, causing an error in transverse shear modulus. Although the use of RSM provides a substantial increase in convergence rate, its accuracy can still be further improved. As discussed in recent articles (Ghanmi et al., 2013; Sankar et al., 2014), hybrid RSM and particle swarm optimisation (PSO) method was developed and utilised in material identification of composite plates for better accuracy. As demonstrated in Table 2.2 (Sankar et al., 2014), hybrid RSM-PSO yielded the most accurate results with the smallest errors among the different methods, while the convergence rate was reasonably good but not as good as that of solely RSM with the largest error. In recent years, researchers can be seen to be devoting their efforts to investigating this method in material identification, mainly, because of its prominent rate of convergence and accuracy.

Table 2.2: System identification of orthotropic plate using hybrid RSM–PSO method in time domain with 5% noise (Sankar et al., 2014)

System parameters	Actual parameters	Predicted parameters			
		RSM	Improved PSO	Hybrid RSM–PSO	GA (No noise)
$E_1 (N/m^2)$	1.078×10^{11}	1.500×10^{11}	1.029×10^{11}	1.084×10^{11}	1.070×10^{11}
$E_2 (N/m^2)$	8.300×10^9	5.011×10^9	7.884×10^9	8.335×10^9	8.000×10^9
ν_{12}	0.421	0.45	0.38	0.41	0.325
$G_{12} (N/m^2)$	4.200×10^9	4.219×10^9	6.909×10^9	4.022×10^9	4.250×10^9
Avg. error (%)		21.52	21.1	2.25	7.09
Max. error (%)		39.62	64.51	4.23	22.8
CPU time (s)		18.7	3508.75	3530.38	–

(e) Hybrid algorithms involving GA, ACO and/or PSO

With regard to the reviews of hybrid algorithms that involves GA, ACO and/or PSO, Sheikhalishahi et al. (2013) developed a hybrid GA-PSO approach to tackle reliability redundancy allocation problem. In the proposed approach, GA was specifically used to perform the exploratory search, while PSO was particularly utilised to conduct the exploitative search. However, only selected individuals were passed through PSO

operator to reduce the computational time. Yu et al. (2015) adopted the use of the hybrid GA-PSO algorithm for process planning scheduling in a manufacturing system. In the suggested algorithm, GA was assigned for the traversal of beginning process plans, followed by the use of PSO in choosing the suitable machine for each process as well as figuring the initiation time of every process. Unlike the previous literature, PSO was applied to the entire populations. Ming and Ponnambalam (2008) employed an integrated GA-PSO algorithm for the concurrent design of cellular manufacturing system. The novelty of this research can be seen in the simultaneous application of GA and PSO in making cell formation (CF) and grouping layout (GL) decisions, in which, GA was assigned for CF and PSO was designated for GL. Apart from GA-PSO, Fidanova et al. (2014) suggested the use of hybrid GA-ACO algorithm to determine the parameters of a fermentation process. GA was initially used to search potential solutions in a coarse manner. Then, ACO was assigned to search for a better solution in a more precise manner utilising the information collected by GA. Furthermore, a GA-ACO-Local Search Hybrid algorithm was developed by Xu et al. (2006) to solve quadratic assignment problem. The probability of GA and ACO taking place was set equal (0.5) and local search was then used to further process the product of either GA or ACO to locally search for better solutions. Besides GA-ACO, Teo and Ponnambalam (2008) designed a combined ACO-PSO algorithm to tackle single row layout problem. In this hybrid algorithm, ACO was utilised initially to roughly search the feasible solutions, while PSO was then used to exploit the information garnered by ACO to search for better solutions at a more thorough pace. Gigras et al. (2015) adopted the use of a hybrid ACO-PSO algorithm for robotic path planning. The concept of pheromone intensity in ACO and the concept of velocity in PSO were utilised collaboratively to identify the shortest path to improve the convergence rate. Hybrid algorithms involving the integration of GA-PSO, GA-ACO, and ACO-PSO have been exhaustively

developed and applied in various fields since decades ago for their great advantages. In most cases, GA is used for diversification and the other is utilised for intensification. Meanwhile, for the hybridization between ACO and PSO, ACO is normally used for exploration and PSO is assigned for exploitation. Although extensive efforts have been devoted to developing hybrids involving two basic algorithms, the application of hybrids encompassing more than two basic algorithms in material identification is uncommon and thus, the collaboration between these three algorithms can be a potential approach.

2.4.3 Uncertainty

In real life applications, the presence of uncertainty is inevitable. Generally, uncertainty can be classified as aleatory and epistemic (Agarwal et al., 2004; Oberkampf et al., 2001). Aleatory uncertainty refers to the inherent randomness in the system, while epistemic uncertainty incurs because of the limited knowledge of the problem and its affecting factors. In the study of engineering structures, uncertainties can be treated as random variables and problems dealing with uncertainties can be referred to as stochastic problems. To solve such problems, probability approaches are the best solutions. The FEM is known to be a useful numerical method for solving wide-ranging problems. Nevertheless, its applicability in problems involving uncertainty is limited by its deterministic nature. Consequently, this drawback leads to the advent of the stochastic finite element method (SFEM). The SFEM has been prevalently used to study the reliability and analyse the robustness of uncertain structures (Xia et al., 2014). Notably, a number of variants of the SFEM have been developed, namely, Monte Carlo simulation (MCS) (Guoliang et al., 1993), perturbation method (Yong & Zhang, 1993) and the spectral stochastic finite element method (SSFEM) (Adhikari, 2011). Each method possesses a different strategy in dealing with the uncertainties. For further information, the details of these variants can be retrieved

from (Arregui-Mena et al., 2016). Numerous studies have been performed adopting such methods in investigating the effects of uncertainties on beam and/or plate structures. Wan et al. (2017) investigated the effects of the stiffener uncertainty on the vibration of plate structures. A beam-stiffened plate model is built for simulation purpose. The beam uncertainty incurs relatively little effect on the real part (amplitude) the beam mobility than that of the imaginary part (phase), given that the amount of beam uncertainty is within the allowable range. It can be deduced that the presence of uncertainties of stiffeners has little effect on the structure-borne-sound transmission between ribs and the panel foundations. Xu et al. (2016) performed a study of the stochastic free vibration characteristics of a functionally graded material (FGM) beam. From the findings, the means of the modal frequencies are substantially dependent on the slenderness ratio, whereas the scatterings of the frequencies are less affected by the slenderness ratio. The uncertainties of the constituent material properties (e.g. elastic modulus, Poisson's ratio, density) have significant influences on the scattering of the modal parameters than those of the constituent material distribution (volume fraction index). The means of mode shapes deviate substantially with slenderness ratios, while the scatterings of mode shapes are sensitive to the randomness in mass densities and demonstrate no significant changes with the randomness in slenderness ratio, elastic moduli and material distribution. Sepahvand (2017) adopted the generalised polynomial chaos (gPC) expansion to quantify the uncertainty in the damping and frequency response function of composite plate structures. The findings reveal that the effects of uncertainties at lower modes are insignificant and thus, negligible. Grover et al. (2017) adopted a robust stochastic finite element analysis technique on the basis of first-order perturbation technique (FOPT) to study the effects of parametric uncertainties on the response of laminated composite and sandwich plates. For the anti-symmetric cross-ply plates, A 10% uncertainty in the longitudinal elastic modulus was found affecting the

response by 5% for a moderately thick anti-symmetric cross-ply plate. Besides, the boundary condition has a considerable influence on the static response. A 10% uncertainty in the longitudinal elastic modulus incurs about 20% and 10% variations in the responses for thin and moderately thick sandwich plates, respectively. It is concluded that the response of the structure is dependent on the presence of material uncertainties and the quantitative response is also affected by the boundary conditions, lamination sequence and span-thickness ratio of the structure.

2.4.4 Summary

At present, impulse technique turns out to be the most widely-used experimental approach used in the research of material identification because of the ease of implementation, inexpensive procedures and wide-ranging applicability on various structures. Hence, in the present research, impulse technique is adopted in conducting experimental measurement. With regard to forward methods, the Finite Element Method (FEM) emerges as the primary choice for forward computation of modal parameters in material identification due to its great flexibility and robustness to any boundary conditions and geometrical shapes. Nevertheless, in the aspect of accuracy, the Fourier method is relatively better than the FEM. In the meantime, a great number of studies have been conducted using the Fourier method in vibration analysis; nevertheless, sources pertaining to the application of the Fourier method in material identification are limited. Therefore, in the current study, the Fourier method is employed as the forward method for its high stability, accuracy and robustness. From the viewpoint of derivative-based optimisation methods, a nonlinear least squares method has been widely used to deal with problems involving the combined use of error functions (natural frequencies, mode shapes, nodal lines, damping). As of today, the integrated use of different error functions is drawing many interests due to its remarkable effectiveness. Therefore, in the present investigation, a two-stage weighted

least square method is proposed, in which, stage 1 involves the use of natural frequency error function and stage 2 involves the use of mode shape error function. Referring to meta-heuristic optimisation methods, hybrid algorithms involving the integration of GA-PSO, GA-ACO, and ACO-PSO have been extensively developed and adopted into various applications due to their great effectiveness. It can be observed that developing hybrids involving two basic algorithms is no longer a new practice as well as in the meantime, hybrids adopting more than two basic algorithms can hardly be found in material identification. Therefore, in the present research, the application and collaboration of these three basic algorithms in material identification are investigated as it is believed that the weaknesses of respective algorithms can be minimised by the strengths of the other algorithms, thus, improving the overall performance. Natural frequency error function has been widely explored and applied in material identification. On the contrary, the use of FRF error function in material identification is scarce. From the viewpoint of accuracy, the use of FRF in material identification can be relatively better than that of the conventional natural frequency error function such that the experimental FRFs do not undergo processing procedures, thereby preserving the data credibility, unlike those of the experimental natural frequencies.

2.5 Mathematical theory

The mathematical theories of the selected forward method, namely, Fourier method and the relevant inverse methods, namely, derivative-based method and meta-heuristic optimisation methods are presented.

2.5.1 Forward method (Fourier method)

A forward method is used to evaluate the natural frequencies and modes shapes of the analytical model with inputs of elastic properties, as derived by Khov et al. (2009). Equation (2.10) describes the motion of a thin orthotropic plate without considering the

effects due to transverse shear deformation and rotary inertia. It is noted that for a thin orthotropic plate, $D_{11} = E_1 h^3 / 12 (1 - \nu_{12} \nu_{21})$, $D_{22} = E_2 h^3 / 12 (1 - \nu_{12} \nu_{21})$, $D_{12} = \nu_{12} D_{22}$, $D_{66} = G_{12} h^3 / 12$, $D_{16} = 0$, $D_{26} = 0$, in which, E_1 and E_2 are the elastic moduli, h is the plate thickness, ν_{12} and ν_{21} are the Poisson's ratios and G_{12} is the shear modulus. In the present study, the subscripts '1' and '2' of elastic constants can be directly referred to as 'x' and 'y', respectively, since the fibre-reinforced composite material is not the subject of interest. A relationship between the stiffness rigidities, D_{ij} and the plate's deflection displacement, $W(x, y)$ is established. The displacement function is defined in a more robust form of the Fourier series expansion with the inclusion of several supplemental terms to accommodate several sets of boundary conditions, as demonstrated in equation (2.11). A system equation can be derived by substituting equation (2.11) into equation (2.10), and rearranged into equation (2.12).

$$D_{11} \frac{\partial^4 W}{\partial x^4} + 4D_{16} \frac{\partial^4 W}{\partial x^3 \partial y} + 2(D_{12} + 2D_{66}) \frac{\partial^4 W}{\partial x^2 \partial y^2} + 4D_{26} \frac{\partial^4 W}{\partial x \partial y^2} + D_{22} \frac{\partial^4 W}{\partial y^4} - \rho h \omega^2 W(x, y) = q(\omega, x, y) \quad (2.10)$$

$$W(x, y) = \sum_{m=0}^{\infty} \sum_{n=0}^{\infty} A_{mn} \cos(\lambda_{am} x) \cos(\lambda_{bn} y) + \sum_{l=1}^4 (\xi_b^l(y) \sum_{m=0}^{\infty} c_m^l \cos(\lambda_{am} x) + \xi_a^l(x) \sum_{m=0}^{\infty} d_m^l \cos(\lambda_{bn} y)) \quad (2.11)$$

$$(D_{11} \lambda_{am}^4 + D_{22} \lambda_{bn}^4 + 2(D_{12} + 2D_{66}) \lambda_{am}^2 \lambda_{bn}^2) A_{mn} + \sum_{l=1}^4 (D_{11} \beta_n^l \lambda_{am}^4 - 2(D_{12} + 2D_{66}) \lambda_{am}^2 \bar{\beta}_n^l + D_{22} \bar{\beta}_n^l) c_m^l + \sum_{l=1}^4 (D_{11} \alpha_m^l \lambda_{bn}^4 - 2(D_{12} + 2D_{66}) \lambda_{bn}^2 \bar{\alpha}_m^l + D_{22} \bar{\alpha}_m^l) d_n^l - \rho h \omega^2 (A_{mn} + \sum_{l=1}^4 (\beta_n^l c_m^l + \alpha_m^l d_n^l)) = q_{mn} \quad (2.12)$$

In matrix form, it can be written as:

$$(\tilde{\mathbf{K}}\mathbf{A} + \mathbf{B}\mathbf{P}) - \rho h \omega^2 (\tilde{\mathbf{M}}\mathbf{A} + \mathbf{F}\mathbf{P}) = \mathbf{q} \quad (2.13)$$

The natural frequencies and mode shapes of an orthotropic plate can then be obtained from solving a standard matrix characteristic equation (2.14) with $\mathbf{q} = \mathbf{0}$, in which the eigenvector \mathbf{A} for a given eigenvalue contains the Fourier coefficients for the corresponding mode shapes. It is notable that in the FEM, the natural frequencies and mode shapes of a structure can be simply obtained by evaluating the eigenvalues and

eigenvectors, respectively. However, in the case of the Fourier method, the evaluated eigenvectors do not directly represent the identified mode shapes of a structure; instead, as mentioned before, these eigenvectors are defined as the Fourier coefficients that are used to evaluate mode shapes. Given the boundary conditions equations, $\mathbf{HP} = \mathbf{QA}$, as discussed by Khov et al. (2009), equation (2.13) can be written in the form of

$$(\mathbf{K} - \rho h \omega^2 \mathbf{M})\mathbf{A} = \mathbf{q} \quad (2.14)$$

where, the stiffness matrix, $\mathbf{K} = \tilde{\mathbf{K}} + \mathbf{BH}^{-1}\mathbf{Q}$ and the mass matrix, $\mathbf{M} = \tilde{\mathbf{M}} + \mathbf{FH}^{-1}\mathbf{Q}$. The detailed derivations of the forward method (Fourier method) in determining the dynamic parameters of a structure were presented in the article written by Khov et al. (2009).

Furthermore, the frequency response function (FRF) of the plate model can be generated using the following formula, involving the evaluated natural frequencies as well as mode shapes.

$$\alpha_{ij}(\omega) = -\omega^2 \sum_{r=1}^N \frac{\varphi_{ir}\varphi_{jr}}{\omega_r^2 - \omega^2 + 2i\omega\omega_r\xi_r} \quad (2.15)$$

where, α_{ij} is the FRF for input at position i and output at position j , ω denotes the angular frequency, φ_{ir} and φ_{jr} indicate the r^{th} mode shape at position i and j , ω_r is the r^{th} mode angular natural frequency and ξ_r is the r^{th} mode damping ratio.

2.5.2 Inverse method

An inverse method is used to update and determine the four typical elastic properties of plates under different sets of boundary conditions. Generally, inverse methods can be categorised into derivative-based methods and meta-heuristic optimisation methods. The theories of these methods are elaborated as follows:

2.5.2.1 Derivative-based method

Material identification begins with the definition of objective function. The aim is to determine elastic properties that constitute natural frequencies and mode shapes that are close to those benchmark natural frequencies and mode shapes. Hence, the objective function can be defined as the discrepancy between experimental and evaluated natural frequencies or mode shapes. In real life cases, the presence of uncertainty is inevitable, thus, regularization is needed to control the changes in elastic properties. Referring to the article written by (Mottershead et al., 2011), a weighted least squares method is used in constructing the non-destructive identification approach. The theories used in stage 1 and stage 2 as well as the formulations of termination criteria are presented as follows:

(a) *Stage 1: The use of natural frequencies*

In stage 1, the natural frequency error function is utilised, and the identification procedures are obtained from literature, with the inclusion of regularisation parameter to control the effects induced by experimental uncertainties (Mottershead et al., 2011). The overall objective function in stage 1 is defined as follows:

$$J = \boldsymbol{\epsilon}^T \mathbf{W}_\epsilon \boldsymbol{\epsilon} + \vartheta \Delta \mathbf{Pr}^T \mathbf{W}_x \Delta \mathbf{Pr} \quad (2.16)$$

where, $\boldsymbol{\epsilon}$ is the difference between the measured and evaluated eigenvalues, $\Delta \mathbf{Pr}$ is the change in flexural rigidities, \mathbf{W}_ϵ and \mathbf{W}_x are the weighting matrices that define the importance of $\boldsymbol{\epsilon}$ and $\Delta \mathbf{Pr}$, respectively, and ϑ is a scalar parameter that is known as the regularisation parameter that controls the influence of the first term (residual norm) and second term (stiffness change norm) of the objective function. This regularisation parameter ranges from 0 to 0.3, depending on the suitability of respective applications. By minimising the objective function J , the solution can be computed as follows:

$$\Delta \mathbf{Pr} = [\mathbf{S} \mathbf{W}_\epsilon \mathbf{S} + \vartheta \mathbf{W}_x]^{-1} \mathbf{S} \mathbf{W}_\epsilon \boldsymbol{\epsilon} \quad (2.17)$$

Let $\aleph_m = \rho h \omega_m^2 = \rho h (2\pi f_m)^2$ be the measured eigenvalue, and $\aleph_a = \rho h \omega_a^2 = \rho h (2\pi f_a)^2$ be the evaluated eigenvalue. Hence, the discrepancy between measured and evaluated eigenvalues is defined as follows:

$$\epsilon = [\aleph_m - \aleph_a] \quad (2.18)$$

where, ρ is the density, h is the thickness, f_m is the measured natural frequency, and f_a is the evaluated natural frequencies. The weighting matrices can be defined as follows:

$$\mathbf{W}_\epsilon = \left(\frac{1}{\text{diag}(\lambda_m)} \right)^2 \quad (2.19)$$

$$\mathbf{W}_x = \frac{\text{mean}(\gamma)}{\text{mean}(\gamma^{-1})} \gamma^{-1}, \gamma = \text{diag}[\mathbf{S}^T \mathbf{W}_\epsilon \mathbf{S}] \quad (2.20)$$

where, \mathbf{S} is the sensitivity matrix that defines derivative of evaluated eigen-frequencies with respect to stiffness rigidities. These derivatives are obtained through the differentiation of the undamped eigenvalue equation, as demonstrated in equation (2.21).

$$S_{ij} = \frac{\partial \lambda_{ia}}{\partial Pr_j} = A_{ia}^T \left(-\lambda_{ia} \frac{\partial M}{\partial Pr_j} + \frac{\partial K}{\partial Pr_j} \right) A_{ia} \quad (2.21)$$

$$\mathbf{S} = \begin{bmatrix} \frac{\partial \lambda_1}{\partial Pr_1} & \dots & \frac{\partial \lambda_1}{\partial Pr_N} \\ \vdots & \ddots & \vdots \\ \frac{\partial \lambda_M}{\partial Pr_1} & \dots & \frac{\partial \lambda_M}{\partial Pr_N} \end{bmatrix} \quad (2.22)$$

where, λ_{ia} is the evaluated eigen-frequency, A_{ia} is the corresponding eigenvector containing the Fourier coefficients, $\frac{\partial M}{\partial Pr_j}$ is the derivatives of mass matrix with respect to elastic properties and $\frac{\partial K}{\partial Pr_j}$ is the derivative of stiffness matrix with respect to elastic properties.

(b) Stage 2: The use of mode shapes

In stage 2, mode shape error function is used and the overall objective function in stage 2 is slightly different from that of in stage 1, as defined below.

$$\mathbf{J} = \boldsymbol{\epsilon}^T \mathbf{W}_\epsilon \boldsymbol{\epsilon} + \Delta \mathbf{Pr}^T \boldsymbol{\mu} \mathbf{W}_x \Delta \mathbf{Pr} \quad (2.23)$$

By minimising the objective function \mathbf{J} , the solution can be computed as follows:

$$\Delta \mathbf{Pr} = [\mathbf{S} \mathbf{W}_\epsilon \mathbf{S} + \boldsymbol{\mu} \mathbf{W}_x]^{-1} \mathbf{S} \mathbf{W}_\epsilon \boldsymbol{\epsilon} \quad (2.24)$$

In stage 2, mode shape error function is used and the difference between measured and evaluated mode shapes is written as follows.

$$\boldsymbol{\epsilon} = [\varphi_m - \varphi_a] \quad (2.25)$$

where, φ_m is the measured mode shapes and φ_a is the evaluated mode shapes, respectively, $\Delta \mathbf{Pr}$ is the change in stiffness rigidities, \mathbf{W}_ϵ and \mathbf{W}_x are the weighting matrices that define the importance of $\boldsymbol{\epsilon}$ and $\Delta \mathbf{Pr}$, respectively, and $\boldsymbol{\mu}$ in this case is the diagonal matrix of regularization parameters controlling the influence of the first term (residual norm) and second term (stiffness change norm) of the objective function. The difference between ϑ and $\boldsymbol{\mu}$ is that in stage 2, the regularization parameters for each stiffness rigidity can be selectively defined. Similarly, this regularization parameter ranges from 0 to 0.3, depending on the suitability of respective applications. The weighting matrices can be defined as follows:

$$\mathbf{W}_\epsilon = \left(\frac{1}{\text{diag}(\varphi_m)} \right)^2 \quad (2.26)$$

$$\mathbf{W}_x = \frac{\text{mean}(\gamma)}{\text{mean}(\gamma^{-1})} \gamma^{-1}, \gamma = \text{diag}[\mathbf{S}^T \mathbf{W}_\epsilon \mathbf{S}] \quad (2.27)$$

where, \mathbf{S} is the sensitivity matrix that defines derivative of evaluated mode shapes with respect to stiffness rigidities. The computation of these derivatives is relatively different from that of commonly-used finite element updating method. The derivations are elaborated as follows:

Equation (2.11) is reinstated as follows:

$$\begin{aligned} W(x, y) = & \sum_{m=0}^{\infty} \sum_{n=0}^{\infty} A_{mn} \cos(\lambda_{am}x) \cos(\lambda_{bn}y) + \\ & \sum_{l=1}^4 (\xi_b^l(y) \sum_{m=0}^{\infty} c_m^l \cos(\lambda_{am}x) + \xi_a^l(x) \sum_{m=0}^{\infty} d_m^l \cos(\lambda_{bn}y)) \end{aligned} \quad (2.11)$$

The mode shape of a plate at a particular mode can be obtained from equation (2.11) by inserting the corresponding evaluated eigenvectors and supplemental terms into the equation. The number of nodes can be defined arbitrarily by defining the coordinates (x , y). Given that mode shapes are obtained from equation (2.11), the derivatives of mode shapes can as well be obtained through the differentiation of equation (2.11), as demonstrated below.

$$\begin{aligned} \frac{\partial W(x, y)}{\partial Pr_j} = & \sum_{m=0}^{\infty} \sum_{n=0}^{\infty} \left(A_{mn} \frac{\partial (\cos(\lambda_{am}x) \cos(\lambda_{bn}y))}{\partial Pr_j} \right. \\ & \left. + \frac{\partial A_{mn}}{\partial Pr_j} (\cos(\lambda_{am}x) \cos(\lambda_{bn}y)) \right) \\ & + \sum_{l=1}^4 \left(\zeta_b^l(y) \sum_{m=0}^{\infty} \left(c_m^l \frac{\partial \cos(\lambda_{am}x)}{\partial Pr_j} + \frac{\partial c_m^l}{\partial Pr_j} \cos(\lambda_{am}x) \right) \right. \\ & \left. + \zeta_a^l(x) \sum_{m=0}^{\infty} \left(d_m^l \frac{\partial \cos(\lambda_{bn}y)}{\partial Pr_j} + \frac{\partial d_m^l}{\partial Pr_j} \cos(\lambda_{bn}y) \right) \right) \end{aligned} \quad (2.28)$$

$$\begin{aligned} \frac{\partial W(x, y)}{\partial Pr_j} = & \sum_{m=0}^{\infty} \sum_{n=0}^{\infty} \left(0 + \frac{\partial A_{mn}}{\partial Pr_j} (\cos(\lambda_{am}x) \cos(\lambda_{bn}y)) \right) \\ & + \sum_{l=1}^4 \left(\zeta_b^l(y) \sum_{m=0}^{\infty} \left(0 + \frac{\partial c_m^l}{\partial Pr_j} \cos(\lambda_{am}x) \right) \right. \\ & \left. + \zeta_a^l(x) \sum_{m=0}^{\infty} \left(0 + \frac{\partial d_m^l}{\partial Pr_j} \cos(\lambda_{bn}y) \right) \right) \end{aligned} \quad (2.29)$$

$$\begin{aligned} \frac{\partial W(x, y)}{\partial Pr_j} = & \sum_{m=0}^{\infty} \sum_{n=0}^{\infty} \left(\frac{\partial A_{mn}}{\partial Pr_j} (\cos(\lambda_{am}x) \cos(\lambda_{bn}y)) \right) \\ & + \sum_{l=1}^4 \left(\zeta_b^l(y) \sum_{m=0}^{\infty} \left(\frac{\partial c_m^l}{\partial Pr_j} \cos(\lambda_{am}x) \right) \right. \\ & \left. + \zeta_a^l(x) \sum_{m=0}^{\infty} \left(\frac{\partial d_m^l}{\partial Pr_j} \cos(\lambda_{bn}y) \right) \right) \end{aligned} \quad (2.30)$$

The derivatives of eigenvectors can be easily obtained using the method suggested by Fox and Kapoor (1968). The derivations are presented as follows:

$$\frac{\delta A_i}{\delta Pr_j} = \sum_{k=1}^N a_k^i A_k, A_i = [A_{00}, A_{10}, \dots, A_{mn}]^T, i = 1, 2, \dots, M \quad (2.31)$$

$$\text{if } i = k, a_k^i = -\frac{1}{2} A_i^T \frac{\delta M}{\delta Pr_j} A_i \quad (2.32)$$

$$\text{if } i \neq k, a_k^i = \frac{A_i^T \frac{\delta K}{\delta Pr_j} A_i - \lambda_i A_i^T \frac{\delta M}{\delta Pr_j} A_i}{\lambda_i - \lambda_k} \quad (2.33)$$

where, A_i denote i^{th} eigenvector, x_j indicates j^{th} parameter, and λ_i represents i^{th} eigenvalue. Meanwhile, it is found that the derivatives of stiffness matrix and the mass matrix are involved in the formulations of the eigenvectors derivatives, as shown in equations (2.31-2.33). Therefore, according to the forward formulations of stiffness matrix and mass matrix which define $\mathbf{K} = \tilde{\mathbf{K}} + \mathbf{B}\mathbf{H}^{-1}\mathbf{Q}$ and $\mathbf{M} = \tilde{\mathbf{M}} + \mathbf{F}\mathbf{H}^{-1}\mathbf{Q}$, respectively, the derivatives of both \mathbf{K} and \mathbf{M} can be obtained as follows:

$$\frac{\partial \mathbf{K}}{\partial Pr_j} = \frac{\partial \tilde{\mathbf{K}}}{\partial Pr_j} + \frac{\partial \mathbf{B}}{\partial Pr_j} \mathbf{H}^{-1} \mathbf{Q} + \mathbf{B} \frac{\partial \mathbf{H}^{-1}}{\partial Pr_j} \mathbf{Q} + \mathbf{B} \mathbf{H}^{-1} \frac{\partial \mathbf{Q}}{\partial Pr_j} \quad (2.34)$$

$$\frac{\partial \mathbf{M}}{\partial Pr_j} = \frac{\partial \tilde{\mathbf{M}}}{\partial Pr_j} + \frac{\partial \mathbf{F}}{\partial Pr_j} \mathbf{H}^{-1} \mathbf{Q} + \mathbf{F} \frac{\partial \mathbf{H}^{-1}}{\partial Pr_j} \mathbf{Q} + \mathbf{F} \mathbf{H}^{-1} \frac{\partial \mathbf{Q}}{\partial Pr_j} \quad (2.35)$$

In both Equations (2.34-2.35),

$$\frac{\partial \tilde{\mathbf{M}}}{\partial Pr_j} = 0 \quad (2.36)$$

$$\frac{\partial \mathbf{F}}{\partial Pr_j} = 0 \quad (2.37)$$

With the use of $\mathbf{H}^{-1}\mathbf{H} = \mathbf{I}$, we can obtain the following equation:

$$\frac{\partial \mathbf{H}^{-1}}{\partial Pr_j} = -\mathbf{H}^{-1} \frac{\partial \mathbf{H}}{\partial Pr_j} \mathbf{H}^{-1} \quad (2.38)$$

Furthermore, the derivatives of supplemental terms $\frac{\partial c_m^l}{\partial Pr_j}$ and $\frac{\partial d_n^l}{\partial Pr_j}$ can be obtained from the following derivations.

$$\mathbf{HP} = \mathbf{QA} \quad (2.39)$$

$$\mathbf{P} = \mathbf{H}^{-1}\mathbf{QA} \quad (2.40)$$

$$\frac{\partial \mathbf{P}}{\partial Pr_j} = \frac{\partial \mathbf{H}^{-1}}{\partial Pr_j} \mathbf{QA} + \mathbf{H}^{-1} \frac{\partial \mathbf{Q}}{\partial Pr_j} \mathbf{A} + \mathbf{H}^{-1} \mathbf{Q} \frac{\partial \mathbf{A}}{\partial Pr_j} \quad (2.41)$$

where, $\mathbf{P} = [c_0^1, c_1^1, \dots, c_m^l, d_0^1, d_1^1, \dots, d_n^l]$, $\mathbf{A} = [A_1, \dots, A_M]$, and \mathbf{H} and \mathbf{Q} are the coefficient matrices. For further understanding, the detailed explanation of these terms

can be found in the article written by Khov et al. (2009). It is notable that in the FEM, the natural frequencies and mode shapes of a structure can be simply obtained by evaluating the eigenvalues and eigenvectors, respectively. However, in the case of the Fourier method, the evaluated eigenvectors do not directly represent the identified mode shapes of a structure; instead, these eigenvectors represent double Fourier series coefficients, A_{mn} , that are used to compute mode shapes. Discernible differences can be found in the derivations of the proposed inverse method and the existing FEM-based inverse methods that are more straightforward.

(c) **Termination criteria**

In the present study, three termination criteria are defined, namely, the maximum number of iterations, the minimum improvement percentage and the minimum value of convergence. The updating process is terminated when either of the criteria is met. In this research, the value of convergence is referred to as correlation coefficients, which can be defined by the errors of the selected modal parameters. In stage 1, the value of convergence is defined by the weighted absolute relative difference (*CCABS*) between the evaluated and reference natural frequencies, as demonstrated in equation (2.42).

$$CCABS = \frac{1}{N} \sum_{i=1}^N C_{R_i} \frac{|f_{m_i} - f_{a_i}|}{f_{m_i}} \quad (2.42)$$

where, f_{m_i} and f_{a_i} are the measured and evaluated natural frequencies of mode i and C_{R_i} is the weighting factor. Meanwhile, in stage 2, the value of convergence (*CCMDISP*) is defined by the absolute relative difference between the measured and evaluated modal displacements, as described in equation (2.43).

$$CCMDISP = \frac{1}{N \cdot M} \sum_{i=1}^N \sum_{j=1}^M \frac{|\varphi_{m_{ij}} - \varphi_{a_{ij}}|}{\varphi_{m_{ij}}} \quad (2.43)$$

where, $\varphi_{m_{ij}}$ and $\varphi_{a_{ij}}$ are the measured and evaluated modal displacement of node j of mode i .

2.5.2.2 Meta-heuristic optimisation method

In the current section, the fundamental theories of genetic algorithm (GA), ant colony optimisation (ACO) and particle swarm optimisation (PSO) are presented. These theories are involved in the composition of the proposed meta-heuristic hybrid optimisation method, which is known as, hybrid GA-ACO-PSO. The mechanisms of the proposed method are thoroughly explicated in conjunction with relevant equations and formulas. Lastly, different types of objective functions used in the research are defined and presented.

(a) Genetic Algorithm (GA)

GA was first developed by Holland (1992) and since then, its potential advantages favour its widespread application in multiples fields. The basic idea of GA was inspired by the principle of genetic evolution in living organisms. Selection, crossover, mutation and elitism are the basic operators in genetic algorithms. An objective function is used to evaluate the fitness of each individual and the selection of individuals for further evolution or/and reproduction is made based on the fitness survival theory introduced by Darwin (1869). Crossover of genetic codes between pairs of chromosomes promotes local exploitation within a promising region while mutation of genetic codes in each chromosome encourages global exploration within a designated search area.

(b) Ant Colony Optimisation (ACO)

ACO was first invented by Dorigo and Caro (1999), emulating the foraging behaviour of real ants, in which they manage to build the shortest path between their settlement and the feeding source. Pheromone trails are used as a communication tool to construct the paths. A higher intensity of accumulated pheromones indicates a higher

possibility of prioritising the path as the preferred one, and finally, generating the shortest solution path. The pheromone, τ_{ij} on the edge connecting cities i and j after iteration t is updated using equation as follows:

$$\tau_{ij}(t+1) = (1 - ev) \cdot \tau_{ij} + \sum_{k=1}^m \Delta\tau_{ij}^k \quad (2.44)$$

$$\Delta\tau_{ij}^k = \begin{cases} Q/L_k & \text{if ant } k \text{ uses edge } (i,j) \text{ in its tour,} \\ 0 & \text{otherwise,} \end{cases} \quad (2.45)$$

where, ev denotes the evaporation rate between iteration t and $t+1$, m represents the number of ants, Q is a constant, and L_k defines the length of tour built by k^{th} ant. The possibility of an ant k heading from city i to city j depends on the amount of accumulated pheromones, and hence, the probability function constituting the amount of pheromone is expressed as follows:

$$p_{ij}^k = \begin{cases} \frac{\tau_{ij}^\alpha \cdot \eta_{ij}^\beta}{\sum_{c_{il_{ant}} \in N(s^p)} \tau_{il_{ant}}^\alpha \cdot \eta_{il_{ant}}^\beta} & \text{if } c_{ij} \in N(s^p), \\ 0 & \text{otherwise,} \end{cases} \quad (2.46)$$

where, $N(s^p)$ is the set of cities available for k^{th} ant, l_{ant} denotes an unvisited city by k^{th} ant, α and β represent the relative significance of the trail over the path information, $\eta_{ij} = 1/d_{ij}$ with d_{ij} denoting the distance between cities i and j .

(c) **Particle Swarm Optimisation (PSO)**

PSO was first constructed by Kennedy and Eberhart (1995), mimicking the social character of animals, such as a flock of birds, a school of fish and a swarm of bees to solve optimisation problems. Unlike GA, PSO utilises the information of local and global best positions of particles to solve optimisation problems. The formulations of PSO are defined as follows:

$$\vec{v}_{k+1} = \vec{a} \otimes \vec{v}_k + \vec{b}_1 \otimes \vec{r}_1 \otimes (\vec{p}_1 - \vec{x}_k) + \vec{b}_2 \otimes \vec{r}_2 \otimes (\vec{p}_2 - \vec{x}_k) \quad (2.47)$$

$$\vec{x}_{k+1} = \vec{c} \otimes \vec{x}_k + \vec{d} \otimes \vec{v}_{k+1} \quad (2.48)$$

where, \vec{v}_{k+1} is the updated velocity, \otimes indicates element-by-element vector multiplication, k is the number of iteration, \vec{v}_k is the previous velocity, \vec{a} is the momentum factor, \vec{r}_1 and \vec{r}_2 are random numbers within the range from 0 to 1, \vec{p}_1 is the previous best position, \vec{p}_2 is the globally best position in the whole neighbourhood, \vec{b}_1 and \vec{b}_2 are the strength of attraction, \vec{x}_{k+1} is the updated position, \vec{x}_k is the previous position, \vec{c} and \vec{d} are the coefficients (normally unity). The assignment of input variables in the equations above decides the exploration and exploitation processes, depending on types of problems.

(d) Meta-heuristic optimisation method (Hybrid GA-ACO-PSO)

The primary intention of combining GA, ACO, and PSO is to minimise each other weaknesses and in the meantime, to promote respective strengths and therefore, transforming into a better hybrid algorithm. It should be highlighted that instead of eliminating the random initialization of GA, the effect of random initialization is subdued by passing the products of GA through ACO and PSO operators. In the composition of the proposed algorithm, ACO is assigned for exploratory search, while PSO is designated for exploitative search. The products of GA are further processed by ACO and PSO to well distribute and organize the search coverage and thus, neutralize the biased effect of random initialization. Consequently, this enhances the searching process. The collaboration between GA and ACO enhances exploratory search such that ACO evades repeated tours from occurring and the presence of pheromone trails probability function makes the search to be more directive and organized. Meanwhile, the integration between GA and PSO improves exploitative search, in which, PSO is assigned to solely focus on exploitative search. In return, with the introduction of different operators and new features, GA enhances the convergence rate and subdues

the substantial dependency on the array of pheromones in ACO, as well as further boosts the exploitative search in PSO. Two types of mutation operators, namely, two-point standard mutation and refined mutation are suggested in this algorithm. In early iterations, standard mutation is utilised collaboratively with the concept of the unrepeated tour in ACO to evade local entrapment, while refined mutation is used in later iterations to supplement the PSO exploitative search. Two main features, namely, fixed refined mutation and logarithmically-spaced refined mutation are introduced in the refined mutation. The details of the features, as well as the flow of the proposed meta-heuristic hybrid GA-ACO-PSO, are described as follows:

(i) *Step 1: Initialization*

The number of generations, number of populations and number of dimensions (design variables) are specified accordingly. Before running the algorithm, input variables for ACO (such as pheromone initial intensity, number of paths, constant value) and input variables for PSO (such as momentum factor, strength of attraction) are specified appropriately. The lower and upper boundaries of each design variable are predefined. Once the assignment of inputs is done, the algorithm is set to run. The algorithm begins with the random generation of two populations, namely, the ant population and the particle population. It is noted that the number of ant population is equal to the number of particle population. These randomly-generated solutions are then used to initialise the GA operators. Fitness value of each set of the vector is then evaluated.

(ii) *Step 2: Selection, crossover, mutation, elitism*

Selection is made based on the fitness values, depending on the types of problems (minimisation). Vectors possessing better fitness values stand a higher possibility of getting selected for the crossover operation. Selected vectors of ACO and PSO are then

carried on to the one-point inter-crossover operation. Subsequently, the mutation operation is conducted, followed by the fitness evaluation. Two different types of mutation operators, namely, two-point standard mutation and refined mutation are proposed. In early iterations, standard mutation is used for exploratory search. The concept of the unvisited route in ACO is adopted to avoid the repetition of tours, and thus, might improve the convergence rate. Meanwhile, in later iterations when there is no unvisited route in the list or when the iteration exceeds half of its assigned value, the standard mutation is replaced by the refined mutation. The reason of introducing the refined mutation is to further improve the exploitative search, which is mainly contributed by PSO. Before proceeding to variable updating, elitism is performed on the list of vectors containing vectors of before and after evolution processes with the best individual remained at the top of the list and the worst at the bottom. The number of elite individuals that are remained for the next iteration corresponds to the predefined number of populations. In the proposed algorithm, the odd-numbered elite individuals obtained from the list with promising fitness values are eventually treated as the new populations of ACO. Comparison of the fitness level between the new population and the previous population is made before undergoing evolution processes to promote exploration in the coming iteration. Solutions from the previous population will be replaced with the solutions from the new population if their fitness levels are relatively inferior to those from the new population. Meanwhile, for the case of PSO, the even-numbered elite individuals retrieved from the list of elitism are used to update the particles best and global best positions, hence, initiating the algorithm in the next iteration. Notably, the initial velocity vectors are set equal to zero and these vectors are involved in the computation starting from the second iteration after the replacement of the PSO-evaluated solutions by the elite individuals. Subsequently, before the next iteration takes place, the velocity vectors are updated with values obtained from the

subtraction between the evaluated and elite solutions to retain the exactness of the velocity vectors.

(1) *Crossover*

The equations of crossover in the proposed algorithm are defined as follows:

$$\vec{x}_{cross1} = [(rand1 \times \vec{x}_1(1:co)) + ((1 - rand1) \times \vec{x}_2(1:co)), (rand1 \times \vec{x}_2(co + 1:end)) + ((1 - rand1) \times \vec{x}_1(co + 1:end))] \quad (2.49)$$

$$\vec{x}_{cross2} = [(rand2 \times \vec{x}_2(1:co)) + ((1 - rand2) \times \vec{x}_1(1:co)), (rand2 \times \vec{x}_1(co + 1:end)) + ((1 - rand2) \times \vec{x}_2(co + 1:end))] \quad (2.50)$$

where \vec{x}_{cross1} and \vec{x}_{cross2} are the vectors after undergoing crossover process, $rand1$ and $rand2$ are random numbers ranging from 0 to 1, \vec{x}_1 and \vec{x}_2 denote the pair of vectors from ACO and PSO, and co indicates the crossover point.

(2) *Mutation*

Standard mutation

The equations of two-point standard mutation are expressed as follows:

$$x_{1new} = LB_1 + \alpha \times (UB_1 - LB_1) \quad (2.51)$$

$$x_{2new} = LB_2 + \beta \times (UB_2 - LB_2) \quad (2.52)$$

$$\alpha = (x_1 - LB_1)/(UB_1 - LB_1) \quad (2.53)$$

$$\beta = (x_2 - LB_2)/(UB_2 - LB_2) \quad (2.54)$$

where, x_{1new} and x_{2new} are the two mutated variables randomly selected from a vector \vec{x} , LB and UB are the predefined lower and upper boundaries of the variables, and x_1 and x_2 are the two variables before undergoing mutation process. In order to avoid any repeated tours in standard mutation, all the possible routes are constructed based on the permutation of different path number for each design variable. The route for each of the mutated design variables is determined and the visited routes are deleted from the list.

The repeated route is replaced with another random pick of route from the list of the unvisited routes.

Refined mutation

In the present research, two refined mutation features, namely, fixed refined mutation and logarithmically-spaced refined mutation are proposed. The general concept of refined mutation is defined as follows:

$$percent = aa + rand \times (bb - aa) \quad (2.55)$$

$$lb = x \times (1 - percent) \quad (2.56)$$

$$ub = x \times (1 + percent) \quad (2.57)$$

$$x_{new} = lb + rand \times (ub - lb) \quad (2.58)$$

where, aa and bb represent the lower and upper boundaries of percentage that need to be specified, $percent$ indicates the randomly picked percentage within the specified range, x is one of the variables randomly selected from the best solution vector, lb and ub denote the lower and upper boundaries of variable, x and x_{new} is the mutated variable. The concept of refined mutation is depicted in Figure 2.7, in which, x_2 has been picked for refined mutation. Notably, the lower boundary or/and upper boundary in refined mutation are set equal to the predefined boundaries in case that the predefined values are exceeded. The difference between the fixed refined mutation and logarithmically-spaced refined mutation consists in the assignment of aa and bb . For fixed refined mutation, these parameters are fixed throughout the entire iterations, while, for logarithmically-spaced refined mutation, these parameters are defined in a descending logarithmical manner over iterations.

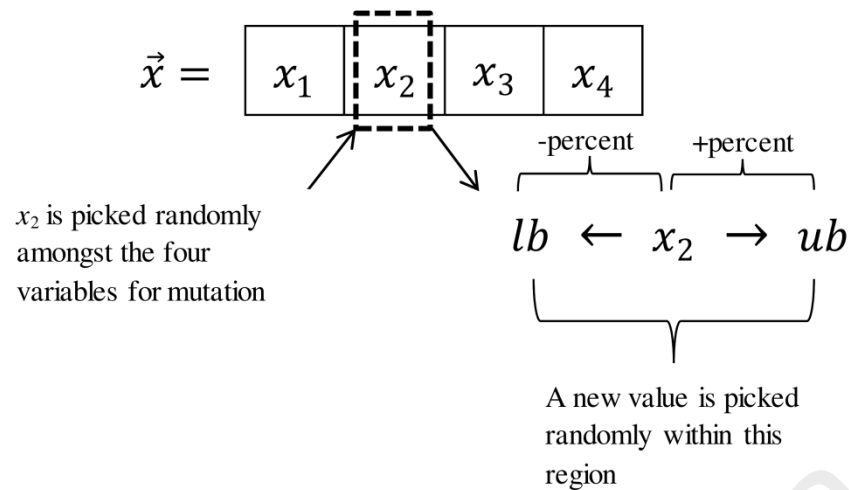


Figure 2.7: Concept of refined mutation

(iii) **Step 3: Variable updating**

The intensity of pheromone in ACO is updated using Equations (2.44-2.45), while for PSO, the velocities of particles are assigned randomly, as well as the local and best positions of the particle are determined and inserted into Equations (2.47-2.48) to initiate the algorithm in the second iteration.

(iv) **Step 4: Solution construction**

In the next iteration of ACO, the solutions are constructed by using equation (2.59) and (2.60) as shown below. The concept of combined discrete and continuous probability distribution scheme is demonstrated in Figure 2.8, as shown below. LB and UB are the lower and upper boundaries of the designated search areas for each design variable, x_i . The predefined search range of the design variables is divided equally by the predefined discrete total number of paths. Random pick of each design variable is then made within the region of respective selected paths. In details, the concept begins with a probabilistic pick of a discrete path by each ant for each design variable, in which, the path number is discrete. It is noted that each path is bounded by respective boundaries and each path is selected probabilistically based on the intensity of pheromones. As seen from Figure 2.8, ant 1 selects paths [2, 3, 4, 5] for variables $[x_1, x_2, x_3, x_4]$, respectively. Once a discrete path is selected by an ant for each design

variable, a random pick of each design variable is done within the boundaries of the selected discrete path, in which, each of the design variable is continuous. The ‘circles’ denote the ants or solutions with respective routes.

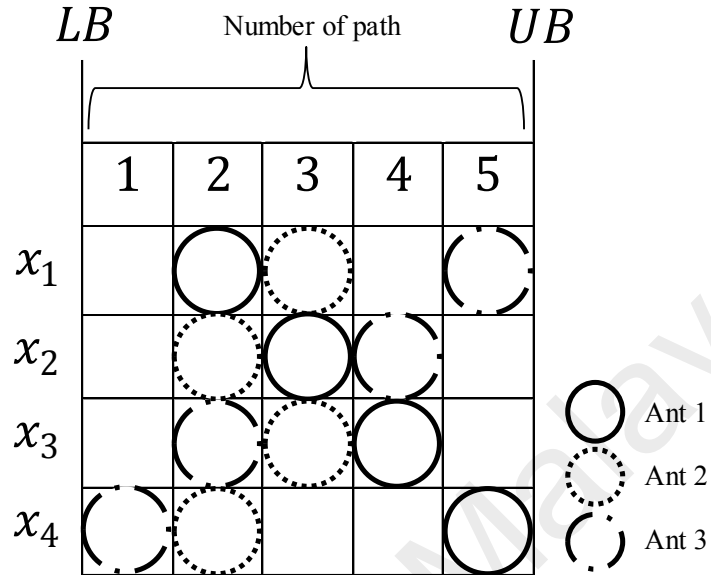


Figure 2.8: Concept of combined discrete and continuous probability distribution scheme

Instead of using equation (2.46) as mentioned above, solutions are probabilistically constructed based on the following probability equation (2.59):

$$p_{ij}^k = \frac{\tau_{ij}}{\sum_{j=1}^n \tau_{ij}} \quad (2.59)$$

where, τ_{ij} is the pheromone intensity for i^{th} design variable at j^{th} path. At initial stage, the values of pheromone intensity for each path are set equal to unity and thus, the probability of selecting either path is the same for the first iteration. The discrete path number is picked based on equation (2.59) and the solution is randomly picked within a continuous range of a path number using equation (2.60) as shown below. It is noted that the use of this probability scheme is to mainly assist the exploration search in GA.

$$x_i^k = \frac{(path_{number} + rand - 1) \times (UB_i - LB_i)}{Number\ of\ paths} + LB_i \quad (2.60)$$

where, x_i^k is the i^{th} design variable of k^{th} ant, $path_{number}$ is the path number that is picked based on the probability of pheromone accumulation (initially, all the probability

are set equal to unity) , *rand* denotes the random number ranges from 0 to 1, UB_i and LB_i are upper and lower boundaries of i^{th} design variable, and *Number of paths* indicates the predefined total number of paths. Meanwhile, in PSO, the previous velocities and the previous solution vectors are updated using equation (2.47-2.48), thus, constituting new velocities and solution vectors in the next iteration. The proposed hybrid algorithm continues operating until the maximum number of generation is achieved. For repeatability investigation, five independent runs are initiated. The complete course of the proposed hybrid algorithm is presented in Figure 2.9.

University of Malaya

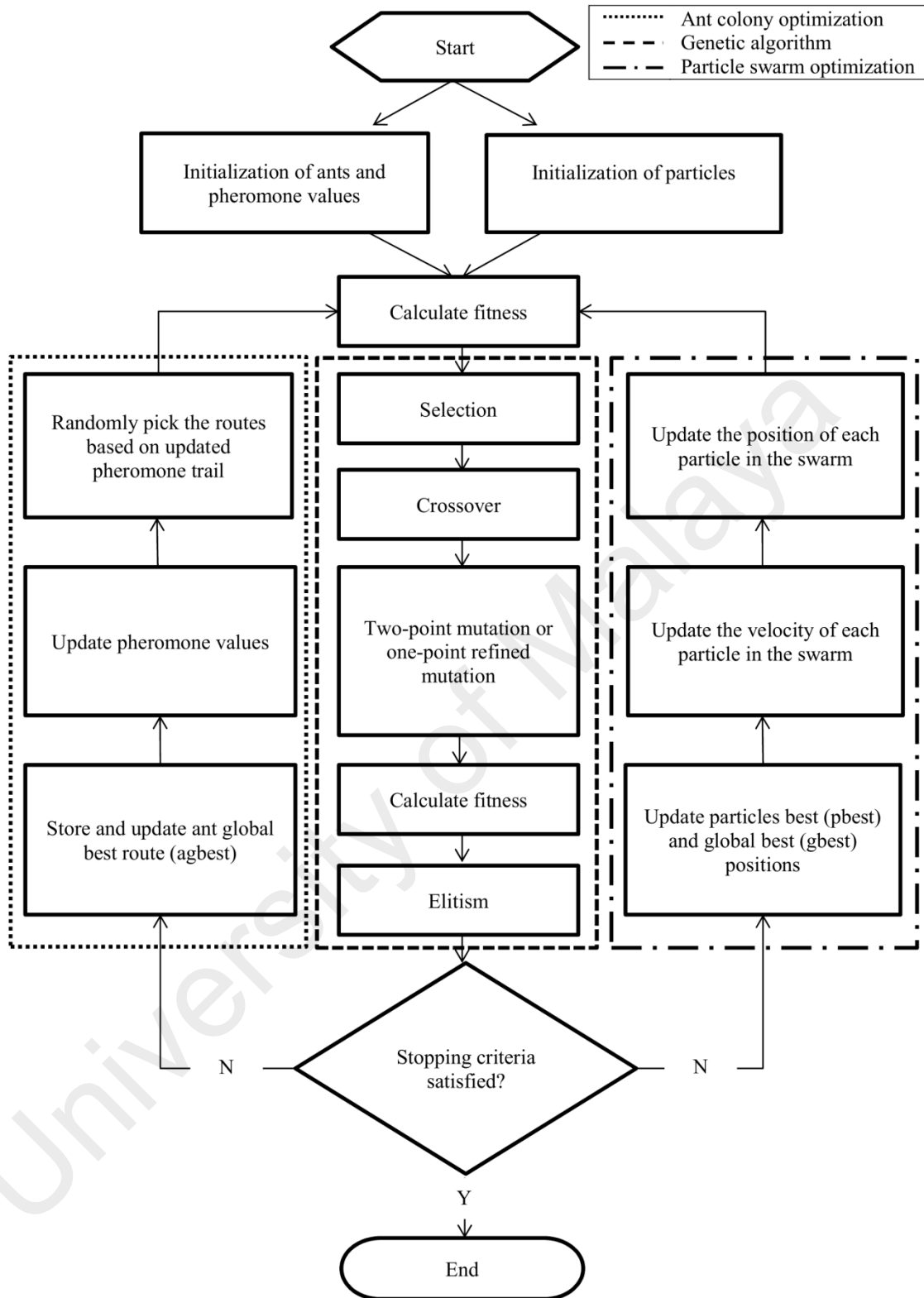


Figure 2.9: The proposed hybrid GA-ACO-PSO algorithm

(e) **Objective function**

The performances of the proposed meta-heuristic hybrid optimisation method adopting three different types of error functions, namely, natural frequency error function, mode shape error function and frequency response function (FRF) error function are investigated and compared. The natural frequency error function is firstly used in the applicability study of the proposed method in material identification and utilised in the comparative study of the proposed method and the other established methods. The effects of using the proposed method incorporated with three different types of error functions, namely, natural frequency error function, mode shape error function and frequency response function (FRF) error function, in material identification are investigated. In the validation stage, a two-stage approach is adopted to accommodate the effects of uncertainties; stage 1 adopts the natural frequency error function, whereas stage 2 involves the FRF error function. The formulations of the error functions are described as follows:

(i) **Natural frequency**

In the present study, the first type of objective function can be expressed in terms of discrepancy of natural frequencies as follows:

$$\begin{aligned} \text{Minimise} \quad & f(x) = \sum_{i=1}^N \left(\frac{fr_i - \bar{f}r_i}{fr_i} \right)^2 \\ \text{subject to} \quad & 0 < \frac{G_{xy}}{E_x} < 1 \\ & 0 < \frac{G_{xy}}{E_y} < 1 \\ & LB_i \leq x_i \leq UB_i \quad ; \quad i = 1, 2, 3, \dots, n \end{aligned} \quad (2.61)$$

where, f is the cost function of the design variable $x = [x_1, x_2, x_3, \dots, x_n]$, fr_i is the evaluated natural frequencies, $\bar{f}r_i$ is the reference or experimental natural frequencies, LB_i and UB_i are the lower and upper boundaries of the elastic properties, respectively. The elastic properties are the in-plane longitudinal elastic modulus (E_x), in-plane

transverse elastic modulus (E_y), in-plane shear modulus (G_{xy}) and major Poisson's ratio (ν_{xy}). As shown in equation (2.61), two additional constraints are introduced to mitigate uncertainties as well as to avoid premature convergence.

(ii) **Mode shape**

Apart from using the natural frequency, the mode shape for each mode of vibration can be used and expressed in terms of modal assurance criterion (MAC) values as follows:

$$MAC = \frac{|\phi_{X_i}^{HT} \phi_{A_i}|^2}{(\phi_{X_i}^{HT} \phi_{X_i})(\phi_{A_i}^{HT} \phi_{A_i})} \quad (2.62)$$

where, superscript *HT* denotes Hermitian transpose, ϕ_{X_i} and ϕ_{A_i} are the i^{th} complex experimental (reference) and analytical mode shapes, respectively. The MAC value ranges from 0 to 1, where 1 indicates perfect resemblance between the experimental and analytical modes. The objective function involving the use of mode shapes can be expressed as follows:

$$\begin{aligned} \text{Minimise} \quad & f(x) = N - \sum_{i=1}^N MAC_i \\ \text{subject to} \quad & 0 < \frac{G_{xy}}{E_x} < 1 \\ & 0 < \frac{G_{xy}}{E_y} < 1 \\ & LB_i \leq x_i \leq UB_i \quad ; \quad i = 1, 2, 3, \dots, n \end{aligned} \quad (2.63)$$

where, f is the cost function of the design variable $x = [x_1, x_2, x_3, \dots, x_n]$, N is the total number of modes, LB_i and UB_i are the lower and upper boundaries of the elastic properties, respectively. The elastic properties are the in-plane longitudinal elastic modulus (E_x), in-plane transverse elastic modulus (E_y), in-plane shear modulus (G_{xy}) and major Poisson's ratio (ν_{xy}). As shown in equation (2.63), two additional constraints are introduced to mitigate uncertainties as well as to avoid premature convergence.

(iii) **Frequency response function (FRF)**

Signature assurance criterion (SAC) or frequency response assurance criterion (FRAC) is a criterion measuring the shape similarity between two frequency response functions (FRFs). The value of SAC ranges from 0 to 1, where, 1 indicates perfectly identical shapes between both the correlated FRFs, whereas, 0 denotes the opposite. The formula is expressed as follows:

$$SAC = \frac{|\alpha_{X_i}^{HT} \alpha_{A_i}|^2}{(\alpha_{X_i}^{HT} \alpha_{X_i})(\alpha_{A_i}^{HT} \alpha_{A_i})} \quad (2.64)$$

where, α_{X_i} = experimental or reference FRF

α_{A_i} = analytical FRF

On the other hand, cross signature scale factor (CSF) is a factor evaluating the amplitude discrepancies between two FRFs. The value of CSF ranges from 0 to 1, where, 1 indicates zero amplitude discrepancy between both the correlated FRFs, while 0 denotes the opposite. The formula is expressed as follows:

$$CSF = \frac{2|\alpha_{X_i}^{HT} \alpha_{A_i}|}{(\alpha_{X_i}^{HT} \alpha_{X_i}) + (\alpha_{A_i}^{HT} \alpha_{A_i})} \quad (2.65)$$

where, α_{X_i} = experimental or reference FRF

α_{A_i} = analytical FRF

By combining both the SAC and CSF correlation analysis, the reliability of the results will be much reassured since both the aspect of shape and magnitude are taken into account in the correlation analysis. The objective function can be expressed as follows:

$$\begin{aligned} \text{Minimise} \quad & f(x) = \left[\left(N - \sum_{i=1}^N SAC_i \right) + \left(N - \sum_{i=1}^N CSF_i \right) \right] \\ \text{subject to} \quad & 0 < \frac{G_{xy}}{E_x} < 1 \end{aligned}$$

$$0 < \frac{G_{xy}}{E_y} < 1$$

$$LB_i \leq x_i \leq UB_i \quad ; \quad i = 1, 2, 3, \dots, n \quad (2.66)$$

where, f is the cost function of the design variable $x = [x_1, x_2, x_3, \dots, x_n]$, N is the total number of nodes, LB_i and UB_i are the lower and upper boundaries of the elastic properties, respectively. The elastic properties are the in-plane longitudinal elastic modulus (E_x), in-plane transverse elastic modulus (E_y), in-plane shear modulus (G_{xy}) and major Poisson's ratio (ν_{xy}). As shown in equation (2.66), two additional constraints are introduced to mitigate uncertainties as well as to avoid premature convergence.

University of Malaysia

CHAPTER 3: RESEARCH METHODOLOGY

3.1 Introduction

This chapter consists of three main sections. The procedures of executing the proposed two-stage derivative-based method are first presented. Next, the procedures of verifying the proposed meta-heuristic hybrid optimisation method are described. Lastly, the procedures of conducting experimental validation on both the proposed methods are explained.

3.2 Method 1: Two-stage derivative-based method

In this method, a two-stage approach is adopted, where, in stage 1, the method developed by Ismail et al. (2013) is used to determine the two in-plane elastic moduli, in-plane shear modulus and major Poisson's ratio. In stage 2, the proposed method, which involves mode shapes, is utilised to improve the identifiability of the in-plane shear modulus and Poisson's ratio. Before the developed method is undertaken for real specimen application, it is tested and verified using plates retrieved from Deobald and Gibson (1988), namely, aluminium and graphite epoxy plates. In this context, these plates are known as the reference plates for better interpretation. The effects of using the developed method on two different reference plates are studied. The aluminium plate is known to be isotropic, such that, the elastic properties are independent of the location and orientation at a point in the body, while, the graphite epoxy composite plate is known to be orthotropic, such that, the elastic properties are different in three mutually perpendicular directions at a point in the body. The dimensions and material properties of the aluminium and graphite epoxy plates are presented in Table 3.1. These dimensions and material properties are used as the input parameters of the Fourier method developed by Khov et al. (2009) to generate the benchmark natural frequencies and mode shapes. The generated benchmark modal parameters are then used as the reference parameters in the inverse identification process. The effects of using the

proposed method on the reference plates under different sets of boundary conditions (F-F-F, C-F-F-F, C-C-F-C, where, C: Clamped, F: Free) are investigated as well. It should be highlighted that for most identification approaches, the objective function is defined by a weighted combination of natural frequencies and mode shapes discrepancies, while in the present research, a separate definition of objective function for natural frequencies and mode shapes discrepancies is proposed to simplify the derivation and computation efforts. The accuracy, repeatability and convergence of the proposed two-stage derivative-based method in identifying the elastic properties of the aluminium and graphite epoxy plates are investigated and discussed. The accuracy is evaluated in terms of absolute percentage error of the evaluated properties with respect to the reference values, while, the repeatability is evaluated in terms of standard deviation. Lastly, the convergence is evaluated in terms of computational time. The details of both stages are elaborated in the following sub-sections.

Table 3.1: Dimensions and elastic properties of reference plates

Boundary condition	a, b (mm)	H (mm)	ρ (kgm^{-3})	E_x (GPa)	E_y (GPa)	G_{xy} (GPa)	ν_{xy}	ν_{yx}
Aluminium								
F-F-F-F	254	3.160	2770	72.4	72.4	28.0	0.33	0.33
C-F-F-F								
C-C-F-C								
Graphite epoxy								
F-F-F-F	254	1.483	1584	127.9	10.27	7.312	0.22	0.0177
C-F-F-F		1.688						
C-C-F-C		1.379						

3.2.1 Stage 1: Natural frequencies

The updating procedures are similar to those explained by Ismail et al. (2013). In the present research, three termination criteria, namely, the maximum number of iterations, the minimum improvement percentage and the minimum value of convergence, are introduced. In the investigation of reference plates, regularization can be omitted since uncertainties are presumably absent, and thus, regularization parameter is set equal to

zero. In this study, the in-plane elastic moduli, in-plane shear modulus and major Poisson's ratio are updated using the first six natural frequencies. The procedures of conducting stage 1 are elaborated as follows:

- i. Estimate initial values for four parameters of the analytical model.
- ii. Specify the termination criteria, including, the maximum number of iterations, the minimum improvement percentage and the minimum value of convergence.
- iii. Input the reference or measured natural frequencies and the regularization parameter (if needed).
- iv. Utilise the forward method to produce the eigen frequencies.
- v. Evaluate the derivatives with respect to each parameter and build the \mathbf{S} matrix.
- vi. Evaluate the error difference between the evaluated and reference or measured natural frequencies, and build the ϵ matrix.
- vii. Estimate $\Delta \mathbf{Pr}$ and update the four parameters.
- viii. Repeat steps 4-7 until either of the three termination criteria is met.

3.2.2 Stage 2: Mode shapes

The updating procedures are similar to those of stage 1. However, few settings must be configured, and the approach is slightly different from that in stage 1. In stage 1, a regularisation parameter is selected on the basis of the graph of stiffness change norm against residual norm and applied on all the involved design variables. In stage 2, regularisation parameters are introduced individually to each of the design variables to control the changes in each of the design variables individually. Certainly, the selection of inappropriate regularisation parameters may cause the proposed method to lose its effectiveness. Therefore, in this study, regularisation parameters are selected on the

basis of the theoretical relationship between the elastic properties and the optimising parameters (e.g. natural frequencies and mode shapes), as well as the information obtained from published articles (Pagnotta, 2008; Tam et al., 2017). The results obtained in stage 1 are used as the initial values in stage 2. In reference studies, the in-plane shear modulus and major Poisson's ratio can be selectively directed to stage 2 based on the quality of the results obtained in stage 1. In ideal cases, the in-plane elastic moduli do not undergo stage 2 because of their sufficiently high accuracy attained in stage 1 to avoid further deterioration. On the contrary, in experimental studies, the four elastic properties are subjected to stage 2, with consideration of the presence of uncertainties that may have provided several gaps for improvement after stage 1. The elastic moduli are taken into account under the condition that the changes in these elastic moduli are confined. Changes in the in-plane shear modulus and major Poisson's ratio are relatively less restricted by assigning appropriate regularisation parameters because mode shapes are relatively local and theoretically much related to both of these properties. In this study, the difference between the experimental and evaluated mode shapes ($\epsilon = [\varphi_m - \varphi_a]$) is much smaller than that between the experimental and evaluated natural frequencies ($\epsilon = [\mathfrak{N}_m - \mathfrak{N}_a]$). Therefore, a scaling factor is needed to amplify the difference between the experimental and evaluated mode shapes in stage 2. The scaling factor can be defined on the basis of the difference between the experimental and evaluated mode shapes. Scaling can be performed by multiplying the values involving mode shapes with a multiple of 10 (e.g. 10, 100, 1000, etc.), depending on suitability. The process begins with the selection of the smallest number (i.e. 10) and increases gradually by multiples of 10. The scaling is regarded well defined when the maximum change in the parameters lies within 10% of the parameters determined from the former iteration and when the identification outcome converges to its solution. In addition, an overestimation of the scaling factor will cause severe divergence, whereas

an underestimation will stagnate the updating process. Hence, the appropriate scaling factor should be selected. Generally, the procedures of conducting stage 2 are presented as follows:

- i. Use the four parameters obtained from stage 1 as the initial values.
- ii. Specify the termination criteria, including, the maximum number of iterations, the minimum improvement percentage and the minimum value of convergence.
- iii. Input the reference or measured mode shapes and the regularization parameters (if needed), as well as scaling factor.
- iv. Utilise the forward method to produce the mode shapes.
- v. Evaluate the derivatives with respect to each parameter and build the \mathbf{S} matrix.
- vi. Evaluate the error difference between the evaluated and reference or measured mode shape modal displacements, and build the ϵ matrix.
- vii. Estimate $\Delta \mathbf{Pr}$ and update the four parameters.
- viii. Repeat steps 4-7 until either of the three termination criteria is met.

3.3 Method 2: Meta-heuristic hybrid optimisation method (Hybrid GA-ACO-PSO)

In the present section, the general flow of the proposed hybrid GA-ACO-PSO algorithm is first explained. Next, the procedures of examining the feasibility of the proposed method in solving test functions and established engineering design problems are presented. Subsequently, the procedures of conducting a study on the applicability of the proposed algorithm in material identification are elaborated. Lastly, the procedures of performing an investigation on the effects of using the proposed method with three different error functions in material identification are explicated.

3.3.1 General flow of algorithm

The detailed theories of the proposed hybrid algorithm has been presented and explained in the previous chapter. Generally, the algorithm begins with the initialization of populations. The initial populations are divided equally into two groups, in which, each group passes through the ant colony optimisation (ACO) and particle swarm optimisation (PSO) operators, respectively. The products of each operator are subsequently processed and evolved via genetic algorithm (GA) operators. The parent populations as well as the evolved populations are then ranked and selected for further evolution in the next generation. The iterations continue until the termination criterion is achieved. In the present study, only one termination criterion, namely, the maximum number of generations or iterations is specified due to the reason of equal and fair comparison in the aspect of accuracy, repeatability and convergence with respect to other algorithms. The pseudo code demonstrating the flow of the algorithm is presented in Figure 3.1.

```

Objective function  $f(x), x = (x_1, \dots, x_d)$ 
Generate initial population of ants,  $x_{ant}$  and particles,  $x_{particle}$ 
while ( $count \leq MaxGeneration$ )
  Initialize pheromone intensity
  if  $count > 0$ 
    Update velocity,  $v_{particle}$  and position of particle,  $x_{particle}$ 
  end
  Evaluate fitness of ants,  $F_{ant}$ , followed by fitness of particles,  $F_{particle}$ 
  Crossover
  if ( $count \leq n$ )
    Standard mutation
  else
    Refined mutation
  end
  Evaluate fitness of crossover and mutated individuals,  $F_{new}$ 
  Rank the solutions
  Divide solutions into 2 parts: population of ants (odd number) and particles (even number)
  if  $count = 0$ 
    Find best solution from the new solutions
    global best,  $agbest = x_{best\ new\ ant}$ 
  else
    Update  $agbest$ 
  end
  if  $count = 0$ 
    Find best solution from the new solutions
    global best,  $gbest = x_{best\ new\ particle}$ 
    population best,  $pbest = x_{new\ particle}$ 
  else
    Update  $gbest$  and  $pbest$ 
  end
  Update pheromone intensity
end

```

Figure 3.1: Pseudo code of the proposed hybrid algorithm

3.3.2 Verification of the proposed method using test functions and engineering design problems

Firstly, 10 sets of test functions and four sets of engineering design problems are used to verify the feasibility of the proposed method. Two different features, namely, fixed refined mutation and logarithmically-spaced refined mutation are introduced. The effects of feature variations in solving test functions and engineering design problems are investigated. Next, the effects of parameter variations in solving test functions are studied. The performance of the proposed method in solving test function and engineering design problems is then investigated and compared with those of conventional algorithms (i.e. GA, ACO, PSO) and other established algorithms.

Notably, before proceeding to the verification of the proposed method, the effects of variation in the input parameters are investigated comprehensively. Given that the number of evaluations is fixed, the numbers of generations and populations can be adjusted to achieve a fixed number of evaluations. Various combinations of the numbers of generations and populations leading to a fixed number of evaluations are investigated. The effects of increasing the number of paths, evaporation rate, and constant used in the ACO algorithm and the proposed method are investigated. The effects of increasing the strength of attraction and varying the momentum factor used in the PSO algorithm and the proposed method are also studied. Variations in the parameters of the two different features used in the proposed method are also investigated. Subsequently, selection of appropriate input parameters is made on the basis of the results obtained from the studies.

3.3.2.1 Test functions

The main reason of conducting this study is to investigate the feasibility of the proposed meta-heuristic hybrid optimisation method in solving unconstrained problems (test functions) in the presence of multimodality before it is adopted for material identification. It is notable that the involving test functions are normally referred to as unconstrained problems, such that, they are only bounded by search region boundaries. A total of 10 test functions are used to evaluate the performance of the proposed hybrid algorithm, in which, the first six ($F_1 - F_6$) are multimodal functions and the last four ($F_7 - F_{10}$) are unimodal functions. The details of the test functions can be found in Appendix A. It can be seen that the expression as well as the designated search region of each test function are distinctively varied from one another and this indirectly studies the robustness of the proposed algorithm. Furthermore, the number of dimensions, N used in the research and the optimum solutions for the 10 test functions are presented in Table 3.2. In the present study, all the functions are to be minimised. For each function,

30 runs of simulations are executed. The research begins with the study of the effects of feature variations, followed by the study of the effects of parameter variations, the study of the performance comparison between the proposed and conventional algorithms and lastly, the study of the performance comparison between the proposed and established algorithms.

Table 3.2: Number of dimensions used and the optimum solutions for test functions

Function	Name	Dimension, N	Global optimum	
			$F(x)$	x
F_1	Ackley	30	0	$[0, \dots, 0]^N$
F_2	Griewangk	30	0	$[0, \dots, 0]^N$
F_3	Rastrigin	30	0	$[0, \dots, 0]^N$
F_4	Rosenbrock	30	0	$[1, \dots, 1]^N$
F_5	Schwefel	30	0	$[420.9687, \dots, 420.9687]^N$
F_6	Weierstrass	30	0	$[0, \dots, 0]^N$
F_7	Schwefel P2.22	30	0	$[0, \dots, 0]^N$
F_8	Sphere	30	0	$[0, \dots, 0]^N$
F_9	Styblinski-Tang	30	$-39.16599N$	$[-2.903534, \dots, -2.903534]^N$
F_{10}	Zakharov	30	0	$[0, \dots, 0]^N$

(a) Effects of feature variations in solving test functions

Firstly, the effects of feature variations are investigated. Basically, two features, namely, fixed refined mutation (feature 1) and logarithmically-spaced refined mutation (feature 2) are introduced. For feature 1, parameter aa is fixed equal to 0.001, while parameter bb is fixed equal to $2aa$, which is equivalent to 0.002. For feature 2, the command “*logspace*” in the proposed hybrid algorithm is used to generate a logarithmically-spaced vector in descending order. When $logspace = 2,500$, from $10^{0.01}$ to $10^{0.00001}$, a total of 2,500 logarithmically-spaced intervals are generated within the defined range. In the current study, parameter aa is specified as the logarithmically-spaced vector in descending order from $10^{0.01}$ to $10^{0.00001}$, while parameter bb is defined as $2aa$. In the language of Matlab, it can be written as “*logspace* (0.01, 0.00001, 2500)”. It should be informed that only one refined mutation point is involved in both

feature 1 and feature 2. The complete input settings of the proposed method in this study are presented in Table 3.3. This study is conducted to investigate and compare the effectiveness of the two proposed features in solving the test functions and the relatively best feature is selected for further investigation. It is notable that the performance is evaluated in terms of average minimised function value error (accuracy) and standard deviation (repeatability).

(b) Effects of parameter variations in solving test functions

Based on the outcomes obtained from the previous study, the relatively best feature is selected. Parameters, such as *aa* and *bb*, as well as the number of mutation points may affect the performance of the selected feature. To determine the relatively best combination of parameters in solving unconstrained problems, the effects of variations in the mentioned parameters are investigated. The input settings for the proposed algorithm are presented in Table 3.3. The effectiveness of parameter variations is evaluated in terms of average minimised function value error (accuracy) and standard deviation (repeatability). Average ranking of Friedman test is conducted to determine the relatively best combination of parameters.

(c) Performance comparison between the proposed and conventional algorithms in solving test functions

Adopting the relatively best combination of parameters which is determined from the previous study, the performance of the proposed algorithm in solving test functions is subsequently evaluated and compared with those of the conventional algorithms, namely, genetic algorithm (GA), ant colony optimisation (ACO) and particle swarm optimisation (PSO). The input settings for the algorithms are presented in Table 3.3. The number of evaluations is set to 200,040 for all the involved algorithms by fixing the number of generations (5,000) and the number of populations for the reason of equal

and fair comparison. In the present study, the number of evaluations includes those from the initialization stage as well. Basically, the number of evaluations can be interpreted as the number of times that the minimisation of the objective function has taken place. The number of evaluations for GA, ACO and PSO can be calculated based on equation (3.1), while for the proposed hybrid algorithm, the number of evaluations can be computed based on equation (3.2).

$$\begin{aligned}
 & \textit{Number of evaluations} \\
 & = \textit{Number of generations (Number of populations)} \\
 & + \textit{Number of initial populations}
 \end{aligned} \tag{3.1}$$

$$\begin{aligned}
 & \textit{Number of evaluations} \\
 & = 2 (\textit{Number of generations (Number of populations)}) \\
 & + \textit{Number of initial populations}
 \end{aligned} \tag{3.2}$$

The optimal number of path used in ACO and hybrid algorithm is found to be 30 and 25, respectively. Notably, a higher number of path leads to a higher degree of exploitative search. Hence, it can be seen that in the hybrid algorithm, the contribution of ACO operator is mainly focalised on the exploratory search. On the other hand, the constant is a fixed number involved in the pheromone intensity updating of ACO. It is specified based on the type of objective function and the optimal constant used in this context is 10,000 for both the ACO and hybrid algorithms. Besides, the strength of attraction and the momentum factor in PSO are specified referring to (Garg, 2016); while for the proposed hybrid algorithm, those parameters are set lower so that the PSO operator in the algorithm could concentrate more on the exploitative search. The command “*linspace*” in PSO, is used to generate a linearly-spaced vector within a specified range in descending order, for instance, when *linspace*= 5,000, from 0.9 to 0.4, a total of 5,000 linearly-spaced interval are generated within the specified range. In this study, *linspace* is specified corresponding to the number of generation. Moreover, the number of crossover is the number of selected individual to undergo crossover process and similarly, the number of mutation is the number of selected individual to

undergo mutation process. Apart, the command “*logspace*” in the proposed hybrid algorithm is used to generate a logarithmically-spaced vector in descending order, such that, when $logspace = 2,500$, from $10^{0.01}$ to $10^{0.00001}$, a total of 2,500 logarithmically-spaced interval are generated within the defined range. The best parameters aa and bb as well as D , as determined in the previous study are utilised in this comparative study. The accuracy, repeatability and the convergence of the involved algorithms are evaluated, in terms of average minimised function value error, standard deviation and average computational time, respectively.

Table 3.3: Input settings for GA, ACO, PSO and the proposed hybrid algorithm

Input variables		Settings			
		GA	ACO	PSO	Hybrid
1.	Number of generation	5,000	5,000	5,000	5,000
2.	Number of populations	40	40	40	20
3.	Number of evaluations	200,040	200,040	200,040	200,040
4.	Number of dimensions (design variables)	30	30	30	30
5.	ACO populations	–	40	–	10
6.	Initial intensity of pheromone for every vectors	–	1	–	1
7.	Number of paths	–	30	–	25
8.	Evaporation rate	–	0	–	0
9.	Constant	–	10,000	–	10,000
10.	PSO populations	–	–	40	10
11.	Strength of attraction, \vec{b}_1, \vec{b}_2	–	–	1.5, 1.5	1.05, 1.05
12.	Momentum factor, \vec{a}	–	–	[0.9,0.4]; <i>linSPACE</i> =5,000	[0.5,0.1]; <i>linSPACE</i> =5,000
13.	Number of crossover	20	–	–	10
14.	Number of standard (or refined) mutation	20	–	–	10 (10)
15.	Initialization of refined mutation after k^{th} generation	–	–	–	$2,500^{th}$
16.	The percentage range of design variables in refined mutation, aa & bb	–	–	–	$aa = [0.01, 1.0000E-05]$; $bb = 2aa$; <i>logSPACE</i> = 2,500

(d) Performance comparison between the proposed and published algorithms in solving test functions

Furthermore, the performance of the proposed algorithm in solving test functions is as well compared with those of published algorithm, including, CPSO-H (Van den Bergh & Engelbrecht, 2004), CLPSO (Liang et al., 2006), APSO (Zhan et al., 2009), GOPSO (Wang et al., 2011), DNSCLPSO (Wang et al., 2013) and DNSPSO (Wang et al., 2013). The maximum number of evaluations is set to 200,040 (including initial evaluations) and the number of generation is fixed to 5,000 as well as the number of populations is defined as 40 (20 for the proposed hybrid algorithm). The input settings for the proposed hybrid algorithm are shown in Table 3.3. It should be noted that only the accuracy and repeatability are investigated and compared, while, the study of convergence (average computational time) is not conducted due to the need of rebuilding and rerunning those established algorithms using a particular computing device for fair and equal comparison. Average ranking of Friedman test is conducted on the accuracy and repeatability of the compared algorithms to determine the relatively best performing algorithm.

3.3.2.2 Engineering design problems

The present study is conducted to investigate the viability of the proposed hybrid algorithm in solving constrained problems (engineering design problems). The optimisation problems to be used for verification include Himmelblau's non-linear optimisation problem, pressure vessel design optimisation problem, welded beam design optimisation problem and gear train design optimisation problem. For each design problem, 30 runs of simulations are executed. Each design problem is first defined and explained, followed by the study of the effects of feature variations, the study of the effects of parameter variations, the study of the performance comparison

between the proposed and conventional algorithms as well as the study of the performance comparison between the proposed and established algorithms.

(a) **Definition**

(i) **Himmelblau's non-linear optimisation problem**

A great number of researchers have been utilising this example as a benchmark to verify newly-developed algorithms since decades ago. This problem is originated by Himmelblau (1972) and it comprises five positive design variables, six non-linear inequality constraints, and 10 boundary conditions, which can be defined as follows:

Minimise

$$f(x) = 5.3578547x_3^2 + 0.8356891x_1x_5 + 37.293239x_1 - 40792.141 \quad (3.3)$$

$$0 \leq g_1(x) \leq 92$$

$$90 \leq g_2(x) \leq 110$$

$$20 \leq g_3(x) \leq 25$$

$$g_1(x) = 85.334407 + 0.0056858x_2x_5 + \mathbf{0.0006262}x_1x_4 - 0.0022053x_3x_5$$

$$g_2(x) = 80.51249 + 0.0071317x_2x_5 + 0.0029955x_1x_2 + 0.0021813x_3^2$$

$$g_3(x) = 9.300961 + 0.0047026x_3x_5 + 0.0012547x_1x_3 + 0.0019085x_3x_4$$

$$78 \leq x_1 \leq 102$$

$$33 \leq x_2 \leq 45$$

$$27 \leq x_3, x_4, x_5 \leq 45$$

Several algorithms have been validated employing this example, including genetic algorithm (GA), cuckoo search, harmony search, simplex search, particle swarm optimisation (PSO) and hybrid PSO-GA. Two slightly different cases of constrained functions have been used, in which the parameter 0.0006262 (in bold) in $g_1(x)$ has been used for case 1 and replaced with 0.00026 for case 2.

(ii) **Pressure vessel design optimisation problem**

In general, a pressure vessel is a container invented to store or to contain fluids at a designated pressure, as visualized in Figure 3.2. In this example, the design of a compressed air pressure vessel with working pressure of 2000 *psi* and a maximum

volume of $750ft^3$ is to be optimised to minimise the total material and manufacturing cost incurred (Kannan & Kramer, 1994). Pressure vessels are usually manufactured in cylindrical shape with both ends capped with hemispherical heads.

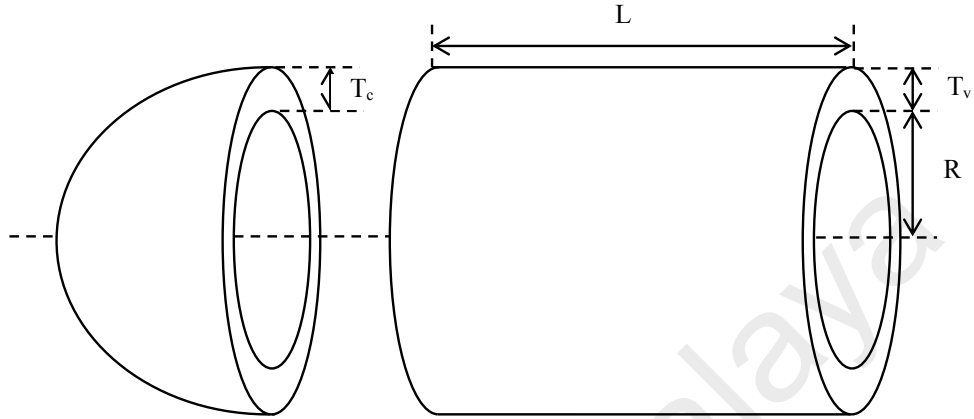


Figure 3.2: Schematic diagram of a pressure vessel

The working pressure and the volume have been fixed according to requirements, and the design variables to be determined include the thickness of the vessel, $T_v = x_1$, the thickness of the hemispherical caps, $T_c = x_2$, the inner radius of the vessel, $R = x_3$, and the length of the vessel excluding the caps, $L = x_4$. T_c and T_v are integers that are multiples of 0.0625 in , whereas, R and L are continuous. The design variables can be expressed in the form of vector, $x = [x_1, x_2, x_3, x_4]$ and the problem can be interpreted as follows:

Minimise

$$f(x) = 0.6224x_1x_3x_4 + 1.7781x_2x_3^2 + 3.1661x_1^2x_4 + 19.84x_1^2x_3 \quad (3.4)$$

$$g_1(x), g_2(x), g_3(x), g_4(x) \leq 0$$

$$g_1(x) = -x_1 + 0.0193x_3$$

$$g_2(x) = -x_2 + 0.0095x_3$$

$$g_3(x) = -\pi x_3^2 x_4 - \frac{4}{3} \pi x_3^3 + 1296000$$

$$g_4(x) = x_4 - 240$$

$$1 \times 0.0625 \leq x_1, x_2 \leq 99 \times 0.0625$$

$$10 \leq x_3, x_4 \leq 200$$

(iii) **Welded beam design optimisation problem**

As depicted in Figure 3.3, this welded beam design problem was first proposed by Rao (2009), with the objective of minimising the manufacturing cost of the welded beam by optimising the design parameters, including the thickness of the weld, $T_w = x_1$, the length of the welded joint, $l = x_2$, the height of the beam, $h = x_3$, and the width of the beam, $w = x_4$. A vector, $x = [x_1, x_2, x_3, x_4]$ is formed for simple representation. The equation below represents the objective function and the constraints are listed. Table 3.4 shows the representation of the symbols, as well as the input specifications of the problem.

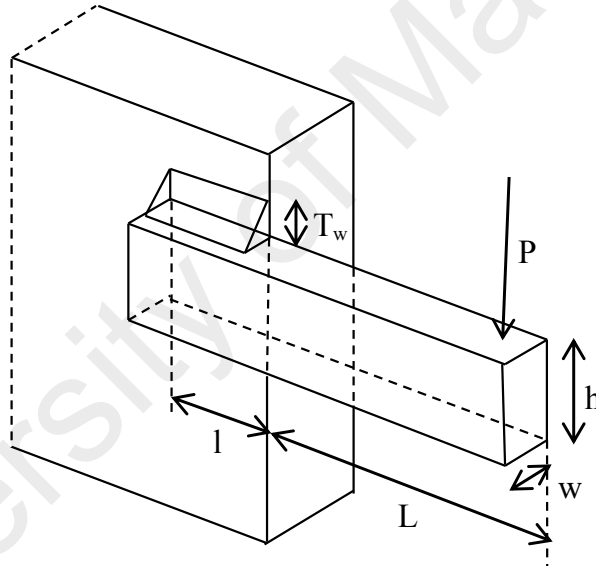


Figure 3.3: Welded beam schematic diagram

Minimise

$$f(x) = 1.10471x_1^2x_2 + 0.04811x_3x_4(14 + x_2) \quad (3.5)$$

$$g_1(x), g_2(x), g_3(x), g_4(x), g_5(x), g_6(x), g_7(x) \leq 0$$

$$g_1(x) = \tau(x) - \tau_{max}$$

$$g_2(x) = \sigma(x) - \sigma_{max}$$

$$g_3(x) = x_1 - x_4$$

$$g_4(x) = 0.125 - x_1$$

$$g_5(x) = \delta(x) - 0.125$$

$$g_6(x) = P - P_c(x)$$

$$g_7(x) = 0.10471x_1^2 + 0.04811x_3x_4(14 + x_2) - 5$$

$$0.1 \leq x_1, x_4 \leq 2$$

$$0.1 \leq x_2, x_3 \leq 10$$

$$\tau(x) = \sqrt{\left(\frac{P}{\sqrt{2}x_1x_2}\right)^2 + 2\left(\frac{P}{\sqrt{2}x_1x_2}\right)\left(\frac{MR}{J}\right)\left(\frac{x_2}{2R}\right) + \left(\frac{MR}{J}\right)^2}$$

$$M = P\left(L + \frac{x_2}{2}\right)$$

$$J(x) = 2\left\{\sqrt{2}x_1x_2\left[\frac{x_2^2}{4} + \left(\frac{x_1 + x_3}{2}\right)^2\right]\right\}$$

$$R = \sqrt{\frac{x_2^2}{4} + \left(\frac{x_1 + x_3}{2}\right)^2}$$

$$\sigma(x) = \frac{6PL}{x_4x_3^2}$$

$$\delta(x) = \frac{6PL^3}{Ex_4x_3^3}$$

$$P_c(x) = \frac{4.013E\sqrt{\frac{x_3^2x_4^6}{36}}}{L^2}\left(1 - \frac{x_3}{2L}\sqrt{\frac{E}{4G}}\right)$$

Table 3.4: Notations for welded beam design problem

	Representation	Values
1.	Weld's maximum shear stress, τ_{max}	13,600 <i>psi</i>
2.	Beam's maximum stress, σ_{max}	30,000 <i>psi</i>
3.	Load applied, P	6,000 <i>lb</i>
4.	Beam length, L	14 <i>in</i>
5.	Shear Modulus, G	12E+06 <i>psi</i>
6.	Young's Modulus, E	30E+06 <i>psi</i>
7.	Weld's Shear stress, τ	-
8.	Beam's normal stress, σ	-
9.	Bar buckling load, P_c	-
10.	Beam deflection, δ	-

(iv) Gear train design optimisation problem

Generally, gear train can be defined as a system that is composed of a combination of various types of gears mounted on a frame, forming a complete working mechanism. This optimisation problem involves no constraints and was first presented by Sandgren (1990), with the intention of determining the best combination of four gears with a different number of teeth that would minimise the gear ratio. Since the number of teeth of the gearwheel is definite, the design variables to be identified would only involve

integers. The formulations associated with the gear ratio and the number of teeth ($x = [x_1, x_2, x_3, x_4]$) are shown as follows:

$$\begin{aligned} &\text{Minimise} \\ &f(x) = \left(\frac{1}{6.931} - \frac{x_1 x_2}{x_3 x_4} \right)^2 \quad (3.6) \\ &12 \leq x_1, x_2, x_3, x_4 \leq 60 \\ &\text{Gear Train} = \frac{x_1 x_2}{x_3 x_4} \end{aligned}$$

(b) Effects of feature variations in solving engineering design problems

The effects of feature variations in solving constrained problems are first examined. As mentioned before, two features, namely, fixed refined mutation (feature 1) and logarithmically-spaced refined mutation (feature 2) are proposed. The details of the proposed features have been explained in the previous section. The effectiveness of the proposed features is compared in terms of the best, average and worst minimised objective function values (accuracy), as well as the standard deviation (repeatability). The best performing feature is selected for subsequent application.

(c) Effects of parameter variations in solving engineering design problems

In this study, the effects of parameter variations in the selected feature are investigated. Parameters, such as, aa and bb , as well as the number of mutation points are varied and the relatively best combination of parameters is determined based on the performance, which is evaluated in terms of the best, average and worst minimised objective function values (accuracy), as well as the standard deviation (repeatability). Average ranking of Friedman test is performed to identify the relatively best combination of parameters.

(d) Performance comparison between the proposed and conventional algorithms in solving engineering design problems

Adopting the best combination of parameters evaluated from the previous study, the performance of the proposed algorithm in solving engineering design problems is then evaluated and compared with those of the conventional algorithms, namely genetic algorithm (GA), ant colony optimisation (ACO) and particle swarm optimisation (PSO). The input settings for the conventional algorithms are similar to those used previously, as shown in Table 3.3, except for the maximum number of generations and evaluations. There are slight adjustments in the input settings for the proposed hybrid algorithm and the maximum number of iterations or generations, as well as evaluations varies according to design problems, as present in Table 3.5. It is noted that the maximum number of iterations and evaluations are fixed constant for all the involved algorithms in each design problem. The accuracy is evaluated in terms of the best, average and worst minimised objective function values, while, the repeatability is evaluated in terms of the standard deviation. On the other hand, the convergence is evaluated in terms of convergence rate and computational time.

Table 3.5: Input settings for the proposed algorithm

Input variables		Himmelblau's problem	Pressure vessel design problem	Welded beam design problem	Gear train design problem
1.	Number of generation	800	500	500	100
2.	Number of populations	20	20	20	20
3.	Number of evaluations	32,040	20,040	20,040	4,040
4.	Number of dimensions (design variables)	5	4	4	4
5.	ACO populations	10	10	10	10
6.	Initial intensity of pheromone for every vectors	1	1	1	1
7.	Number of paths	25	25	25	25
8.	Evaporation rate	0	0	0	0
9.	Constant	10,000	10,000	10,000	10,000
10.	PSO populations	10	10	10	10
11.	Strength of attraction, \vec{b}_1, \vec{b}_2	1.5, 1.5	1.5, 1.5	2.0, 2.0	1.5, 1.5
12.	Momentum factor, \vec{a}	[0.9, 0.6]; <i>linespace</i> = 800	[0.9, 0.6]; <i>linespace</i> = 500	[0.9, 0.6]; <i>linespace</i> = 500	[0.9, 0.6]; <i>linespace</i> = 100
13.	Number of crossover	10	10	10	10
14.	Number of standard (or refined) mutation	10 (10)	10 (10)	10 (10)	10 (10)
15.	Initialization of refined mutation after k^{th} generation	400 th	250 th	250 th	50 th
16.	The percentage range of design variables in refined mutation, aa & bb	$aa = 0.0010$; $bb = 2aa$;	$aa = 0.0010$; $bb = 2aa$;	$aa = 0.0010$; $bb = 2aa$;	$aa = 0.0100$; $bb = 2aa$;

(e) Performance comparison between the proposed and published algorithms in solving engineering design problems

Lastly, the performance of the proposed algorithm in solving engineering design problems is compared with those of the published algorithms. The input settings for the proposed hybrid algorithm are presented in Table 3.5 and 30 runs of simulations are executed. The accuracy of the proposed hybrid algorithm is evaluated in terms of the best, average and worst solutions, while, the repeatability is evaluated in terms of the standard deviation and the convergence is evaluated in terms of the maximum number of evaluations.

3.3.3 Application in vibrational material identification

Before the proposed meta-heuristic hybrid method is adopted for real specimen application, similarly, it is verified using the reference plates, namely, aluminium and graphite epoxy plates (Deobald & Gibson, 1988). The specifications of the aluminium and graphite epoxy plates are presented in Table 3.1. In the present study, the Fourier method introduced by Khov et al. (2009) is employed in the identification process as the forward method. It should be noted that in this study, only the commonly-used natural frequency error function is utilised in the identification process. The reference natural frequencies of the aluminium plate are generated using the mentioned published Fourier method with inputs of actual material properties taken from (Deobald & Gibson, 1988). On the other hand, for the graphite epoxy plate, the reference natural frequencies generated using the Fourier method are retrieved from (Khov et al., 2009). Three different sets of general boundary conditions, namely, F-F-F-F, C-F-F-F and C-C-F-C (C: Clamped; F: Free) are investigated. The accuracy of the proposed method is studied and compared in terms of minimised objective function values. The determined elastic properties are subsequently compared with the benchmark properties for quantitative verification. For repeatability study, five runs of simulations are executed and the standard deviations are evaluated. Furthermore, convergence study is conducted for different types of materials and different sets of boundary conditions.

The identification process involves minimisation of the objective function. The input settings for genetic algorithm (GA), ant colony optimisation (ACO), particle swarm optimisation (PSO) and the proposed hybrid GA-ACO-PSO are listed in Table 3.6. The number of evaluations is set constant (i.e., 20) for all the involved algorithms by fixing the number of generations and number of populations for the reason of equal and fair comparison. As mentioned before in the previous section, the number of evaluations for

GA, ACO and PSO can be calculated based on equation (3.1), while for the proposed hybrid algorithm, the number of evaluations can be determined using equation (3.2).

In the present study, four dimensions are involved, namely, in-plane longitudinal elastic modulus (E_x), in-plane transverse elastic modulus (E_y), in-plane shear modulus (G_{xy}) and major Poisson's ratio (ν_{xy}). Similar to the previous section, the optimal number of path used in ACO and hybrid algorithm that yield the best results in material identification is found to be 30 and 25, respectively. The optimal constant used in this context is 10,000 for both ACO and hybrid algorithm. The strength of attraction and the momentum factor in PSO are defined based on the suggested values in (Garg, 2016); whilst for hybrid algorithm, those parameters are defined lower in values. As explained before, the *linspace* is specified according to the number of generations.

Table 3.6: Input settings for GA, ACO, PSO and the proposed hybrid algorithm in material identification

Input variables		Settings			
		GA	ACO	PSO	Hybrid
1.	Number of generations	20	20	20	20
2.	Number of populations	40	40	40	20
3.	Number of evaluations	840	840	840	840
4.	Number of dimensions (design variables)	4	4	4	4
5.	ACO populations	-	40	-	10
6.	Initial intensity of pheromone for every vectors	-	1	-	1
7.	Number of paths	-	30	-	25
8.	Evaporation rate	-	0	-	0
9.	Constant	-	10000	-	10000
10.	PSO populations	-	-	40	10
11.	Strength of attraction, \vec{b}_1, \vec{b}_2	-	-	1.5, 1.5	1.05, 1.05
12.	Momentum factor, \vec{a}	-	-	[0.9,0.4]; linspace =20	[0.5,0.1]; linspace =20
13.	Number of crossover	20	-	-	10
14.	Number of standard (or refined) mutation	20	-	-	10 (10)
15.	Initialization of refined mutation after k^{th} generation	-	-	-	10 th
16.	The percentage range of design variables in refined mutation, aa & bb	-	-	-	$aa = 0.02$; $bb = 0.05$;

3.3.4 Comparative study of different error functions

In the present context, the emphasis is placed on the study of the effects of using the proposed meta-heuristic hybrid approach with different types of error functions, namely, natural frequency error function, mode shape error function and frequency response function (FRF) error function. The performance of each the involved error function is compared and discussed. It is noteworthy that only the graphite epoxy plate under F-F-F-F (F: Free) boundary condition is investigated since the feasibility of the proposed method on different types of plates under different sets of boundaries conditions has been verified in the previous study. The dimensions and material properties of the graphite epoxy plate taken from literature (Deobald & Gibson, 1988) are shown in Table 3.1 in the previous section. These dimensions and material properties are used as the input parameters of the Fourier method developed by Khov et al. (2009) to generate the benchmark natural frequencies and mode shapes as well as the frequency response functions (FRFs). The generated benchmark parameters are then used as the reference parameters in the inverse problem. The input settings for the proposed hybrid algorithm are summarized in Table 3.7. The input settings for the conventional algorithms are similar to those presented in Table 3.6 in previous section, except for the number of populations, number of generations and number of evaluations. The number of evaluations is set constant (240) for all the involved algorithms by fixing the number of generations and number of populations, based on equation (4.3) and equation (4.4), as mentioned in the previous section. The accuracy of the proposed hybrid algorithm with different error functions is evaluated in terms of minimised error function values, as well as the absolute percentage error of the identified elastic properties. The repeatability is evaluated in terms of standard deviation of the identified elastic properties, while, the convergence is evaluated in terms of computational time.

Table 3.7: Input settings for hybrid algorithm in FRF-based material identification

	Input variables	Settings
1.	Number of generations	5
2.	Number of populations	20
3.	Number of evaluations	240
4.	Number of dimensions (design variables)	4
5.	ACO populations	10
6.	Initial intensity of pheromone for every vectors	1
7.	Number of paths	25
8.	Evaporation rate	0.9
9.	Constant	10000
10.	PSO populations	10
11.	Strength of attraction, \vec{b}_1, \vec{b}_2	1.05, 1.05
12.	Momentum factor, \vec{a}	[0.5,0.1]; <i>linspace</i> =5
13.	Number of crossover	10
14.	Number of standard (or refined) mutation	10 (10)
15.	Initialization of refined mutation after k^{th} generation	3 rd
16.	The percentage range of design variables in refined mutation, aa & bb	$aa = 0.02; bb = 0.05$

3.4 Experimental validation

Experimental validation is an experimental test conducted involving the use of real specimens to validate the feasibility of the proposed methods in identifying the elastic properties of the real specimens. In this context, these real specimens are referred to as experimental plates for better interpretation. Two experimental plates, namely, acrylonitrile-butadiene-styrene (ABS) plate and aluminium composite panel (ACP) are studied since the ABS plate is an isotropic material with great impact resistance and it is commonly used in automotive interior design industries, prototype construction industries, etc., while the ACP is an orthotropic material with great weather versatility and it is often utilised in building exterior and interior design industries, commercial signage design industries, etc. The results obtained from the destructive test (ABS plate) as well as from theoretical calculation (ACP) are needed to validate the results obtained from the proposed non-destructive technique. As highlighted, since there is no specific standard available for the identification of the material properties of the ACP using destructive test, theoretical calculation is thus performed. In this context, the details of

the destructive test and theoretical calculation are first presented, followed by the explanation of the non-destructive test. As mentioned, non-destructive test involves two main procedures, namely, experimental measurement and numerical evaluation. These procedures are hence explained in the following sub-sections.

3.4.1 Destructive test

Destructive tensile test is conducted to determine the elastic properties of the acrylonitrile-butadiene-styrene (ABS) plate, involving the use of an INSTRON universal testing instrument, as demonstrated in Figure 3.4. The standard procedures of conducting tensile test on ABS specimen can be found in the ASTM D683 standard, entitled “Standard test Method for Tensile Properties of Plastics”. Initially, the ABS plate is cut into pieces of specimens according to the standard shape and dimensions stated in the ASTM D638 standard, as depicted in Figure 3.5 and Table 3.8. A total of 10 pieces of specimens are produced, in which, five of the specimens are cut in the direction parallel to the x-axis of the plate, and the others are cut in the direction parallel to the y-axis of the plate. The gauge length and the width of each specimen are then measured and recorded. After that, the specimen is placed in between the grips of the INSTRO universal testing instrument. To minimise the possibility of slippage, the specimen is tightened considerably. The input settings for the tensile test machine program are specified appropriately, in which the maximum load is set equal to 1200N and the speed is set equal to 5mm/min. Upon reaching the maximum load, the machine comes to a halt. The width and the length of the specimen are subsequently measured and recorded. Furthermore, several precautionary measures need to be taken to avoid or reduce experimental errors. Before conducting tensile test, the specimens should be thoroughly inspected for any deformities to avoid inaccurate outcomes. Apart, slippage of grips should as well be avoided by making sure the grips are tightened appropriately as well as the surfaces of grips are in good condition.



Figure 3.4: INSTRON universal testing instrument

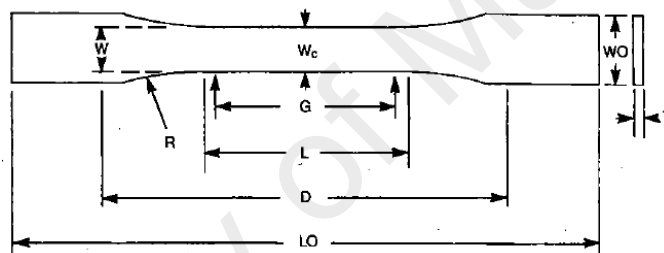


Figure 3.5: Schematic diagram of specimen for thickness of 3mm

Table 3.8: Dimension of specimen

Dimensions	Reading (mm)	Tolerances (mm)
W- Width of narrow section	13	± 0.5
L- Length of narrow section	57	± 0.5
WO- Width overall, min	19	+6.4
LO- Length overall, min	165	No max
G- Gage length	50	± 0.25
D- Distance between grips	115	± 5
R- Radius of fillet	76	± 1

3.4.2 Theoretical calculation

The aluminium composite panel (ACP) can be regarded as a composite plate as it is made of layers of different materials, comprising a layer of polyethylene core embedded in between two layers of the aluminium sheets. It is commonly used in building exterior and interior design industries due to its great weather versatility and durability.

Unfortunately, there is no specific test standard for determining the elastic properties of the ACP. Therefore, in this case, theoretical calculation appears to be the most relevant measure in evaluating the elastic properties, involving the use of established fibre-reinforced composite material formula, known as “The Rule of Mixture”, as presented below (Reddy, 2004).

Assumptions:

- Perfect bonding exists between the aluminium sheet and polyethylene core.
- The panel is a continuum, no gaps or empty spaces exist.
- The panel behaves as a linear elastic material
- The panel is transversely-isotropic, which is a class of orthotropic material that has the same properties in a single x-y plane, therefore the elastic modulus in x and y directions are the same.

The Rule of Mixtures is applied to calculate the elastic modulus, E and Poisson’s ratio, ν .

$$\text{Elastic Modulus, } E = E_f v_f + E_m v_m \tag{3.6}$$

$$\text{Poisson's ratio, } \nu_{xy} = \nu_f v_f + \nu_m v_m \tag{3.7}$$

where,

E = Elastic modulus of composite material

E_f = Elastic modulus of fiber, in this case is polyethylene

E_m = Elastic modulus of matrix, in this case is aluminium

v_f = Volume fraction of fiber, in this case is polyethylene

v_m = Volume fraction of matrix, in this case is aluminium

ν_f = Poisson's ratio of fiber, in this case is polyethylene

ν_m = Poisson's ratio of matrix, in this case is aluminium

3.4.3 Non-destructive test

3.4.3.1 Experimental measurement

Experimental modal analysis (EMA) is conducted to acquire the dynamic characteristics of the real specimens, expressed in terms of natural frequencies, mode shapes and damping properties. In the research, two experimental plates, namely, acrylonitrile-butadiene-styrene (ABS) plate and aluminium composite panel (ACP) with dimensions of $300\text{mm} \times 300\text{mm} \times 3\text{mm}$ each, as well as density of 1075kgm^{-3} and 1520kgm^{-3} , respectively, are investigated. Referring to (Hwang et al., 2009), semi-elastic strings are attached to the two diagonal corner edges of the plate to simulate F-F-F-F boundary condition, as demonstrated in Figure 3.6. The reason of only investigating F-F-F-F (F: Free) boundary condition consists in its simple implementation without requiring any customized clamping system, unlike those of other boundary conditions. Based on the dimensions of the plate, a grid of 5×5 is defined, and 25 measurement points are present in each plate, where the distance between adjacent points is 75mm . The equipment involved include an impact hammer, an accelerometer, a multi-channel Data Acquisition (DAQ) hardware, a DAQ software (DASYLab), a curve fitting software (ME'Scope), and a matrix-calculation software (Matrix Laboratory (MATLAB) software). The experimental set-up is demonstrated in Figure 3.7 and Figure 3.8. As seen from the figures, the plate is bounded by semi-elastic strings to simulate F-F-F-F boundary condition. The impact hammer is connected to the multi-channel DAQ hardware and it is used to strike the plate mechanically. The accelerometer is mounted on the surface of the plate at a particular point to measure the response of the plate (acceleration). It is connected to the multi-channel DAQ hardware and this DAQ hardware is connected to a laptop that is equipped with DAQ software and other post-processing software. The specifications of equipment are presented in Table 3.9.

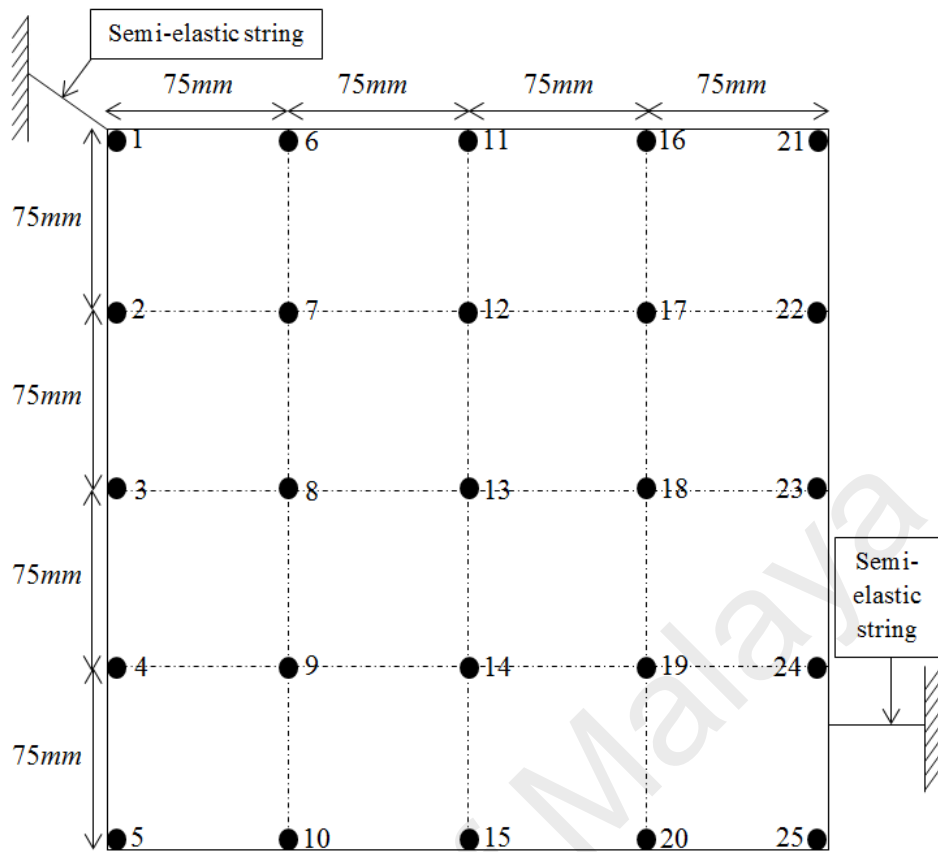


Figure 3.6: Schematic diagram of plate

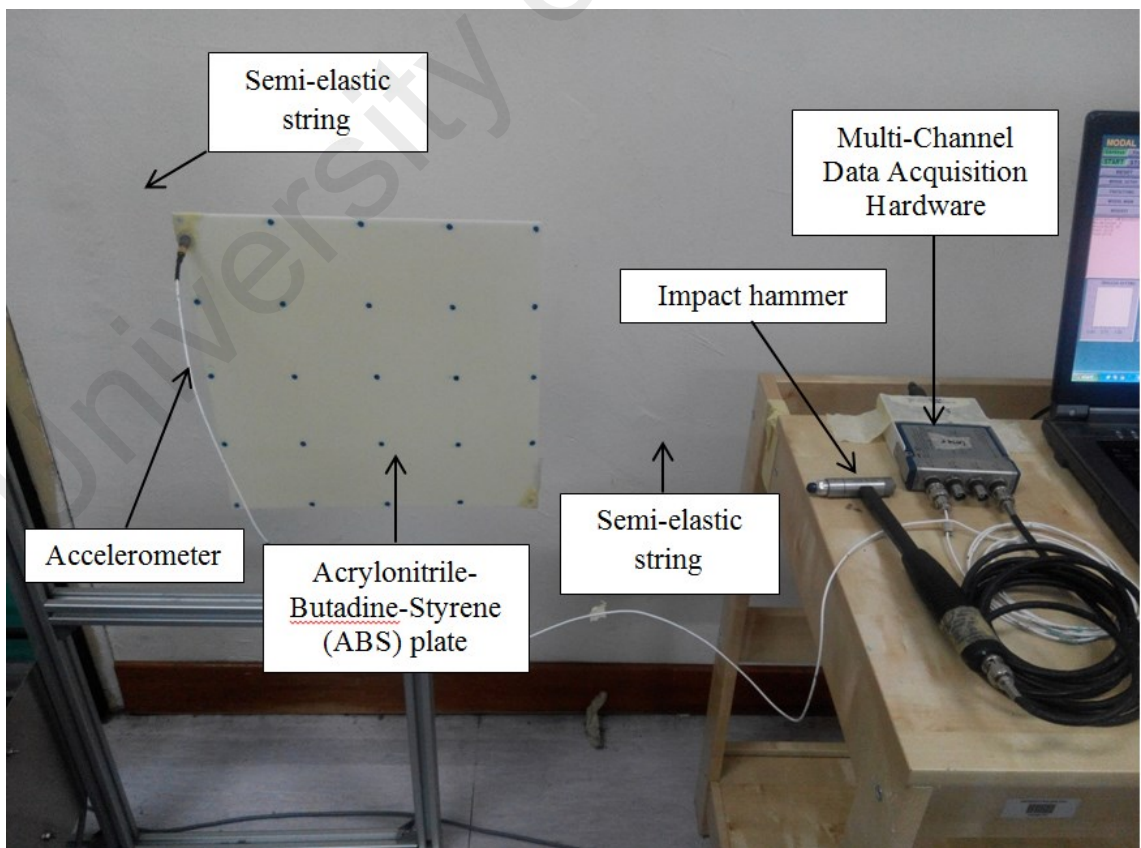


Figure 3.7: Experimental set-up for ABS plate

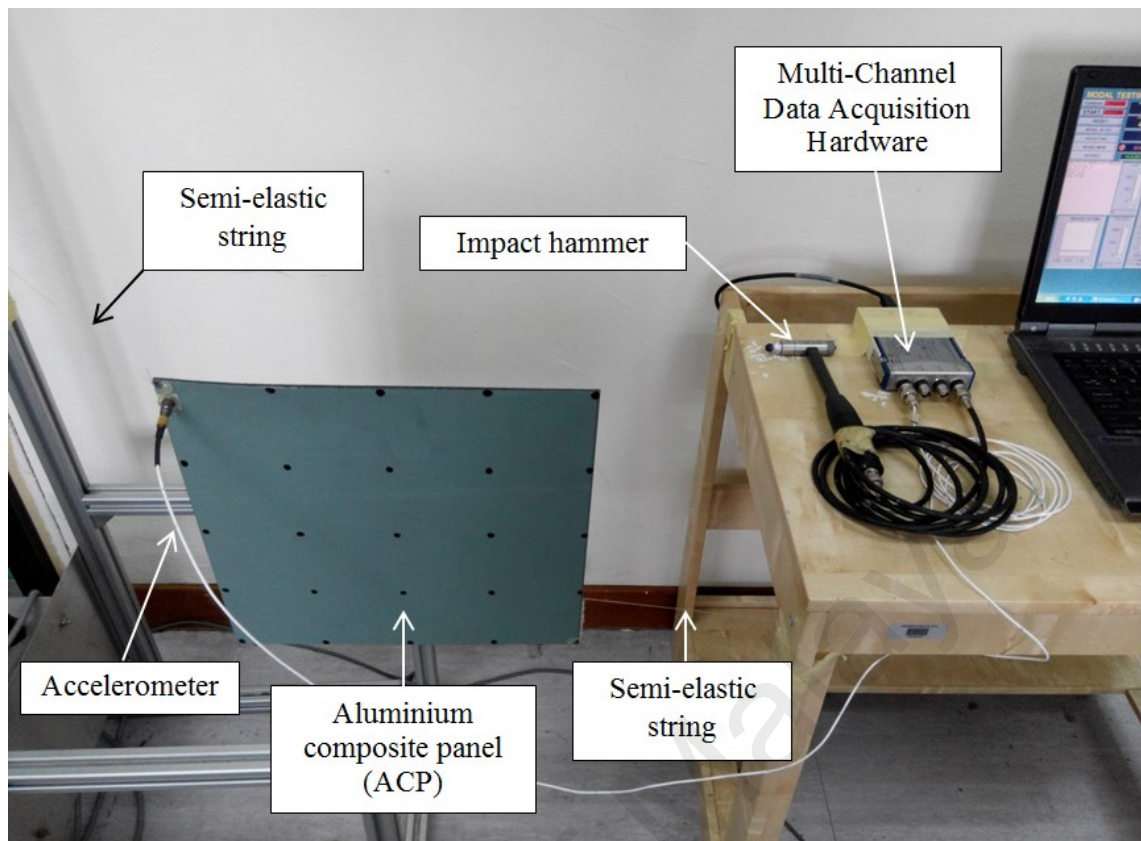


Figure 3.8: Experimental set-up for ACP

Table 3.9: Apparatus and equipment specifications

No.	Equipment/Material	Specification/Purpose
1.	Acrylonitrile-butadiene-styrene (ABS) plate	Dimension: $300\text{mm} \times 300\text{mm} \times 3\text{mm}$ Density: 1075kgm^{-3}
2.	Aluminium composite panel (ACP)	Dimension: $300\text{mm} \times 300\text{mm} \times 3\text{mm}$ Density: 1520kgm^{-3}
3.	PCB Impact Hammer (Model 086C03)	Sensitivity: 2.16mV/N Tip type: Medium tip with vinyl cover Hammer mass: 0.16kg Frequency range: 2.5kHz Amplitude range: $\pm 2200\text{N peak}$
4.	PCB Accelerometer (Model 352B68 SN 6149)	Sensitivity: 100mV/g Frequency range: $0.5 - 10000\text{Hz}$ Amplitude range: $\pm 4900\text{m/s}^2 \text{ peak}$
5.	NI USB Dynamic Signal Acquisition Module, Model NI-USB 9234	Number of channel: 4 ADC resolution: Type of ADC: delta sigma (with analogue pre-filtering)
6.	DASYLab [®] v10.0	Sampling rate: 2.048kS/s Block size: 4.096kS Channel 1: Accelerometer Channel 0: Impact hammer Averaging: 5 To perform FRF measurement
7.	ME'scopeVES 4.0.0.99	To perform curve fitting for modal parameters extraction from FRFs data
8.	MATLAB [®] R2013a	To perform identification process

In experiments, collected data often come with uncertainties and these uncertainties are predominantly due to the presence of various errors, namely, prediction errors, measurement errors and implementation errors. In the present study, implementation and measurement errors are the emphasis since these errors might incur during the acquisition of vibration data. Uncertainties can be reduced experimentally and handled numerically. To minimise uncertainties incurred during experimental measurement, several important issues pertaining to experimental set-up should be taken into serious attention before conducting the experiment. These include the identification of the boundary condition of the real structure, the suitability of measurement grid (number of measurement degree of freedoms (DOFs)), as well as impact and response received locations (input and output DOFs), the hardness suitability of impact hammer tip, as well as the suitability of block size and sampling rate. By addressing these issues appropriately, the level of uncertainties incurred during experiment could greatly be reduced. It is noteworthy that these issues are dependent on the specimen dimensions, as well as the resonant frequency range of the specimen. The first five natural modes of the plates are utilised in this research and a total of 25 measurement DOFs are defined over each plate of similar dimensions. The impact location (input DOF) is roved from point 1 to point 25, while the response received location (output DOF) is fixed at a particular point. In order to accurately capture all the modes of interest, it is necessary to place the accelerometer appropriately at locations that incur high responses of the corresponding modes, instead of those that are near to the nodal axes of the corresponding modes. Therefore, EMA is carried out a few times by placing the accelerometer at arbitrary locations to figure out the best locations for accurate acquisition of the modes of interest. In this study, point 1, point 3 and point 15 are discovered to be the best locations for capturing all the first five modes.

3.4.3.2 Numerical evaluation

(a) *Method 1: Two-stage derivative-based method*

For validation purposes, the proposed algorithm is tested on real specimens, namely, acrylonitrile-butadiene-styrene (ABS) plate and aluminium composite panel (ACP). Only F-F-F-F (F: Free) boundary condition is studied due to the ease of implementation, unlike the other boundary conditions requiring proper clamping or supporting devices for effective execution. The details of stage 1 and stage 2 are elaborated as follows:

(i) *Stage 1: The use of natural frequencies*

There are slight differences in the procedures between the reference and experimental plates. In the study of experimental plates, considering the presence of uncertainties during experimental measurement, regularization is deemed necessary to accommodate the effects due to uncertainties. In the study of the acrylonitrile-butadiene-styrene (ABS) plate, since experimental results are involved, regularization is needed to accommodate the effects due to uncertainties. As stated in (Link, 1999), the recommended value of regularization parameter ranges from 0 to 0.3 depending on problem suitability. The regularization parameter is often selected based on the plot of stiffness change norm against residual norm (L-curve), such that the selected parameter is placed in the trade-off range between the stiffness change norm and residual norm. In this study, the regularization parameters for all the four elastic properties are defined by 0.0030, selected based on the plot of stiffness change norm against residual norm. Similarly, in the investigation of the aluminium composite panel (ACP), the selected regularization parameters are 0.0030 for all the four elastic properties, as referred to the graph of stiffness change norm against residual norm (L-curve) in stage 1. The in-plane elastic moduli, in-plane shear modulus and major Poisson's ratio are updated using first five natural frequencies and the updating procedures are similar to those explained above.

(ii) ***Stage 2: The use of mode shapes***

The updating procedures are slightly different from those of reference plates. Instead of only involving the in-plane shear modulus (G_{xy}) and major Poisson's ratio (ν_{xy}) in stage 2, the elastic moduli (E_x, E_y) are also updated in stage 2 because of the additional room for improvement caused by the presence of uncertainties. It is well known that the in-plane elastic moduli are relatively more sensitive to natural frequencies, and logically, the accuracy of elastic moduli determined in stage 1 can be inferred to be sufficiently good. Since the presence of uncertainties is inevitable during experiment, these elastic moduli should be taken into account as well under the condition that the changes in the elastic moduli are confined while the changes in the in-plane shear modulus and major Poisson's ratio are relatively less restricted by assigning appropriate values of regularization. In stage 2, the regularization parameters for the elastic moduli are both defined by the maximum recommended value of 0.3000, while the regularization parameters for the in-plane shear modulus and Poisson's ratio are both set equal to 0.0500 as suggested in (Link, 1999). In addition, the scaling factor for both the acrylonitrile-butadiene-styrene (ABS) plate and aluminium composite panel (ACP) are defined by 100 and 10, respectively.

(b) ***Method 2: Meta-heuristic optimisation method (Hybrid GA-ACO-PSO)***

The proposed method with the relatively best error function is adopted in the study and it has been proven that the use of the frequency response function (FRF) error function is relatively more effective in identifying the in-plane shear modulus and Poisson's ratio as compared to the use of the natural frequency error function. It is known that the presence of uncertainties in experiment is inevitable. In a consequence, to mitigate the effects due to uncertainties, a slightly different two-stage approach is adopted for identifying the elastic properties of the acrylonitrile-butadiene-styrene (ABS) plate and aluminium composite panel (ACP), in which, the natural frequency error

function is employed initially to determine the elastic properties of the ABS plate and ACP within bounded search regions. In stage 2, the search areas are narrowed down and the FRF error function is utilised to specifically improve the identifiability of the in-plane shear modulus and Poisson's ratio. It should be highlighted that before proceeding to stage 2, it is important to select relevant FRFs for effective execution of the identification process. In the reference studies, all the first five modes are taken into account and the entire 25 sets of FRFs are involved in the computation. The drawback of this approach without adopting any scheme of FRF selection consists in its limited ability in handling uncertainties. Therefore, in the experimental studies, before proceeding to stage 2, a two-level FRF selection scheme is introduced. The first level involves the mode selection which is made based on the sensitivity of modes with respect to the elastic properties of the plates. The selection of modes is required basically to specify and narrow down the frequency range of the FRFs. Modes that are sensitive to the in-plane shear modulus, as well as the Poisson's ratio, are of great interests for this study as the involvement of the FRFs containing these modes in stage 2 is believed to be important in improving the identifiability of both the parameters. Subsequently, in the second level, the selection of FRF is made by referring to the node position (or impact location) that lies in the high response regions of the mode of interest determined from the first level. Those FRFs yielded from the impact locations incurring high responses of modes that are sensitive to the in-plane shear modulus and the Poisson's ratio are said to be useful and helpful in improving the identifiability of both the parameters. In some cases, those FRFs obtained from the impact locations incurring relatively low responses of modes can as well be useful under the condition that the presence of modes of interest in the FRFs must be pronouncedly visible. The input settings for the proposed hybrid algorithm in both stage 1 (natural frequency error function) and stage 2 (FRF error function) are similar to those presented in Table 3.7.

CHAPTER 4: RESULTS AND DISCUSSIONS

4.1 Introduction

This chapter comprises four main sections. It begins with the study of the two-stage derivative-based method, followed by the investigation of the meta-heuristic hybrid optimisation method. In the following section, the two proposed methods are validated experimentally and lastly, the performance comparison between the two-stage derivative-based method and meta-heuristic hybrid optimisation method is presented and discussed.

4.2 Method 1: Two-stage derivative-based method

This study consists of four sections, namely, accuracy study, repeatability study, convergence study and analysis of the results. In the first three sections, the identification results are presented and discussed, while, in the last section, the results obtained are critically analysed and justified. Notably, the benchmark natural frequencies and mode shapes, as well as the sensitivity graphs of the aluminium and graphite epoxy plates under different sets of boundary conditions are demonstrated in Appendix B.

4.2.1 Accuracy of two-stage derivative-based method in reference plates

In the investigation of the aluminium plate, it can be observed from Table 4.1 that the absolute percentage errors of elastic moduli and in-plane shear modulus with respect to reference values during stage 1 are relatively small (below 2%) if compared to those of the identified Poisson's ratio (around 9%). The in-plane shear modulus determined during stage 1 are found to be sufficiently good in terms of accuracy with comparatively low absolute percentage errors (below 1.3%) due to the issues associated with material isotropy. For isotropic materials, the sensitivity of natural frequencies with respect to the in-plane shear modulus is claimed to be relatively higher than those for composite

materials. In this study, the reference aluminium plate is known to be isotropic, therefore, in the absence of uncertainty, stage 1 is said to be sufficient for the identification of the in-plane shear modulus. Since the absolute percentage error of the evaluated Poisson's ratio are comparatively larger (around 9%), it is necessary to further improve the identifiability of the Poisson's ratio. Therefore, stage 2 is performed and the absolute percentage error of the Poisson's ratio can be seen experiencing a significant reduction from around 9% in stage 1 to around 4% in stage 2. Indirectly, this shows that a considerable sensitivity exists between mode shape and the Poisson's ratio which leads to the accurate identification of the Poisson's ratio and therefore, necessitating the implementation of stage 2. Meanwhile, the in-plane shear modulus experiences a slight deterioration in stage 2 under F-F-F-F boundary condition by at most 0.1254%. This occurrence can be explained by the isotropic stiffness rigidity that relates the Poisson's ratio and in-plane shear modulus, such that, when the stiffness rigidity experiences changes, the Poisson's ratio and in-plane shear modulus are affected as well.

Table 4.1: Identification results of aluminium plate under three different boundary conditions

	Ref.	Stage 1: Natural frequency		Stage 2: Mode shape	
		Initial	Updated	Initial	Updated
F-F-F-F					
E_x (GPa)	72.4	55	72.1630 [0.3273]	72.1630	72.1630 [0.3273]
E_y (GPa)	72.4	55	72.0349 [0.5043]	72.0349	72.0349 [0.5043]
G_{xy} (GPa)	28	15	27.7922 [0.7421]	27.7922	27.7571 [0.8675]
ν_{xy}	0.33	0.3	0.2999 [9.1212]	0.2999	0.3179 [3.6667]
C-F-F-F					
E_x (GPa)	72.4	55	72.6179 [0.3010]	72.6179	72.6179 [0.3010]
E_y (GPa)	72.4	55	72.5016 [0.1403]	72.5016	72.5016 [0.1403]
G_{xy} (GPa)	28	15	27.9399 [0.2146]	27.9399	27.9364 [0.2271]
ν_{xy}	0.33	0.3	0.2997 [9.1818]	0.2997	0.3147 [4.6364]
C-C-F-C					
E_x (GPa)	72.4	55	73.8295 [1.9745]	73.8295	73.8295 [1.9745]
E_y (GPa)	72.4	55	73.4772 [1.4878]	73.4772	73.4772 [1.4878]
G_{xy} (GPa)	28	15	28.3556 [1.2700]	28.3556	28.3763 [1.3439]
ν_{xy}	0.33	0.3	0.3009 [8.8182]	0.3009	0.3139 [4.8788]
#[n]denotes the absolute percentage error with respect to the reference value.					

In the study of the graphite epoxy plate, as shown in Table 4.2, the overall identified elastic moduli are relatively more accurate with absolute percentage errors of not more than 2.4% in stage 1, while, the absolute percentage errors of the in-plane shear modulus and the major Poisson's ratio with respect to the reference values are more than 2.6% in stage 1. Therefore, the use of mode shapes in stage 2 is suggested to improve the identifiability of the in-plane shear modulus and the major Poisson's ratio. From Table 4.2, the identified in-plane shear modulus in stage 2 under three different boundary conditions is more accurate with absolute percentage errors reduced from the most 4.6444% in stage 1 to the least 1.1816% in stage 2, while the absolute percentage errors of the Poisson's ratio are reduced from the most 9.0909% to the least 1.5000%. The maximum percentage of improvement for both the in-plane shear modulus and Poisson's ratio are 3.0717% and 6.2273%, respectively. This indirectly implies that a considerable influence exists between mode shapes and the evaluated in-plane shear modulus as well as the identified major Poisson's ratio.

Table 4.2: Identification results of graphite epoxy plate under three different boundary conditions

	Ref.	Stage 1: Natural frequency		Stage 2: Mode shape	
		Initial	Updated	Initial	Updated
F-F-F-F					
E_x (GPa)	127.9	110	127.8279 [0.0564]	127.8279	127.8279 [0.0564]
E_y (GPa)	10.27	9	10.4585 [1.8354]	10.4585	10.4585 [1.8354]
G_{xy} (GPa)	7.312	6	6.9724 [4.6444]	6.9724	7.1783 [1.8285]
ν_{xy}	0.22	0.2	0.2000 [9.0909]	0.2000	0.2058 [6.4545]
C-F-F-F					
E_x (GPa)	127.9	110	128.2560 [0.2783]	128.2560	128.2560 [0.2783]
E_y (GPa)	10.27	9	10.5074 [2.3116]	10.5074	10.5074 [2.3116]
G_{xy} (GPa)	7.312	6	7.0010 [4.2533]	7.0010	7.2256 [1.1816]
ν_{xy}	0.22	0.2	0.2015 [8.4091]	0.2015	0.2067 [6.0455]
C-C-F-C					
E_x (GPa)	127.9	110	127.4364 [0.3625]	127.4364	127.4364 [0.3625]
E_y (GPa)	10.27	9	10.2500 [0.1947]	10.2500	10.2500 [0.1947]
G_{xy} (GPa)	7.312	6	7.1158 [2.6833]	7.1158	7.2189 [1.2732]
ν_{xy}	0.22	0.2	0.2030 [7.7273]	0.2030	0.2233 [1.5000]

[#][n]denotes the absolute percentage error with respect to the reference value.

4.2.2 Repeatability of two-stage derivative-based method in reference plates

Five independent runs of this approach are executed using a fixed set of initial values. The results for each run turn out the same and hence, indicating 100% repeatability. This can be explained by the nature of the method, in which, it is known to be deterministic. In contrast to a probabilistic derivative-based method, such as bayesian estimation approach, in which, each run of simulation leads to different outcomes even with the same input of initial guesses, the present deterministic approach shows superiority in the aspect of repeatability over the probabilistic derivative-based approach.

4.2.3 Convergence of two-stage derivative-based method in reference plates

From Table 4.3, it can be observed that the updating process of stage 2 consumes relatively more computational time as compared to that of stage 1 due to the relatively bulk involvement of local information associated with mode shapes in stage 2 as well as the relatively tedious procedures of obtaining the derivatives of mode shapes with respect to design parameters. Despite consuming a maximum average computational time of 446.5720 seconds, which is equivalent to about seven minutes, the proposed two-stage derivative-based method can be considered the better method in the aspect of computational time, if compared to most of the meta-heuristic algorithms. The complete sets of computational time under each boundary condition are presented in Appendix C.

Table 4.3: Average computational time of the proposed two-stage derivative-based method

BC	Aluminium plate			Graphite epoxy plate		
	Stage 1 (s)	Stage 2 (s)	Total (s)	Stage 1 (s)	Stage 2 (s)	Total (s)
F-F-F-F	11.8644	325.2434	337.1078	11.9040	272.1712	284.0752
C-F-F-F	11.8410	434.7310	446.5720	22.9507	163.5534	186.5041
C-C-F-C	29.3750	271.8027	301.1777	17.3910	217.3293	234.7203

4.2.4 Analysis of the proposed two-stages derivative-based method in reference plates

Derivative-based method is known to be dependent on the initial values. Initial values that are further from the true values will cause divergence and thereby, affecting the solution quality. To effectively apply the proposed method, the range of the true values of the material must be known in advance. Otherwise, the application of this method is less effective. Instead of investigating the effects of using different sets of starting values, the feasibility of the proposed method is verified using different plates under different types of boundary conditions and the results reveal that the proposed method is effective in identifying the true elastic properties.

Results obtained from reference studies suggest that for purely isotropic materials under a condition where uncertainties are presumably absent, the use of the natural frequency error function (stage 1) is sufficient for effective identification of the elastic moduli and in-plane shear modulus. The use of mode shape error function (stage 2) is recommended to improve the Poisson's ratio. The use of the natural frequency error function in stage 1 for composite materials provides several gaps for improvement in the identified in-plane shear modulus and Poisson's ratio. These findings can be explained by the reduced equation of the in-plane shear modulus derived from the stiffness matrix. The in-plane shear modulus of isotropic materials is theoretically related to the elastic modulus $\left(G = \frac{E}{2(1-\nu)}\right)$ which is relatively more sensitive to natural frequencies. Therefore, in the absence of uncertainties, a condition equivalent to an ideal case, the use of the natural frequency error function in stage 1 is sufficient in determining the in-plane shear modulus of isotropic materials. The in-plane shear modulus of orthotropic composite materials is theoretically an independent parameter. Hence, the use of the mode shape error function in stage 2 is necessary to further

improve the identifiability of the in-plane shear modulus. In experimental studies, these discoveries can be relevant references in accommodating the presence of uncertainties.

In the study of composite material, the identifiability of the in-plane shear modulus does also show an overall improvement after the use of mode shape in stage 2 due to the relationship between shear modulus and twisting modes. By fundamental definition, shear modulus is the ratio of shear stress to shear strain. Stress is a global parameter and can be found in shear modulus as well as Young's modulus. Since natural frequency is also a global parameter, the use of natural frequency error function is sufficiently good to identify shear modulus and Young's modulus. However, for shear modulus, the accuracy can be further improved by involving the use of mode shapes as shear modulus is much related to twisting modes (Hendrickson, 1963). These modes are unique and sometimes they are not symmetric and not uniform. Due to their uniqueness, the presence of twisting modes in the identification process appears to be more significant and influential to the change in in-plane shear modulus if compared to normal bending modes. In the present study, the first six non-rigid body modes are involved in the identification of the aluminium and graphite epoxy reference plates. In the investigation of the aluminium plate, mode 1, 4 and 5 are twisting modes under F-F-F-F boundary condition, while mode 2, 5 and 6 are twisting modes under C-F-F-F boundary condition, whereby under C-C-F-C boundary condition, mode 3, 5 and 6 are twisting modes. Meanwhile, in the study of graphite epoxy plate, mode 1, 3, and 6 are twisting modes under F-F-F-F boundary condition, while mode 1, 3, 4, 5, and 6 are twisting modes under C-F-F-F boundary condition and lastly, mode 2, 4, 5, and 6 are twisting modes under C-C-F-C boundary conditions. Therefore, by using a two-stage approach involving natural frequencies and mode shapes, the identifiability of in-plane shear modulus can be further improved.

Furthermore, the inclusion of mode shapes has also been proven vital in improving the identifiability of the Poisson's ratio and the results above indirectly imply that mode shapes are considerably sensitive with respect to the Poisson's ratio. Relatively, the Poisson's ratio can be said to be more sensitive to bending modes than twisting modes. This phenomenon can be explained by the composition of the Poisson's ratio, that defines the coupling effect between the normal deformations in two orthogonal directions (Lauwagie T. et al., 2010):

$$v_{ij} = -\frac{\varepsilon_i}{\varepsilon_j} \quad (4.1)$$

where, ε_i is the normal strain in the i -direction, while ε_j is the normal strain in the j -direction induced by the coupling effect. In a simple interpretation, Poisson's ratio can be known as the ratio of shortening strain (ε_i) to tensile strain (ε_j). Scientifically, the Poisson's ratio is associated with mode shapes as it involves coupled strains, while mode shapes are fundamentally composed of the displacement of nodes. In fact, a relationship between strain and displacement does exist, such that strain is often expressed as mode curvature and displacement is obtained via the second integration of the mode curvature (strain) (Wang et al., 2014). Both strain and displacement are much related to the motion of an object that defines mode shapes. Compared to natural frequency, mode shape is more localized in the sense that the flexural or twisting movement of the plate is entirely determined and expressed in terms of displacement at each designated node of the plate at a particular natural frequency. Unlike a natural frequency, more information and details can be explored and retrieved from a mode shapes. Referring to the fundamental formula of the Poisson's ratio which is defined by the ratio of shortening strain and tensile strain, it can be logically related to bending modes such that in these bending modes, the shortening and tensile effects due to the bending motion are more significant as compared to those of twisting modes. Hence, it

draws a relatively close relationship between the Poisson's ratio and bending modes. In the study of the aluminium plate, mode 2 and 3 are bending modes under F-F-F-F boundary condition, while mode 1, 3 and 4 are bending modes under C-F-F-F boundary condition, whereby under C-C-F-C boundary condition, mode 1, 2 and 4 are bending modes. Meanwhile, in the study of the graphite epoxy plate, mode 2, 4, and 5 are bending modes under F-F-F-F boundary condition, while mode 2 is bending modes under C-F-F-F boundary condition and lastly, mode 1 and 3 are bending modes under C-C-F-C boundary conditions. Consequently, it can be observed that the use of mode shape error function in stage 2 does improve the identifiability of the Poisson's ratio. In short, the use of the proposed two-stage approach is recommended for effective identification of the in-plane shear modulus and the Poisson's ratio of a composite structure.

4.3 Method 2: Meta-heuristic hybrid optimisation method (Hybrid GA-ACO-PSO)

The present study consists of three main sections, including, verification using test functions and engineering design problems, application in vibrational material identification and lastly, comparative study of different error functions. The first section presents and discusses the results obtained from the feasibility study of the proposed hybrid method in solving unconstrained (test functions) and constrained (engineering design problems) problems. The next section demonstrates and analyses the results obtained from the applicability study of the proposed hybrid method in material identification involving the commonly-used error function. In the last section, the effectiveness of the proposed hybrid algorithm incorporated with different error functions is investigated and discussed. Notably, the benchmark natural frequencies and mode shapes, as well as the sensitivity graphs of the aluminium and graphite epoxy plates under different sets of boundary conditions are demonstrated in Appendix B.

4.3.1 Verification using test functions and engineering design problems

The applicability of the proposed hybrid algorithm on test functions (unconstrained, unimodal, multimodal) and engineering design problems (constrained) (Himmelblau, 1972; Kannan & Kramer, 1994; Rao, 2009; Sandgren, 1990) are validated in this section. Basically, there are two main sections, namely, test functions and engineering design problems. For each section, there are four sub-sections, namely, effects of feature variations, effects of parameter variations, performance comparison between the proposed and conventional algorithms and lastly, performance comparison between the proposed and published algorithms. It should be noted that the data are presented in four decimal places.

4.3.1.1 Test functions

(a) Effects of feature variations in solving test functions

Two features, namely, fixed refined mutation (feature 1) and logarithmically-spaced refined mutation (feature 2) are proposed. The accuracy and repeatability of the features are studied and compared in terms of average minimised function value error ($f_i - F_i$) and standard deviation, as shown in Table 4.4. Between feature 1 and feature 2, the least average minimised function value and standard deviation for each function are shown in bold. Feature 2 performs better when dealing with multimodal problems as compared to feature 1. This can be explained by the strength of feature 2 in inducing an logarithmic increase in the search precision over iterations. For feature 1, the search pace is fixed constant, thereby, restricting the change in the search precision. Between multimodal and unimodal problems, feature 1 is more effective in solving unimodal problems. Feature 1 also exhibits superiority in solving unimodal functions over feature 2. The reason consists in the effective match between the constant search precision of feature 1 with the order of magnitude of the solution, and hence, yielding better results. Overall,

the logarithmically-spaced refined mutation (feature 2) can be claimed to be the better choice in solving unconstrained problems.

Table 4.4: Average minimised function value error and standard deviation achieved by the proposed hybrid algorithm with different features

	Test functions	Average minimised function value errors ($f_i - F_i$)		Standard deviation	
		Feature 1	Feature 2	Feature 1	Feature 2
	Multimodal				
F_1	Ackley	1.1772E+00	8.8818E-16	1.1427E+00	0.0000E+00
F_2	Griewangk	3.1084E-01	3.2933E-03	2.1346E-01	6.1861E-03
F_3	Rastrigin	1.2689E+01	0.0000E+00	5.7347E+00	0.0000E+00
F_4	Rosenbrock	4.6365E+01	2.6569E+01	2.2434E+01	1.0254E+00
F_5	Schwefel	1.0486E+03	5.8070E+02	5.0515E+02	3.2303E+02
F_6	Weierstrass	2.3423E+00	0.0000E+00	1.0035E+00	0.0000E+00
	Unimodal				
F_7	Schwefel P2.22	2.3768E-01	1.1757E-54	1.0959E-01	1.7281E-54
F_8	Sphere	5.1542E-04	3.7596E-90	4.7599E-04	1.6592E-89
F_9	Styblinski-Tang	0.0000E+00	7.1340E-02	0.0000E+00	2.2734E-02
F_{10}	Zakharov	1.7263E+01	2.0131E+01	7.1408E+00	1.1865E+01

(b) Effects of parameter variations in solving test functions

The values of aa and bb , as well as the number of mutation points may affect the performance of logarithmically-spaced refined mutation (feature 2). To determine the relatively best combination of parameters in solving unconstrained problems, the effects due to variations in the mentioned parameters are investigated. Several values of aa and bb are investigated, including, $aa = [(1.0000, 0.1000), (1.0000, 0.0100), (1.0000, 0.0010), (0.1000, 0.0100), (0.1000, 0.0010), (0.1000, 0.0001), (0.0100, 0.0010), (0.0100, 0.0001), (0.0100, 1.0000E-05)]$ and $bb = 2aa$. For each parameter aa and bb , various number of mutation points are studied, such as $D = [10, 6, 3, 1]$, in which, out of 30 dimensions, there are 10, 6, 3, or 1 dimension(s) undergone the proposed refined mutation. The accuracy of each combination of parameters is evaluated in terms of average minimised function value errors ($f_i - F_i$), as presented in Appendix D. The values (in bold) are the least average minimised function value errors. To identify the best combination of parameters at a statistical level, average ranking of Friedman test is conducted, as shown in Table 4.5 and Table 4.6. Parameter $aa = (0.01, 0.00001)$ yields

the least ranking value, indicating the relatively most effective parameter among all the variations. The sequence from the most to the least effective parameter aa is listed as follows: (0.0100-0.00001), (0.0100-0.0010), (0.0100-0.0001), (0.1000-0.0001), (0.1000-0.0010), (0.1000-0.0100), (1.0000-0.0100), (1.0000-0.0010), (1.0000-0.1000). Furthermore, the use of 10 refined mutation points is found to be the relatively best choice, as shown in Table 4.6.

Table 4.5: Friedman test on aa variations

No.	Parameter aa	Ranking
1	1.0000–0.1000	7.1500
2	1.0000–0.0100	6.1375
3	1.0000–0.0010	6.1625
4	0.1000–0.0100	5.1125
5	0.1000–0.0010	4.5125
6	0.1000–0.0001	4.4125
7	0.0100–0.0010	3.7375
8	0.0100–0.0001	4.3125
9	0.0100–1.0000E–05	3.4625

Table 4.6: Friedman test on D variations

No.	Parameter D	Ranking
1	10	2.2944
2	6	2.3167
3	3	2.6000
4	1	2.7889

(c) Performance comparison between the proposed and conventional algorithms in solving test functions

Under a fixed number of evaluations, the accuracy, repeatability and convergence of all the involved algorithms are investigated, in terms of average minimised function value errors, standard deviations and average computational time, as presented in Table 4.7, Table 4.8 and Table 4.9, respectively. From Table 4.7 and Table 4.8, it can be seen that the proposed hybrid algorithm outperforms the other conventional algorithms, in terms of accuracy and repeatability for all the 10 test functions. This can be explained by the more complete search coverage of the proposed hybrid algorithm, in which, the

collaboration between genetic algorithm (GA) and ant colony optimisation (ACO) enhances the exploratory search, while the incorporation between genetic algorithm (GA) and particle swarm optimisation (PSO) improves the exploitative search. However, the proposed hybrid algorithm is found to be less convincing in terms of computational time, in which, it consumes the third least computational time among the four algorithms. This drawback is said to be caused by the time-consuming procedures of ACO operator in the composition of the proposed hybrid algorithm. The effect of this drawback may not be significant when it is used in complex practical applications, such as, material identification, etc. Overall, the proposed hybrid algorithm is proven to be the relatively best choice among all the algorithms in solving unconstrained problem due to its promising accuracy and repeatability as well as its satisfactory convergence.

Table 4.7: Average minimised function value error ($f_i - F_i$) achieved by GA, ACO, PSO and the proposed hybrid algorithm

	Test functions	GA	ACO	PSO	Proposed
	Multimodal				
F_1	Ackley	5.5367E-01	7.8042E+00	6.2996E+00	8.8818E-16
F_2	Griewangk	9.9315E-01	5.6317E+00	2.8562E+01	0.0000E+00
F_3	Rastrigin	1.2400E-01	1.0574E+02	1.2844E+02	0.0000E+00
F_4	Rosenbrock	5.4078E+01	9.0607E+01	1.5869E+02	2.6349E+01
F_5	Schwefel	1.3815E+03	4.8440E+02	3.2182E+03	3.3993E+01
F_6	Weierstrass	4.0285E-01	1.0914E+01	1.0998E+01	0.0000E+00
	Unimodal				
F_7	Schwefel P2.22	3.2906E-01	2.3460E+01	7.9540E+00	2.3980E-197
F_8	Sphere	9.6391E-02	1.4398E+00	1.3029E+00	0.0000E+00
F_9	Styblinski-Tang	5.8215E+01	2.6548E+02	1.2046E+02	7.1340E-02
F_{10}	Zakharov	1.7549E+02	1.0656E+02	5.0452E+01	5.4603E-135

Table 4.8: Standard deviation achieved by GA, ACO, PSO and the proposed hybrid algorithm

	Test functions	GA	ACO	PSO	Proposed
	Multimodal				
F_1	Ackley	7.4119E-01	6.5273E-01	1.6687E+00	0.0000E+00
F_2	Griewangk	5.2668E-01	1.6215E+00	1.4879E+01	0.0000E+00
F_3	Rastrigin	2.0830E-01	6.2155E+00	3.1032E+01	0.0000E+00
F_4	Rosenbrock	3.0371E+01	2.6881E+01	9.7180E+01	1.0623E+00
F_5	Schwefel	1.1541E+03	1.5281E+02	7.2036E+02	1.2081E+01
F_6	Weierstrass	6.9991E-01	9.0727E-01	2.2248E+00	0.0000E+00
	Unimodal				
F_7	Schwefel P2.22	4.0579E-01	5.6364E+00	2.5258E+00	0.0000E+00
F_8	Sphere	1.6115E-01	3.2818E-01	1.1344E+00	0.0000E+00
F_9	Styblinski-Tang	2.9139E+01	1.2145E+02	3.9523E+01	2.2734E-02
F_{10}	Zakharov	6.2568E+01	2.8334E+01	2.9283E+01	2.9404E-134

Table 4.9: Average computational time (s) consumed by GA, ACO, PSO and the proposed hybrid algorithm

	Test functions	GA	ACO	PSO	Proposed
	Multimodal				
F_1	Ackley	6.7591	34.0530	3.9075	17.5637
F_2	Griewangk	6.5775	33.3621	2.7232	17.2906
F_3	Rastrigin	6.0198	32.8629	2.1511	16.6845
F_4	Rosenbrock	6.2386	43.0278	2.2772	18.0221
F_5	Schwefel	6.1859	32.4051	3.1556	16.5884
F_6	Weierstrass	65.9326	91.4274	63.4896	78.1854
	Unimodal				
F_7	Schwefel P2.22	5.6452	32.3744	2.5993	19.5688
F_8	Sphere	5.6424	32.1542	2.6287	16.0283
F_9	Styblinski–Tang	6.6552	33.0512	3.6925	17.1748
F_{10}	Zakharov	7.8900	35.0688	4.8395	17.8307

(d) Performance comparison between the proposed and published algorithms in solving test functions

A comparative study of the proposed hybrid algorithm with respect to established algorithms, namely, CPSO-H (Van den Bergh & Engelbrecht, 2004), CLPSO (Liang et al., 2006), APSO (Zhan et al., 2009), GOPSO (Wang et al., 2011), DNSCLPSO (Wang et al., 2013) and DNPSO (Wang et al., 2013) in solving unconstrained test functions is conducted. For equal and fair comparison, in the proposed method, the maximum number of evaluations (200,040 including initial evaluations) and the number of generation (5,000) as well as the number of populations (20 for the proposed algorithm, 40 for the published algorithm) are set similar to those used in the published algorithms. 30 runs of simulations are conducted as well as the average minimised function value errors and standard deviations are recorded, as presented in Table 4.10 and Table 4.11. It should be noted that the comparison in terms of average computational time is not included due to the need of rebuilding and rerunning those established algorithms using a particular computing device for fair and equal comparison. Results are presented in two decimal places as they are originally presented in two decimal places by Wang et al. (2013). Five functions are tested and as seen from Table 4.10 and Table 4.11, the proposed hybrid algorithm performs better in terms of accuracy and repeatability if

compared to those established algorithms. Average ranking of Friedman test is conducted as well and the least ranking value indicates the best performing algorithm, as shown in Table 4.12. The performance of the algorithms from best to worst is listed as follows: Proposed, DNSPSO, GOPSO, DNSCLPSO, CPSO-H, CLPSO, and lastly, APSO.

Table 4.10: Average minimised function value error ($f_i - F_i$) achieved by established algorithms and the proposed hybrid algorithm

Test functions	CPSO-H	CLPSO	APSO	GOPSO	DNSCLPSO	DNSPSO	Proposed
Ackley	2.25E-14	1.85E-07	1.09E-14	3.43E-15	5.89E-16	5.89E-16	8.88E-16
Griewangk	1.90E-02	4.37E-09	1.20E-02	0.00E+00	0.00E+00	0.00E+00	0.00E+00
Rastrigin	3.32E+00	1.50E-04	6.27E+00	0.00E+00	2.20E+00	0.00E+00	0.00E+00
Weierstrass	4.74E-15	5.62E-07	4.77E-02	1.04E-08	0.00E+00	1.40E-13	0.00E+00
Sphere	1.29E-36	1.23E-13	9.60E-66	0.00E+00	1.23E-50	0.00E+00	0.00E+00

Table 4.11: Standard deviation achieved by established algorithms and the proposed hybrid algorithm

Test functions	CPSO-H	CLPSO	APSO	GOPSO	DNSCLPSO	DNSPSO	Proposed
Ackley	3.07E-14	2.70E-07	1.94E-14	1.59E-15	0.00E+00	0.00E+00	0.00E+00
Griewangk	8.81E-02	5.06E-08	9.14E-02	0.00E+00	0.00E+00	0.00E+00	0.00E+00
Rastrigin	1.18E+01	6.96E-04	1.28E+01	0.00E+00	1.96E+00	0.00E+00	0.00E+00
Weierstrass	3.67E-14	1.38E-06	4.08E-01	2.19E-08	0.00E+00	5.29E-14	0.00E+00
Sphere	7.61E-36	3.09E-13	1.57E-65	0.00E+00	2.86E-50	0.00E+00	0.00E+00

Table 4.12: Friedman test on accuracy and repeatability

No.	Algorithms	Accuracy	Repeatability
1	CPSO-H	5.6000	5.4000
2	CLPSO	5.8000	5.8000
3	APSO	5.8000	6.0000
4	GOPSO	3.1000	3.1000
5	DNSCLPSO	3.1000	3.2000
6	DNSPSO	2.4000	2.5000
7	Proposed	2.2000	2.0000

4.3.1.2 Engineering design problems

(a) *Effects of feature variations in solving engineering design problems*

As mentioned in the previous section, the two proposed features are fixed refined mutation (feature 1) and logarithmically-spaced refined mutation (feature 2). The details of the features can be referred to in the previous section. As proven in the previous

section, feature 2 is more effective than feature 1 in solving unconstrained problems in the presence of multimodality. However, in the application of engineering design problems, feature 1 shows great superiority over feature 2 in terms accuracy and repeatability, as presented in Table 4.13. This can be explained by the great compatibility between the fixed refined mutation (feature 1) and the nature of the engineering design problems. Feature 2 with relatively high search precision is found to be less effective in solving the engineering problems due to the relatively large order of magnitude of the solution as well as the restriction imposed on the change in the solution, such that, in some cases, the solutions are only allowed be expressed in terms of the multiples of a specified number. Hence, it can be seen that feature 1 outperforms feature 2 in achieving the least best, average and worst minimised objective function values (in bold) as well as the least standard deviation (in bold) for all the design problems. In short, feature 1 can be claimed to be the better choice in solving engineering design problems.

Table 4.13: Best, average and worst minimised objective function values as well as standard deviation achieved by the proposed hybrid algorithm with different features

Problems	Best	Average	Worst	Standard deviation
Himmelblau's				
Case 1				
Feature 1	-30665.5387	-30661.9060	-30638.7590	6.6061
Feature 2	-30665.5366	-30651.1961	-30530.8256	28.2546
Case 2				
Feature 1	-31025.5602	-31024.9575	-31021.0604	1.2189
Feature 2	-31025.5601	-31023.9266	-30990.1009	6.3263
Pressure vessel				
Feature 1	6059.7143	6387.6266	6820.5797	231.8850
Feature 2	6060.0994	6553.2902	7351.5945	340.5299
Welded beam				
Feature 1	1.7249	1.7431	1.8140	0.0253
Feature 2	1.7284	1.7589	1.8363	0.0290
Gear train				
Feature 1	2.7009E-12	9.1212E-10	4.5033E-09	1.1793E-09
Feature 2	2.7009E-12	1.1627E-09	6.1933E-09	1.2592E-09

(b) *Effects of parameter variations in solving engineering design problems*

The values of aa and bb may influence the performance of fixed refined mutation (feature 1). Hence, the effects due to variations in the mentioned parameters are studied to identify the relatively most effective parameters in handling constrained problems. Several values of aa and bb are investigated, including, $aa = [0.1000, 0.0100, 0.0010, 0.0001, 1.0000E-05]$ and $bb = 2aa$. The best, average and worst minimised objective function values as well as the standard deviations for all the problems are presented in Appendix E. Parameter $aa = 0.0010$ demonstrates great dominance over the others in achieving the least best, average, and worst minimised objective function values as well as standard deviations (in bold) for the first three problems. However, for gear train design problem, parameter $aa = 0.0100$ outperforms the other variations. Overall, parameter $aa = 0.0010$ is proven to be the relatively best choice of parameter, yielding the least values in the aspects of the best, average and worst evaluated solutions as well as the standard deviations of the evaluated solutions in the Friedman test (in bold), as demonstrated in Table 4.14. The sequence from the most to the least effective parameter aa in terms of the best evaluated solution is arranged as follows: 0.0010, 1.0000E-05, 0.0001, 0.1000 and lastly, 0.0100, while, the sequence from the best to the worst parameter aa in terms of the standard deviation is arranged as follows: 0.0010, 0.0100, 0.1000, 0.0001 and lastly, 1.0000E-05.

Table 4.14: Friedman test on parameter variations

No.	Parameter aa	Best	Average	Worst	Standard deviation
1.	0.1000	3.2500	2.5000	2.5833	2.6667
2.	0.0100	3.4167	1.8333	1.5833	1.6667
3.	0.0010	1.5833	1.0000	1.4167	1.1667
4.	0.0001	2.2500	3.3333	3.0833	3.0000
5.	1.0000E-05	2.0000	3.8333	3.8333	4.0000

(c) Performance comparison between the proposed and conventional algorithms in solving engineering design problems

The performance of the proposed hybrid algorithm in handling engineering design problems is studied and compared with those of conventional algorithms. The accuracy, repeatability and convergence are investigated and discussed.

(i) Accuracy and repeatability of meta-heuristic hybrid optimisation method in solving engineering design problems

In the study of engineering design problems, the accuracy of algorithms can be evaluated in terms of best, average, and worst minimised objective function values, while the repeatability can be evaluated in terms of standard deviations. As shown in Table 4.15, the proposed hybrid algorithm outperforms genetic algorithm (GA), ant colony optimisation (ACO) and particle swarm optimisation (PSO) in achieving the least best, average and worst minimised objective function values as well as the least standard deviation in Himmelblau's problem case 1. For case 2, the proposed hybrid algorithm still yields the least best minimised objective function value, however, PSO performs better in terms of repeatability (the least standard deviation). In pressure design problem, the proposed hybrid algorithm and PSO outperform GA and ACO, in terms of accuracy (best minimised objective function values), while the proposed hybrid algorithm demonstrates slight superiority in achieving the least standard deviation over PSO. In welded beam and gear train design problems, the proposed algorithm dominates in both the aspects of accuracy and repeatability. As a whole, it can be observed that GA relatively performs the worst in the aspect of accuracy and repeatability primarily due to inferiority in exploration performed by the standard mutation operator. On account of the strong dependence on the array of pheromone intensity leading to biased evaluation, ACO is also found to be less promising in the aspect of accuracy and repeatability. Furthermore, the reason leading to the

considerably great performance of PSO in terms of accuracy and repeatability can be explained by the balanced distribution between intensification and diversification. However, overall, the proposed hybrid algorithm relatively performs the best in the aspect of accuracy and repeatability as compared to those conventional algorithms, and this is attributable to its more complete search coverage.

Table 4.15: Best, average and worst minimised objective function values as well as standard deviation achieved by GA, ACO, PSO and the proposed hybrid algorithm

Problems	Best	Average	Worst	Standard deviation
Himmelblau's				
Case 1				
GA	-30234.3196	-29843.0334	-29476.4048	180.2950
ACO	-30545.5765	-30172.7197	-29396.6277	256.1369
PSO	-30665.5365	-30660.2530	-30589.9784	14.7625
Proposed	-30665.5387	-30661.9060	-30638.7590	6.6061
Case 2				
GA	-30481.1240	-30205.2505	-29839.6100	152.3820
ACO	-30879.4371	-30601.5052	-30221.8405	181.4626
PSO	-31025.5589	-31025.3516	-31021.2128	0.7766
Proposed	-31025.5602	-31024.9575	-31021.0604	1.2189
Pressure vessel				
GA	9338.6924	15756.4664	26533.9533	4437.4555
ACO	6361.3903	6887.0627	7668.7851	347.8406
PSO	6059.7143	6225.4735	7332.8415	280.3232
Proposed	6059.7143	6387.6266	6820.5797	231.8850
Welded beam				
GA	2.5853	3.5690	4.7892	0.6544
ACO	2.0948	3.3591	4.6244	0.7140
PSO	1.7250	1.7559	2.1777	0.0800
Proposed	1.7249	1.7431	1.8140	0.0253
Gear train				
GA	1.1661E-10	4.7066E-07	1.3320E-05	2.3866E-06
ACO	2.7009E-12	1.1156E-09	1.3125E-08	2.3846E-09
PSO	2.3078E-11	2.1080E-09	6.5123E-09	1.9745E-09
Proposed	2.7009E-12	9.7022E-10	2.3576E-09	8.8056E-10

(ii) ***Convergence of meta-heuristic hybrid optimisation method in solving engineering design problems***

In this context, convergence rate refers to the ability of an algorithm to converge to the solution involving lower number of evaluations. As seen from Figure 4.1 and Figure 4.2 (Himmelblau's problem), GA and ACO seem to have trapped at local minima in

early iterations, while the proposed hybrid algorithm and PSO demonstrate great performance in convergence rate. From Figure 4.3 (pressure vessel design problem), GA can be seen to have difficulty in finding the global solution since the beginning of iterations, while ACO shows slight superiority over GA but still falls into local minima in later iterations. The proposed hybrid algorithm is found leading PSO in terms of convergence in early iterations, however, in later iterations, PSO is found to be ahead of it. In welded beam design problem, GA and ACO are again found to have fallen into local traps, as shown in Figure 4.4. PSO still outperforms the proposed hybrid algorithm in terms of convergence rate. Lastly, from Figure 4.5 (gear train design problem), GA seems to have converged earlier than the rest, but it is trapped at local minima, whereas, the proposed hybrid algorithm performs the best in terms of convergence among all the algorithms. From a general perspective, it can be seen that GA experiences severe premature convergence due to issues pertaining to standard mutation of GA (exploration), as mentioned previously. In some cases, ACO exhibits considerably good convergence rate on account of its more directive search ability as well as its ability in eliminating redundant and repeated solutions. Unfortunately, falling into local traps is still the main concern due to the strong dependence on the pheromone intensity. Overall, PSO can be claimed to be slightly better than the proposed hybrid algorithm in terms of convergence rate as the drawbacks of GA operator in the aspect of convergence rate compromises the overall convergence rate of the proposed hybrid algorithm.

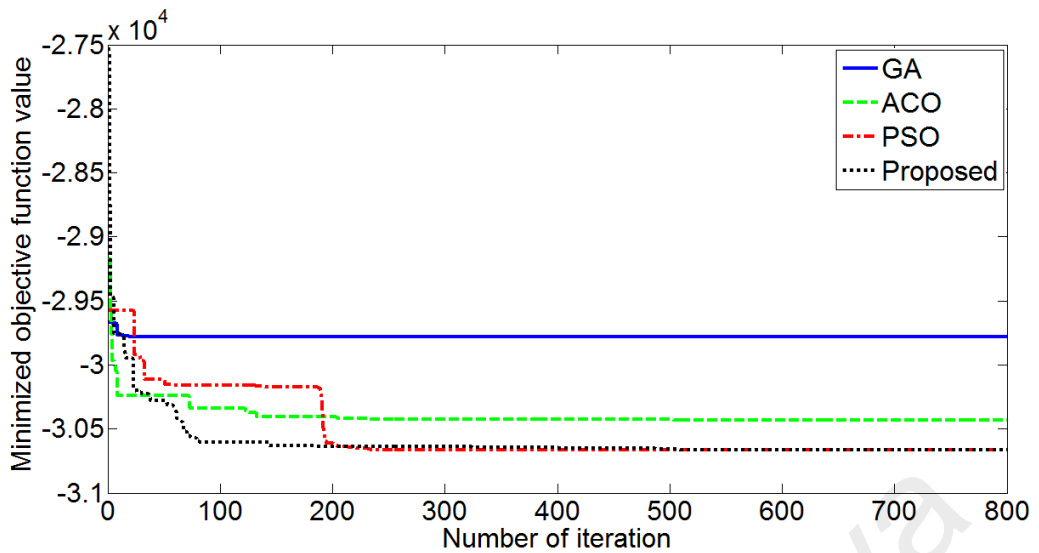


Figure 4.1: Convergence rate achieved by GA, ACO, PSO and the proposed hybrid algorithm for Himmelblau's non-linear optimisation problem case 1

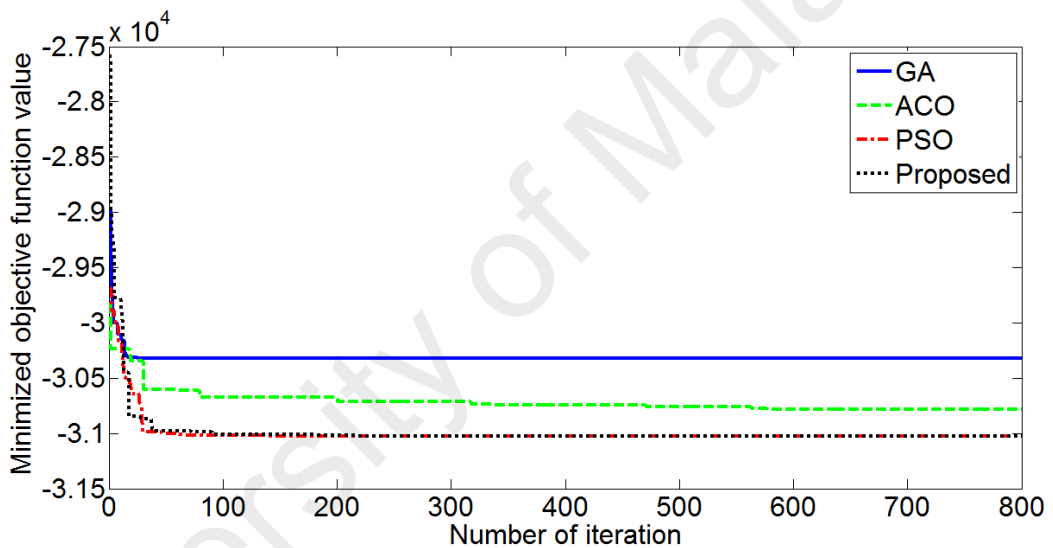


Figure 4.2: Convergence rate achieved by GA, ACO, PSO and the proposed hybrid algorithm for Himmelblau's non-linear optimisation problem case 1

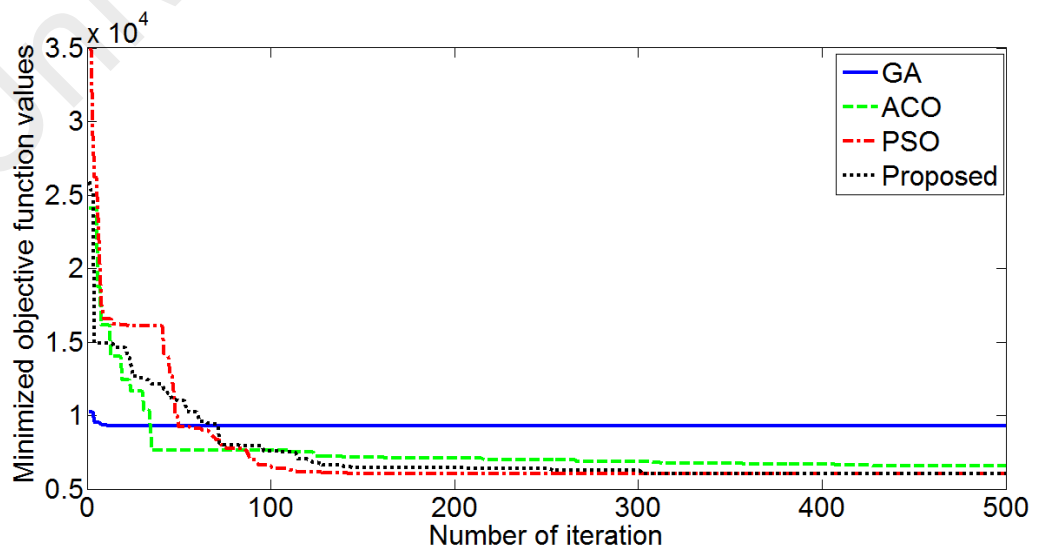


Figure 4.3: Convergence rate achieved by GA, ACO, PSO and the proposed hybrid algorithm for pressure vessel design optimisation problem

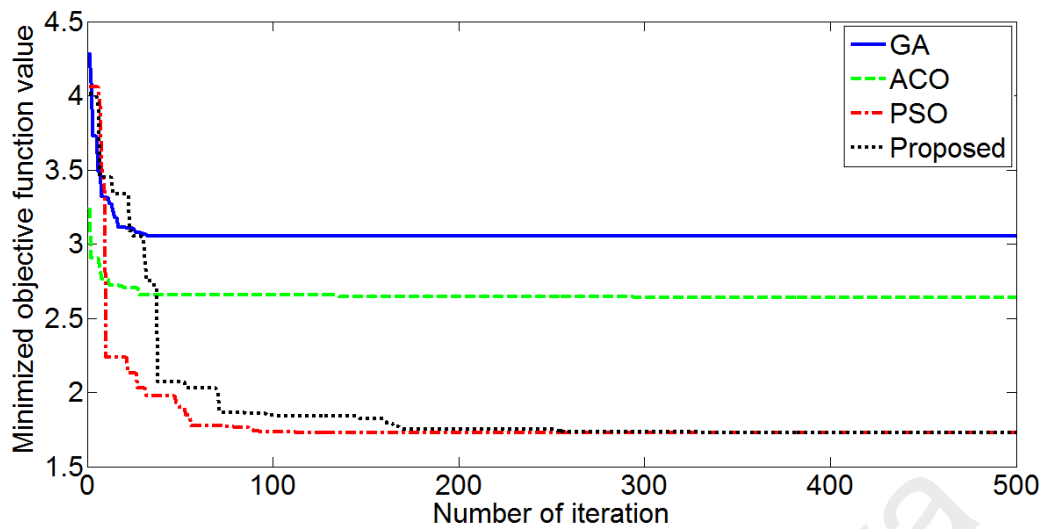


Figure 4.4: Convergence rate achieved by GA, ACO, PSO and the proposed hybrid algorithm for welded beam design optimisation problem

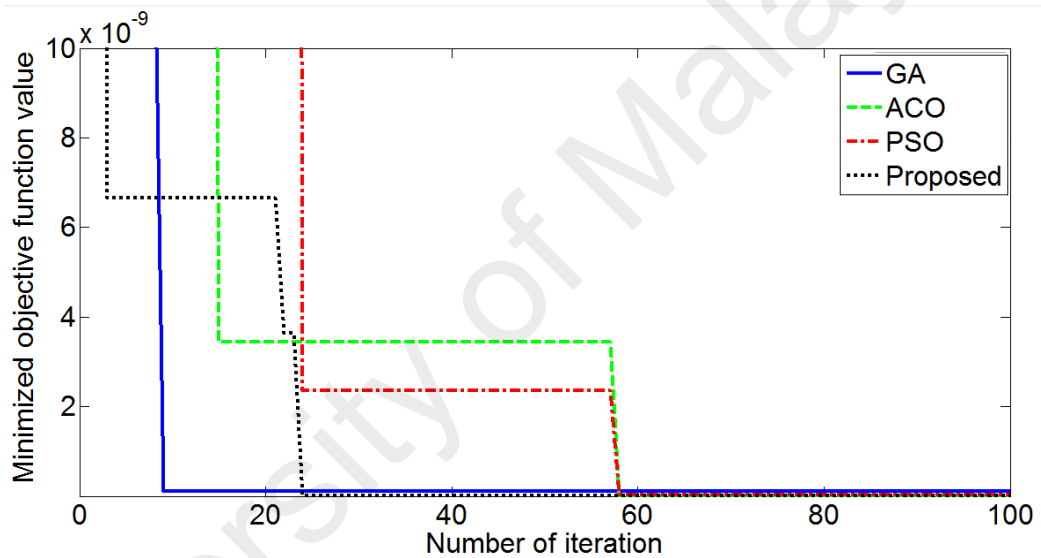


Figure 4.5: Convergence rate achieved by GA, ACO, PSO and the proposed hybrid algorithm for gear train design optimisation problem

Computational time refers to the total time consumed by the algorithm to converge to its solution. When dealing with Himmelblau's problem (case 1), PSO (0.5414s) consumes the least computational time compared to the proposed hybrid algorithm (1.9146s), GA (1.7780s) and ACO (2.1166s), as shown in Figure 4.6. The maximum computational time difference is about 1.6 seconds. On the other hand, from Figure 4.7 (case 2), the sequence from the least to most time-consuming algorithms is listed as follows: PSO (0.6261s), the proposed hybrid algorithm (1.7642s), GA (1.8213s) and lastly, ACO (1.9871s). The maximum difference is about 1.4 seconds. In the application

of pressure vessel design problem, the proposed hybrid algorithm is found to have consumed the most computational time (1.6525s), followed by GA (1.3600s), ACO (1.3497s) and lastly, PSO (0.5793s), as demonstrated in Figure 4.8. The maximum computational time difference is around 1.1 seconds. In the study of welded beam design problem, the most time-consuming algorithm is found to be ACO (1.4922s), tailed by the proposed hybrid algorithm (1.4558s), GA (1.3241s) and lastly, PSO (0.6741s), as depicted in Figure 4.9. The maximum computational time difference is approximately 0.9 seconds. Furthermore, from Figure 4.10 (gear train design problem), PSO still dominates in terms of computational time (0.0787s), followed by ACO (0.2442s), GA (0.2462s), and lastly, the hybrid algorithm (0.2760s). The maximum computational time difference is about 0.2 seconds. As a whole, PSO outperforms the other algorithms in consuming the least computational time, while, the proposed hybrid algorithm consumes considerably lesser computational time if compared to GA and ACO. The involvement of simple formulations is the main reason contributing to the least consumption of computational time in PSO. Despite the proposed hybrid algorithm showing inferiority in computational time, this shortcoming is relatively insignificant in practical applications, such as, in material identification.

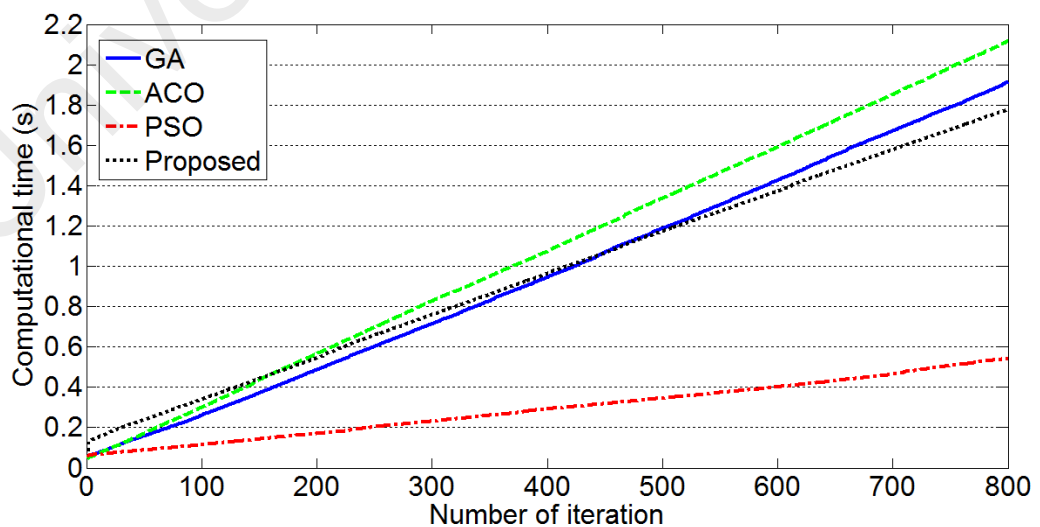


Figure 4.6: Computational time consumed by GA, ACO, PSO and the proposed hybrid algorithm for Himmelblau's non-linear optimisation problem case 1

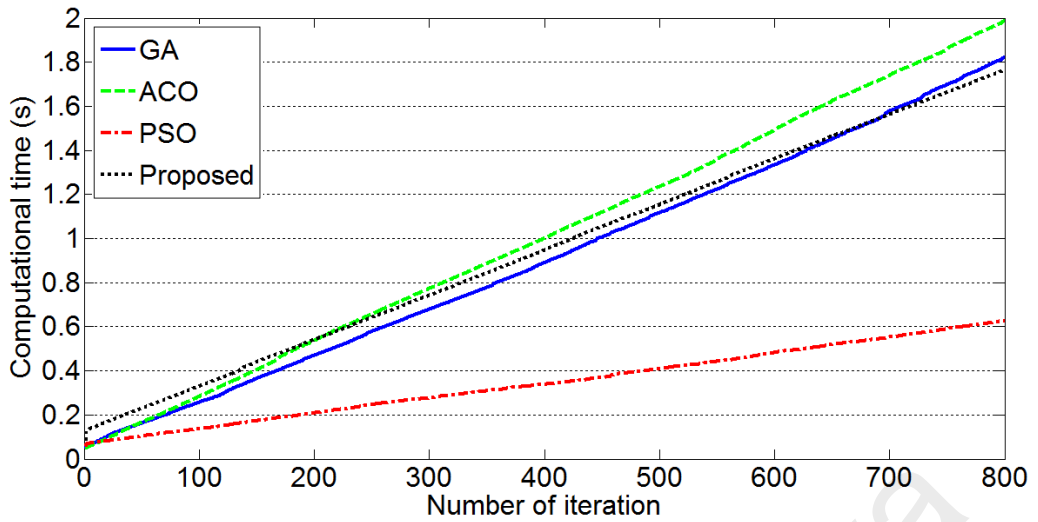


Figure 4.7: Computational time consumed by GA, ACO, PSO and the proposed hybrid algorithm for Himmelblau's non-linear optimisation problem case 2

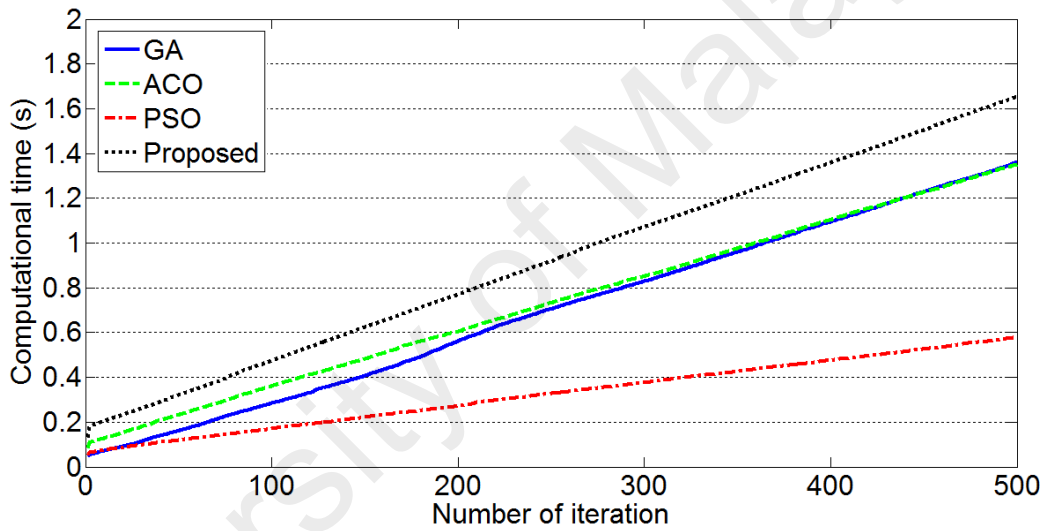


Figure 4.8: Computational time consumed by GA, ACO, PSO and the proposed hybrid algorithm for pressure vessel design optimisation problem

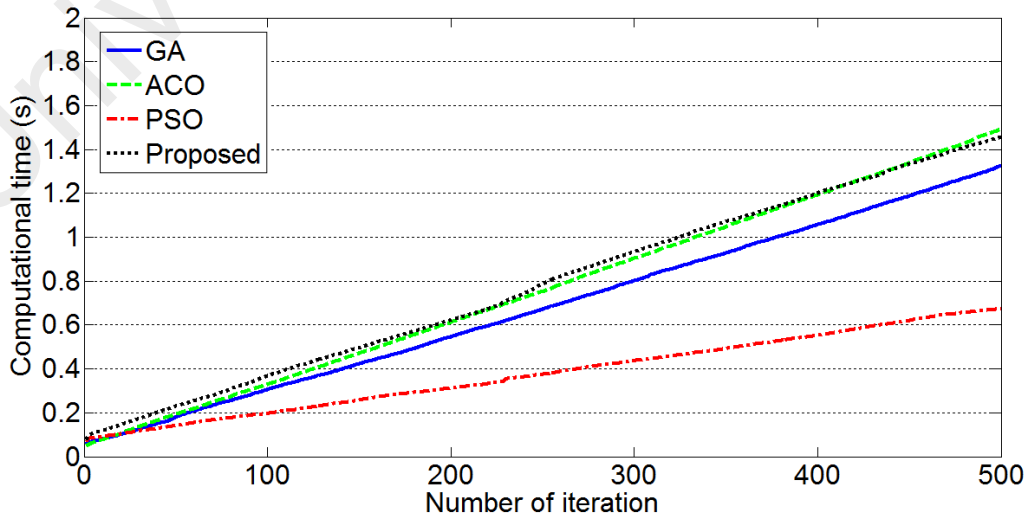


Figure 4.9: Computational time consumed by GA, ACO, PSO and the proposed hybrid algorithm for welded beam design optimisation problem

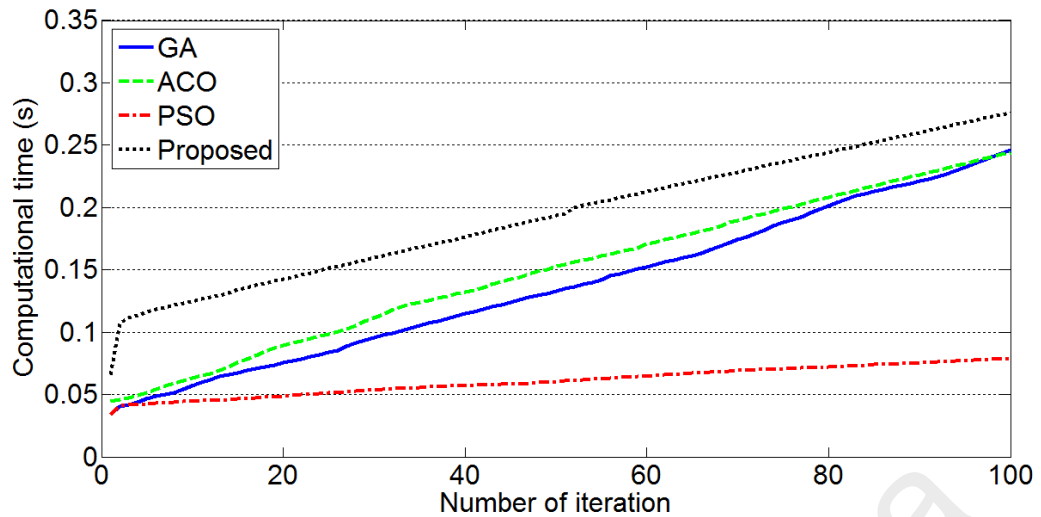


Figure 4.10: Computational time consumed by GA, ACO, PSO and the proposed hybrid algorithm for gear train design optimisation problem

(d) Performance comparison between the proposed and published algorithms in solving engineering design problems

Unlike the other sections, which, are organized into the sub-sections of accuracy study, repeatability study and convergence study, the present study is divided into four sub-sections, comprising, Himmelblau's non-linear optimisation problem, pressure vessel design optimisation problem, welded beam design optimisation problem and gear train design optimisation problem for better interpretation since a relatively large number of published algorithms are taken into comparison in each of the design problem.

(i) Himmelblau's non-linear optimisation problem

Comparisons of the developed algorithm with respect to the previous ones have been made and presented in Table 4.16. From Table 4.16, some of the past researches can be observed providing undesirable solutions as the constraints have been violated. The proposed algorithm demonstrates great performances in terms of accuracy with solution, $x = [78.0000, 33.0000, 29.9953, 45.0000, 36.7758]$ and $f(x) = -30665.5387$ for case 1, as well as $x = [78.0000, 33.0000, 27.0710, 45.0000, 44.9692]$ and $f(x) = -31025.5602$

for case 2. The values in bold refers to the relatively best solutions. The proposed hybrid algorithm is seen to be better in terms of accuracy if compared to those of (Deb, 2000; Gandomi et al., 2013; Himmelblau, 1972; Homaifar et al., 1994; Lee & Geem, 2005) for case 1 and to those of (Coello, 2000a; Coello, 2000b; Fesanghary et al., 2008; Omran & Salman, 2009) for case 2. In the aspect of repeatability, the proposed method performs better than most of the other algorithm, as shown in Table 4.17. Furthermore, the maximum number of evaluations of the proposed hybrid algorithm is found to be relatively lower than those of (Deb, 2000; He et al., 2004; Lee & Geem, 2005; Mehta & Dasgupta, 2012) for case 1, and that of (Shi & Eberhart, 1998) for case 2. For case 1, the proposed algorithm requires maximum 32,040 evaluations to converge, while the algorithm developed by He et al. (2004) requires maximum 90,000 evaluations, signifying a reduction of about 64.40%. However, the best solution achieved by the proposed algorithm is slightly inferior by $9.7830E-07\%$. For case 2, as compared to the algorithm developed by Hu et al. (2003), slight inferiority can also be seen (by $3.8678E-06$) in the best solution achieved by the proposed algorithm. Despite, the proposed algorithm exhibits a massive improvement in the number of evaluations by 83.98% with respect to that of (Hu et al., 2003). In general, the proposed algorithm can be claimed as the better algorithm in the aspect of accuracy, repeatability and convergence.

Table 4.16: Comparison of the best solutions for Himmelblau's problem applying different algorithms

Case	Algorithms	Design variables					Constraints			Function value
		x_1	x_2	x_3	x_4	x_5	$0 \leq g_1 \leq 92$	$90 \leq g_2 \leq 110$	$20 \leq g_3 \leq 25$	
1	Homaifar et al. (1994)	80.3900	35.0700	32.0500	40.3300	33.3400	91.6562	99.5369	20.0255	-30005.7000
	Himmelblau (1972)	NA	NA	NA	NA	NA	NA	NA	NA	-30373.9490
	Gandomi et al. (2013)	78.0000	33.0000	29.9962	45.0000	36.7761	92.0000	98.8407	20.0003	-30665.2330
	Lee and Geem (2005)	78.0000	33.0000	29.9950	45.0000	36.7760	92.0000	98.8405	19.9999 ^v	-30665.5000
	Mehta and Dasgupta (2012)	78.0000	33.0000	29.9953	45.0000	36.7758	NA	NA	NA	-30665.5387
	Deb (2000)	NA	NA	NA	NA	NA	NA	NA	NA	-30665.5370
	He et al. (2004)	78.0000	33.0000	29.9953	45.0000	36.7758	93.2854 ^v	100.4048	20.0000	-30665.5390
	Dimopoulos (2007)	78.0000	33.0000	29.9953	45.0000	36.7758	92.0000	98.8405	20.0000	-30665.5400
Proposed (feature 1)	78.0000	33.0000	29.9953	45.0000	36.7758	92.0000	98.8405	20.0000	-30665.5387	
2	Coello (2000a)	78.5958	33.0100	27.6460	45.0000	45.0000	91.9564	100.5451	20.2519	-30810.3590
	Coello (2000b)	78.0495	33.0070	27.0810	45.0000	44.9400	93.2838 ^v	100.4079	20.0019	-31020.8590
	Fesanghary et al. (2008)	78.0000	33.0000	27.0851	45.0000	44.9253	93.2783 ^v	100.3961	20.0000	-31024.3166
	Omran and Salman (2009)	78.0000	33.0000	27.0710	45.0000	44.9692	93.2854 ^v	100.4048	20.0000	-31025.5563
	Shi and Eberhart (1998)	78.0000	33.0000	27.0710	45.0000	44.9690	93.2853 ^v	100.4047	20.0000	-31025.5610
	Hu et al. (2003)	78.0000	33.0000	27.0710	45.0000	44.9692	92.0000	100.4049	20.0000	-31025.5614
	Proposed (feature 1)	78.0000	33.0000	27.0710	45.0000	44.9692	92.0000	100.4048	20.0000	-31025.5602

*NA= Not available, superscript v= violated

Table 4.17: Repeatability study for Himmelblau's problem

Case	Algorithms	Best	Average	Worst	Standard deviation	Number of evaluations
1	Homaifar et al. (1994)	-30005.7000	NA	NA	NA	NA
	Himmelblau (1972)	-30373.9490	NA	NA	NA	NA
	Gandomi et al. (2013)	-30665.2327	NA	NA	11.6231	5,000
	Lee and Geem (2005)	-30665.5000	NA	NA	NA	65,000
	Mehta and Dasgupta (2012)	-30665.5387	NA	NA	NA	62,748
	Deb (2000)	-30665.5370	NA	-29846.6540	NA	250,050
	He et al. (2004)	-30665.5390	-30643.9890	NA	70.0430	90,000
	Dimopoulos (2007)	-30665.5400	NA	NA	NA	NA
Proposed (feature 1)	-30665.5387	-30661.9060	-30638.7590	6.6061	32,040	
2	Coello (2000a)	-30810.3590	NA	NA	NA	1,600
	Coello (2000b)	-31020.8590	-30984.2407	-30792.4077	73.6335	2,100
	Fesanghary et al. (2008)	-31024.3166	NA	NA	NA	28,000
	Omran and Salman (2009)	-31025.5563	NA	NA	NA	50,000
	Shi and Eberhart (1998)	-31025.5610	NA	NA	NA	NA
	Hu et al. (2003)	-31025.5614	-31025.5614	NA	0	200,000
	Proposed (feature 1)	-31025.5602	-31024.9575	-31021.0604	1.2189	32,040

*NA= Not available

(ii) *Pressure vessel design optimisation problem*

This design problem has been solved utilising numerous algorithms in the past and the results of the proposed algorithm and other algorithms are summarized in Table 4.18. In this context, the proposed hybrid algorithm achieves better solution ($x = [0.8125, 0.4375, 42.0984, 176.6366]$ and $f(x) = 6059.7143$) if compared to those of (Coelho, 2010; Coello, 2000b; Coello & Montes, 2002; Deb, 1997; He & Wang, 2007; Kannan & Kramer, 1994; Kaveh & Talatahari, 2010; Lee & Geem, 2005; Mezura-Montes & Coello, 2008; Sandgren, 1990; Zhang & Wang, 1993). The proposed hybrid algorithm is found to have achieved the least best solution, similar to those of (Akay & Karaboga, 2012; Cagnina et al., 2008; Gandomi et al., 2013; He et al., 2004). Furthermore, the suggested algorithm exhibits better repeatability than those of (Coelho, 2010; Gandomi et al., 2013; He et al., 2004; Mezura-Montes & Coello, 2008) with standard deviation of 231.8850, as demonstrated in Table 4.19. In the aspect of convergence, the proposed hybrid algorithm is found to have consumed the least number of evaluations (20,040) among all the compared algorithms. In general, the proposed algorithm emerges as one of the most competitive algorithms in solving this problem.

Table 4.18: Comparison of best solutions for pressure vessel design problem applying different algorithms

Algorithms	Design variables				Function value
	x_1	x_2	x_3	x_4	$f(x)$
Sandgren (1990)	1.1250	0.6250	47.7000	117.7010	8129.1036
Lee and Geem (2005)	1.1250	0.6250	58.2789	43.7549	7198.4330
Kannan and Kramer (1994)	1.1250	0.6250	58.2910	43.6900	7198.0428
Zhang and Wang (1993)	1.1250	0.6250	58.2900	43.6930	7197.7000
Deb (1997)	0.9375	0.5000	48.3290	112.6790	6410.3811
Coello (2000b)	0.8125	0.4375	40.3239	200.0000	6288.7445
He and Wang (2007)	0.8125	0.4375	42.0913	176.7465	6061.0777
Coello and Montes (2002)	0.8125	0.4375	42.0974	176.6541	6059.9460
Mezura-Montes and Coello (2008)	0.8125	0.4375	42.0981	176.6405	6059.7456
Kaveh and Talatahari (2010)	0.8125	0.4375	42.0984	176.6378	6059.7258
Coelho (2010)	0.8125	0.4375	42.0984	176.6372	6059.7208
Akay and Karaboga (2012)	0.8125	0.4375	42.0984	176.6366	6059.7143
Cagnina et al. (2008)	0.8125	0.4375	42.0984	176.6366	6059.7143
Gandomi et al. (2013)	0.8125	0.4375	42.0984	176.6366	6059.7143
He et al. (2004)	0.8125	0.4375	42.0984	176.6366	6059.7143
Proposed (feature 1)	0.8125	0.4375	42.0984	176.6366	6059.7143

Table 4.19: Repeatability study for pressure vessel design problem

Algorithms	Best	Average	Worst	Standard deviation	Number of evaluations
Sandgren (1990)	8129.1036	NA	NA	NA	NA
Lee and Geem (2005)	7198.4330	NA	NA	NA	NA
Kannan and Kramer (1994)	7198.0428	NA	NA	NA	NA
Zhang and Wang (1993)	7197.7000	NA	NA	NA	NA
Deb (1997)	6410.3811	NA	NA	NA	NA
Coello (2000b)	6288.7445	6293.8432	6308.1497	7.4133	900,000
He and Wang (2007)	6061.0777	6147.1332	6363.8041	86.4545	200,000
Coello and Montes (2002)	6059.9460	6177.2533	6469.3220	130.9297	80,000
Mezura-Montes and Coello (2008)	6059.7456	6850.0049	7332.8798	426.0000	25,000
Kaveh and Talatahari (2010)	6059.7258	6081.7812	6150.1289	67.2418	NA
Coelho (2010)	6059.7208	6440.3786	7544.4925	448.4711	NA
Akay and Karaboga (2012)	6059.7143	6245.3081	NA	205.0000	30,000
Cagnina et al. (2008)	6059.7143	6092.0498	NA	12.1725	24,000
Gandomi et al. (2013)	6059.7143	6447.7360	6495.3470	502.6930	NA
He et al. (2004)	6059.7143	6289.9288	NA	305.7800	30,000
Proposed (feature 1)	6059.7143	6387.6266	6820.5797	231.8850	20,040

*NA= Not available

(iii) *Welded beam design optimisation problem*

Several publications can be found adopting this problem for verification purposes. From Table 4.20, the proposed hybrid algorithm of feature 1 can be seen yielding better solution if compared those of the other algorithms (Coello, 2000b; Coello & Montes, 2002; Dimopoulos, 2007; Gandomi et al., 2011; He & Wang, 2007; Hedar & Fukushima, 2006; Mezura-Montes & Coello, 2008), in which, $x = [0.2057, 3.4705, 9.0366, 0.2057]$ and $f(x) = 1.7249$. In the study of repeatability, the proposed algorithm performs satisfactorily and better than those of (Akay & Karaboga, 2012; Cagnina et al., 2008; Coello & Montes, 2002; Gandomi et al., 2011; Hedar & Fukushima, 2006; Mezura-Montes & Coello, 2008) with standard deviation of 0.0253, as shown in Table 4.21. In terms of convergence, the proposed hybrid algorithm is discovered to have undergone the least number of evaluations among all the compared algorithms. The best solution evaluated using the proposed hybrid algorithm is the same as that of algorithm developed by Mehta and Dasgupta (2012); nevertheless, the proposed hybrid algorithm shows 8.8884% of reduction in the number of evaluations. In general, the proposed hybrid algorithm appears to be one of the well-rounded algorithms.

Table 4.20: Comparison of the best solutions for welded beam design problem applying different algorithms

Algorithms	Design variables				Function value
	x_1	x_2	x_3	x_4	$f(x)$
Coello (2000b)	0.2088	3.4205	8.9975	0.2100	1.7483
Mezura-Montes and Coello (2008)	0.1997	3.6121	9.0375	0.2061	1.7373
Gandomi et al. (2011)	0.2015	3.5620	9.0414	0.2057	1.7312
Dimopoulos (2007)	0.2015	3.5620	9.0414	0.2057	1.7312
Coello and Montes (2002)	0.2060	3.4713	9.0202	0.2065	1.7282
He and Wang (2007)	0.2024	3.5442	9.0482	0.2057	1.7280
Hedar and Fukushima (2006)	0.2056	3.4726	9.0366	0.2057	1.7250
Kaveh and Talatahari (2010)	0.2057	3.4711	9.0367	0.2057	1.7249
Mehta and Dasgupta (2012)	0.2057	3.4705	9.0366	0.2057	1.7249
Mezura-Montes et al. (2007)	0.2057	3.4705	9.0366	0.2057	1.7249
Cagnina et al. (2008)	0.2057	3.4705	9.0366	0.2057	1.7249
Akay and Karaboga (2012)	0.2057	3.4705	9.0366	0.2057	1.7249
Hu et al. (2003)	0.2057	3.4705	9.0366	0.2057	1.7249
Proposed (feature 1)	0.2057	3.4705	9.0366	0.2057	1.7249

Table 4.21: Repeatability study for welded beam design problem

Algorithms	Best	Mean	Worst	Standard deviation	Number of evaluations
Coello (2000b)	1.7483	1.7720	1.7858	0.0112	NA
Mezura-Montes and Coello (2008)	1.7373	1.8133	1.9947	0.0705	25,000
Gandomi et al. (2011)	1.7312	1.8787	2.3456	0.2678	50,000
Dimopoulos (2007)	1.7312	NA	NA	NA	NA
Coello and Montes (2002)	1.7282	1.7927	1.9934	0.0747	80,000
He and Wang (2007)	1.7280	1.7488	1.7821	0.0129	NA
Hedar and Fukushima (2006)	1.7250	1.7564	1.8844	0.0424	NA
Kaveh and Talatahari (2010)	1.7249	1.7298	1.7760	0.0092	NA
Mehta and Dasgupta (2012)	1.7249	NA	NA	NA	21,995
Mezura-Montes et al. (2007)	1.7249	1.7250	NA	1.0000E-15	24,000
Cagnina et al. (2008)	1.7249	2.0574	NA	0.2154	24,000
Akay and Karaboga (2012)	1.7249	1.7419	NA	0.0310	30,000
Hu et al. (2003)	1.7249	NA	NA	NA	NA
Proposed (feature 1)	1.7249	1.7431	1.8140	0.0253	20,040

*NA= Not available

(iv) **Gear train design optimisation problem**

There are few literature utilising this problem for validation purposes. From Table 4.22, the proposed hybrid algorithm exhibits dominating performances in terms of accuracy over (Kannan & Kramer, 1994; Sandgren, 1990) with solution of $x = [16, 19, 43, 49]$ and $f(x) = 2.7009E-12$. Apart, as seen from Table 4.23, it is evident that the proposed method shows better repeatability as well as better convergence over (Gandomi et al., 2013). In general, the proposed hybrid algorithm is proven to have performed the best among all the algorithms.

Table 4.22: Comparison of the best solutions for gear train design problem applying different algorithms

Algorithms	Design variables					Function value
	$T_d(x_1)$	$T_b(x_2)$	$T_a(x_3)$	$T_f(x_4)$	Gear ratio	$f(x)$
Sandgren (1990)	18	22	45	60	0.1467	5.7120E-6
Kannan and Kramer (1994)	13	15	33	41	0.1441	2.1460E-8
Deb and Goyal (1996)	16	19	43	49	0.1443	2.7009E-12
Gandomi et al. (2013)	16	19	43	49	0.1443	2.7009E-12
Proposed (feature 1)	16	19	43	49	0.1443	2.7009E-12

Table 4.23: Repeatability study for gear train design problem

Algorithms	Best	Average	Worst	Standard deviation	Number of evaluations
Sandgren (1990)	5.7120E-6	NA	NA	NA	NA
Kannan and Kramer (1994)	2.1460E-8	NA	NA	NA	NA
Deb and Goyal (1996)	2.7009E-12	NA	NA	NA	NA
Gandomi et al. (2013)	2.7009E-12	1.9841E-9	2.3576E-9	3.5546E-9	5,000
Proposed (feature 1)	2.7009E-12	9.7022E-10	2.3576E-9	8.8056E-10	4,040
*NA= Not available					

4.3.2 Application in vibrational material identification

This section consists of four sub-sections, including, accuracy study, repeatability study, convergence study and lastly, robustness study. The results pertaining to the accuracy, repeatability, convergence as well as robustness of the proposed meta-heuristic algorithm are presented and analysed.

4.3.2.1 Accuracy of meta-heuristic hybrid optimisation method in reference plates

Figure 4.11 demonstrate the comparison of minimised objective function values achieved by genetic algorithm (GA), ant colony optimisation (ACO), particle swarm optimisation (PSO) and the proposed hybrid algorithm for the aluminium plate. It is noted that for visual qualitative comparison reason, the graphs shown in Figure 4.11 have been enlarged and the maximum limit of y-axis does not represent the actual minimised values achieved by those algorithms. From Figure 4.11, it can be observed that ACO performs the worst, followed by GA and PSO, while the hybrid algorithm demonstrates the relatively best results. Still, in the study of the aluminium plate, the proposed hybrid algorithm appears to be the relatively best choice with minimised values of $1.5579\text{E-}08$, $2.4244\text{e-}08$ and $7.8573\text{e-}08$ under three different sets of boundary conditions, as presented in Table 4.24, Table 4.25 and Table 4.26, respectively. It can be observed that the evaluated elastic properties deviate by 1.2727% at most from the benchmark properties when utilising the proposed hybrid algorithm. From those observations, it can be inferred that the proposed hybrid algorithm is the better algorithm in the aspect of accuracy in material identification.

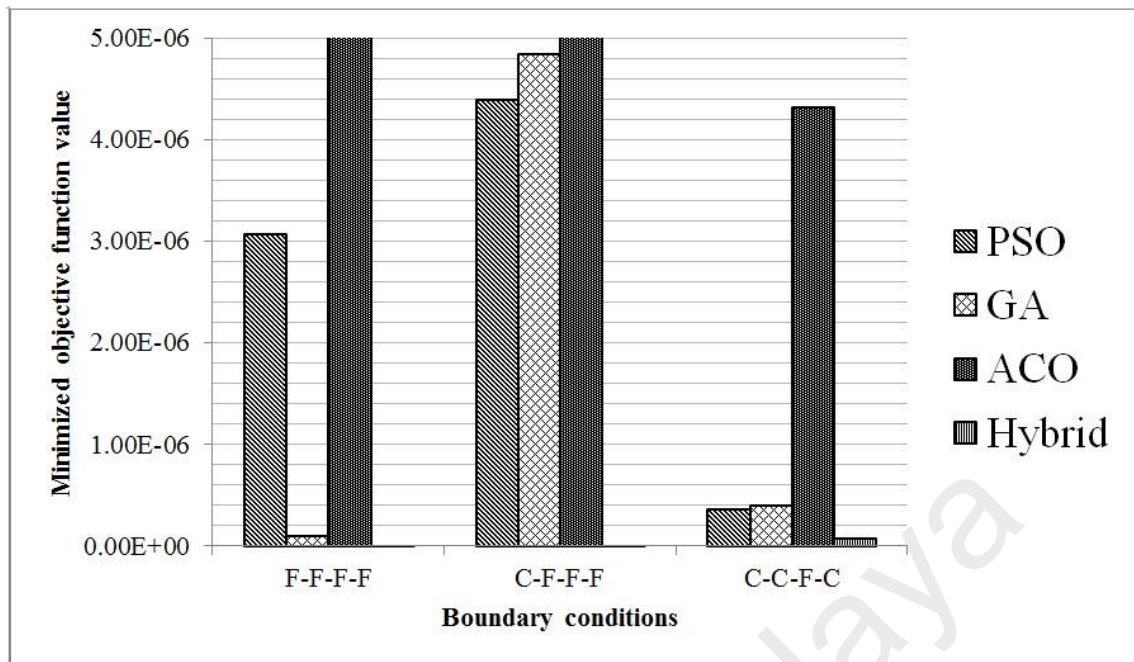


Figure 4.11: Comparison of minimised value for aluminium plate using different algorithms

Table 4.24: Elastic constants obtained for aluminium plate under F-F-F-F boundary condition

	E_x (GPa)	E_y (GPa)	G_{xy} (GPa)	ν_{xy}	Obj. Fun.
PSO	72.4631[0.0872]	72.3508[0.0680]	28.0034[0.0121]	0.3330[0.9091]	3.0826E-06
GA	72.4607[0.0838]	72.3786[0.0296]	27.9958[0.0150]	0.3301[0.0303]	1.1039E-07
ACO	72.7990[0.5511]	72.1331[0.3686]	27.9286[0.2550]	0.3344[1.3333]	8.7278E-06
Proposed	72.4002[0.0003]	72.4211[0.0291]	28.0019[0.0068]	0.3299[0.0303]	1.5579E-08
Benchmark	72.4	72.4	28	0.33	-

#[n]denotes the absolute percentage error with respect to the benchmark value.

Table 4.25: Elastic constants obtained for aluminium plate under C-F-F-F boundary condition

	E_x (GPa)	E_y (GPa)	G_{xy} (GPa)	ν_{xy}	Obj. Fun.
PSO	72.3556[0.0613]	73.0242[0.8622]	28.0288[0.1029]	0.3158[4.3030]	4.4058E-06
GA	72.4287[0.0396]	72.8125[0.5698]	28.0457[0.1632]	0.3159[4.2727]	4.8509e-06
ACO	72.4018[0.0025]	70.7281[2.3091]	27.9373[0.2239]	0.3553[7.6667]	2.5178E-05
Proposed	72.4057[0.0079]	72.4130[0.0180]	27.9956[0.0157]	0.3295[0.1515]	2.4244e-08
Benchmark	72.4	72.4	28	0.33	-

#[n]denotes the absolute percentage error with respect to the benchmark value.

Table 4.26: Elastic constants obtained for aluminium plate under C-C-F-C boundary condition

	E_x (GPa)	E_y (GPa)	G_{xy} (GPa)	ν_{xy}	Obj. Fun.
PSO	72.1016[0.4122]	72.2972[0.1420]	27.7662[0.8350]	0.3390[2.7273]	3.6406e-07
GA	72.2092[0.2635]	72.2842[0.1599]	27.8983[0.3632]	0.3355[1.6667]	4.0050e-07
ACO	73.5411[1.5761]	72.7066[0.4235]	28.6222[2.2221]	0.3028[8.2424]	4.3167e-06
Proposed	72.3456[0.0751]	72.3924[0.0105]	27.8143[0.6632]	0.3342[1.2727]	7.8573e-08
Benchmark	72.4	72.4	28	0.33	-

#[n]denotes the absolute percentage error with respect to the benchmark value.

In the investigation of the graphite epoxy plate, it can be seen from Figure 4.12 that PSO, GA and the proposed hybrid algorithm yield considerably better outcomes as compared to ACO. Similarly, for the reason of visual qualitative comparison, the graphs shown in Figure 4.12 have been enlarged, as mentioned above. The results suggest that PSO and GA can be the probable alternatives as it can be observed that the values are comparatively close but marginally inferior to those of the proposed hybrid algorithm. In comparison of the four algorithms, the proposed hybrid algorithm yields the best results under every set of boundary conditions with values of $2.8081E-08$, $1.2745E-07$ and $3.5636E-08$, as shown in Table 4.27, Table 4.28 and Table 4.29, respectively. Meanwhile, the absolute percentage errors of the determined elastic properties with respect to benchmark properties using the proposed hybrid algorithm are found to be below 3%. These consequently verify the accuracy of the proposed hybrid algorithm in material identification.

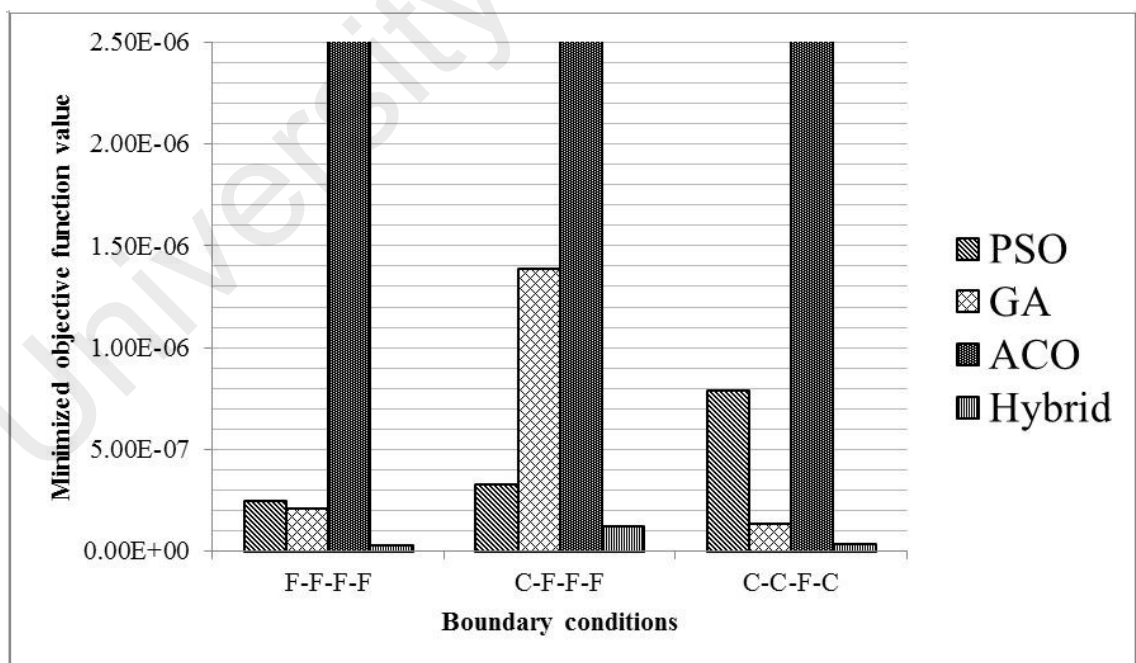


Figure 4.12: Comparison of minimised value for graphite epoxy plate using different algorithms

Table 4.27: Elastic constants obtained for graphite epoxy plate under F-F-F-F boundary condition

	$E_x(GPa)$	$E_y(GPa)$	$G_{xy}(GPa)$	ν_{xy}	Obj. Fun.
PSO	127.8802[0.0155]	10.2697[0.0029]	7.3092[0.0383]	0.2067[6.0455]	2.5121E-07
GA	127.8441[0.0437]	10.2668[0.0312]	7.3117[0.0041]	0.2316[5.2727]	2.1230E-07
ACO	128.4253[0.4107]	10.2508[0.0182]	7.3072[0.0656]	0.1756[20.182]	6.9808E-06
Proposed	127.8654[0.0271]	10.2696[0.0039]	7.3134[0.0191]	0.2183[0.7727]	2.8081E-08
Benchmark	127.9	10.27	7.312	0.22	-
#[n]denotes the absolute percentage error with respect to the benchmark value.					

Table 4.28: Elastic constants obtained for graphite epoxy plate under C-F-F-F boundary condition

	$E_x(GPa)$	$E_y(GPa)$	$G_{xy}(GPa)$	ν_{xy}	Obj. Fun.
PSO	127.8159[0.0658]	10.2619[0.0789]	7.3263[0.1956]	0.2368[7.6364]	3.2977E-07
GA	127.8445[0.0434]	10.2391[0.3009]	7.3410[0.3966]	0.1957[11.045]	1.3924E-06
ACO	128.2228[0.2524]	10.3010[0.3019]	7.2463[0.8985]	0.2630[19.545]	8.0426E-06
Proposed	127.9189[0.0148]	10.2781[0.0789]	7.3118[0.0027]	0.2140[2.7273]	1.2745E-07
Benchmark	127.9	10.27	7.312	0.22	-
#[n]denotes the absolute percentage error with respect to the benchmark value.					

Table 4.29: Elastic constants obtained for graphite epoxy plate under C-C-F-C boundary condition

	$E_x(GPa)$	$E_y(GPa)$	$G_{xy}(GPa)$	ν_{xy}	Obj. Fun.
PSO	127.6372[0.2055]	10.2642[0.0565]	7.2971[0.2038]	0.2362[7.3636]	7.9172E-07
GA	128.0523[0.1191]	10.2709[0.0088]	7.2975[0.1983]	0.2186[0.6364]	1.3538E-07
ACO	128.3453[0.3482]	10.2966[0.2590]	7.2949[0.2339]	0.2159[1.8636]	5.2515E-06
Proposed	127.8287[0.0557]	10.2688[0.0117]	7.3164[0.0602]	0.2203[0.1364]	3.5636E-08
Benchmark	127.9	10.27	7.312	0.22	-
#[n]denotes the absolute percentage error with respect to the benchmark value.					

The improvement percentages of the identified elastic properties when using the proposed algorithm with respect to those using conventional algorithms are presented in Table 4.30. It shows that the accuracy of the determined E_x and E_y using the proposed hybrid algorithm in comparisons to those of using other algorithms is improved by 2.2911% and 0.3836% at most for the aluminium and graphite epoxy plates, respectively. Furthermore, the evaluated in-plane shear modulus of the aluminium and graphite epoxy plates utilising the proposed hybrid algorithm is found to be more accurate by at most 1.5589% and 0.8958%, respectively when comparing to those of using traditional algorithms. Significant improvements can as well be seen in the identified Poisson's ratio of the aluminium plate (by 7.5151% at most) and graphite epoxy plate (by 19.410% at most) when applying the proposed hybrid algorithm.

Overall, the proposed hybrid algorithm is proven to be slightly more superior to the others in the aspect of accuracy.

Table 4.30: Improvement percentage of identified elastic properties using the proposed algorithm with respect to those of using other algorithms

	$E_x(\%)$	$E_y(\%)$	$G_{xy}(\%)$	$\nu_{xy}(\%)$
Aluminium	0.0317-1.501	0.0005-2.2911	0.0053-1.5589	0.3940-7.5152
Graphite epoxy	0.0166-0.3836	0.0143-0.2473	0.0192-0.8958	0.5000-19.410

4.3.2.2 Repeatability of meta-heuristic hybrid optimisation method in reference plates

In the study of the aluminium plate, it can be seen that from Figure 4.13, the proposed hybrid algorithm yields the relatively least standard deviations under all the three boundary conditions as compared to those of conventional algorithms. As presented in Table 4.31, Table 4.32 and Table 4.33, the proposed hybrid algorithm performs the best in the aspect of repeatability with standard deviations of 2.7751E-07, 1.9999E-07 and 1.8245E-07 under three different boundary conditions, respectively.

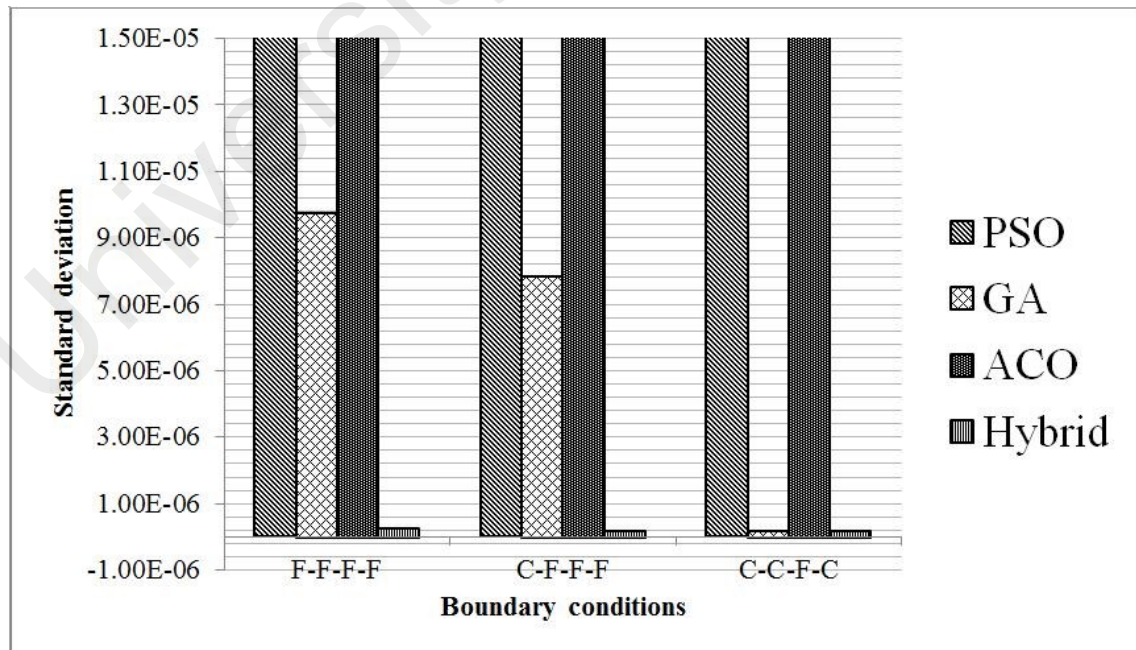


Figure 4.13: Comparison of repeatability for aluminium plate using different algorithms

Table 4.31: Repeatability study using different type of algorithms for aluminium plate under F-F-F-F boundary condition

	Best	Average	Worst	Std. dev.
PSO	3.0826E-06	1.8734E-05	5.2624E-05	1.8059E-05
GA	1.1039E-07	7.5095E-06	2.6547E-05	9.7445E-06
ACO	8.7278E-06	1.3182E-04	2.5658E-04	8.7483E-05
Proposed	1.5579E-08	4.0034E-07	8.7327E-07	2.7751E-07

Table 4.32: Repeatability study using different type of algorithms for aluminium plate under C-F-F-F boundary condition

	Best	Average	Worst	Std. dev.
PSO	4.4058E-06	2.2551E-05	8.1018E-05	2.9593E-05
GA	4.8509E-06	1.3303E-05	2.2814E-05	7.8665E-06
ACO	2.5178E-05	9.2809E-05	2.4608E-04	7.9389E-05
Proposed	2.4244E-08	2.2518E-07	5.2392E-07	1.9999E-07

Table 4.33: Repeatability study using different type of algorithms for aluminium plate under C-C-F-C boundary condition

	Best	Average	Worst	Std. dev.
PSO	3.6406E-07	1.3024E-05	4.3623E-05	1.6081E-05
GA	4.0050E-07	6.6893E-07	8.8026E-07	2.0707E-07
ACO	4.3167E-06	2.4678E-05	8.4013E-05	2.9836E-05
Proposed	7.8573E-08	2.6036E-07	5.9360E-07	1.8245E-07

In the study of the graphite epoxy plate, similarly, the proposed hybrid algorithm exhibits superiority in the aspect of repeatability over the conventional algorithms, as depicted in Figure 4.14. The standard deviations for graphite epoxy plate under three different sets of boundary conditions are 2.7751E-07, 1.9999E-07, and 1.8245E-07, as demonstrated in Table 4.34, Table 4.35 and Table 4.36, respectively. The great repeatability of the proposed method in material identification can be explained by the effective search coverage, in which, the exploratory search is contributed by the collaboration between genetic algorithm (GA) and ant colony optimisation (ACO) operator, while the exploitative search is contributed by the cooperation between genetic algorithm (GA) and particle swarm optimisation (PSO).

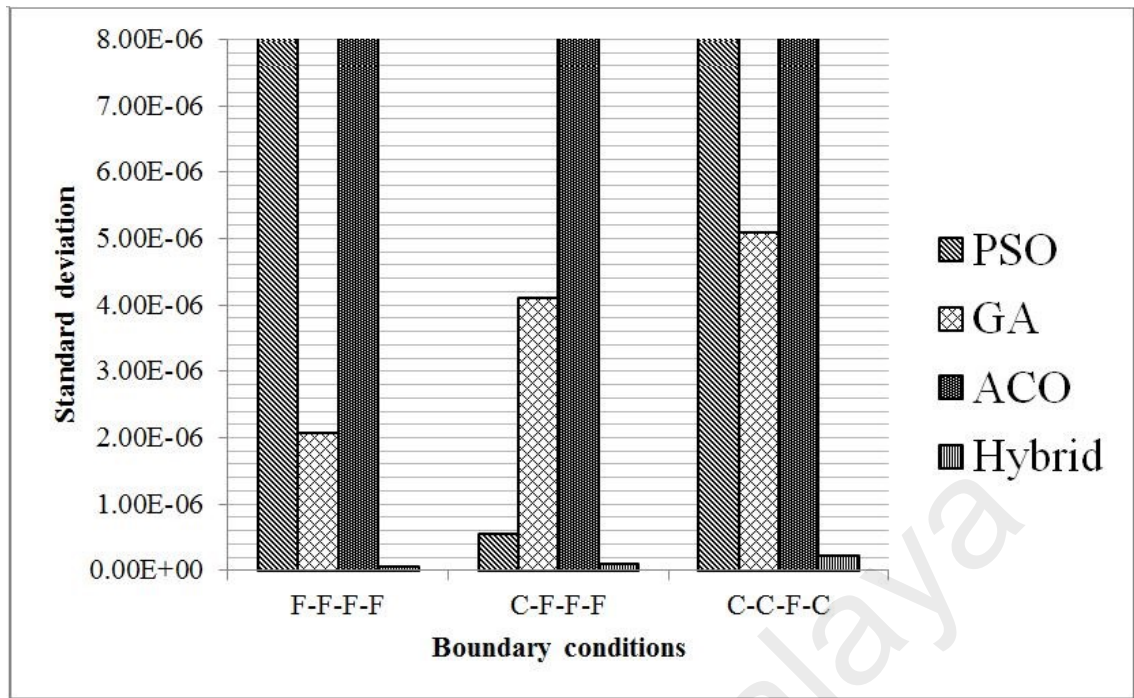


Figure 4.14: Comparison of repeatability for graphite epoxy plate using different algorithms

Table 4.34: Repeatability study using different type of algorithms for graphite epoxy plate under F-F-F-F boundary condition

	Best	Average	Worst	Std. dev.
PSO	2.5121E-07	3.3108E-04	1.6394E-03	6.5418E-04
GA	2.1230E-07	1.8251E-06	5.6053E-06	2.0889E-06
ACO	6.9808E-06	4.7169E-04	1.5170E-03	5.5143E-04
Proposed	2.8081E-08	1.6298E-07	2.3106E-07	7.7340E-08

Table 4.35: Repeatability study using different type of algorithms for graphite epoxy plate under C-F-F-F boundary condition

	Best	Average	Worst	Std. dev.
PSO	3.2977E-07	1.0014E-06	1.9707E-06	5.4871E-07
GA	1.3924E-06	5.2336E-06	1.2572E-05	4.1214E-06
ACO	8.0426E-06	2.3155E-04	5.4768E-04	1.8497E-04
Proposed	1.2745E-07	2.2914E-07	3.8962E-07	1.0473E-07

Table 4.36: Repeatability study using different type of algorithms for graphite epoxy plate under C-C-F-C boundary condition

	Best	Average	Worst	Std. dev.
PSO	7.9172E-07	3.4247E-05	1.5742E-04	6.1708E-05
GA	1.3538E-07	3.1563E-06	1.3302E-05	5.0936E-06
ACO	5.2515E-06	4.9431E-04	1.6992E-03	6.2138E-04
Proposed	3.5636E-08	2.4207E-07	6.7863E-07	2.3007E-07

Besides, from Table 4.37, the proposed hybrid algorithm leads the rest of the algorithms in terms of repeatability by at most $8.7205E-05$ and $6.5410E-04$ in difference of standard deviation for the aluminium and graphite epoxy plates, respectively. This can be a useful reference for future development of the proposed algorithm in improving the repeatability in material identification.

Table 4.37: Difference of standard deviation of the proposed hybrid algorithm with respect to those of other algorithms

	F-F-F-F	C-F-F-F	C-C-F-C
Aluminium	9.4670E-06	7.6665E-06	2.4620E-08
	-	-	-
	8.7205E-05	7.9189E-05	2.9654E-05
Graphite epoxy	2.0116E-04	4.4398E-07	4.8635E-06
	-	-	-
	6.5410E-04	1.8487E-04	6.2115E-04

4.3.2.3 Convergence of meta-heuristic hybrid optimisation method in reference plates

In this section, the convergence rate in sequence of the number of iteration is firstly investigated, followed by the study of computational time. Figure 4.15, Figure 4.16 and Figure 4.17 depict the convergence behaviours of the four algorithms for the aluminium plate under F-F-F-F, C-F-F-F and C-C-F-C (C: Clamped, F: Free) boundary conditions, respectively. Figure 4.15 shows the convergence plot for the aluminium plate under F-F-F-F boundary condition. As expected, the hybrid algorithm exhibits as good convergence rate as that of ant colony optimisation (ACO), while those of genetic algorithm (GA) and particle swarm optimisation (PSO) come after. In Figure 4.16, the hybrid algorithm demonstrates its great dominance in convergence rate over the other algorithms, in which, it leads to a great decrease in the objective function values after the first iteration. Under C-C-F-C boundary condition (Figure 4.17), the hybrid algorithm surpasses the other algorithms in terms of convergence rate in early iterations,

however, in iteration 6, PSO converges slightly sooner than that of the hybrid algorithm.

Despite, the proposed hybrid algorithm yields considerably good results.

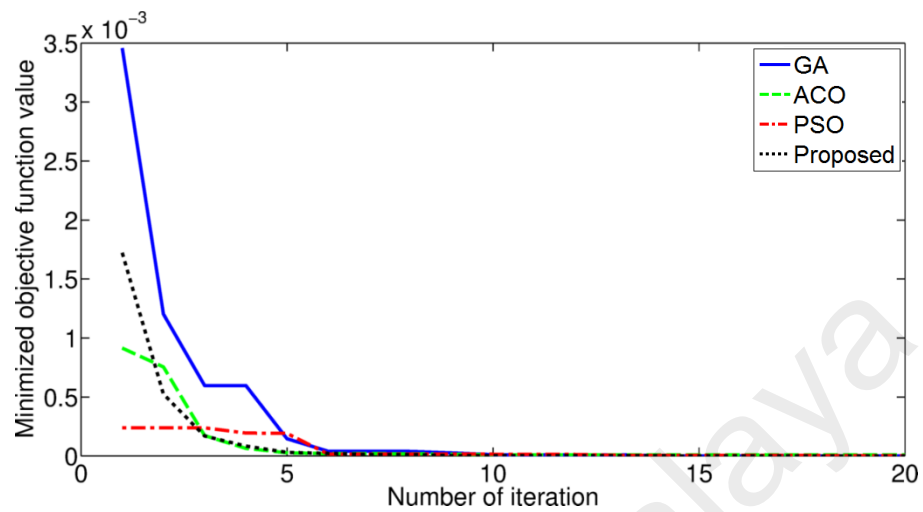


Figure 4.15: Convergence rate of different types of algorithms for aluminium plate under F-F-F-F boundary condition

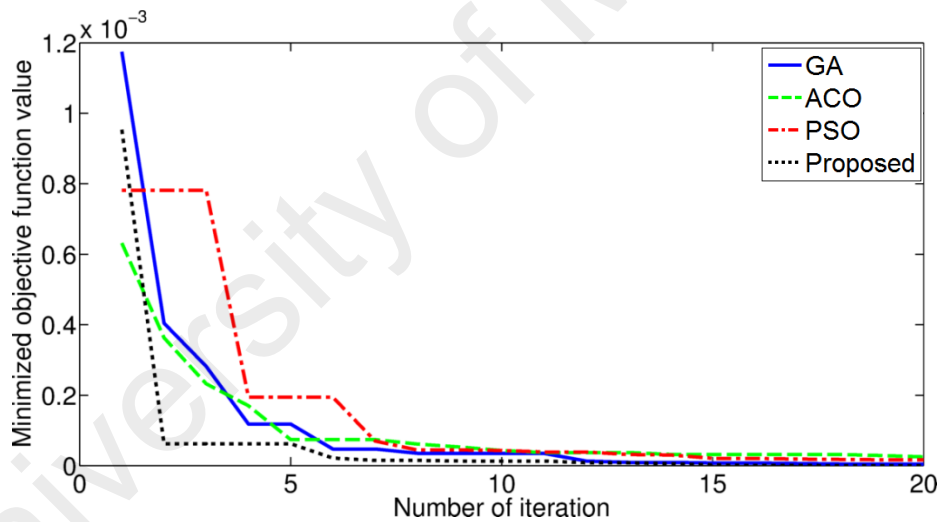


Figure 4.16: Convergence rate of different types of algorithms for aluminium plate under C-F-F-F boundary condition

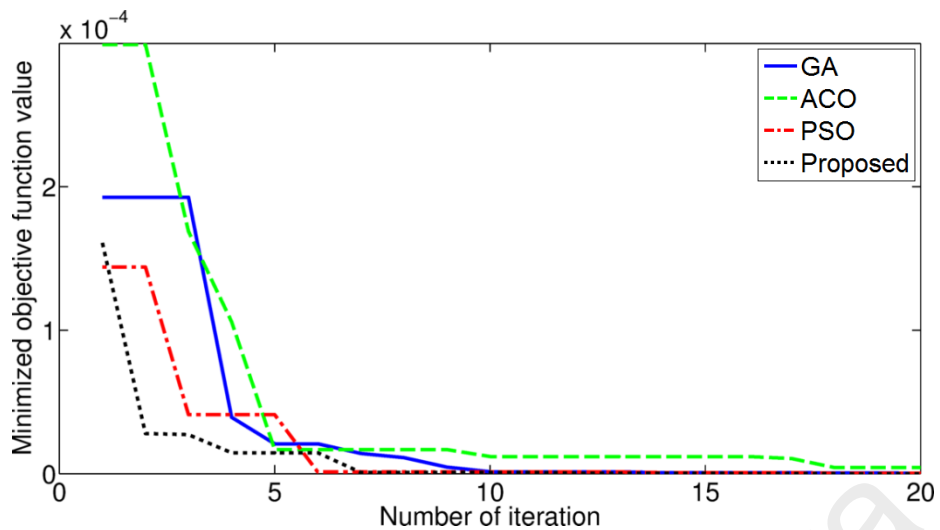


Figure 4.17: Convergence rate of different types of algorithms for aluminium plate under C-C-F-C boundary condition

On the other hand, Figure 4.18, Figure 4.19, and Figure 4.20 demonstrate the convergence graphs of the four algorithms for the graphite epoxy plate under F-F-F-F, C-F-F-F and C-C-F-C boundary conditions, respectively. From Figure 4.18, it can be observed that from iteration 1 to 3, a drastic reduction occurs in the objective function values of the proposed hybrid algorithm before it is further reduced in iteration 6. In view of other algorithms, the initial values are comparatively smaller and the reduction of objective function values is not as much as that of the proposed hybrid algorithm. Meanwhile, under C-F-F-F boundary condition, the proposed hybrid algorithm exhibits considerably similar convergence rate as those of GA and ACO starting from iteration 3, as depicted in Figure 4.19. The proposed hybrid algorithm experiences a great drop in the objective function value from iteration 1 to 3. As shown in Figure 4.20, it can be observed that the proposed hybrid algorithm performs the best, in which it yields the least minimised objective function value at the highest rate among all the algorithms.

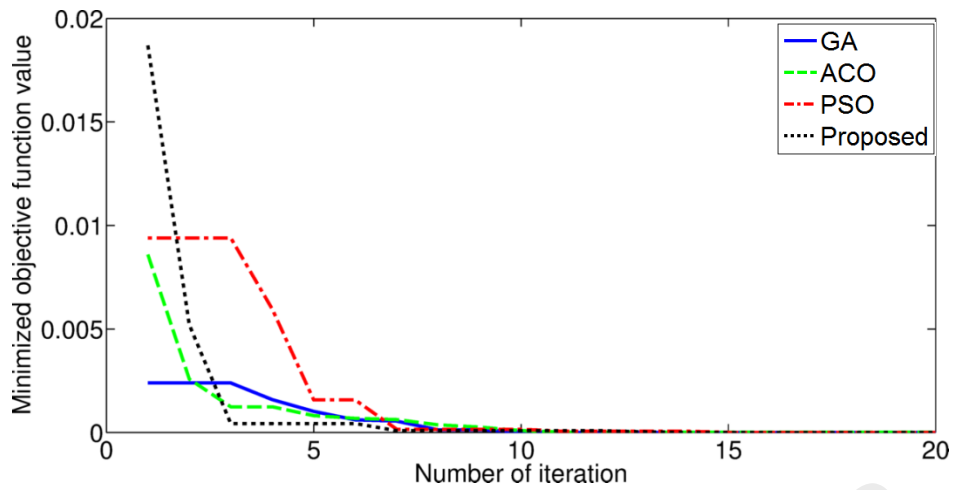


Figure 4.18: Convergence rate of different types of algorithms for graphite epoxy plate under F-F-F-F boundary condition

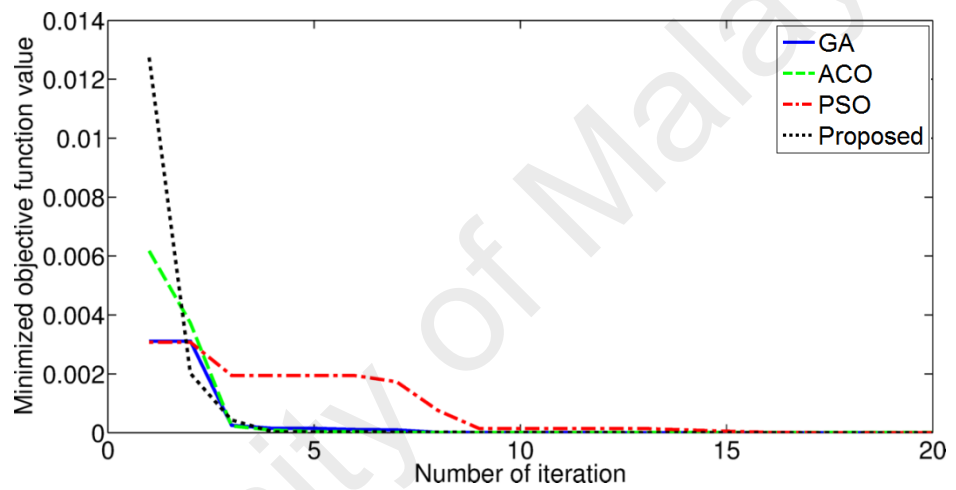


Figure 4.19: Convergence rate of different types of algorithms for graphite epoxy plate under C-F-F-F boundary condition

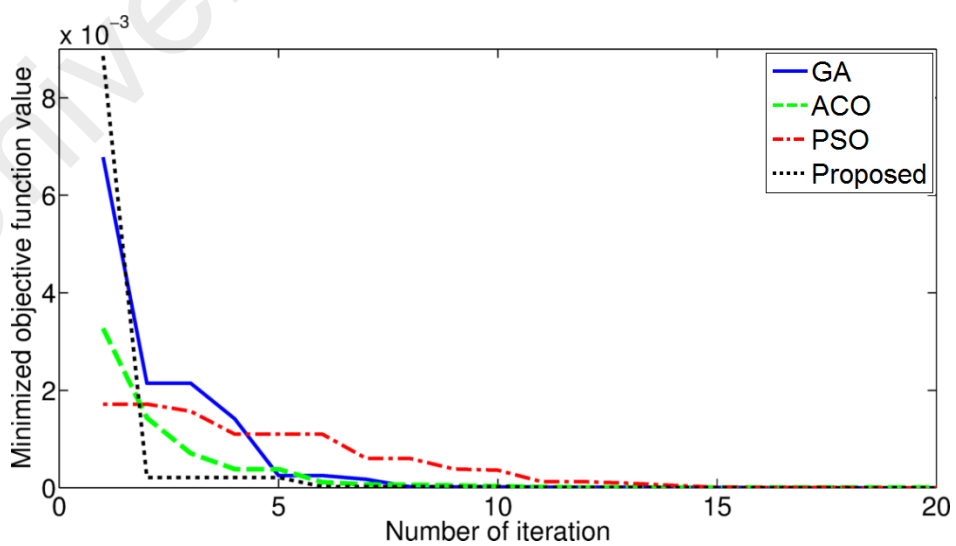


Figure 4.20: Convergence rate of different types of algorithms for graphite epoxy plate under C-C-F-C boundary condition

Overall, it can be observed that in early iterations, the proposed hybrid algorithm converges to its solution at a comparatively higher rate. This phenomenon occurs due to the equal contribution of work load from both the ACO and PSO operators, in which ACO operator is assigned for exploratory search, while PSO operator is designated for exploitative search. The biased effect due to random initialization of GA operator is compromised via the use of ACO and PSO operators and in the next iteration, those processed outcomes, in which, ones from the products of exploration search (ACO) and the other from the products of exploitative search (PSO) are subsequently merged and evolved again via the use of GA operators. Therefore, at the end, the rate of minimisation can be seen on the rise in comparison to those of other involved algorithms due to well distribution of search coverage.

Apart from the investigation of convergence rate, technically, algorithm that consumes much computational time can be referred to as computationally expensive (high computational cost). A slight difference exists between convergence rate and computational time in the present study, in which, convergence rate refers to the ability of the algorithm to converge involving lower number of evaluations, whereby, computational time refers to the total time consumed by the algorithm to converge to its solution. In this context, the number of evaluations for each algorithm is fixed constant for equal comparison purposes and the computational time of each algorithm for the aluminium and graphite epoxy plates are presented in Figure 4.21 and Figure 4.22, respectively. The results show that under a fixed number of evaluations, the computational time of the involved algorithms is almost similar with time difference not exceeding 12 seconds. The proposed hybrid algorithm is found tailing the rest of the algorithms in terms of computational time (3928s), in which, genetic algorithm (GA), ant colony optimisation (ACO) and particle swarm optimisation (PSO) consume 3922s, 3926s and 3924s, respectively. The time difference between the proposed hybrid

algorithm and the least time-consuming GA is found to be around 6 seconds, indicating 0.1530% in difference with respect to the time consumed by GA. Despite, comparing to the accuracy improvement of the proposed hybrid algorithm, the drawback of the proposed hybrid algorithm in the aspect of computational time is as well overshadowed by its relatively more significant accuracy improvement, where, the accuracy of the identified E_x , E_y , G_{xy} , and v_{xy} using the proposed hybrid algorithm are improved by at most 1.501%, 2.2911%, 1.5589% and 7.5152%, respectively with respect to those of using conventional algorithms, as demonstrated in Table 4.30. Furthermore, in the study of the graphite epoxy plate under F-F-F-F boundary condition, the proposed hybrid algorithm is found consuming the most computational time (3872s) if compared to GA (3860s), ACO (3867s) and PSO (3864s). In comparison to the least time-consuming GA, the proposed algorithm is found to have lagged behind by 12 seconds at most, which is equivalent to 0.3109% in difference. Despite, the shortcoming of the proposed algorithm in this aspect is offset by its relatively larger accuracy improvement, as shown in Table 4.30, garnering 0.3836%, 0.2473%, 0.8958% and 19.41% of improvement at most for E_x , E_y , G_{xy} , and v_{xy} , respectively. Generally, the relatively rapid convergence of the hybrid algorithm in sequence of iterations, its high repeatability as well as its excellent capability in searching for the global minimum are said to have compensated its shortcoming in the aspect of computational time.

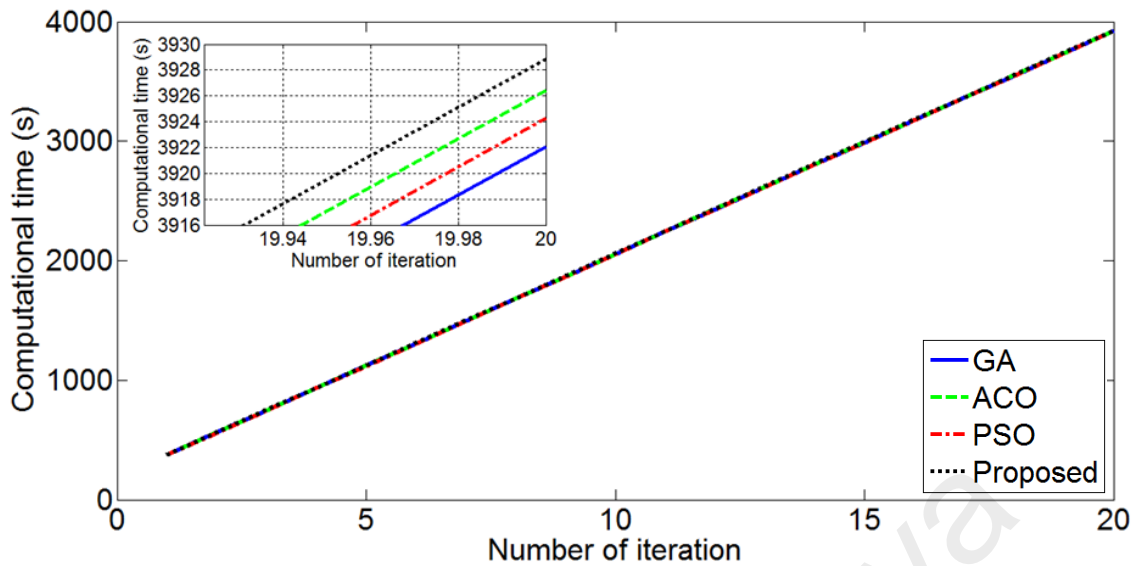


Figure 4.21: Computational time of different types of algorithms for aluminium plate under F-F-F-F boundary condition

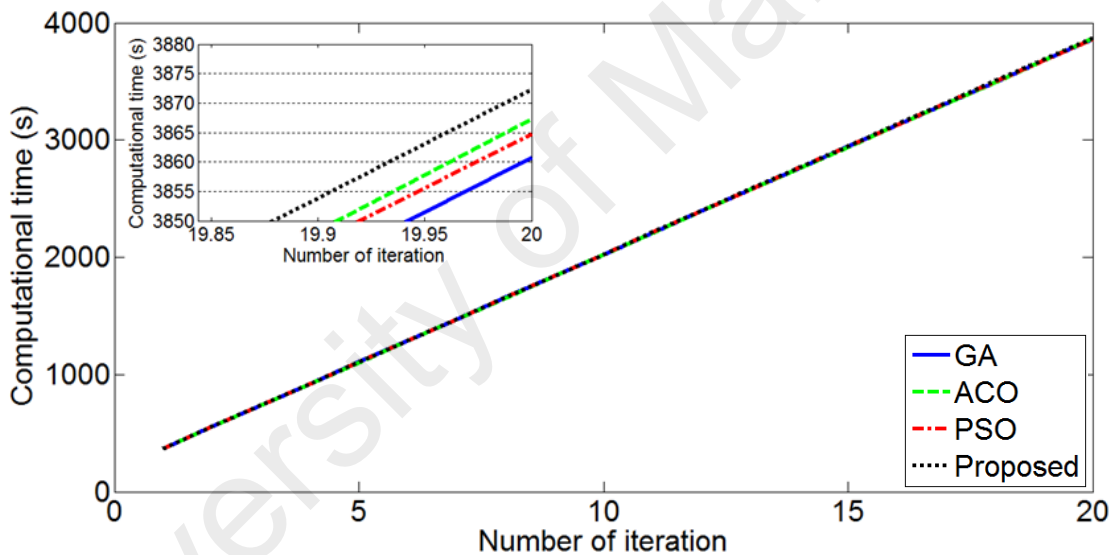


Figure 4.22: Computational time of different types of algorithms for graphite epoxy plate under F-F-F-F boundary condition

4.3.2.4 Robustness of meta-heuristic hybrid optimisation method in reference plates

In real cases, experimental data often comes with uncertainties and these uncertainties are predominantly due to the presence of various errors, namely, prediction errors, measurement errors and implementation errors. In the present study, implementation and measurement errors are the emphasis since these errors might incur

during the acquisition of vibration data. Uncertainties can be reduced experimentally and handled numerically. To minimise uncertainties incurred during experimental measurement, several important issues pertaining to experimental set-up should be taken into serious attention before conducting the experiment. These include the identification of the boundary condition of the real structure, the suitability of impact location and impact grid, the hardness suitability of impact hammer tip as well as the suitability of block size and sampling rate. By addressing these issues appropriately, the level of uncertainties incurred during experiment could greatly be reduced. It is noteworthy that these issues are in fact dependent on the specimen dimensions as well as the resonant frequency range of the specimen. Even though several precautionary steps have been strictly followed during experiment, it is learnt that in reality, the presence of uncertainties in the measured data are inevitable; therefore, it is necessary to curb these uncertainties numerically. In numerical evaluation, in order to accommodate these uncertainties as well as to avoid premature convergence, constraints should be introduced. In the present study, two additional inequality constraints are defined to mitigate the presence of uncertainties, in which, the ratio of in-plane shear modulus (G_{xy}) to in-plane longitudinal elastic modulus (E_x) as well as the ratio of in-plane shear modulus (G_{xy}) to in-plane transverse elastic modulus (E_y) are restricted to be within the range of 0 to 1. Furthermore, since the range of elastic properties is unknown in practical applications, the search boundaries of elastic properties can initially be set large enough to encompass possible search areas. In addressing uncertainties in the measured results, the influence of these errors/uncertainties on the end outcomes are studied and presented. Three different levels of errors, namely, 1%, 5% and 10% are artificially introduced into the “measured” natural frequencies and these “erroneous” natural frequencies are subsequently used as the reference parameters in the proposed hybrid algorithm. The uncertainties (i.e. 1%, 5% and 10%) are assigned in the way that

the specified amount represents the upper limit of the range of the uncertainty. For example, a 10% uncertainty indicates an uncertainty that lies within the range of 0 to 10%. Five sets of computations are executed and the set with the relatively best minimised objective function value is chosen and presented in Table 4.38 and Table 4.39. The reason of introducing three levels of errors is to investigate the influence of increasing errors on the absolute percentage error of the identified elastic properties. The error level is set up to 10% considering it is in the worst-case scenario. Apart, this investigation is extended to the graphite epoxy and aluminium plates to study the effects of the types of plate on the absolute percentage error of identified elastic properties in the presence of errors. It is noted that the absolute percentage error is evaluated on the basis of the absolute percentage error between the identified elastic properties and the actual reference elastic properties. From Table 4.38 and Table 4.39, the identified elastic moduli (E_x and E_y), as well as the identified in-plane shear modulus (G_{xy}) experience elevated deviations as the error level rises from 1% to 10% with the absolute percentage error ranging from 0.01% to 8%. On the other hand, the evaluated Poisson's ratio (ν_{xy}) fluctuates within the range of 0.02% to 13% in the presence of increasing level of error. This occurrence could possibly due to the insignificant influence of natural frequency on the identified Poisson's ratio, ν_{xy} . During initialization of numerical evaluation, the value of Poisson's ratio is first randomly assigned. Because of the insignificant influence of natural frequencies on the Poisson's ratio, great changes in natural frequency induce little changes in the Poisson's ratio, causing the identified Poisson's to be locally trapped near its initial value. Therefore, it can be observed that the identified Poisson's ratio fluctuates and deviates more from its actual value if compared to the other elastic constants. Overall, the proposed hybrid algorithm is proven to be able to produce reliable identification results in the presence of errors, regardless of types of material as well as boundary conditions.

Table 4.38: Identified elastic properties of aluminium plate in the presence of increasing errors

	$E_x(GPa)$	$E_y(GPa)$	$G_{xy}(GPa)$	ν_{xy}
Benchmark	72.4	72.4	28	0.33
F-F-F-F				
1%	72.5913 [0.2642]	72.4991 [0.1369]	28.0085 [0.0304]	0.3290 [0.3030]
5%	71.1711 [1.6974]	72.2650 [0.1865]	28.2343 [0.8368]	0.3190 [3.3333]
10%	73.9361 [2.1217]	77.4832 [7.0210]	28.2909 [1.0389]	0.2947 [10.6970]
C-F-F-F				
1%	72.4563 [0.0778]	71.9042 [0.6848]	27.7964 [0.7271]	0.3524 [6.7879]
5%	71.1265 [1.7590]	71.5846 [1.1262]	27.6695 [1.1804]	0.3626 [9.8788]
10%	70.3329 [2.8551]	68.9921 [4.7070]	28.5882 [2.1007]	0.2999 [9.1212]
C-C-F-C				
1%	72.7744 [0.5171]	72.4439 [0.0606]	27.9578 [0.1507]	0.3243 [1.7273]
5%	71.0602 [1.8506]	71.9986 [0.5544]	29.7598 [6.2850]	0.3212 [2.6667]
10%	69.8662 [3.4997]	67.1080 [7.3094]	30.2124 [7.9014]	0.3091 [6.3333]
#[n]denotes the absolute percentage error with respect to the benchmark value.				

Table 4.39: Identified elastic properties of graphite epoxy plate in the presence of increasing errors

	$E_x(GPa)$	$E_y(GPa)$	$G_{xy}(GPa)$	ν_{xy}
Benchmark	127.9	10.27	7.312	0.22
F-F-F-F				
1%	128.1903 [0.2270]	10.2659 [0.0399]	7.3114 [0.0082]	0.2470 [12.2727]
5%	129.1287 [0.9607]	10.1255 [1.4070]	7.3225 [0.1436]	0.2209 [0.4091]
10%	129.7710 [1.4629]	10.7189 [4.3710]	7.2655 [0.6359]	0.2443 [11.0455]
C-F-F-F				
1%	127.2377 [0.5178]	10.3559 [0.8364]	7.2500 [0.8479]	0.2267 [3.0455]
5%	126.4558 [1.1292]	10.5217 [2.4508]	7.1893 [1.6781]	0.2120 [3.6364]
10%	124.2640 [2.8428]	10.9467 [6.5891]	7.5320 [3.0088]	0.2205 [0.2273]
C-C-F-C				
1%	127.4838 [0.3254]	10.1851 [0.8267]	7.3196 [0.1039]	0.2282 [3.7273]
5%	123.1655 [3.7017]	10.4110 [1.3729]	7.0117 [4.1069]	0.2293 [4.2273]
10%	118.9493 [6.9982]	10.4508 [1.7605]	7.6814 [5.0520]	0.2344 [6.5455]
#[n]denotes the absolute percentage error with respect to the benchmark value.				

4.3.3 Comparative study of different error functions

The results of using the natural frequency error function, mode shape error function and frequency response function (FRF) error function embedded in the proposed hybrid algorithm are presented in this section. Five sets of simulations have been executed and the best set of evaluated elastic properties with the least minimised value is shown in bold, as depicted in Appendix F. Three different types of objective functions have been

utilised and since the sensitivity of each type of objective function with respect to the change in elastic properties is varied, the minimised objective function values are not compared among different types of objective functions used. On the other hand, the computational time of using three different types of error functions is investigated and compared, as presented in Appendix F. The discussion begins with the study of accuracy of using the proposed hybrid algorithm with different error functions, followed by the study of repeatability and lastly, the study of convergence.

4.3.3.1 Accuracy of meta-heuristic hybrid optimisation method with different error functions in reference plates

As shown in Figure 4.23, the absolute percentage error of evaluated E_x using frequency response function (FRF) error function is found to be the least with 0.00172%, followed by those of using natural frequency error function with 1.1651% and mode shape error function with 6.8312%. The error can be seen to be experiencing reduction by approximately 1.2% and 6.8% when using FRF error function with respect to those of using natural frequency and mode shape error functions, respectively. Meanwhile, in Figure 4.24, approximately 6.3% of improvement is visible in the accuracy of the determined E_y when replacing the use of mode shape error function with the use of FRF error function. In the meantime, there is only around 0.9% difference between those of using FRF error function and natural frequency error function. Similarly, as depicted in Figure 4.25, the use of FRF error function exhibit about 7% and 1% greater superiority in determining reliable G_{xy} over the use of mode shape and natural frequency error functions, respectively. Apart, in Figure 4.26, the use of mode shape error function surpasses both the use of natural frequency error function and FRF error function in terms of accuracy of the evaluated ν_{xy} by roughly 27% and 2%, respectively and thus, emerging as the best choice of error function in identifying Poisson's ratio. In the meantime, the use of FRF error function produces considerably

good and reliable Poisson's ratio with 2.2727% of absolute percentage error and about 25% of reduction with respect to that of natural frequency error function only. From Figure 4.23, Figure 4.24, Figure 4.25 and Figure 4.26, it is found that the use of the natural frequency as well as FRF objective functions lead to excellent outcomes, especially the in-plane longitudinal elastic modulus, in-plane transverse elastic modulus and in-plane shear modulus with comparatively small absolute percentage errors. However, discernible inferiority can be seen in determining the major Poisson's ratio when using either of the aforementioned objective function. Instead, the mode shape objective function exhibits convincing ability in evaluating reliable Poisson's ratio with significantly small absolute percentage error. However, the drawback consists in its disability in yielding reliable and accurate elastic moduli and shear modulus. It can be deduced that the absolute percentage errors of the outcomes yielded using FRF lie in between those of natural frequencies and mode shapes. This can be explained by the fundamental equation of the FRFs, which are composed of natural frequencies, mode shapes as well as damping properties.

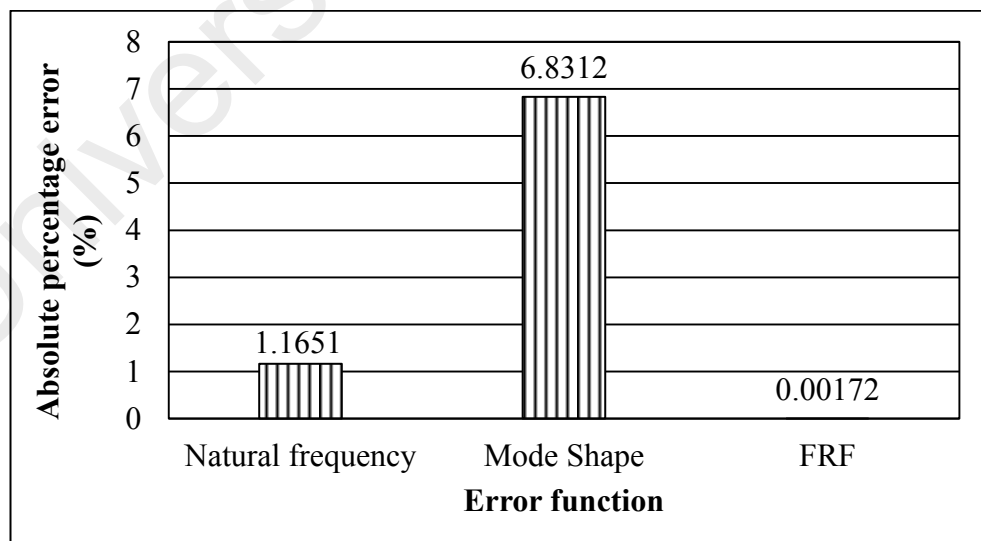


Figure 4.23: Absolute percentage error of evaluated E_x

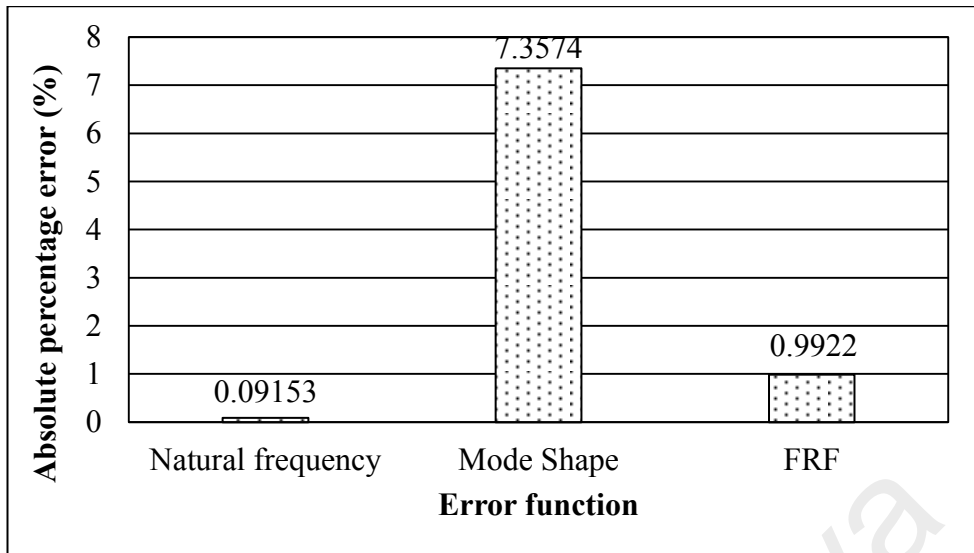


Figure 4.24: Absolute percentage error of evaluated E_y

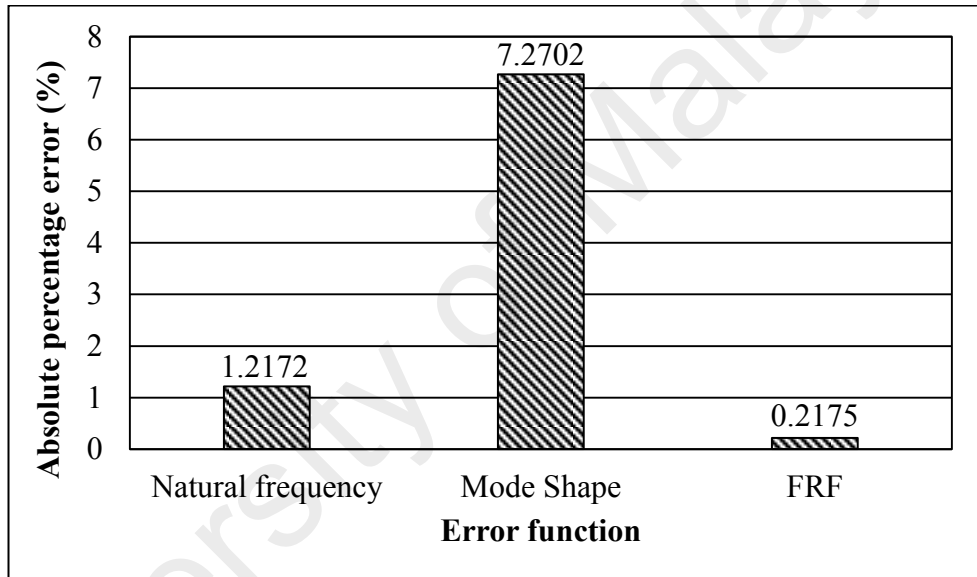


Figure 4.25: Absolute percentage error of evaluated G_{xy}

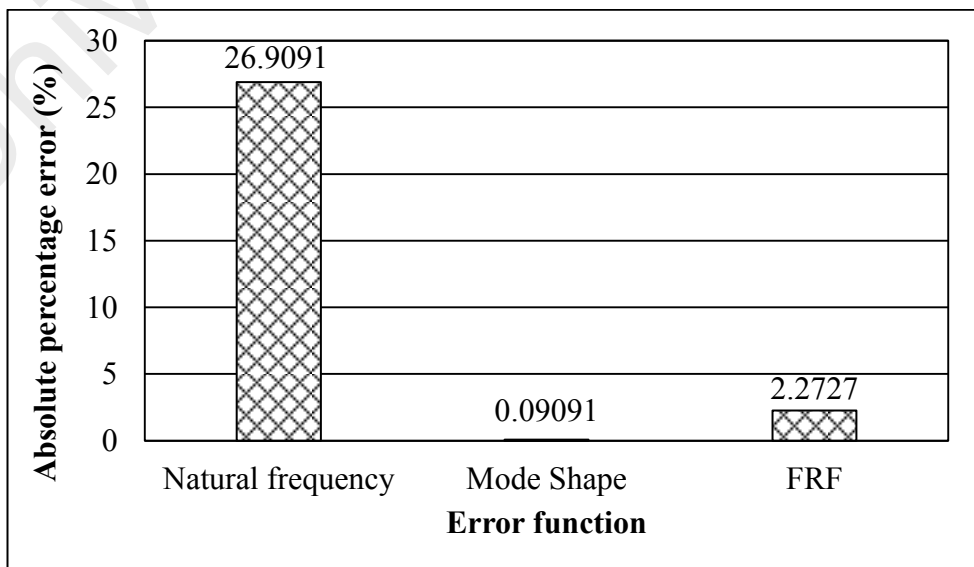


Figure 4.26: Absolute percentage error of evaluated v_{xy}

4.3.3.2 Repeatability of meta-heuristic hybrid optimisation method with different error functions in reference plates

In the study of repeatability, from Figure 4.27, the use of the frequency response function (FRF) error function yields the lowest standard deviation (0.9247) of evaluated E_x with about 3 and 14 in difference with respect to those in natural frequency and mode shape error functions, respectively. As demonstrated in Figure 4.28, even though the standard deviations of identified E_y using the FRF error function is not the lowest (0.1734), its repeatability is convincingly good as the difference of standard deviation with respect to the lowest (0.0131) is not as large as those of evaluated longitudinal elastic modulus. Meanwhile, in Figure 4.29, the repeatability of evaluated G_{xy} using the FRF error function is found the best with standard deviation of 0.08607, followed by the natural frequency error function and mode shape error function with standard deviations of 0.1302 and 0.8531, respectively. In view of the evaluated ν_{xy} as depicted in Figure 4.30, the use of the mode shape error function yields the lowest standard deviation (0.006279), tailed by the use of the FRF error function (0.01315) and the use of the natural frequency error function (0.03505). In general view of Figure 4.27, Figure 4.28, Figure 4.29 and Figure 4.30, the standard deviations of the evaluated E_x , E_y and G_{xy} using the FRF error function are found relatively lower than those of using the mode shape error function. Comparable and even better repeatability can as well be observed in the identified E_x , E_y and G_{xy} when using the FRF error function if compared to those of using the natural frequency error function. On the contrary, the use of the mode shape error function leads to excellent repeatability in the determined ν_{xy} if compared to those of using the natural frequency and FRF error functions, as shown in Figure 4.30. Therefore, it can be addressed that the repeatability of using the FRF error function consists in the trade-off range between those of using the natural frequency and mode shape error functions.

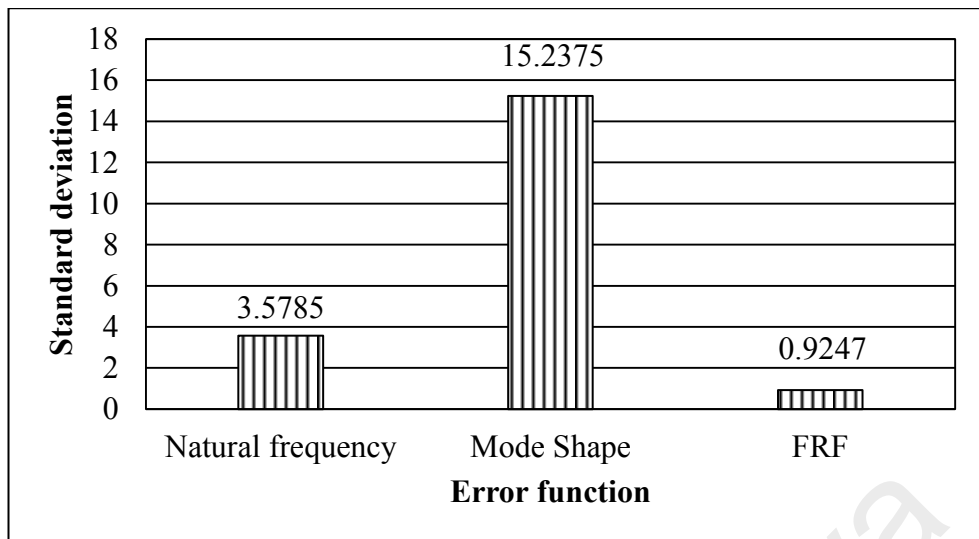


Figure 4.27: Standard deviation of the evaluated E_x

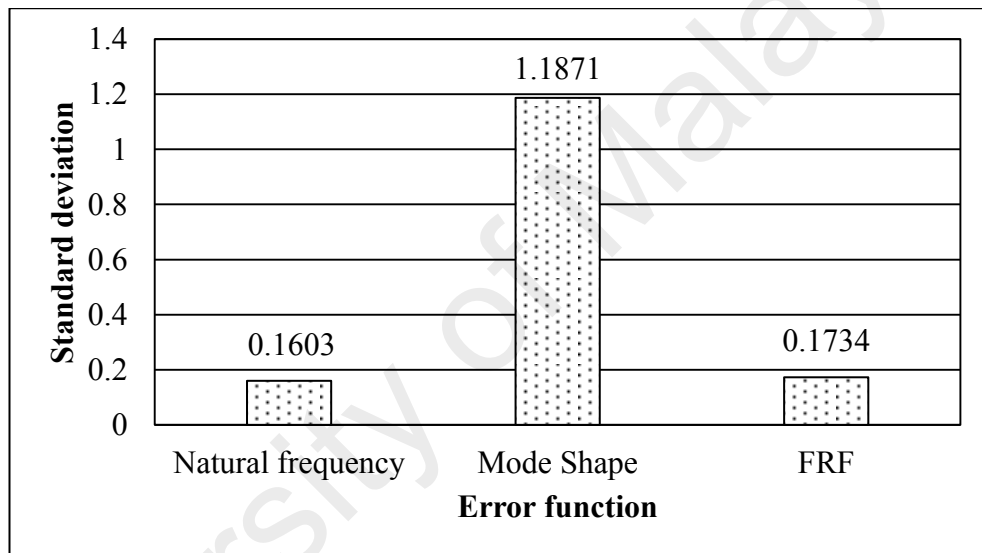


Figure 4.28: Standard deviation of the evaluated E_y

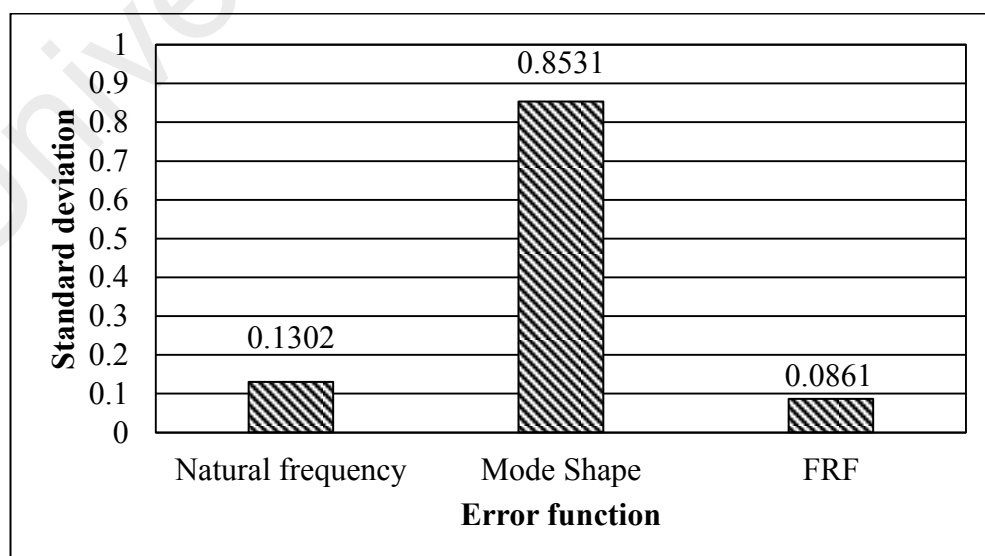


Figure 4.29: Standard deviation of the evaluated G_{xy}

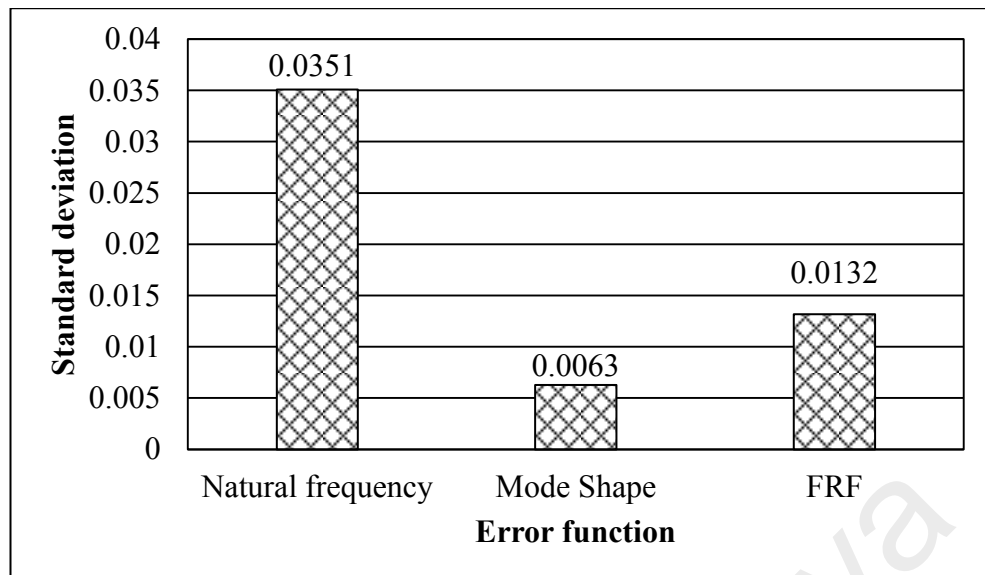


Figure 4.30: Standard deviation of the evaluated v_{xy}

4.3.3.3 Convergence of meta-heuristic hybrid optimisation method with different error functions in reference plates

Furthermore, convergence study is conducted by observing and comparing the computational time consumed by respective error function in identifying the elastic properties of the graphite epoxy plate under the condition that the number of evaluations is fixed. It should be noted that the least computational time consumed by respective error function among five sets of simulations is compared and presented in Figure 4.31. It can be observed that the use of the natural frequency error function consumes the least computational time, with a value of 1277.3374 seconds, followed by the use of the frequency response function (FRF) error function with a value of 2015.4959 seconds and lastly, the use of the mode shape error function consumes the most computational time with a value of 2146.2799 seconds. Widely regarded as a global parameter due to its uniqueness in defining corresponding mode at a particular frequency, the use of the natural frequency error function in material identification appears to be relatively simple in the aspect of procedures and thus, consuming lesser computational time as compared to the use of the mode shape error function as well as FRF error function. More computational time is needed when utilising the mode shape error function due to the

involvement of a greater number of localized parameters, such as the unit displacements of nodes for each vibrational mode. Composed of natural frequencies, mode shapes and damping properties, the use of the FRF error function exhibits the characteristics of those parameters and thus, the computational time is also influenced by those parameters. As compared to mode shapes, FRFs are relatively more localized as well as more information can be retrieved and observed from FRFs. Therefore, it can be seen that the use of the FRF error function consumes relatively more computational time as compared to the use of the mode shape error function. Despite, from the perspective of practical applications, this drawback can be compensated by the processing time consumed during the extraction of experimental natural frequencies and mode shapes from experimental FRF data, in which, these procedures are not required in the use of the FRF error function. As a whole, the use of the FRF error function can be claimed to be the better alternative, accounting for its relatively more complete and satisfactory performances in the aspects of accuracy, repeatability and convergence. The complete sets of computational time are presented in Appendix F.

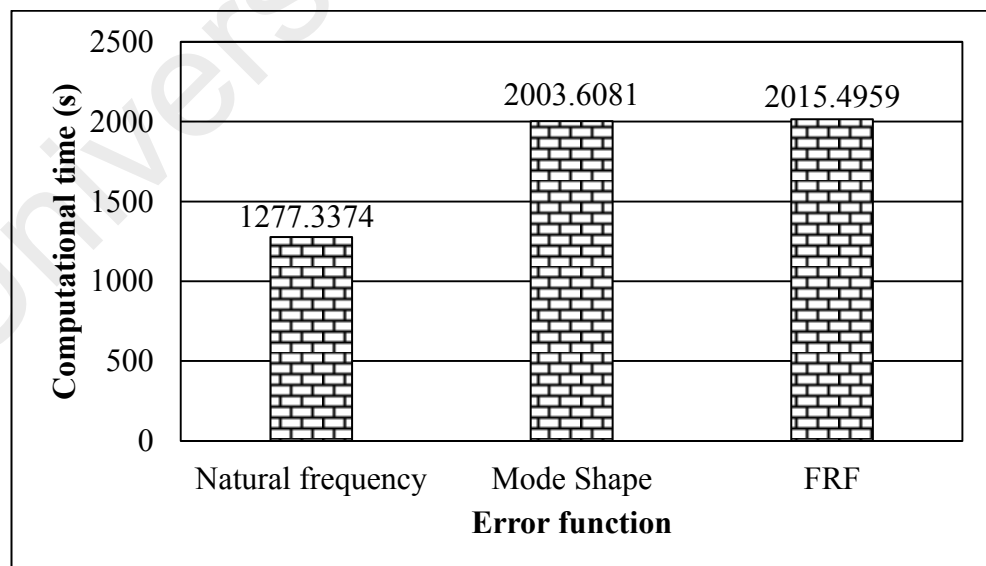


Figure 4.31: Computational time of using different types of error functions

4.3.3.4 Analysis of meta-heuristic hybrid optimisation method with different error functions in reference plates

The analysis and explanation of the results are considerably similar to those of two-stage derivative-based method which involves natural frequencies and mode shapes. The figures above indirectly imply that the sensitivity of natural frequencies with respect to the elastic and shear moduli is relatively higher in comparison to that of the Poisson's ratio. On the contrary, mode shapes are found to be more sensitive to the changes in the Poisson's ratio than those in elastic and shear moduli. As mentioned before, this phenomenon can be associated with the composition of the Poisson's ratio, which is regarded as the ratio of shortening strain to tensile strain. Based on the basic definition of Poisson's ratio, a relationship does exist between the Poisson's ratio and mode shapes as both are fundamentally composed of strains. Mode shapes are defined in terms of nodes' displacements, and these displacements can be obtained via the second order integration of mode curvature (strain). Hence, it can be observed that the use of the mode shape error function yields excellent Poisson's ratio, but not the other elastic properties. With the use of the frequency response functions (FRFs) that are composed of natural frequencies, mode shapes and damping properties, the outcomes are found to be experiencing a great improvement due to the contributions from both natural frequencies and modes shapes.

Apart, the results show that the use of the FRF error function yields better shear modulus compared to both the natural frequency and mode shape error function. The main reason consists in the relation between shear modulus and twisting modes. By general definition, shear modulus is the ratio of shear stress to shear strain. Stress, which is a global parameter, can be found in shear modulus as well as in elastic modulus. Since natural frequency is a global parameter, the use of natural frequency error function is sufficiently good to identify shear modulus and elastic modulus.

However, for shear modulus, it is much related to twisting modes (Hendrickson, 1963), in which, these modes are unique and sometimes they are not symmetric and not uniform. In the present study, the first six non-rigid body modes are involved in the identification process and mode 1, 3 and 6 are found to be twisting modes. Due to their uniqueness, the presence of twisting modes appears to be more significant and distinctive compared to normal bending modes, that are much related to elastic modulus. Therefore, by involving FRFs, which are composed of both natural frequencies and mode shapes, the identifiability of shear modulus can be further improved.

Referring to the use of the mode shape error function, the reliability of the evaluated shear modulus is questionable due to the great influence of stress, which is a global parameter compared to that of strain, which is a local parameter. Even though mode shape is much related to shear strain in the composition of shear modulus, the influence of mode shape on shear modulus, is marginally significant. Therefore, the sole use of the mode shape error function shows inferiority in identifying shear modulus.

4.4 Experimental validation

The results of the destructive test for the acrylonitrile-butadiene-styrene (ABS) plate as well as theoretical calculation for the aluminium composite panel (ACP) are first presented. In the following sections, the results of the proposed non-destructive test are then presented and compared with those obtained from the destructive test and theoretical calculation.

4.4.1 Destructive test

The final benchmark elastic properties of acrylonitrile-butadiene-styrene (ABS) plate obtained from tensile test are presented in Table 4.40.

Table 4.40: Benchmark elastic properties of ABS plate obtained from tensile test

Elastic Properties	Benchmark value obtained from tensile test
$E_x (GPa)$	2.3782
$E_y (GPa)$	2.3050
$G_{xy} (GPa)$	0.8763
ν_{xy}	0.3370

4.4.2 Theoretical calculation

On the other hand, the final benchmark elastic properties of the aluminium composite panel (ACP) obtained from theoretical calculations are presented in Table 4.41.

Table 4.41: Benchmark elastic properties of ACP obtained from theoretical calculation

Elastic Properties	Benchmark value obtained from calculation
$E_x (GPa)$	10.3079
$E_y (GPa)$	10.3079
$G_{xy} (GPa)$	3.8465
ν_{xy}	0.3656

4.4.3 Non-destructive test**4.4.3.1 Method 1: Two-stage derivative-based method****(a) Accuracy of two-stage derivative-based method in experimental plates**

In the study of the acrylonitrile-butadiene-styrene (ABS) plate, from Table 4.42, the identified G_{xy} and ν_{xy} can be seen experiencing a relatively great improvement in accuracy after stage 2 with the absolute percentage errors reduced by 8.7416% and 7.4481%, respectively. This can be explained by the considerable sensitivity of mode shapes with respect to the evaluated G_{xy} and ν_{xy} . On the other hand, relatively small changes can be observed in the identified E_x and E_y after stage 2 as the changes in E_x and E_y are controlled by the suggested regularization parameters.

Table 4.42: Identification results of ABS plate under F-F-F-F boundary condition

F-F-F-F	Static	Stage 1: Natural frequency		Stage 2: Mode shape	
		Initial	Updated	Initial	Updated
E_x (GPa)	2.3782	2.9000	2.6428 [11.1261]	2.6428	2.6245 [10.3566]
E_y (GPa)	2.3050	2.9000	2.6702 [15.8438]	2.6702	2.6760 [16.0954]
G_{xy} (GPa)	0.8763	1.0500	0.9549 [8.9698]	0.9549	0.8783 [0.2282]
ν_{xy}	0.3370	0.3000	0.3035 [9.9407]	0.3035	0.3286 [2.4926]

[#][n]denotes the absolute percentage error with respect to the static test value.

Apart from that, Table 4.43 presents the experimental natural frequencies and mode shapes obtained from experimental modal analysis (EMA) as well as the evaluated natural frequencies and mode shapes obtained using the proposed two-stage derivative-based method. The emphasis is placed on the evaluated mode shapes in stage 1 and stage 2. From a qualitative perspective, a high degree of resemblance can be observed in between all the experimental and evaluated mode shapes as well as there is no discernible difference shown in between the mode shapes obtained from stage 1 and stage 2. Based on the presented mode shapes, mode 1, mode 4 and mode 5 are apparently known to be twisting modes, whereby mode 2 and mode 3 are bending modes. From Table 4.44, it can be seen that mode 2, mode 3, mode 4 and mode 5 experience a reduction in the average node displacement differences after stage 2, thus, it can be directly interpreted that the identifiability of the G_{xy} and the ν_{xy} are mainly contributed by these modes. From the fundamental equations of the shear modulus and Poisson's ratio, the influence of twisting modes on the shear modulus is known to be relatively more significant than that on the Poisson's ratio. Between bending and twisting modes, the influence of bending mode on the Poisson's ratio is relatively more significant. Therefore, it can be inferred that the accuracy of the G_{xy} is further improved, mainly due to the contribution from mode 4 and mode 5 which are regarded as twisting modes, whereby, the accuracy of the ν_{xy} can be seen to have improved after stage 2, mainly due to the influence of mode 2 and mode 3 which are the bending modes. Overall, it can be seen that the weighted absolute relative difference between the

experimental and evaluated modal displacements (*CCMDISP*) is reduced from 1.0318 in stage 1 to 0.9909 in stage 2 . This shows that despite the reduction in *CCMDISP* is small, the implementation of stage 2 with the aid of scaling factors is important in improving the identifiability of the G_{xy} and v_{xy} .

Table 4.43: Comparison of experimental and evaluated natural frequencies and mode shapes for ABS plate

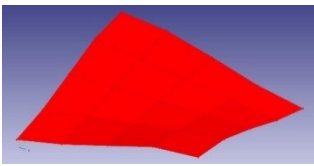
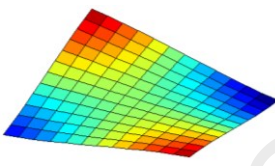
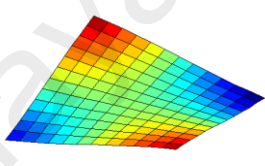
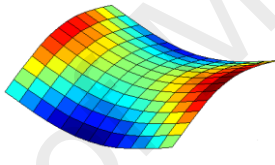
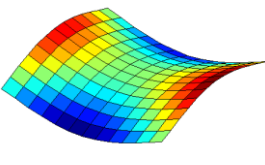
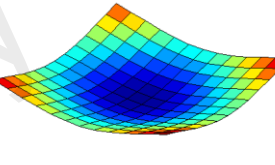
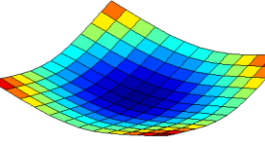
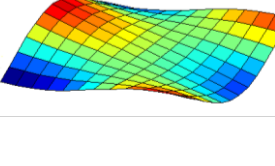
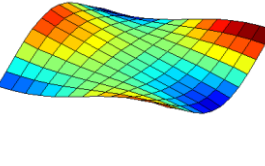
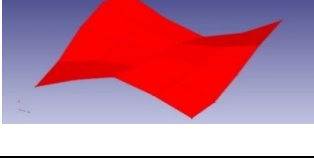
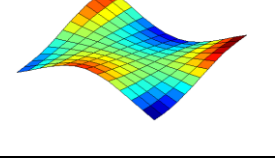
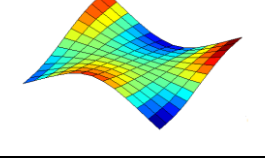
Mode	Experimental measurement	Numerical evaluation	
		Stage 1	Stage 2
1	31.90 Hz 	32.9334 Hz 	31.9337 Hz 
2	47.70 Hz 	48.4408 Hz 	47.8930 Hz 
3	61.70 Hz 	61.6635 Hz 	62.2511 Hz 
4	84.80 Hz 	85.8236 Hz 	84.4028 Hz 
5	84.90 Hz 	85.9887 Hz 	84.7198 Hz 

Table 4.44: Average node displacement difference between experimental and evaluated mode shapes for ABS plate

Mode	Average node displacement difference (dimensionless)	
	Stage 1	Stage 2
1	0.4648	0.4656
2	0.3819	0.3542
3	2.8658	2.7029
4	0.8315	0.8277
5	0.6148	0.6043
<i>CCMDISP</i>	1.0318	0.9909

Furthermore, in the investigation of the aluminium composite panel (ACP), from Table 4.45, the evaluated G_{xy} is found to have deteriorated in terms of accuracy by 6.1614%. This can be explained by the use of theoretical calculation to determine the reference elastic properties of ACP, in which, several assumptions have been made upon applying the formulas, and thus, might have compromised the credibility. The evaluated elastic properties are said to be valid and reasonable since the absolute percentage errors are recorded within 20%. Thus, in this case, the evaluated G_{xy} can be claimed to be in good agreement with the reference G_{xy} with absolute error of 16.4513% after stage 2. Meanwhile, the accuracy of the evaluated ν_{xy} is improved by 13.0197% after stage 2. The changes in E_x as well as in E_y are relatively small if compared to the others as controlled by the specified regularization parameters. Overall, the results are reasonably good and stage 2 is proven important to preserve the accuracy of both the G_{xy} and ν_{xy} with absolute percentage errors of not exceeding 20%.

Table 4.45: Identification results of ACP under F-F-F-F boundary condition

F-F-F-F	Cal	Stage 1: Natural frequency		Stage 2: Mode shape	
		Initial	Updated	Initial	Updated
E_x (GPa)	10.3097	12.0000	11.8014 [14.4689]	11.8014	11.8610 [15.0470]
E_y (GPa)	10.3097	11.0000	10.8456 [4.9412]	10.8456	10.7829 [4.5899]
G_{xy} (GPa)	3.8465	3.5000	3.4507 [10.2899]	3.4507	3.2137 [16.4513]
ν_{xy}	0.3656	0.2800	0.2762 [24.4530]	0.2762	0.3238 [11.4333]
#[n]denotes the absolute percentage error with respect to the calculated value.					

As shown in Table 4.46, the experimental natural frequencies and mode shapes are compared with those of evaluated from stage 1 and stage 2. The experimental mode shapes are almost similar to those of evaluated mode shapes and there is no discernible difference shown in between the mode shapes obtained from stage 1 and stage 2. Similar to the ABS plate, mode 1, mode 4 and mode 5 are twisting modes, while mode 2 and mode 3 are bending modes. Mode 1 contributes to the improved identification of the G_{xy} in stage 2, while, mode 2 and mode 3 contributes to the accurate identification of the v_{xy} as it can be observed from Table 4.47 that mode 1, mode 2 and mode 3 incur a reduction in the average node displacement differences. As a whole, it can be observed that the weighted absolute relative difference between experimental and evaluated modal displacements (*CCMDISP*) experiences a small reduction from 1.1406 in stage 1 to 1.1054 in stage 2. Although the reduction is small, the use of stage 2 in conjunction with scaling factors is proven effective in preserving the identifiability of the G_{xy} and v_{xy} with absolute percentage errors maintained within 20% with respect to the benchmark parameters.

Table 4.46: Comparison of experimental and evaluated natural frequencies and mode shapes for ACP

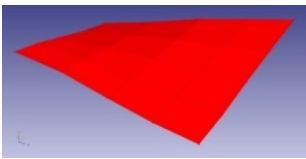
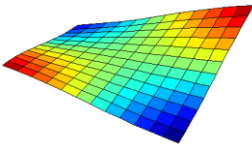
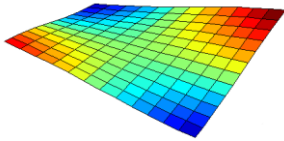
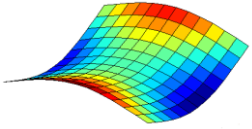
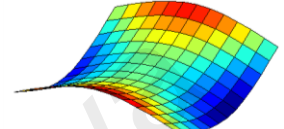
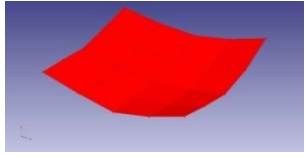
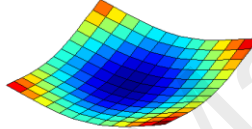
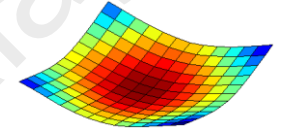
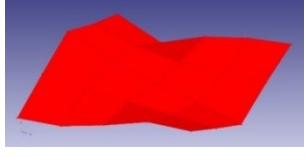
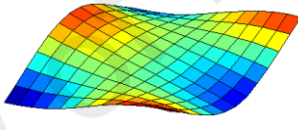
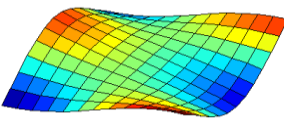
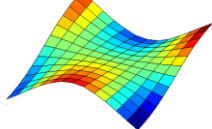
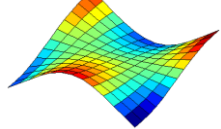
Mode	Experimental measurement	Numerical evaluation	
		Stage 1	Stage 2
1	52.70 Hz 	52.8556 Hz 	51.5486 Hz 
2	82.10 Hz 	85.2059 Hz 	83.2553 Hz 
3	107.00 Hz 	105.2253 Hz 	106.4991 Hz 
4	142.00 Hz 	141.2432 Hz 	139.0896 Hz 
5	149.00 Hz 	143.7471 Hz 	141.9151 Hz 

Table 4.47: Average nodal displacement difference between experimental and evaluated mode shapes for ACP

Mode	Average node displacement difference (dimensionless)	
	Stage 1	Stage 2
1	0.4156	0.4145
2	1.4194	1.3854
3	1.6673	1.4603
4	0.9662	1.0099
5	1.2345	1.2567
<i>CCMDISP</i>	1.1406	1.1054

(b) Repeatability of two-stage derivative-based method in experimental plates

As mentioned, the proposed method is a deterministic approach and the results obtained from five independent runs turn out to be the same. Therefore, it can be inferred that using a fixed set of initial values, the repeatability of this approach appears to be 100% regardless of the number of runs.

(c) Convergence of two-stage derivative-based method in experimental plates

Table 4.48 demonstrates the computational time consumed by the proposed method in identifying the elastic properties of acrylonitrile-butadiene-styrene (ABS) plate. It can be observed that the updating process of stage 2 consumes relatively more time as compared to that of stage 1 due to the consideration of a large number of mode shape information in stage 2 as well as the relatively indirect updating procedures of stage 2. The proposed two-stage derivative-based method consumes about seven minutes of computational time at most in determining the elastic properties of the ABS plate, and this is quite promising as compared to most of the meta-heuristic methods. Depending on the three basic identification stopping criteria, as demonstrated in Table 4.49, it can be observed from Table 4.50 that in stage 1, the first stopping criterion is met, where the maximum number of iteration is achieved (10). In stage 2, the third stopping criterion is satisfied, where the minimum value of convergence is achieved (0.990931). It should be informed that six decimal places are used in the study of convergence due to the relatively small order of magnitude of the convergence value.

Table 4.48: Computational time of ABS plate

Set	Stage 1 (s)	Stage 2 (s)	Total (s)
1	59.0030	359.9599	418.9629
2	58.3020	358.8376	417.1396
3	58.6871	359.2133	417.9004
4	58.1406	359.9401	418.0807
5	58.8989	359.8981	418.7970
Average	58.6063	359.5698	418.1761

Table 4.49: Identification stopping criteria of ABS plate

Stage	Maximum number of iteration	Minimum improvement percentage	Minimum value of convergence
1	10	0.1000	0.0030
2	10	0.0100	1.0000

Table 4.50: Convergence results of ABS plate

Iteration	<i>CCABS</i>	<i>CCMDISP</i>
1	0.012932	1.031773
2	0.011299	1.025390
3	0.009815	1.024478
4	0.008500	1.024344
5	0.007338	1.045571
6	0.006313	0.990931
7	0.005411	-
8	0.004618	-
9	0.003924	-
10	0.003363	-

Furthermore, in the study of the aluminium composite panel (ACP), it is also found that the computational time consumed by the updating process of stage 2 is relatively more than that of stage 1 on account of the involvement of a large number of mode shape parameters as well as the indirect procedures of stage 2. The proposed method consumes about 7 minutes of computational time at most. Notably, the amount of computational time needed is dependent on the termination criteria, namely, maximum number of iteration, minimum improvement percentage and minimum value of convergence, as specified in Table 4.52. From Table 4.53, it can be observed that in stage 1, the second termination criterion is satisfied, where the predefined minimum improvement percentage is achieved at iteration 4 (0.0278%). Meanwhile in stage 2, the

third stopping criterion is met where the solution has converged to the minimum value of convergence (1.105379).

Table 4.51: Computational time of ACP

Set	Stage 1 (s)	Stage 2 (s)	Total (s)
1	23.4339	420.3862	443.8201
2	23.4568	419.5393	442.9961
3	23.4887	419.5177	443.0064
4	23.5556	421.0835	444.6390
5	23.5797	419.3662	442.9458
Average	23.5029	419.9786	443.4815

Table 4.52: Identification stopping criteria of ACP

Stage	Maximum number of iteration	Minimum improvement percentage	Minimum value of convergence
1	10	0.1000	0.0030
2	10	0.0100	1.1100

Table 4.53: Convergence results of ACP

Iteration	<i>CCABS</i>	<i>CCMDISP</i>
1	0.003724	1.140626
2	0.003610	1.115335
3	0.003598	1.122679
4	0.003597	1.118665
5	-	1.116487
6	-	1.117945
7	-	1.105379

4.4.3.2 Method 2: Meta-heuristic hybrid optimisation method (Hybrid GA-ACO-PSO)

(a) Selection of frequency response functions (FRFs)

A two-stage approach with a two-level FRF selection scheme is proposed to accommodate the effects due to uncertainties. Stage 1 involves the use of the natural frequency error function while stage 2 involves the use of the FRF error function. Before proceeding to stage 2, the two-level FRF selection is performed. The first level involves the selection of modes that are sensitive to the target elastic properties (in-plane shear modulus and Poisson's ratio). The mode selection is made based on the

results obtained from a sensitivity study. The second level involves the selection of FRFs based on the node position (or impact location) that lies in the high response regions of the selected modes.

A sensitivity study is conducted in the investigation of experimental plates to serve as a useful reference for the mode selection. As mentioned, the selection of modes is conducted mainly to specify as well as to narrow down the frequency range of the FRFs, hence, improving the identifiability of the in-plane shear modulus and Poisson's ratio. The sensitivity plots of the ABS plate and ACP are demonstrated in Figure 4.32 and Figure 4.33, respectively. It can be observed that the plots of both the ABS plate and ACP are similar, in which, the influence of mode 1, mode 4 and mode 5 on G_{xy} can be seen to be relatively greater as compared to that of mode 2 and mode 3. This can be explained by the twisting behaviours of the aforementioned modes, as depicted in Figure 4.34 and Figure 4.35. The presence of shear strain in these modes is relatively more significant if compared to that of bending strain. Since the in-plane shear modulus is fundamentally related to shear strain, the influence of these modes on the in-plane shear modulus is found to be substantial. Furthermore, in comparison to the rest of the modes, mode 2 and mode 3 are found to be relatively more sensitive to ν_{xy} . The reason consists in the bending characteristics of these modes, as shown in Figure 4.34 and Figure 4.35, in which, the presence of bending strain in these modes is relatively significant than that of shear strain. Since the Poisson's ratio is basically composed of bending strain, these bending modes are thus possessing larger influence on the Poisson's ratio. Therefore, in stage 2, FRFs containing modes that are sensitive to both G_{xy} as well as ν_{xy} can be selectively adopted into the identification process to further improve the identifiability of the in-plane shear modulus and the Poisson's ratio. As compared to natural frequencies, more local information can be retrieved from FRFs as it is basically composed of natural frequencies, mode shapes and damping properties.

Therefore, instead of selectively adopting natural frequencies, which are more global, the use of FRFs in stage is the better option.

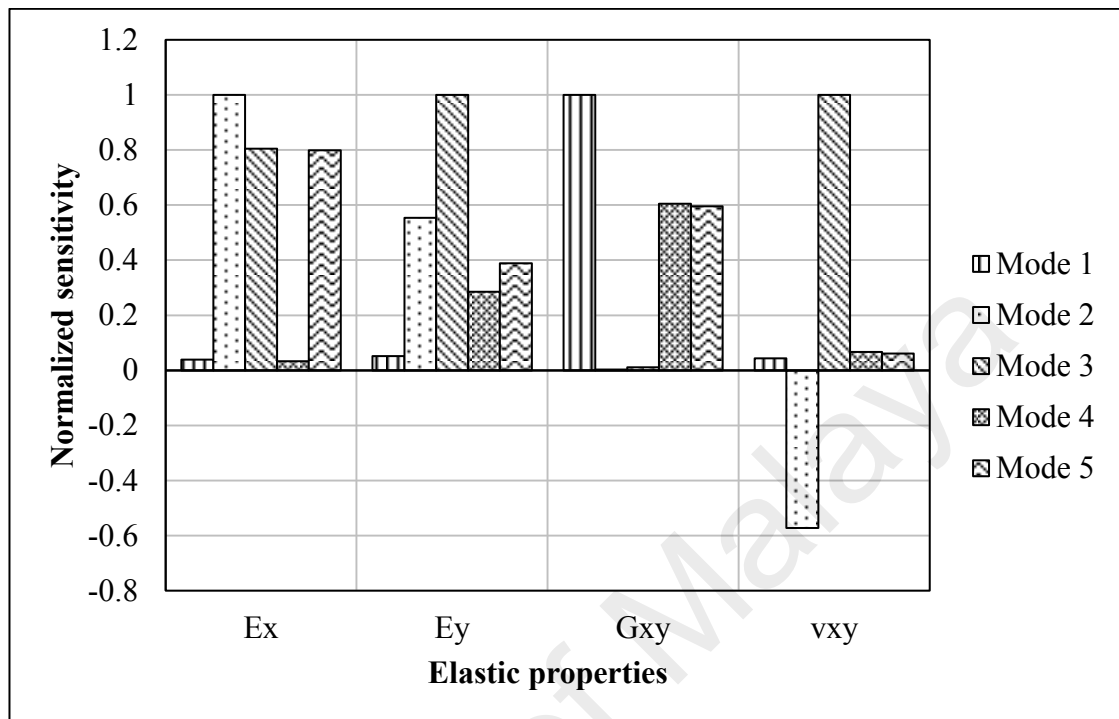


Figure 4.32: Sensitivity graph of ABS plate

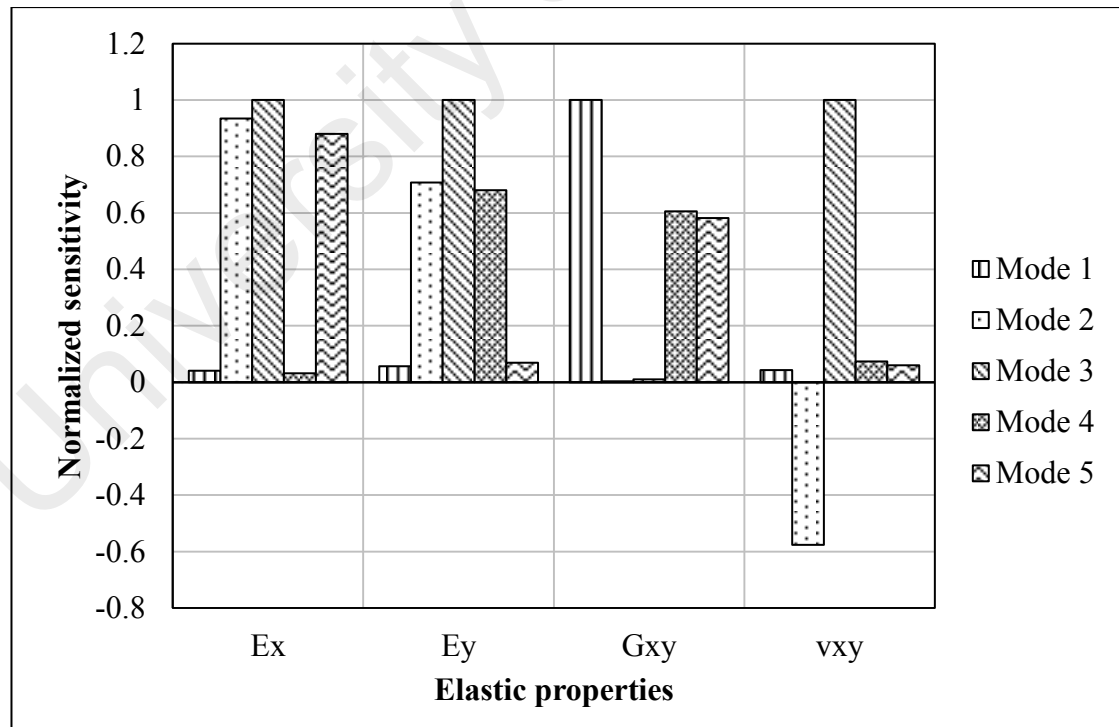


Figure 4.33: Sensitivity graph of ACP

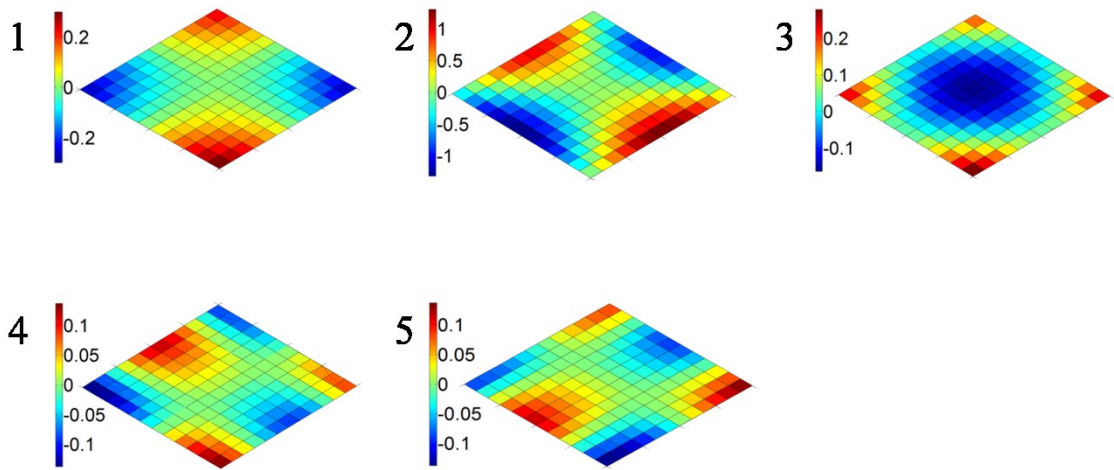


Figure 4.34: Corresponding mode shapes of ABS plate after stage 1

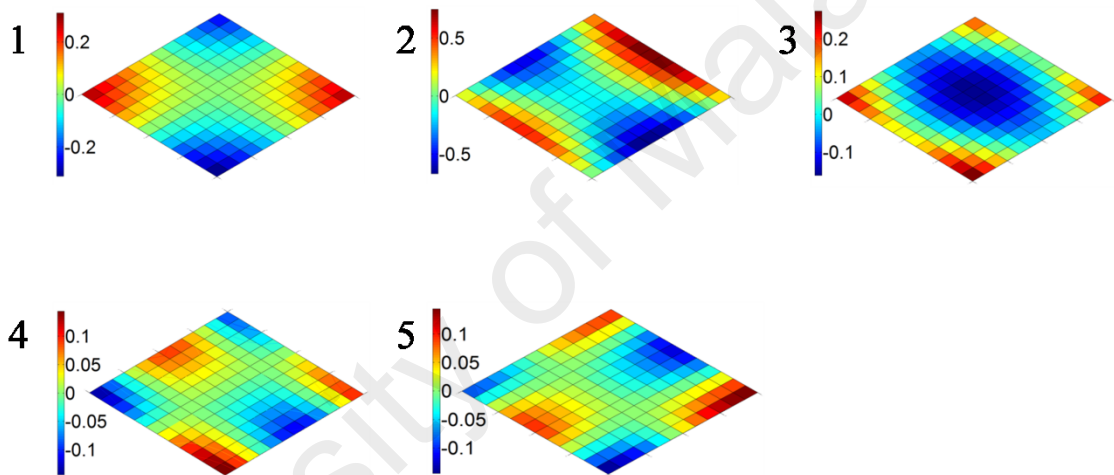


Figure 4.35: Corresponding mode shapes of ACP after stage 1

There are a total of 25 DOFs defined over each plate and each designated DOF possesses respective set of FRF, depending on the input and output DOF. In this context, input DOF refers to the location of impact (roving impact hammer), while, output DOF refers to the location of response received (fixed accelerometer). As demonstrated in Figure 4.36 and Figure 4.37, the corresponding modes of interest for the ABS plate and ACP determined from the first level, which include mode 1 and mode 3, are of great emphasis. In the second level of the FRF selection scheme, four sets of FRFs corresponding to the location of impact at point 5, 9, 21 and 25 with respect to the fixed location of response received at point 1 are selected on account of the dominant contributions of mode 1 and mode 3 in those selected locations, as depicted in Figure

4.36 and Figure 4.37. It can be seen that point 5, 21 and 25 lie in high response regions of mode 1 and mode 3, whilst, point 9 is placed at relatively low response regions of mode 1 and mode 3. Despite located at relatively low response regions of mode 1 and mode 3, the FRF yielded from the location of impact at point 9 is still selected due to the clear visibility of the peaks of mode 1 and mode 3 in the FRF.

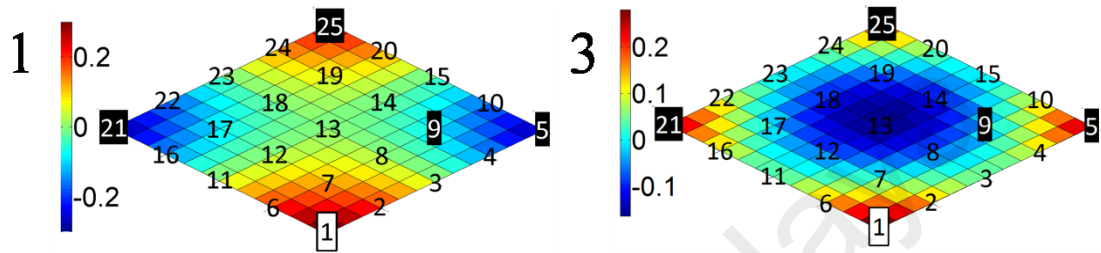


Figure 4.36: 25 measurement DOFs of corresponding modes of the ABS plate determined from the first level FRF selection scheme

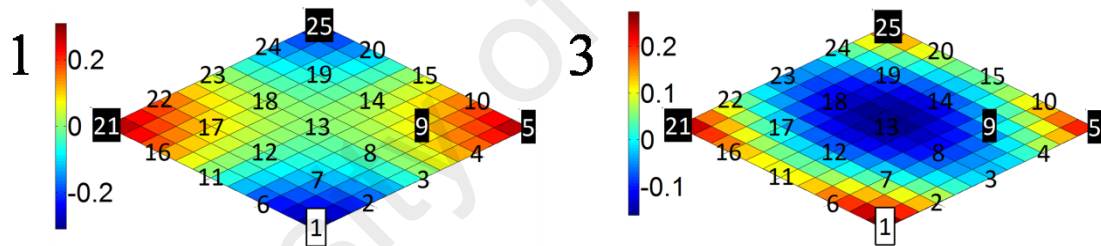


Figure 4.37: 25 measurement DOFs of corresponding modes of ACP determined from the first level FRF selection scheme

(b) Accuracy of meta-heuristic hybrid optimisation method with frequency response function (FRF) error function in experimental plates

Table 4.54 presents the experimental and evaluated natural frequencies of the ABS plate in the first stage. The natural frequencies evaluated in the first stage can be seen to have matched reasonably well with the experimental natural frequencies, garnering the maximum absolute percentage error of 0.9567%. It can as well be observed that the presence of uncertainties in higher modes is relatively more significant, which leads to relatively larger absolute percentage error in higher modes.

Table 4.54: Experimental and evaluated natural frequencies of ABS plate in the first stage

Natural frequency (<i>Hz</i>)	1 st	2 nd	3 rd	4 th	5 th
Experimental	31.90	47.70	61.70	84.80	84.90
Evaluated	32.0077 [0.3376]	47.6636 [0.0763]	61.5580 [0.2301]	83.9887 [0.9567]	84.2800 [0.7303]
#[n] denotes the absolute percentage error with respect to the experimental value.					

In view of FRF, slight changes can be seen on the evaluated FRFs of the ABS plate before and after the second stage, as depicted in Figure 4.38, Figure 4.39, Figure 4.40 and Figure 4.41. It is notable that the level of coincidence between the experimental and evaluated resonance peaks is of greater importance as compared to that of the other local frequencies. From the figures, it can be observed that the resonance peaks indicating mode 1 and mode 3 in the evaluated FRFs experience a slight improvement and coincide well with those of the experimental FRFs after the second stage. Referring to Figure 4.38, Figure 4.39 and Figure 4.40, a noticeable reduction can as well be seen in the magnitude difference between the experimental and evaluated local frequencies after the second stage, with the indications shown in black. Certainly, in some cases, the magnitude difference between the experimental and evaluated local frequencies can be seen in a rise after the second stage, with the notations marked in green. The reason consists in the reach of a compromise, such that, a reduction in magnitude difference of particular local frequencies could somehow cause an increment in magnitude difference of the other. Contrary to the others, Figure 4.41 shows no significant changes in the magnitude difference between the experimental and evaluated FRFs on account of the reach of sufficient improvement.

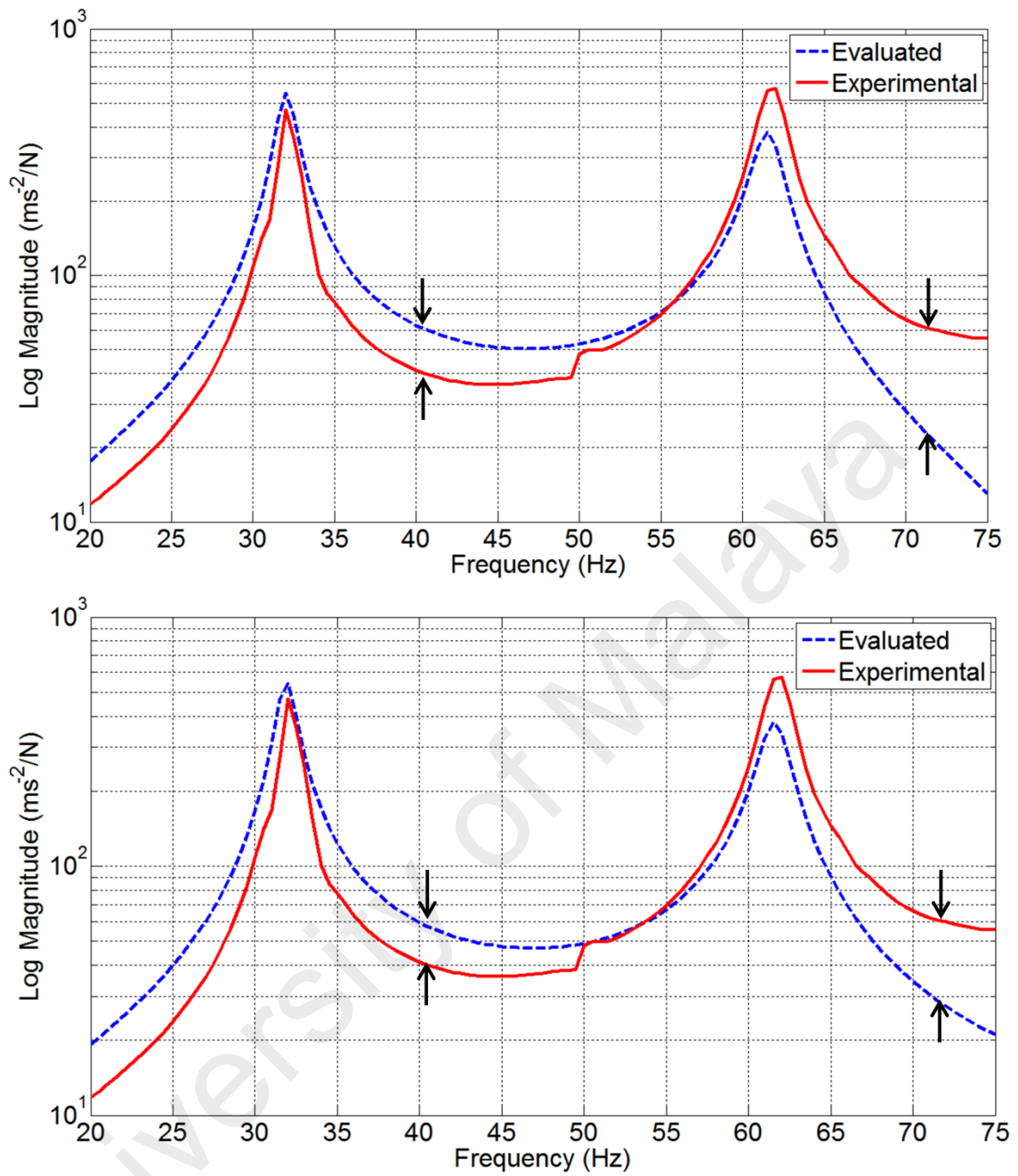


Figure 4.38: Evaluated and experimental FRFs of ABS plate before (top) and after (bottom) the second stage with input DOF at point 5 and output DOF at point 1. Note: Arrow in black indicates a reduction in magnitude difference before and after the second stage.

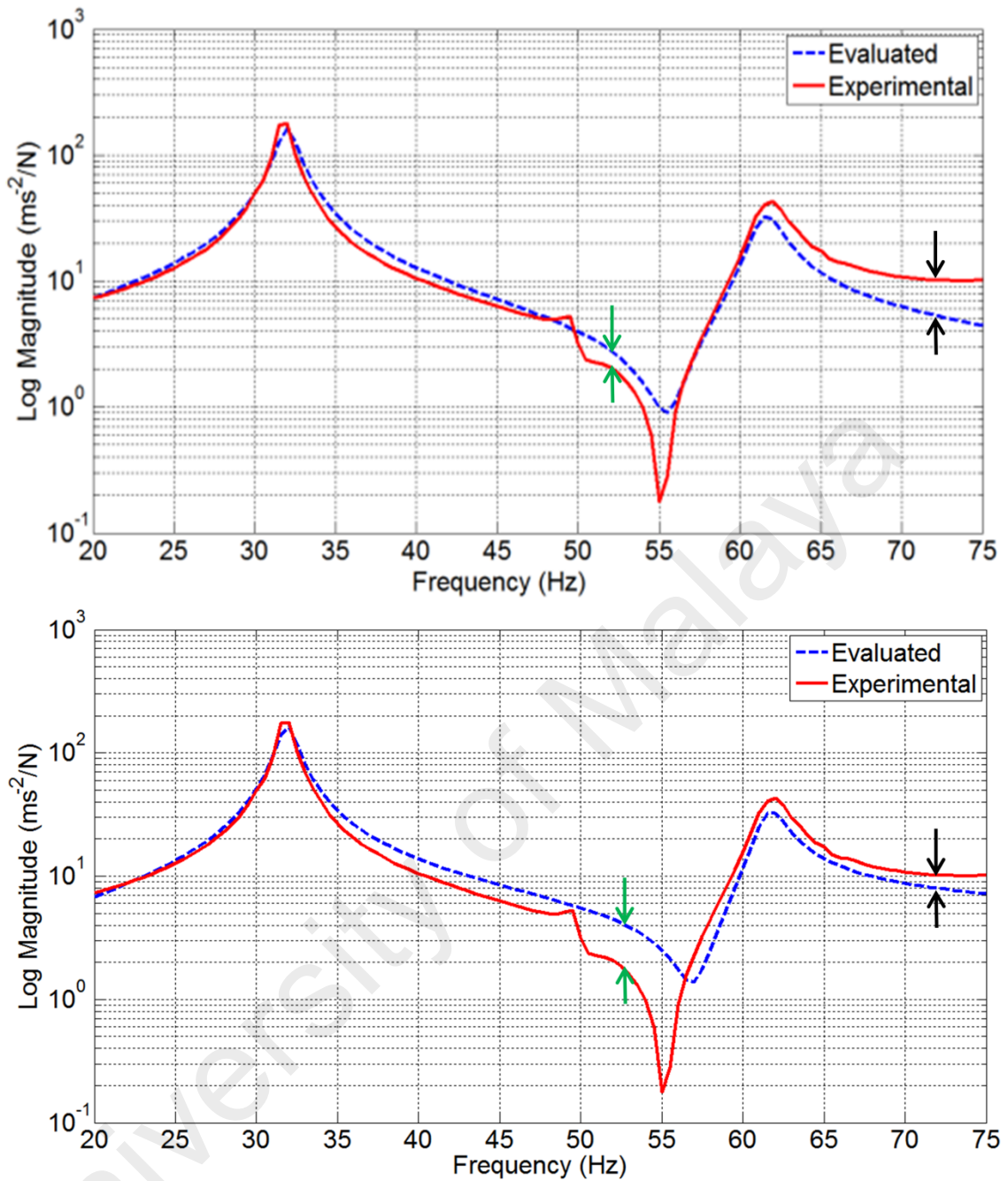


Figure 4.39: Evaluated and experimental FRFs of ABS plate before (top) and after (bottom) the second stage with input DOF at point 9 and output DOF at point 1. Note: Arrow in black indicates a reduction in magnitude difference before and after the second stage, while arrow in green denotes an increment in magnitude difference before and after the second stage.

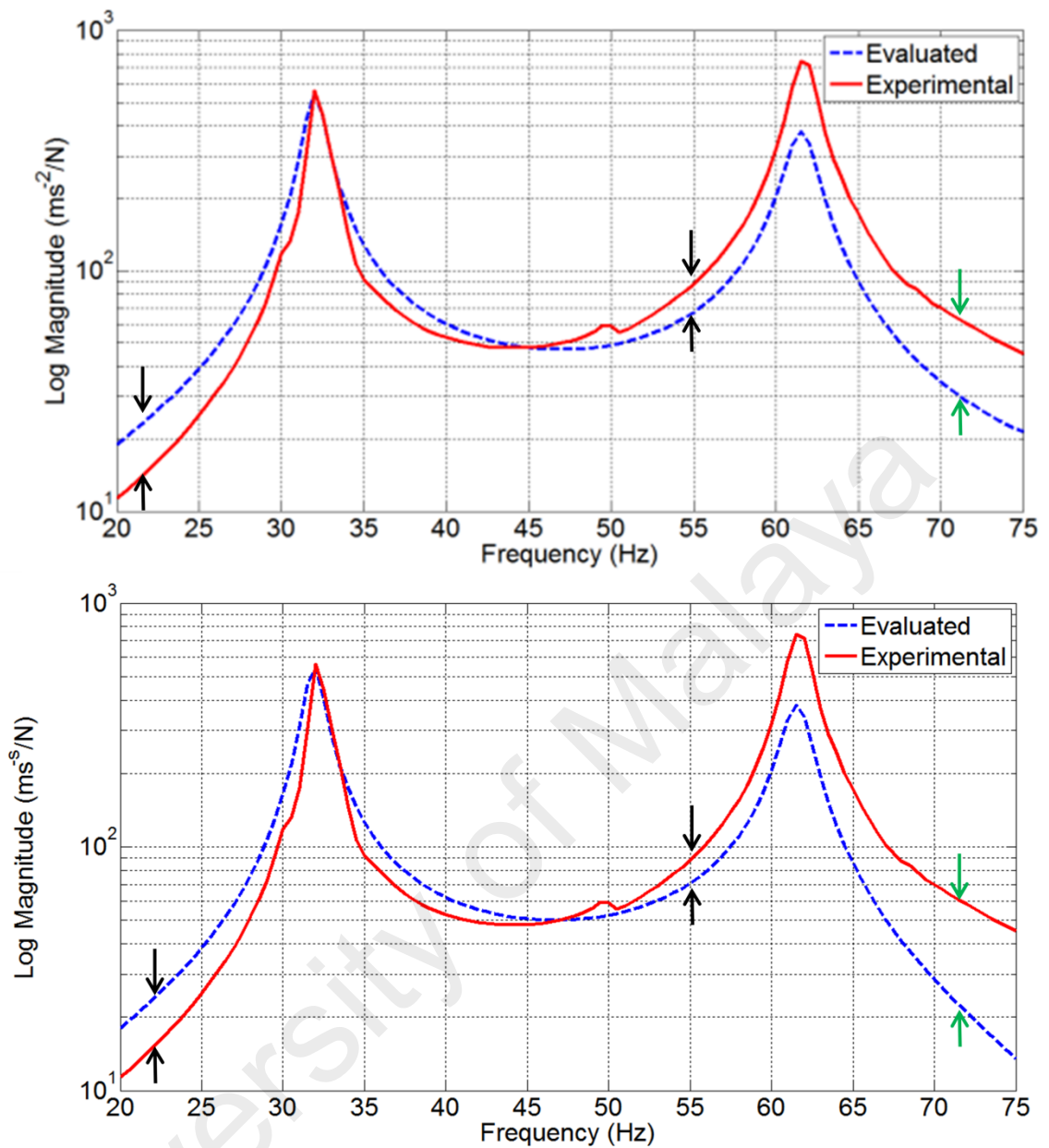


Figure 4.40: Evaluated and experimental FRFs of ABS plate before (top) and after (bottom) the second stage with input DOF at point 21 and output DOF at point 1. Note: Arrow in black indicates a reduction in magnitude difference before and after the second stage, while arrow in green denotes an increment in magnitude difference before and after the second stage.

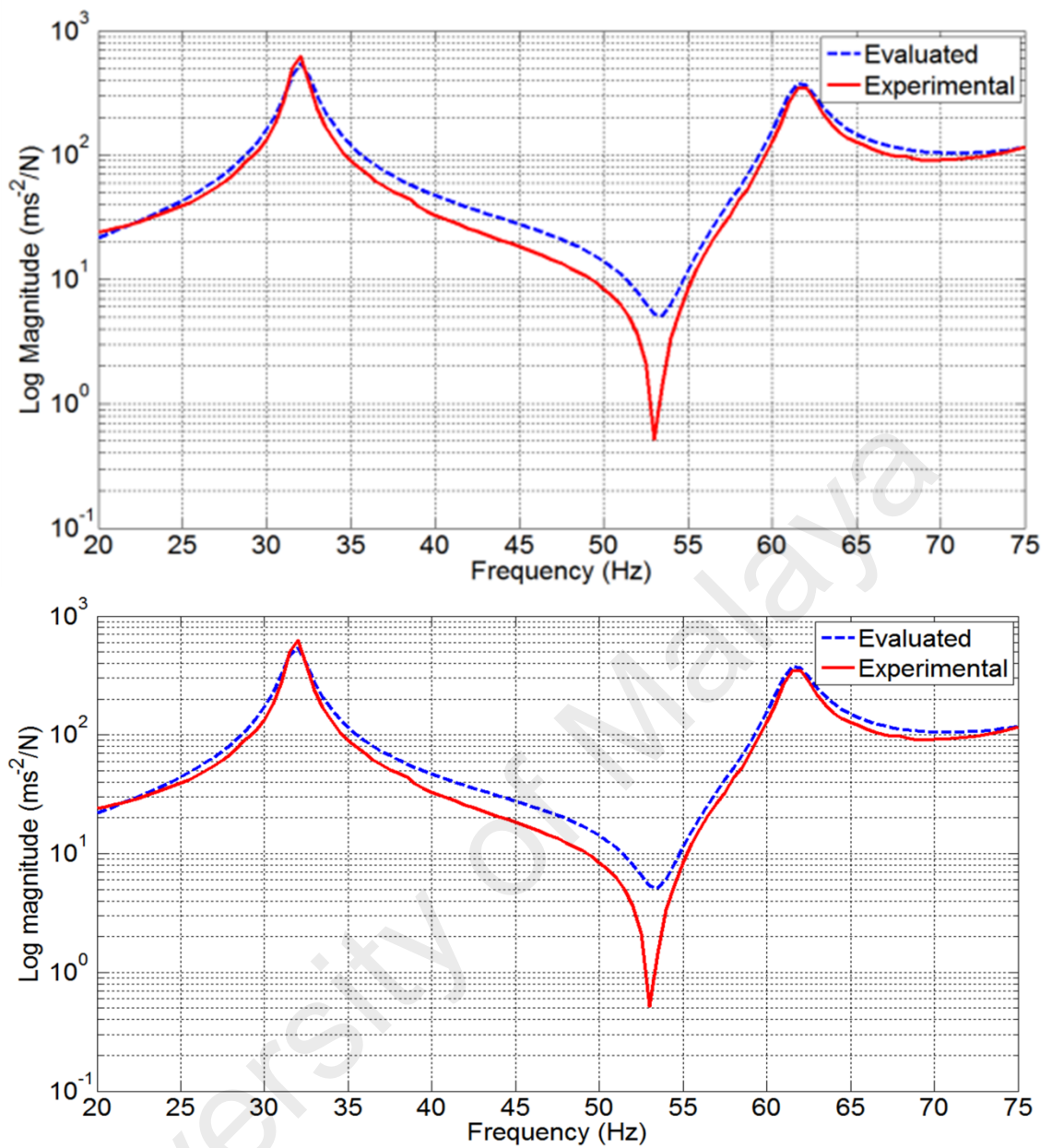


Figure 4.41: Evaluated and experimental FRFs of ABS plate before (top) and after (bottom) the second stage with input DOF at point 25 and output DOF at point 1.

The evaluated elastic properties of the ABS plate using the natural frequency error function in the first stage as well as the FRF error function in the second stage are presented in Table 4.55 and Table 4.56, respectively. In the first stage, the best evaluated E_x , E_y , G_{xy} , and ν_{xy} are reported to be $2.5682GPa$, $2.6156GPa$, $0.8992GPa$ and 0.3188 , respectively with the minimised value of $1.6597E - 04$. On the other hand, in the second stage, the best evaluated E_x , E_y , G_{xy} , and ν_{xy} are discovered to be $2.5864GPa$, $2.5582GPa$, $0.8917GPa$ and 0.3314 , respectively with the minimised value of 1.1228 . Comparison shall not be made upon the minimised values obtained from both stages due to different application of error functions. It can be observed that the absolute percentage error of the evaluated G_{xy} with respect to the benchmark parameter is reduced from 2.6133% in the first stage to 1.7574% in the second stage, while, the absolute percentage error of the evaluated ν_{xy} can as well be seen experiencing a drop from 5.4006% in the first stage to 1.6617% in the second stage. From the overall results, it can be inferred that the application of the FRF error function is able to improve the identifiability of the in-plane shear modulus and the Poisson's ratio of the ABS plate.

Table 4.55: Evaluated elastic properties of ABS plate using natural frequency error function in stage 1

Set	E_x (GPa)	E_y (GPa)	G_{xy} (GPa)	ν_{xy}	Minimised value
Tensile	2.3782	2.3050	0.8763	0.3370	-
LB	1.5000	1.5000	0.5000	0.2000	-
UB	3.5000	3.5000	2.0000	0.4000	-
1	2.6399	2.5671	0.9088	0.3158	1.8516E-04
2	2.5452	2.6499	0.9119	0.3185	1.7074E-04
3	2.6667	2.5047	0.8987	0.3293	2.2873E-04
4	2.5280	2.7476	0.8970	0.3079	2.3707E-04
5*	2.5682 [7.9892]	2.6156 [13.4751]	0.8992 [2.6133]	0.3188 [5.4006]	1.6597E-04
Mean	2.5896 [8.8891]	2.6170 [13.5358]	0.9031 [3.0583]	0.3181 [5.6083]	1.9753E-04

*The set in bold indicates the best set amongst the five sets with the least minimised value.
[#][n] denotes the absolute percentage error with respect to the tensile test value.

Table 4.56: Evaluated elastic properties of ABS plate using FRF error function in stage 2

Set	E_x (GPa)	E_y (GPa)	G_{xy} (GPa)	ν_{xy}	Minimised value
Tensile	2.3782	2.3050	0.8763	0.3370	-
LB	2.3500	2.3500	0.8000	0.3000	-
UB	2.9000	2.9000	1.0000	0.3500	-
1*	2.5864 [8.7545]	2.5582 [10.9848]	0.8917 [1.7574]	0.3314 [1.6617]	1.1228
2	2.6417	2.4608	0.8927	0.3477	1.1241
3	2.5582	2.5163	0.8904	0.3497	1.1254
4	2.5901	2.5527	0.8940	0.3344	1.1333
5	2.7982	2.4600	0.8910	0.3305	1.1267
Mean	2.6349 [10.7939]	2.5096 [8.8764]	0.8920 [1.7916]	0.3387 [2.2028]	1.1265
*The set in bold indicates the best set amongst the five sets with the least minimised value. #[n] denotes the absolute percentage error with respect to the tensile test value.					

Table 4.57 demonstrates the experimental and evaluated natural frequencies of the ACP after first stage identification. It can be observed that the first natural mode experiences the largest deviation with respect to the experimental natural frequency probably due to the presence of deformities at microscopic level, which is not taken into account in the computation. As a whole, the evaluated natural frequencies correlate considerably well with the measured natural frequencies.

Table 4.57: Experimental and evaluated natural frequencies of ACP after the first stage

Natural frequency (Hz)	1 st	2 nd	3 rd	4 th	5 th
Experimental	52.70	82.10	107.00	142.00	149.00
Evaluated	53.9054 [2.2872]	82.2233 [0.1502]	106.5531 [0.4177]	139.5983 [1.6913]	147.4436 [1.0446]
#[n] denotes the absolute percentage error with respect to the experimental value.					

The qualitative correlation level between the evaluated and the experimental FRFs of the ACP can be seen to have improved discernably after undergoing the second stage, as demonstrated in Figure 4.42, Figure 4.43, Figure 4.44 and Figure 4.45. From the figures, three peaks denoting modes 1, 2 and 3 can be seen in the experimental FRFs. With the use of the proposed two-stage approach incorporated with a two-level FRF selection scheme, only modes 1 and 3 are selected and involved in the identification. Therefore,

only the peaks denoting modes 1 and 3 can be seen in the evaluated FRF. As emphasized, the coincidence level of the resonance peaks before the experimental and evaluated FRFs is of greater significance as compared to that of the local frequencies. It can be observed that the resonance peaks of experimental FRFs match considerably well with those of the evaluated FRFs after the second stage. Local frequencies around the vicinity of resonance peaks indicating mode 1 also experience a pronounced reduction in magnitude difference after the second stage, as indicated in black. Likewise, the magnitude difference of certain local frequencies can be seen in a rise with the indications shown in green due to the reach of a compromise, as mentioned before.

University of Malaya

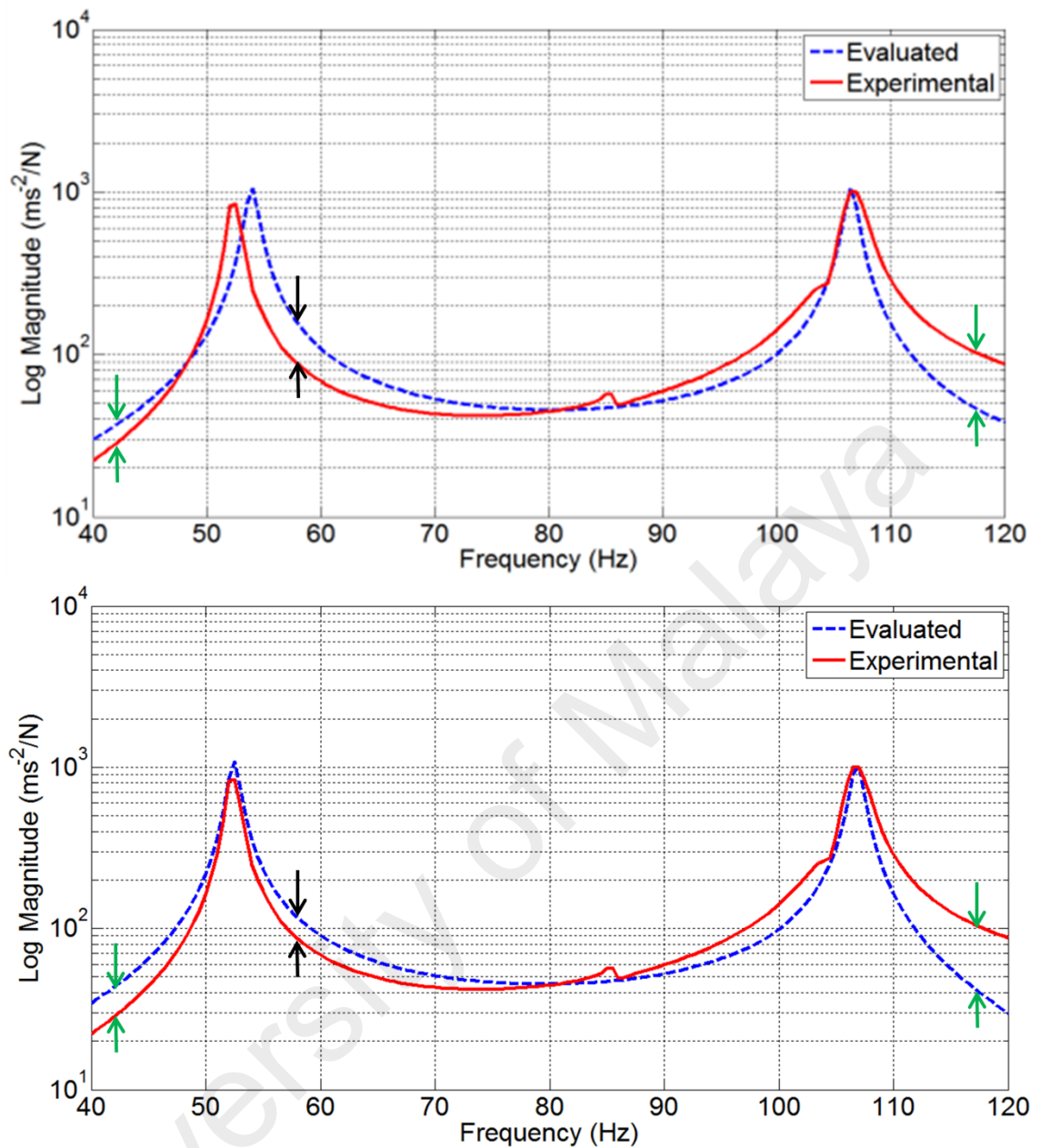


Figure 4.42: Evaluated and experimental FRFs of ACP before (top) and after (bottom) the second stage with input DOF at point 5 and output DOF at point 1. Note: Arrow in black indicates a reduction in magnitude difference before and after the second stage, while arrow in green denotes an increment in magnitude difference before and after the second stage.

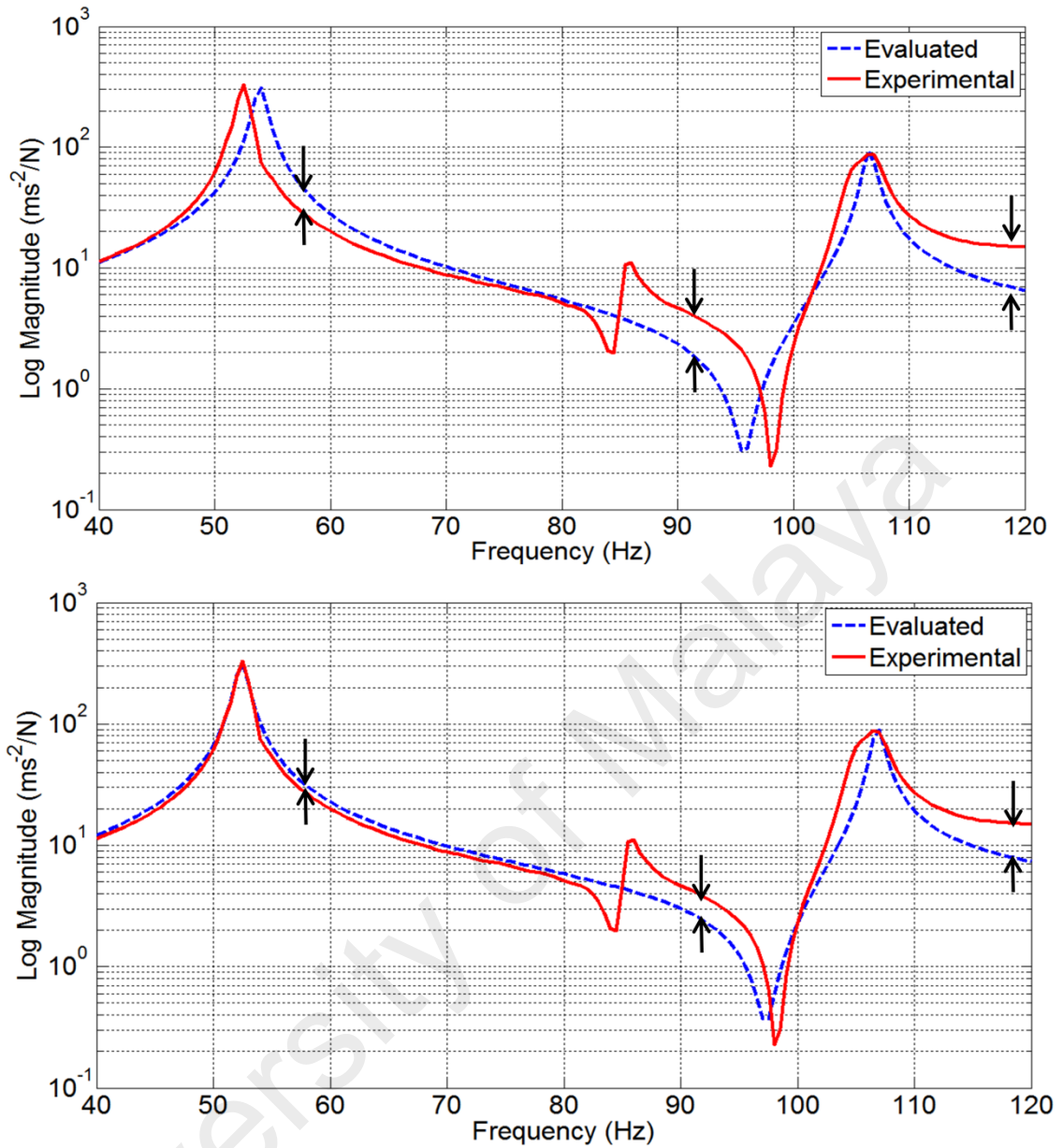


Figure 4.43: Evaluated and experimental FRFs of ACP before (top) and after (bottom) the second stage with input DOF at point 9 and output DOF at point 1. Note: Arrow in black indicates a reduction in magnitude difference before and after the second stage.

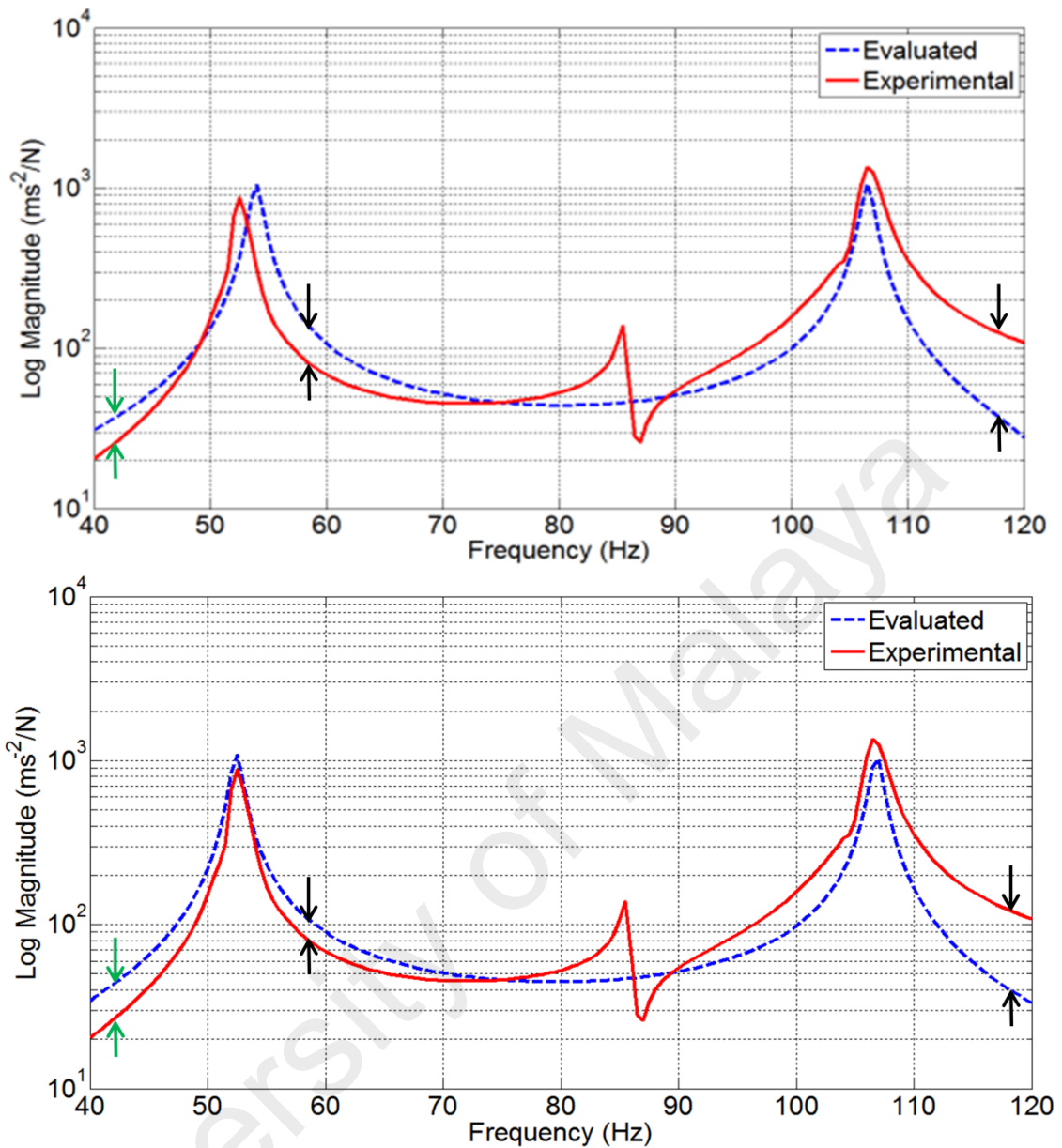


Figure 4.44: Evaluated and experimental FRFs of ACP before (top) and after (bottom) the second stage with input DOF at point 21 and output DOF at point 1. Note: Arrow in black indicates a reduction in magnitude difference before and after the second stage, while arrow in green denotes an increment in magnitude difference before and after the second stage.

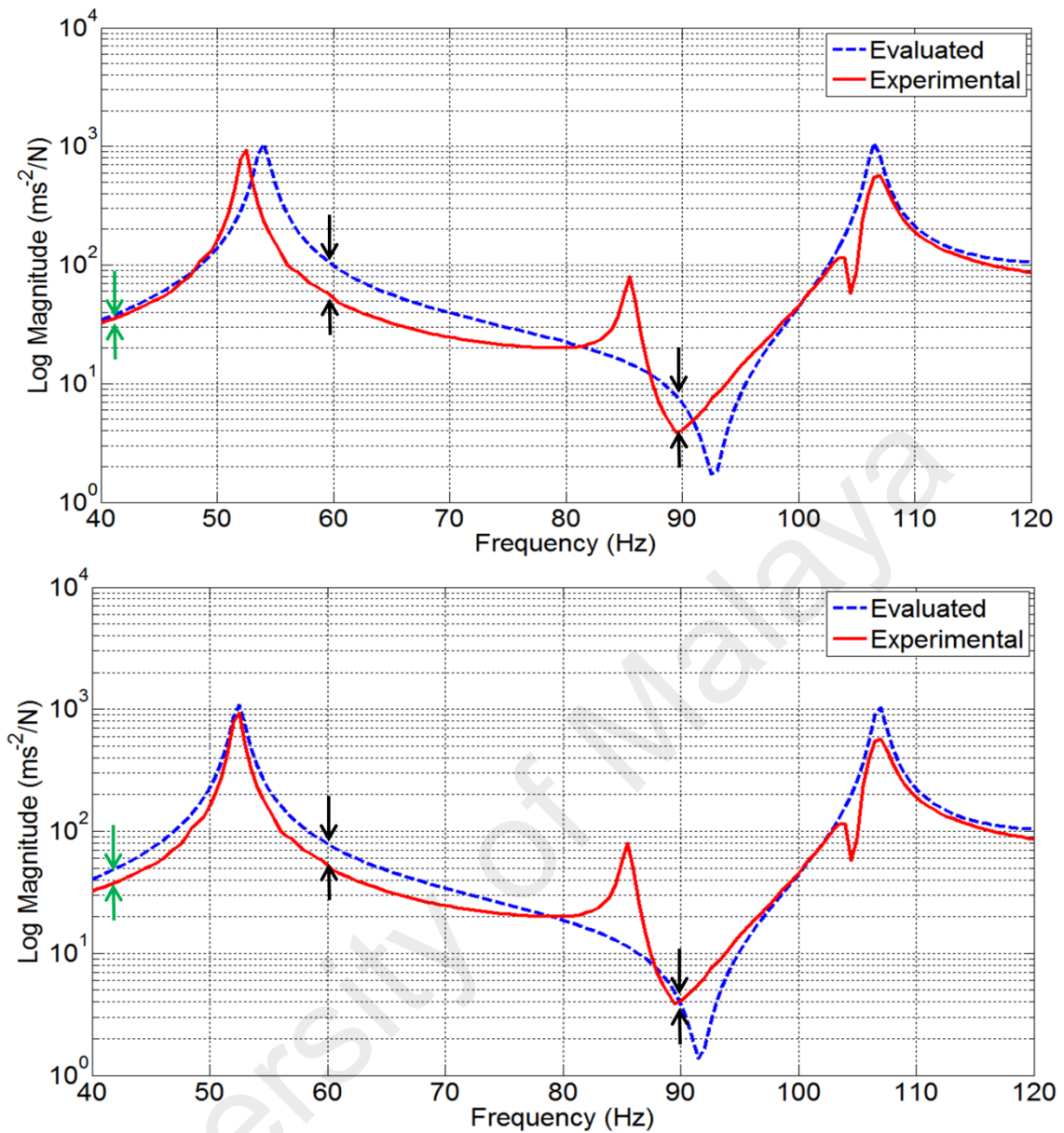


Figure 4.45: Evaluated and experimental FRFs of ACP before (top) and after (bottom) the second stage with input DOF at point 25 and output DOF at point 1. Note: Arrow in black indicates a reduction in magnitude difference before and after the second stage, while arrow in green denotes an increment in magnitude difference before and after the second stage.

Furthermore, in the study of the aluminium composite panel (ACP), the results obtained from stage 1 and stage 2 are presented in, respectively. The elastic properties of the ACP obtained from the first stage and the second stage are presented in Table 4.58 and Table 4.59, respectively. The best evaluated E_x , E_y , G_{xy} , and ν_{xy} using the natural frequency error function are found to be $9.6266GPa$, $12.6695GPa$, $3.6019GPa$ and 0.2433 , respectively with the minimised value of $9.3809E - 04$. Meanwhile, the

best evaluated E_x , E_y , G_{xy} , and ν_{xy} using the FRF error function are discovered to be 11.4612GPa, 10.9005GPa, 3.3863GPa and 0.3184, respectively, with the minimised value of 0.6010. The results show that the identified G_{xy} experiences an increase in the absolute percentage error with respect to benchmark value from 6.3590% in the first stage to 11.9641% in the second stage. On the contrary, a massive improvement can be seen in the accuracy of the identified ν_{xy} with absolute percentage error reduced from 33.4519% in the first stage to 12.9103% in the second stage. This phenomenon may be due to some contradictions arisen between the nature of the real structure and the assumptions made upon performing the theoretical calculation using the well-known formulations, such as, the incorrect hypothesis of a uniform and transversely-isotropic panel. Despite deterioration is shown in the identified in-plane shear modulus with respect to the benchmark value, the evaluated FRFs correlate well with the experimental FRFs after second, as demonstrated before. Overall, it can be deduced that the use of the FRF error function does preserve the identifiability of the in-plane shear modulus and the Poisson's ratio of the ACP with absolute errors maintained below 20%.

Table 4.58: Evaluated elastic properties of ACP using natural frequency error function in stage 1

Set	E_x (GPa)	E_y (GPa)	G_{xy} (GPa)	ν_{xy}	Minimised value
Calculation	10.3097	10.3097	3.8465	0.3656	-
LB	9.0000	9.0000	2.0000	0.2000	-
UB	15.0000	15.0000	4.0000	0.4000	-
1	12.7923	9.7400	3.4414	0.3229	1.1502E-03
2	13.0927	9.5663	3.3504	0.3548	2.2302E-03
3	12.7400	9.8114	3.5889	0.3613	1.0659E-03
4*	9.6266 [6.6258]	12.6695 [22.8891]	3.6019 [6.3590]	0.2433 [33.4519]	9.3809E-04
5	10.5130	12.6308	3.5475	0.2693	1.5205E-03
Mean	11.7529 [13.9985]	10.8836 [5.5666]	3.5060 [8.8522]	0.3103 [15.1258]	1.3795E-03
*The set in bold indicates the best set amongst the five sets with the least minimised value. # [n] denotes the absolute percentage error with respect to the calculated value.					

Table 4.59: Evaluated elastic properties of ACP using FRF error function in stage 2

Set	E_x (GPa)	E_y (GPa)	G_{xy} (GPa)	ν_{xy}	Minimised value
Calculation	10.3097	10.3097	3.8465	0.3656	-
LB	10.0000	10.0000	3.0000	0.2800	-
UB	13.0000	13.0000	4.0000	0.3200	-
1	12.4609	10.4158	3.3946	0.3039	0.6277
2	11.0199	10.9403	3.3612	0.3115	0.6650
3	12.5870	10.3533	3.3657	0.2989	0.6669
4*	11.4612 [11.1691]	10.9005 [5.7305]	3.3863 [11.9641]	0.3184 [12.9103]	0.6010
5	12.1617	11.1326	3.4287	0.2901	0.6241
Mean	11.9381 [15.7948]	10.7485 [4.2562]	3.3873 [11.9381]	0.3046 [16.6849]	0.6369
*The set in bold indicates the best set amongst the five sets with the least minimised value. # [n] denotes the absolute percentage error with respect to the calculated value.					

The results above reveal that the proposed identification method is feasible in improving the identifiability of the in-plane shear modulus and the Poisson's ratio. One of the contributing factors is the introduction of the two-level FRF selection scheme in the identification process. The first level involves the mode selection which is made based on the sensitivity of modes with respect to the in-plane shear modulus and the Poisson's ratio, followed by the second level which involves the selection of FRFs referring to the node position (or the impact location in this study) that lies in the high response regions of the modes of interest determined from the first level.

(c) Repeatability of meta-heuristic hybrid optimisation method with frequency response function (FRF) error function in experimental plates

Table 4.60 and Table 4.61 present the standard deviations of evaluated elastic properties of the acrylonitrile-butadiene-styrene (ABS) plate and aluminium composite panel (ACP), respectively. In the study of the ABS plate, the overall repeatability can be seen to be considerably good with standard deviations of not more than 0.09, whereas, in the study of the ACP, the overall repeatability is relatively less convincing with larger standard deviations (1.4446 at most). This can be explained by the different order of magnitude between the elastic properties of the ABS plate and ACP, in which, the

elastic properties of the ACP are relatively larger than those of ABS, hence, the incurred standard deviations are found to be larger.

Table 4.60: Standard deviations of evaluated elastic properties of ABS plate

	E_x (GPa)	E_y (GPa)	G_{xy} (GPa)	ν_{xy}
Stage 1	0.0542	0.0815	0.0060	0.0069
Stage 2	0.0860	0.0427	0.0013	0.0083

Table 4.61: Standard deviations of evaluated elastic properties of ACP

	E_x (GPa)	E_y (GPa)	G_{xy} (GPa)	ν_{xy}
Stage 1	1.4077	1.4446	0.0961	0.0467
Stage 2	0.6025	0.3080	0.0242	0.0098

(d) Convergence of meta-heuristic hybrid optimisation method with frequency response function (FRF) error function in experimental plates

In this context, the convergence of the proposed algorithm in identifying the elastic properties of the acrylonitrile-butadiene-styrene (ABS) plate and aluminium composite panel (ACP) is investigated in terms of computational time, as presented in Table 4.62 and Table 4.63, respectively. From the tables, it can be observed that stage 2 consumes relatively more computational time as compared to stage 1, mainly due to the involvement of more localised parameters in the application of frequency response function (FRF) error function in stage 2. Overall, the total average computational time is about 3033 seconds, which is approximately equivalent to 51 minutes. As compared to the conventional destructive identification approaches which require complying with certain standard procedures, the proposed method is said to be relatively more promising in terms of computational time.

Table 4.62: Computational time of the proposed meta-heuristic hybrid algorithm in determining the elastic properties of ABS plate

Set	Stage 1 (s)	Stage 2 (s)	Total (s)
1	1099.5481	1929.5738	3029.1219
2	1101.4429	1911.8509	3013.2938
3	1100.7816	1901.0254	3001.8069
4	1104.7591	1934.4297	3039.1888
5	1099.7829	1936.7043	3036.4872
Average	1101.2629	1922.7168	3023.9797

Table 4.63: Computational time of the proposed meta-heuristic hybrid algorithm in determining the elastic properties of ACP

Set	Stage 1 (s)	Stage 2 (s)	Total (s)
1	1097.9476	1932.8024	3030.7500
2	1097.4559	1938.3119	3035.7678
3	1099.3411	1936.5649	3035.9060
4	1096.3115	1905.2580	3001.5695
5	1097.2637	1936.4004	3033.6641
Average	1097.6640	1929.8675	3027.5315

4.5 Comparison between two-stage derivative-based method and meta-heuristic hybrid optimisation method

Table 4.64 presents the results obtained using two-stage derivative-based method as well as the results obtained using meta-heuristic hybrid optimisation method. It should be noted that the evaluated properties with the least absolute percentage errors among both the compared methods are shown in bold. From the table, it can be observed that in the study of the graphite epoxy reference plate, the integrated use of meta-heuristic hybrid optimisation method with frequency response function (FRF) error function yields better E_x , E_y , G_{xy} , and ν_{xy} with values of $127.8978GPa$, $10.1681GPa$, $7.2961GPa$ and 0.2150 , respectively as well as with absolute percentage errors of 0.0017% , 0.9922% , 0.2175% and 2.2727% , respectively. Meanwhile, in the investigation of the ABS experimental plate, the E_x , E_y , G_{xy} , and ν_{xy} evaluated using meta-heuristic hybrid optimisation method are also found to be more accurate with values of $2.5864GPa$, $2.5582GPa$, $0.8917GPa$ and 0.3314 , respectively as well as

with absolute percentage errors of 8.7545%, 10.9848%, 1.7574%, and 1.6617%, respectively. Overall, meta-heuristic hybrid optimisation method can be claimed to be the better method in the aspect of accuracy.

Table 4.64: Comparison of evaluated elastic properties using two-stage derivative-based method and meta-heuristic hybrid optimisation method

	Benchmark	Two-stage derivative-based method	Meta-heuristic hybrid optimisation method
Reference study	Value	Value	Value
Graphite epoxy plate			
E_x (GPa)	127.9	127.8279 [0.0564]	127.8978 [0.0017]
E_y (GPa)	10.27	10.4585 [1.8354]	10.1681 [0.9922]
G_{xy} (GPa)	7.312	7.1783 [1.8285]	7.2961 [0.2175]
ν_{xy}	0.22	0.2058 [6.4545]	0.2150 [2.2727]
Experimental study			
ABS plate			
E_x (GPa)	2.3782	2.6245 [10.3566]	2.5864 [8.7545]
E_y (GPa)	2.3050	2.6760 [16.0954]	2.5582 [10.9848]
G_{xy} (GPa)	0.8763	0.8783 [0.2282]	0.8917 [1.7574]
ν_{xy}	0.3370	0.3286 [2.4926]	0.3314 [1.6617]
ACP			
E_x (GPa)	10.3097	11.8610 [15.0470]	11.4612 [11.1691]
E_y (GPa)	10.3097	10.7829 [4.5899]	10.9005 [5.7305]
G_{xy} (GPa)	3.8465	3.2137 [16.4513]	3.3863 [11.9641]
ν_{xy}	0.3656	0.3238 [11.4333]	0.3184 [12.9103]
#[n]denotes the absolute percentage error with respect to the benchmark value.			

Apart, from the viewpoint of repeatability, the proposed two-stage derivative-based method shows great superiority over meta-heuristic hybrid optimisation method, in which, the standard deviation is found to be 0.0000 when using two-stage derivative-based method, signifying 100% repeatability regardless of number of runs due to the deterministic characteristic of the proposed two-stage derivative-based method.

Table 4.65: Comparison of standard deviations of evaluated elastic properties using two-stage derivative-based method and meta-heuristic hybrid optimisation method

	Two-stage derivative-based method	Meta-heuristic hybrid optimisation method
Reference study		
Graphite epoxy plate		
E_x (GPa)	0.0000	0.9247
E_y (GPa)	0.0000	0.1734
G_{xy} (GPa)	0.0000	0.0861
ν_{xy}	0.0000	0.0132
Experimental study		
ABS plate		
E_x (GPa)	0.0000	0.0860
E_y (GPa)	0.0000	0.0427
G_{xy} (GPa)	0.0000	0.0013
ν_{xy}	0.0000	0.0083
ACP		
E_x (GPa)	0.0000	0.6025
E_y (GPa)	0.0000	0.3080
G_{xy} (GPa)	0.0000	0.0242
ν_{xy}	0.0000	0.0098

From Table 4.66, the proposed two-stage derivative-based method is evident to have consumed relatively lesser overall computational time as compared to the proposed meta-heuristic hybrid optimisation method due to the exploitation of gradient information as well as the relatively smaller allowable search regions used in the two-stage derivative-based method.

Table 4.66: Comparison of average computational time of evaluated elastic properties using two-stage derivative-based method and meta-heuristic hybrid optimisation method

	Two-stage derivative-based method (s)	Meta-heuristic hybrid optimisation method (s)
Reference study		
Graphite epoxy plate	234.7203	2015.4959
Experimental study		
ABS plate	418.1761	3023.9797
ACP	443.4815	3027.5315

Nevertheless, when comparing the aspect of robustness, the meta-heuristic hybrid optimisation method exhibits superiority over the two-stage derivative-based method.

The proposed two-stage derivative-based method is designated only for material identification, whereby, the proposed meta-heuristic hybrid optimisation method is a more universal approach, in which, it can be used in various applications, such as unconstrained unimodal and multimodal problems, constrained engineering design problems as well as material identification. The meta-heuristic hybrid optimisation method is effective in solving problems involving large number of dimensions, while, the proposed two-stage derivative-based method is restricted to relatively low-dimensional material identification problems. In addition, the quality of outcomes when using the two-stage derivative-based method depends substantially on the initial guesses, such that, initial guesses that differ vastly from the actual values would compromise the effectiveness of the proposed method. In contrast, the use of meta-heuristic hybrid optimisation has less restriction on initialization and encompasses relatively much larger search regions. In the other point of view, both methods are applicable in material identification as well as robust to different types of materials and different sets of boundary conditions. In the meantime, both methods are said to be able to handle uncertainties. As a whole, two-stage derivative-based method is better in the aspects of repeatability and convergence rate, whereas, meta-heuristic hybrid optimisation method is better in the aspects of accuracy and robustness. From the perspective of applicability, two-stage derivative-based method is said to be effective in solving unimodal problems, under the condition that the solution of the problem is known beforehand, while, meta-heuristic hybrid optimisation method is claimed to be feasible in solving various problems, including problems with multimodality, constraints and large number of dimensions.

Table 4.67: Robustness of the proposed two-stage derivative-based method and meta-heuristic hybrid optimisation method

Criteria of robustness	Two-stage derivative-based method	Meta-heuristic hybrid optimisation method
Test functions (unconstrained, unimodal, multimodal)	<i>No</i>	<i>Yes</i>
Engineering design problems (constrained)	<i>No</i>	<i>Yes</i>
Large number of dimensions	<i>No</i>	<i>Yes</i>
Large area of search region	<i>No</i>	<i>Yes</i>
Material identification	<i>Yes</i>	<i>Yes</i>
Various types of materials	<i>Yes</i>	<i>Yes</i>
Various sets of boundary conditions	<i>Yes</i>	<i>Yes</i>
Handling of uncertainties	<i>Yes</i>	<i>Yes</i>
<p><i>Yes</i> indicates “<i>Applicable</i>” in fulfilling the criteria of robustness <i>No</i> denotes “<i>Not Applicable</i>” in fulfilling the criteria of robustness</p>		

University of Malaysia

CHAPTER 5: CONCLUSIONS AND RECOMMENDATIONS

5.1 Conclusions

In the present study, two-stage derivative-based method has been developed, in which, the Fourier method is utilised as the forward method, while, a weighted least squares method is used as the inverse method as well as natural frequencies are employed in stage 1 and mode shapes are utilised in stage 2. The feasibility of the proposed method on different types of plates under different sets of boundary conditions has been verified and the proposed method has been proven viable in improving as well as preserving the identifiability of the in-plane shear modulus and Poisson's ratio. This can be explained by the relationship between the in-plane shear modulus and twisting modes as well as the relationship between the Poisson's ratio and bending modes. Basically, shear modulus is defined by the ratio of shear stress to shear strain and in twisting modes, the contribution of shear strain is known to be relatively significant. On the other hand, Poisson's ratio is defined by the ratio of shortening strain to tensile strain and in bending modes, the contribution of these strains are comparatively larger. Therefore, it can be observed that the use of mode shape error function in stage 2 does help in improving the identifiability of the in-plane shear modulus and the Poisson's ratio.

Furthermore, meta-heuristic hybrid optimisation method (Hybrid GA-ACO-PSO) has also been developed. The primary motivation of combining these algorithms is to complement respective weaknesses as well as promote respective strengths, hence, transforming into a better algorithm. In the composition of the proposed method, the collaboration between genetic algorithm (GA) operator and ant colony optimisation (ACO) operator helps in enhancing the exploratory process, while the cooperation between genetic algorithm (GA) operator and particle swarm optimisation (PSO) operator contributes in improving the exploitative process. Two different mutation

operators, namely, fixed refined mutation (feature 1) and logarithmically-spaced refined mutation (feature 2) are introduced to aid the process of intensification. The proposed method with new features has been tested in solving unconstrained test functions and constrained engineering design problems. Feature 2 is found to be relatively effective in dealing with high-dimensional unconstrained test functions in the presence of multimodality due to its ability in inducing an logarithmic increase in the search precision over iterations. Meanwhile, feature 1 is discovered to be relatively effective in tackling constrained engineering design problems on account of its great compatibility with the nature of the engineering design problems. In the following study, the proposed method has been applied in material identification and it demonstrates promising performances in the aspects of accuracy, repeatability, convergence and robustness due to its excellent global search capability.

Apart from that, the use of the proposed meta-heuristic hybrid optimisation method incorporated with different types of error functions, namely, natural frequency error function, mode shape error function and frequency response function (FRF) error function has been studied and the FRF error function has been proven to be the most complete error function, in which, its accuracy and repeatability consist in the trade-off range between those of the natural frequency error function and the mode shape error function. However, the FRF error function consumes the most computational time as compared to the other error functions as it involves a large number of local data. Despite, from the perspective of practical applications, this drawback can be compensated by the processing time consumed during the extraction of experimental natural frequencies and mode shapes from experimental FRF data, in which, these procedures are not required when utilising the FRF error function. As a whole, FRF error function emerges as the better alternative, considering its relatively more complete and satisfactory performances in the aspects of accuracy, repeatability and convergence.

The proposed two-stage derivative-based method and meta-heuristic hybrid optimisation method have been validated experimentally, in which, the results obtained from destructive test and theoretical calculation are compared with those obtained from the proposed non-destructive tests. As mentioned, a non-destructive test involves experimental measurement and numerical evaluation. Experimental modal analysis (EMA) is conducted and the acquired data are subsequently used as the reference parameters in the proposed algorithms. In the proposed two-stage derivative-based method, regularization parameters are introduced to consider the effects due to uncertainties. It has been proven to be feasible in improving the identifiability of the in-plane shear modulus and the Poisson's ratio of experimental plates. Furthermore, in the proposed meta-heuristic hybrid optimisation method, two-stage procedures are adopted as well to mitigate the presence of uncertainties. Stage 1 involves the use of the proposed method incorporated with the natural frequency error function and stage 2 involves the use of the proposed method incorporated with the FRF error function. Selection of FRFs to be used in the identification process is performed based on the sensitivity of natural modes with respect to the elastic parameters as well as based on the location of impact which lies in the high response regions of the selected modes. As a result, it has been proven to be viable in improving the identifiability of the in-plane shear modulus and Poisson's ratio. Overall, two-stage derivative-based method shows better performances in the aspects of repeatability and convergence, while meta-heuristic hybrid optimisation method demonstrates superiority in terms of accuracy and robustness. The perspectives of robustness in the context can be interpreted as the applicability of the method in various types of problems (in the presence of multimodality, constraints), the consideration of a large number of dimensions and a large area of search regions as well as the applicability in material identification

(different types of materials, different sets of boundary conditions, handling of uncertainties).

5.2 Recommendations

There are strengths and weaknesses in both the proposed methods. As mentioned, the proposed two-stage derivative-based method is relatively inferior in the aspects of accuracy and robustness, while, the proposed meta-heuristic hybrid method is relatively less promising in terms of repeatability and convergence. In fact, to circumvent these drawbacks, the organized collaboration between the two proposed methods can be the solution. With the help of meta-heuristic operators which are more precise and global, the search precision of the derivative-based method can be improved and the search region can as well be extended, thus, enhancing the accuracy and robustness. Besides, by introducing the gradient information of the derivative-based method into the meta-heuristic method, the repeatability and convergence can be bettered. Furthermore, the integrated use of two different derivative-based methods can as well be a potential approach. For instance, the combined use of Bayesian estimation method which involves the application of a prior and Newton method which is a root-finding algorithm might be viable in tackling issues pertaining to accuracy and robustness. Apart, developing a meta-heuristic hybrid optimisation method by incorporating three different established algorithms other than the proposed algorithms can also be a topic of interest to improve the overall performance of the approach. From the perspective of applications, the use of the recommended methods in material defect quantification, structural health monitoring as well as self-healing material identification can be a promising scope of study due to the substantial impact in various industries, especially, in manufacturing and construction industries.

REFERENCES

- Adhikari, S. (2011). A reduced spectral function approach for the stochastic finite element analysis. *Computer Methods in Applied Mechanics and Engineering*, 200(21-22), 1804-1821.
- Agarwal, H., Renaud, J. E., Preston, E. L., & Padmanabhan, D. (2004). Uncertainty quantification using evidence theory in multidisciplinary design optimization. *Reliability Engineering & System Safety*, 85(1-3), 281-294.
- Akay, B., & Karaboga, D. (2012). Artificial bee colony algorithm for large-scale problems and engineering design optimization. *Journal of Intelligent Manufacturing*, 23(4), 1001-1014.
- Alfano, M., & Pagnotta, L. (2005). An inverse procedure for determining the material constants of isotropic square plates by impulse excitation of vibration. *Advances in Experimental Mechanics IV*, 3-4, 287-292.
- Alfano, M., & Pagnotta, L. (2006). Determining the elastic constants of isotropic materials by modal vibration testing of rectangular thin plates. *Journal of Sound and Vibration*, 293(1-2), 426-439.
- Alfano, M., & Pagnotta, L. (2007). A non-destructive technique for the elastic characterization of thin isotropic plates. *Ndt & E International*, 40(2), 112-120.
- Alobeid, A., & Cooper, J. E. (1995). A Rayleigh-Ritz approach for the estimation of the dynamic properties of symmetrical composite plates with general boundary-conditions. *Composites Science and Technology*, 53(3), 289-299.
- Araujo, A. L., Lopes, H. M. R., Vaz, M. A. P., Soares, C. M. M., Herskovits, J., & Pedersen, P. (2006a). Parameter estimation in active plate structures. *Computers & Structures*, 84(22-23), 1471-1479.
- Araújo, A. L., Mota Soares, C. M., Herskovits, J., & Pedersen, P. (2002). Development of a finite element model for the identification of mechanical and piezoelectric properties through gradient optimisation and experimental vibration data. *Composite Structures*, 58(3), 307-318.
- Araujo, A. L., Soares, C. M. M., de Freitas, M. J. M., Pedersen, P., & Herskovits, J. (2000). Combined numerical-experimental model for the identification of mechanical properties of laminated structures. *Composite Structures*, 50(4), 363-372.

- Araujo, A. L., Soares, C. M. M., & deFreitas, M. J. M. (1996). Characterization of material parameters of composite plate specimens using optimization and experimental vibrational data. *Composites Part B: Engineering*, 27(2), 185-191.
- Araujo, A. L., Soares, C. M. M., Herskovits, J., & Pedersen, P. (2006b). Parameter estimation in active plate structures using gradient optimisation and neural networks. *Inverse Problems in Science and Engineering*, 14(5), 483-493.
- Arregui-Mena, J. D., Margetts, L., & Mummery, P. M. (2016). Practical application of the stochastic finite element method. *Archives of Computational Methods in Engineering*, 23(1), 171-190.
- Auzins, J., Chate, A., Rikards, R., & Skukis, E. (2015). Metamodeling and robust minimization approach for the identification of elastic properties of composites by vibration method. *Zamm-Zeitschrift Fur Angewandte Mathematik Und Mechanik*, 95(10), 1012-1026.
- Avril, S., Bonnet, M., Bretelle, A. S., Grediac, M., Hild, F., Ienny, P., . . . Pierron, F. (2008). Overview of identification methods of mechanical parameters based on full-field measurements. *Experimental Mechanics*, 48(4), 381-402.
- Ayorinde, E. O. (1995). Elastic constants of thick orthotropic composite plates. *Journal of Composite Materials*, 29(8), 1025-1039.
- Ayorinde, E. O., & Gibson, R. F. (1993). Elastic constants of orthotropic composite materials using plate resonance frequencies, classical lamination theory and an optimized three-mode Rayleigh formulation. *Composites Engineering*, 3(5), 395-407.
- Barkanov, E., Wesolowski, M., Hufenbach, W., & Dannemann, M. (2015). An effectiveness improvement of the inverse technique based on vibration tests. *Computers & Structures*, 146, 152-162.
- Batista, F. B., Albuquerque, E. L., Arruda, J. R. F., & Dias, M. (2009). Identification of the bending stiffness matrix of symmetric laminates using regressive discrete Fourier series and finite differences. *Journal of Sound and Vibration*, 320(4-5), 793-807.
- Berthelot, J. M., & Angoulvant, F. (2002). Measuring the bending stiffnesses of orthotropic and symmetric laminates from flexural vibrations. *Journal of Composite Materials*, 36(4), 443-475.

- Bhat, R. B. (1985). Natural frequencies of rectangular-plates using characteristic orthogonal polynomials in Rayleigh-Ritz method. *Journal of Sound and Vibration*, 102(4), 493-499.
- Bledzki, A. K., Kessler, A., Rikards, R., & Chate, A. (1999). Determination of elastic constants of glass/epoxy unidirectional laminates by the vibration testing of plates. *Composites Science and Technology*, 59(13), 2015-2024.
- Borza, D. N. (2004). Vibration-based identification of isotropic material properties by quasi-binary electronic holography and finite element modelling. *Inverse Problems in Science and Engineering*, 12(1), 45-57.
- Bruno, L., Felice, G., Pagnotta, L., Poggialini, A., & Stigliano, G. (2008). Elastic characterization of orthotropic plates of any shape via static testing. *International Journal of Solids and Structures*, 45(3-4), 908-920.
- Cagnina, L. C., Esquivel, S. C., & Coello Coello, C. A. (2008). Solving engineering optimization problems with the simple constrained particle swarm optimizer. *Informatica (Ljubljana)*, 32(3), 319-326.
- Castellano, A., Foti, P., Fraddosio, A., Marzano, S., & Piccioni, M. D. (2014). Mechanical characterization of CFRP composites by ultrasonic immersion tests: Experimental and numerical approaches. *Composites Part B: Engineering*, 66, 299-310.
- Catania, G., & Sorrentino, S. (2009, February 9-12). *Experimental evaluation of the damping properties of beams and thin-walled structures made of polymeric materials*. Paper presented at the Conference & Exposition on Structural Dynamics, Orlando, Florida USA.
- Chow, S. T., Liew, K. M., & Lam, K. Y. (1992). Transverse vibration of symmetrically laminated rectangular composite plates. *Composite Structures*, 20(4), 213-226.
- Coelho, L. D. (2010). Gaussian quantum-behaved particle swarm optimization approaches for constrained engineering design problems. *Expert Systems with Applications*, 37(2), 1676-1683.
- Coello, C. A. C. (2000a). Treating constraints as objectives for single-objective evolutionary optimization. *Engineering Optimization*, 32(3), 275-308.

- Coello, C. A. C. (2000b). Use of a self-adaptive penalty approach for engineering optimization problems. *Computers in Industry*, 41(2), 113-127.
- Coello, C. A. C., & Montes, E. M. (2002). Constraint-handling in genetic algorithms through the use of dominance-based tournament selection. *Advanced Engineering Informatics*, 16(3), 193-203.
- Cugnoni, J., Gmur, T., & Schorderet, A. (2007). Inverse method based on modal analysis for characterizing the constitutive properties of thick composite plates. *Computers & Structures*, 85(17-18), 1310-1320.
- Cugnoni, J., Gmür, T., & Schorderet, A. (2004). *A mixed numerical–experimental identification method for evaluating the constitutive parameters of composite laminated shells*. Paper presented at the Proceedings of composites testing and model identification, University Press, Bristol.
- Daei, M., & Mirmohammadi, S. H. (2015). A flexibility method for structural damage identification using continuous ant colony optimization. *Multidiscipline Modeling in Materials and Structures*, 11(2), 186-201.
- Daghia, F., de Miranda, S., Ubertini, F., & Viola, E. (2007). Estimation of elastic constants of thick laminated plates within a Bayesian framework. *Composite Structures*, 80(3), 461-473.
- Dahmen, S., Ketata, H., Ben Ghazlen, M. H., & Hosten, B. (2010). Elastic constants measurement of anisotropic Olivier wood plates using air-coupled transducers generated Lamb wave and ultrasonic bulk wave. *Ultrasonics*, 50(4-5), 502-507.
- Darwin, C. (1869). *On the Origin of Species by Means of Natural Selection, or the Preservation of Favoured Races in the Struggle for Life*. London: John Murray.
- De Wilde, W. P., & Sol, H. (1986). Determination of Material Constants Using Experimental Free Vibration Analysis on Anisotropic Plates. In H. Wieringa (Ed.), *Experimental Stress Analysis* (pp. 207-214). Dordrecht, Netherlands: Springer.
- Deb, K. (1997). GeneAS: A Robust Optimal Design Technique for Mechanical Component Design. In D. Dasgupta & Z. Michalewicz (Eds.), *Evolutionary Algorithms in Engineering Applications* (pp. 497-514). Berlin, Heidelberg: Springer.

- Deb, K. (2000). An efficient constraint handling method for genetic algorithms. *Computer Methods in Applied Mechanics and Engineering*, 186(2-4), 311-338.
- Deb, K., & Goyal, M. (1996). A combined genetic adaptive search (GeneAS) for engineering design. *Computer Science and Informatics*, 26(4), 30-45.
- Deobald, L. R., & Gibson, R. F. (1988). Determination of elastic-constants of orthotropic plates by a modal-analysis Rayleigh-Ritz technique. *Journal of Sound and Vibration*, 124(2), 269-283.
- Dickinson, S. M. (1978). The buckling and frequency of flexural vibration of rectangular isotropic and orthotropic plates using Rayleigh's method. *Journal of Sound and Vibration*, 61(1), 1-8.
- Dickinson, S. M., & Dibrasio, A. (1986). On the use of orthogonal polynomials in the Rayleigh-Ritz method for the study of the flexural vibration and buckling of isotropic and orthotropic rectangular-plates. *Journal of Sound and Vibration*, 108(1), 51-62.
- Dimopoulos, G. G. (2007). Mixed-variable engineering optimization based on evolutionary and social metaphors. *Computer Methods in Applied Mechanics and Engineering*, 196(4-6), 803-817.
- Dorigo, M., & Caro, G. D. (1999). The ant colony optimization meta-heuristic. In C. David, D. Marco, G. Fred, D. Dipankar, M. Pablo, P. Riccardo & V. P. Kenneth (Eds.), *New ideas in optimization* (pp. 11-32). London: McGraw-Hill.
- E1876-09, A. (2009). Standard Test Method for Dynamic Young's Modulus, Shear Modulus, and Poisson's Ratio by Impulse Excitation of Vibration. West Conshohocken: ASTM International.
- Fallstrom, K. E. (1991). Determining material properties in anisotropic plates using Rayleigh method. *Polymer Composites*, 12(5), 306-314.
- Fallstrom, K. E., & Jonsson, M. (1991). A nondestructive method to determine material properties in anisotropic plates. *Polymer Composites*, 12(5), 293-305.
- Fallstrom, K. E., & Molin, N. E. (1987). A nondestructive method to determine material properties in orthotropic plates. *Polymer Composites*, 8(2), 103-108.

- Felgar, R. P. (1950). *Formulas for Integrals Containing Characteristic Functions of A Vibrating Beam*. Austin: University of Texas Press.
- Fesanghary, M., Mahdavi, M., Minary-Jolandan, M., & Alizadeh, Y. (2008). Hybridizing harmony search algorithm with sequential quadratic programming for engineering optimization problems. *Computer Methods in Applied Mechanics and Engineering*, 197(33-40), 3080-3091.
- Fidanova, S., Paprzycki, M., & Roeva, O. (2014, Sept 7-10). *Hybrid GA-ACO algorithm for a model parameters identification problem*. Paper presented at the Federated Conference on Computer Science and Information Systems, Warsaw, Poland.
- Fox, R. L., & Kapoor, M. P. (1968). Rates of change of eigenvalues and eigenvectors. *Aiaa Journal*, 6(12), 2426-2429.
- Gandomi, A. H., Yang, X. S., & Alavi, A. H. (2011). Mixed variable structural optimization using firefly algorithm. *Computers & Structures*, 89(23-24), 2325-2336.
- Gandomi, A. H., Yang, X. S., & Alavi, A. H. (2013). Cuckoo search algorithm: a metaheuristic approach to solve structural optimization problems. *Engineering with Computers*, 29(1), 17-35.
- Garg, H. (2016). A hybrid PSO-GA algorithm for constrained optimization problems. *Applied Mathematics and Computation*, 274, 292-305.
- Garshasbinia, N., & Jam, J. E. (2005). Identification of mechanical properties in laminated composite plates using genetic algorithm. *Iranian Polymer Journal*, 14(1), 39-46.
- Ghanmi, S., Bouajila, S., & Guedri, M. (2013). Numerical-experimental updating identification of elastic behavior of a composite plate using new multi-objective optimization procedure. *Journal of Surface Engineered Materials and Advanced Technology*, 3(1), 13-20.
- Gigras, Y., Choudhary, K., Gupta, K., & Vandana. (2015, Mar 11-13). *A hybrid ACO-PSO technique for path planning*. Paper presented at the International Conference on Computing for Sustainable Global Development (INDIACom), New Delhi, India.

- Giraudeau, A., Pierron, F., & Guo, B. Q. (2010). An alternative to modal analysis for material stiffness and damping identification from vibrating plates. *Journal of Sound and Vibration*, 329(10), 1653-1672.
- Glushkov, E., Glushkova, N., Eremin, A., Lammering, R., & Neumann, M. (2014). *Elastic guided wave based assessment of laminate composite material constants*. Paper presented at the 11th European Conference on Non-Destructive Testing (ECNDT), Prague, Czech Republic
- Grover, N., Sahoo, R., Singh, B. N., & Maiti, D. K. (2017). Influence of parametric uncertainties on the deflection statistics of general laminated composite and sandwich plates. *Composite Structures*, 171, 158-169.
- Guoliang, J., Lin, C., & Jiamei, D. (1993). Monte Carlo finite element method of structure reliability analysis. *Reliability Engineering & System Safety*, 40(1), 77-83.
- He, Q., & Wang, L. (2007). An effective co-evolutionary particle swarm optimization for constrained engineering design problems. *Engineering Applications of Artificial Intelligence*, 20(1), 89-99.
- He, S., Prempain, E., & Wu, Q. H. (2004). An improved particle swarm optimizer for mechanical design optimization problems. *Engineering Optimization*, 36(5), 585-605.
- Hearmon, R. F. S. (1959). The frequency of flexural vibration of rectangular orthotropic plates with clamped or supported edges. *Journal of Applied Mechanics*, 26(4), 537-540.
- Hedar, A. R., & Fukushima, M. (2006). Derivative-free filter simulated annealing method for constrained continuous global optimization. *Journal of Global Optimization*, 35(4), 521-549.
- Hendrickson, I. G. (1963). Tuned Q Analysis of Quench and Precipitation Hardening of 4330M and 17-7PH Steels.
- Herskovits, J. (1998). Feasible direction interior-point technique for nonlinear optimization. *Journal of Optimization Theory and Applications*, 99(1), 121-146.
- Himmelblau, D. M. (1972). *Applied nonlinear programming*. New York: McGraw-Hill.

- Holland, J. H. (1992). *Adaptation in Natural and Artificial Systems: An Introductory Analysis with Applications to Biology, Control and Artificial Intelligence*. Cambridge: MIT Press.
- Homaifar, A., Qi, C. X., & Lai, S. H. (1994). Constrained optimization via genetic algorithms. *Simulation*, 62(4), 242-253.
- Hu, X. H., Eberhart, R. C., & Shi, Y. H. (2003, 26 April). *Engineering optimization with particle swarm*. Paper presented at the Proceedings of the 2003 IEEE Swarm Intelligence Symposium, Indianapolis, IN, USA.
- Huang, Y. Q., & Luo, Z. Y. (2013). Vibration response of cement structures under conditions of impact loads. *Materials Testing*, 55(11-12), 897-902.
- Hwang, S. F., & Chang, C. S. (2000). Determination of elastic constants of materials by vibration testing. *Composite Structures*, 49(2), 183-190.
- Hwang, S. F., & He, R. S. (2006). A hybrid real-parameter genetic algorithm for function optimization. *Advanced Engineering Informatics*, 20(1), 7-21.
- Hwang, S. F., Wu, J. C., Barkanovs, E., & Belevicius, R. (2010). Elastic constants of composite materials by an inverse determination method based on a hybrid genetic algorithm. *Journal of Mechanics*, 26(3), 345-353.
- Hwang, S. F., Wu, J. C., & He, R. S. (2009). Identification of effective elastic constants of composite plates based on a hybrid genetic algorithm. *Composite Structures*, 90(2), 217-224.
- Ismail, Z., Khov, H., & Li, W. L. (2011). Identifying material properties of composite materials from vibration data. *World Journal of Engineering*, 20, 471-472.
- Ismail, Z., Khov, H., & Li, W. L. (2013). Determination of material properties of orthotropic plates with general boundary conditions using Inverse method and Fourier series. *Measurement*, 46(3), 1169-1177.
- Jalil, N. S. A. A., Julai, S., & Ramli, R. (2015). Parametric modelling of flexible plate structures using continuous ant colony optimization. *Journal of Simulation*, 9(3), 223-231.

- Kam, T. Y., Chen, C. M., & Yang, S. H. (2009). Material characterization of laminated composite materials using a three-point-bending technique. *Composite Structures*, 88(4), 624-628.
- Kannan, B. K., & Kramer, S. N. (1994). An augmented Lagrange multiplier based method for mixed-integer discrete-continuous optimization and its applications to mechanical design. *Journal of Mechanical Design*, 116(2), 405-411.
- Kaveh, A., & Talatahari, S. (2010). An improved ant colony optimization for constrained engineering design problems. *Engineering Computations*, 27(1-2), 155-182.
- Kennedy, J., & Eberhart, R. C. (1995, Nov 27-Dec 1). *Particle swarm optimization*. Paper presented at the IEEE International Conference on Neural Networks, Seoul, Korea.
- Khov, H., Li, W. L., & Gibson, R. F. (2009). An accurate solution method for the static and dynamic deflections of orthotropic plates with general boundary conditions. *Composite Structures*, 90(4), 474-481.
- Kim, C. S., & Dickinson, S. M. (1985). Improved approximated expressions for the natural frequencies of isotropic and orthotropic rectangular plates. *Journal of Sound and Vibration*, 103(1), 142-149.
- Koide, R. M., França, G. v. Z. d., & Luersen, M. A. (2013). An ant colony algorithm applied to lay-up optimization of laminated composite plates. *Latin American Journal of Solids and Structures*, 10(3), 491-504.
- Kong, K. K., Ong, Z. C., Khoo, S. Y., Ismail, Z., Ang, B. C., Chong, W. T., . . . Rahman, A. G. A. (2014). Identification of material properties of orthotropic composite plate using hybrid non-destructive evaluation approach. *Materials Research Innovations*, 18, 423-428.
- Kovalovs, A., & Rucevskis, S. (2011). *Identification of elastic properties of composite plate*. Paper presented at the Annual Conference on Functional Materials and Nanotechnologies, Riga, Latvia.
- Kutanaei, S. S., & Choobbasti, A. J. (2015). Prediction of combined effects of fibers and cement on the mechanical properties of sand using particle swarm optimization algorithm. *Journal of Adhesion Science and Technology*, 29(6), 487-501.

- Lai, T. C., & Ip, K. H. (1996). Parameter estimation of orthotropic plates by Bayesian sensitivity analysis. *Composite Structures*, 34(1), 29-42.
- Lai, T. C., & Lau, T. C. (1993). Determination of elastic constants of a generally orthotropic plate by modal analysis. *International Journal of Analytical and Experimental Modal Analysis*, 8, 15-33.
- Larsson, D. (1997). Using modal analysis for estimation of anisotropic material constants. *Journal of Engineering Mechanics*, 123(3), 222-229.
- Lauwagie, T., Sol, H., Heylen, W., & Roebben, G. (2004). Determination of the in-plane elastic properties of the different layers of laminated plates by means of vibration testing and model updating. *Journal of Sound and Vibration*, 274(3-5), 529-546.
- Lauwagie, T., Sol, H., Roebben, G., Heylen, W., Shi, Y. M., & Van der Biest, O. (2003). Mixed numerical-experimental identification of elastic properties of orthotropic metal plates. *Ndt & E International*, 36(7), 487-495.
- Lauwagie T., Lambrinou K., Sol H., & W., H. (2010). Resonant-based identification of the Poisson's ratio of orthotropic materials *Experimental Mechanics*(4), 437-447.
- Lee, C. R., & Kam, T. Y. (2006a). Identification of mechanical properties of elastically restrained laminated composite plates using vibration data. *Journal of Sound and Vibration*, 295(3-5), 999-1016.
- Lee, C. R., & Kam, T. Y. (2006b). System identification of partially restrained composite plates using measured natural frequencies. *Journal of Engineering Mechanics*, 132(8), 841-850.
- Lee, C. R., Kam, T. Y., & Sun, S. J. (2007). Free-vibration analysis and material constants identification of laminated composite sandwich plates. *Journal of Engineering Mechanics*, 133(8), 874-886.
- Lee, K. S., & Geem, Z. W. (2005). A new meta-heuristic algorithm for continuous engineering optimization: Harmony search theory and practice. *Computer Methods in Applied Mechanics and Engineering*, 194(36-38), 3902-3933.
- Leiderman, R., & Castello, D. A. (2016). Detecting and classifying interfacial defects by inverse ultrasound scattering analysis. *Wave Motion*, 65, 119-129.

- Li, N., Ben Tahar, M., Aboura, Z., & Khellil, K. (2016). A dynamic analysis approach for identifying the elastic properties of unstitched and stitched composite plates. *Composite Structures*, 152, 959-968.
- Liang, J. J., Qin, A. K., Suganthan, P. N., & Baskar, S. (2006). Comprehensive learning particle swarm optimizer for global optimization of multimodal functions. *Ieee Transactions on Evolutionary Computation*, 10(3), 281-295.
- Lin, Y. H., & Chang, C. L. (2009). Determining elastic constants of material using optimization method and vibration test. *Materials Science Forum*, 628-629, 89-96.
- Lin, Y. H., & Chang, C. L. (2010). Using modal analysis and optimization to determine elastic constants of thick composite plates. *Key Engineering Materials*, 419-420, 473-476.
- Link, M. (1999). Updating of Analytical Models: Basic Procedures and Extensions. In J. M. M. Silva & N. M. M. Maia (Eds.), *Modal Analysis and Testing* (pp. 281-304). Dordrecht, Netherlands: Springer.
- Liu, L., Sun, S. Z., Yu, H., Yue, X., & Zhang, D. (2016). A modified Fuzzy C-Means (FCM) clustering algorithm and its application on carbonate fluid identification. *Journal of Applied Geophysics*, 129, 28-35.
- Majumdar, A., Maiti, D. K., & Maity, D. (2012). Damage assessment of truss structures from changes in natural frequencies using ant colony optimization. *Applied Mathematics and Computation*, 218(19), 9759-9772.
- Maletta, C., & Pagnotta, L. (2004). On the determination of mechanical properties of composite laminates using genetic algorithms. *International Journal of Mechanics and Materials in Design*, 1(2), 199-211.
- Marzani, A., & De Marchi, L. (2013). Characterization of the elastic moduli in composite plates via dispersive guided waves data and genetic algorithms. *Journal of Intelligent Material Systems and Structures*, 24(17), 2135-2147.
- Matter, M., Gmur, T., Cugnoni, J., & Schorderet, A. (2007). Improved modal characterization of the constitutive parameters in multilayered plates. *Composites Science and Technology*, 67(6), 1121-1131.

- Matter, M., Gmur, T., Cugnoni, J., & Schorderet, A. (2009). Numerical-experimental identification of the elastic and damping properties in composite plates. *Composite Structures*, 90(2), 180-187.
- Matter, M., Gmur, T., Cugnoni, J., & Schorderet, A. (2011). Identification of the elastic and damping properties in sandwich structures with a low core-to-skin stiffness ratio. *Composite Structures*, 93(2), 331-341.
- Mcintyre, M. E., & Woodhouse, J. (1988). On measuring the elastic and damping constants of orthotropic sheet materials. *Acta Metallurgica*, 36(6), 1397-1416.
- Mehta, V. K., & Dasgupta, B. (2012). A constrained optimization algorithm based on the simplex search method. *Engineering Optimization*, 44(5), 537-550.
- Mezura-Montes, E., & Coello, C. A. C. (2008). An empirical study about the usefulness of evolution strategies to solve constrained optimization problems. *International Journal of General Systems*, 37(4), 443-473.
- Mezura-Montes, E., Coello, C. A. C., Velazquez-Reyes, J., & Munoz-Davila, L. (2007). Multiple trial vectors in differential evolution for engineering design. *Engineering Optimization*, 39(5), 567-589.
- Ming, L. C., & Ponnambalam, S. G. (2008, Oct 12-15). *A hybrid GA/PSO for the concurrent design of cellular manufacturing system*. Paper presented at the IEEE International Conference on Systems, Man and Cybernetics (SMC), Singapore.
- Mottershead, J. E., Link, M., & Friswell, M. I. (2011). The sensitivity method in finite element model updating: A tutorial. *Mechanical Systems and Signal Processing*, 25(7), 2275-2296.
- Muthurajan, K. G., Sanakaranarayanan, K., & Rao, B. N. (2004). Evaluation of elastic constants of specially orthotropic plates through vibration testing. *Journal of Sound and Vibration*, 272(1-2), 413-424.
- Oberkampf, W., Helton, J., & Sentz, K. (2001). *Mathematical Representation of Uncertainty*. Paper presented at the 19th AIAA Applied Aerodynamics Conference, Anaheim, CA, USA. <https://doi.org/10.2514/6.2001-1645>
- Omran, M. G. H., & Salman, A. (2009). Constrained optimization using CODEQ. *Chaos Solitons & Fractals*, 42(2), 662-668.

- Pagnotta, L. (2008). Recent progress in identification methods for the elastic characterization of materials. *International Journal of Mechanics*, 2(4), 129-140.
- Pagnotta, L., & Stigliano, G. (2008). Elastic characterization of isotropic plates of any shape via dynamic tests: Theoretical aspects and numerical simulations. *Mechanics Research Communications*, 35(6), 351-360.
- Pagnotta, L., & Stigliano, G. (2009). Elastic characterization of isotropic plates of any shape via dynamic tests: Practical aspects and experimental applications. *Mechanics Research Communications*, 36(2), 154-161.
- Petrone, G., & Meruane, V. (2017). Mechanical properties updating of a non-uniform natural fibre composite panel by means of a parallel genetic algorithm. *Composites Part A: Applied Science and Manufacturing*, 94, 226-233.
- Ragauskas, P., & Belevičius, R. (2009). Identification of material properties of composite materials. *Aviation*, 13(4), 109-115.
- Rao, S. S. (2009). *Engineering Optimization: Theory And Practice* (Fourth ed.). New Jersey, USA: John Wiley & Sons.
- Rebillat, M., & Boutillon, X. (2011). Measurement of relevant elastic and damping material properties in sandwich thick plates. *Journal of Sound and Vibration*, 330(25), 6098-6121.
- Reddy, J. N. (2004). *Mechanics of Laminated Composite Plates and Shells: Theory and Analysis, Second Edition*: Taylor & Francis.
- Reddy, J. N. (2006). *Theory and Analysis of Elastic Plates and Shells* (Second ed.). Boca Raton, Florida, USA: CRC Press, Taylor & Francis Group.
- Rikards, R., Abramovich, H., Green, T., Auzins, J., & Chate, A. (2003). Identification of elastic properties of composite laminates. *Mechanics of Advanced Materials and Structures*, 10(4), 335-352.
- Rikards, R., Chate, A., & Gailis, G. (2001). Identification of elastic properties of laminates based on experiment design. *International Journal of Solids and Structures*, 38(30-31), 5097-5115.

- Rikards, R., Chate, A., Steinchen, W., Kessler, A., & Bledzki, A. K. (1999). Method for identification of elastic properties of laminates based on experiment design. *Composites Part B: Engineering*, 30(3), 279-289.
- Ručevskis, S. (2014). Identification of elastic constants of carbon/epoxy composite plates. *Scientific Journal of the Series of Scientific Journal of RTU*, 4, 193-207.
- Saito, A., Nishikawa, Y., Yamasaki, S., Fujita, K., Kawamoto, A., Kuroishi, M., & Nakai, H. (2016). Equivalent orthotropic elastic moduli identification method for laminated electrical steel sheets. *Mechanical Systems and Signal Processing*, 72-73, 607-628.
- Sale, M., Rizzo, P., & Marzani, A. (2011). Semi-analytical formulation for the guided waves-based reconstruction of elastic moduli. *Mechanical Systems and Signal Processing*, 25(6), 2241-2256.
- Sandgren, E. (1990). Nonlinear integer and discrete programming in mechanical design optimization. *Journal of Mechanical Design*, 112(2), 223-229.
- Sankar, P. A., Machavaram, R., & Shankar, K. (2014). System identification of a composite plate using hybrid response surface methodology and particle swarm optimization in time domain. *Measurement*, 55, 499-511.
- Sato, J., Hutchings, I. M., & Woodhouse, J. (2008). Determination of the dynamic elastic properties of paper and paperboard from the low-frequency vibration modes of rectangular plates. *Appita Journal*, 61(4), 291-296.
- Schwaar, M., Gmur, T., & Frieden, J. (2012). Modal numerical-experimental identification method for characterising the elastic and damping properties in sandwich structures with a relatively stiff core. *Composite Structures*, 94(7), 2227-2236.
- Schwarz, B. J., & Richardson, M. H. (1999, October). *Experimental Modal Analysis*. Paper presented at the Proceedings of the CSI Reliability Week, Orlando, FL.
- Sepahvand, K. (2017). Stochastic finite element method for random harmonic analysis of composite plates with uncertain modal damping parameters. *Journal of Sound and Vibration*, 400, 1-12.
- Sheikhalishahi, M., Ebrahimipour, V., Shiri, H., Zaman, H., & Jeihoonian, M. (2013). A hybrid GA-PSO approach for reliability optimization in redundancy allocation

problem. *International Journal of Advanced Manufacturing Technology*, 68(1-4), 317-338.

Shi, Y., & Eberhart, R. (1998, 4-9 May). *A modified particle swarm optimizer*. Paper presented at the Proceedings of IEEE International Conference on Evolutionary Computation, Washington, DC, USA.

Silva, M. F. T., Borges, L. M. S. A., Rochinha, F. A., & de Carvalho, L. A. V. (2004). A genetic algorithm applied to composite elastic parameters identification. *Inverse Problems in Science and Engineering*, 12(1), 17-28.

Sol, H. (1986). *Identification of anisotropic plate rigidities using free vibration data*. (PhD Thesis), University of Brussels.

Sol, H., Hua, H., De Visscher, J., Vantomme, J., & De Wilde, W. P. (1997). A mixed numerical/experimental technique for the nondestructive identification of the stiffness properties of fibre reinforced composite materials. *Ndt & E International*, 30(2), 85-91.

Sun, K., Zhao, Y., & Hu, H. (2015). Identification of temperature-dependent thermal-structural properties via finite element model updating and selection. *Mechanical Systems and Signal Processing*, 52, 147-161.

Tam, J. H., Ong, Z. C., Lau, C. L., Ismail, Z., Ang, B. C., & Khoo, S. Y. (2017). Identification of material properties of composite plates using Fourier-generated frequency response functions. *Mechanics of Advanced Materials and Structures*, 1-10.

Teo, Y. T., & Ponnambalam, S. G. (2008, Aug 23-26). *A hybrid ACO/PSO heuristic to solve single row layout problem*. Paper presented at the IEEE International Conference on Automation Science and Engineering, Arlington, VA, USA.

Van den Bergh, F., & Engelbrecht, A. P. (2004). A cooperative approach to particle swarm optimization. *Ieee Transactions on Evolutionary Computation*, 8(3), 225-239.

Vishnuvardhan, J., Krishnamurthy, C. V., & Balasubramaniam, K. (2007). Genetic algorithm reconstruction of orthotropic composite plate elastic constants from a single non-symmetric plane ultrasonic velocity data. *Composites Part B-Engineering*, 38(2), 216-227.

- Wan, Y. P., Zhang, P. P., Huang, Z. Y., Ji, L., & Jovic, M. (2017). Parameter uncertainty effects of stiffeners on the vibration of plates. *Transactions of Famena*, 41(3), 1-12.
- Wang, H., Sun, H., Li, C. H., Rahnamayan, S., & Pan, J. S. (2013). Diversity enhanced particle swarm optimization with neighborhood search. *Information Sciences*, 223, 119-135.
- Wang, H., Wu, Z. J., Rahnamayan, S., Liu, Y., & Ventresca, M. (2011). Enhancing particle swarm optimization using generalized opposition-based learning. *Information Sciences*, 181(20), 4699-4714.
- Wang, W. T., & Kam, T. Y. (2000). Material characterization of laminated composite plates via static testing. *Composite Structures*, 50(4), 347-352.
- Wang, Z. C., Geng, D., Ren, W. X., & Liu, H. T. (2014). Strain modes based dynamic displacement estimation of beam structures with strain sensors. *Smart Materials and Structures*, 23(12).
- Warburton, G. B. (1954). The vibration of rectangular plates. *Proceedings of the Institution of Mechanical Engineers*, 168(1), 371-384.
- Wesolowski, M., Barkanov, E., Rucevskis, S., Chate, A., & Delfa, G. L. (2009, July 27-31). *Characterisation of elastic properties of laminated composites by non-destructive techniques*. Paper presented at the ICCM International Conferences on Composite Materials, United Kingdom, Edinburgh.
- Xia, B. Z., Yu, D. J., & Liu, J. (2014). Transformed perturbation stochastic finite element method for static response analysis of stochastic structures. *Finite Elements in Analysis and Design*, 79, 9-21.
- Xu, Y., & Gao, T. (2016). Optimizing thermal-elastic properties of C/C–SiC composites using a hybrid approach and PSO algorithm. *Materials*, 9(4), 222.
- Xu, Y. F., & Zhu, W. D. (2013). Operational modal analysis of a rectangular plate using non-contact excitation and measurement. *Journal of Sound and Vibration*, 332(20), 4927-4939.
- Xu, Y. L., Lim, M. H., Ong, Y. S., & Tang, J. (2006, July 8-12). *A GA-ACO-local search hybrid algorithm for solving quadratic assignment problem*. Paper presented at the Proceedings of the 8th annual conference on Genetic and Evolutionary Computation Conference (GECCO), Seattle, Washington, USA.

- Xu, Y. L., Qian, Y., & Song, G. B. (2016). Stochastic finite element method for free vibration characteristics of random FGM beams. *Applied Mathematical Modelling*, 40(23-24), 10238-10253.
- Yong, Y. K., & Zhang, Z. (1993). A perturbation method for finite-element modeling of piezoelectric vibrations in quartz plate resonators. *Ieee Transactions on Ultrasonics Ferroelectrics and Frequency Control*, 40(5), 551-562.
- Yu, L., & Xu, P. (2010, 12-14 Jan. 2010). *An ACO-based algorithm for structural health monitoring*. Paper presented at the 2010 Prognostics and System Health Management Conference, Macao, China.
- Yu, M. R., Zhang, Y. J., Chen, K., & Zhang, D. (2015). Integration of process planning and scheduling using a hybrid GA/PSO algorithm. *International Journal of Advanced Manufacturing Technology*, 78(1-4), 583-592.
- Zhan, Z. H., Zhang, J., Li, Y., & Chung, H. S. H. (2009). Adaptive particle swarm optimization. *Ieee Transactions on Systems Man and Cybernetics Part B-Cybernetics*, 39(6), 1362-1381.
- Zhang, C., & Wang, H. P. (1993). Mixed-discrete nonlinear optimization with simulated annealing. *Engineering Optimization*, 17(3), 263-280.

LIST OF PUBLICATIONS AND PAPERS PRESENTED

1. Tam, J. H., Ong, Z. C., Ismail, Z., Ang, B. C., & Khoo, S. Y. (2017). Identification of material properties of composite materials using non-destructive vibrational evaluation approaches: A review. *Mechanics of Advanced Materials and Structures*, 24(12), 971-986. doi: 10.1080/15376494.2016.11967988 (published)
2. Tam, J. H., Ong, Z. C., Ismail, Z., Ang, B. C., & Khoo, S. Y. (2017). Identification of material properties of composite plates using Fourier-generated Frequency Response Functions. *Mechanics of Advanced Materials and Structure*, UMCM-2016-0392. doi: 10.1080/15376494.2017.1365980 (Accepted)
3. Tam, J. H., Ong, Z. C., Ismail, Z., Ang, B. C., & Khoo, S. Y. (2017). Inverse identification of elastic properties of composite materials using hybrid GA-ACO-PSO algorithm. *Inverse Problems in Science & Engineering*, GIPE-2017-0091. doi: 10.1080/17415977.2017.1411911 (Accepted)
4. Tam, J. H., Ong, Z. C., Ismail, Z., Ang, B. C., & Khoo, S. Y. (2017). A new hybrid GA-ACO-PSO algorithm for solving various engineering design problems. *International Journal of Computer Mathematics*, GCOM-2016-0446-B. (Accepted)
5. Tam, J. H., Ong, Z. C., Ismail, Z., Ang, B. C., & Khoo, S. Y. (2017). Inverse identification of composite material properties. *Experimental Mechanics*, EXME-S-17-00413. (Under Review)
6. Tam, J. H., Ong, Z. C., Ho, K. W., Ismail, Z., Ang, B. C., Khoo, S. Y., Li, W. L. (2018). Composite material identification using a two-stage meta-heuristic hybrid approach incorporated with a two levels FRF selection scheme. (To be submitted)
7. Tam, J. H., Ong, Z. C., Ismail, Z., Ang, B. C., & Khoo, S. Y. (2017, 24-25 Oct). Identification of material properties of orthotropic composite plate using experimental frequency response function data. Paper presented at the 3rd International Conference on the Science and Engineering of Materials (ICoSEM) 2017, Kuala Lumpur, Malaysia. (attended)